AD-A117 862 COLORADO UNIV AT BOULDER F/G 20/9
PLASMA WAVE TURBULENCE AND PARTICLE HEATING CAUSED BY ELECTRON --ETC(U)
MAY 82 M V GOLDMAN AFOSR-80-0022
UNCLASSIFIED CU-1533143 AFOSR-TR-82-0592 NL

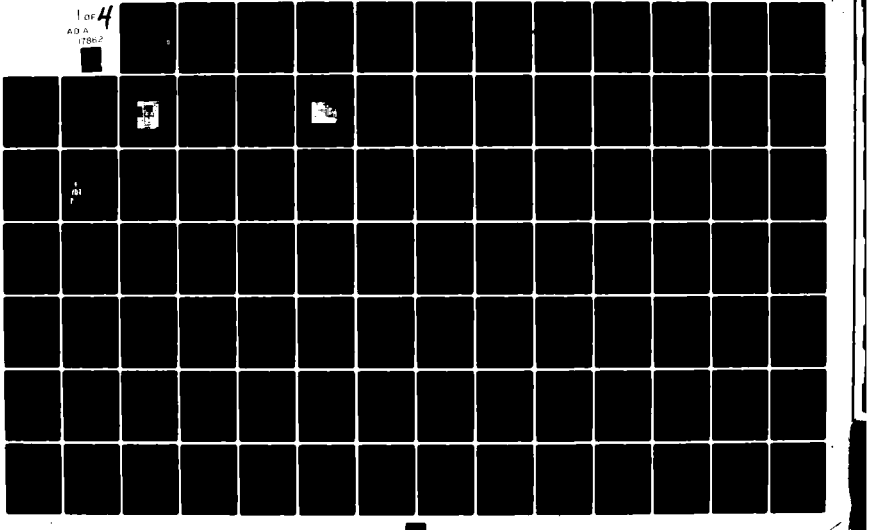

AFOSR-TR- 82-0592

(3)

AD A117052

AIR FORCE OFFICE OF SCIENTIFIC RESEARCH

Interim Report: October 1980 - September 1981

Plasma Wave Turbulence and Particle Heating Caused by Electron Beams, Radiation and Pinches

Martin V. Goldman, Principal Investigator

AFOSR-80-0022

CU# 1533143

DTIC
ELECTE
AUG 5 1982
D
H

Copy available to DTIC does not permit fully legible reproduction

DTIC FILE COPY

May, 1982

Approved for public release; distribution unlimited.

82 08 03 017

DISCLAIMER NOTICE

THIS DOCUMENT IS BEST QUALITY PRACTICABLE. THE COPY FURNISHED TO DTIC CONTAINED A SIGNIFICANT NUMBER OF PAGES WHICH DO NOT REPRODUCE LEGIBLY.

UNCLASSIFIED

SECURITY CLASSIFICATION OF THIS PAGE (When Data Entered)

REPORT DOCUMENTATION PAGE	READ INSTRUCTIONS BEFORE COMPLETING FORM
1. REPORT NUMBER **AFOSR-TR- 82-0592** 2. GOVT ACCESSION NO. AD-A117 562	3. RECIPIENT'S CATALOG NUMBER
4. TITLE (and Subtitle) PLASMA WAVE TURBULENCE AND PARTICLE HEATING CAUSED BY ELECTRON BEAMS, RADIATION AND PINCHES	5. TYPE OF REPORT & PERIOD COVERED INTERIM 1 Oct 80 - 30 Sep 81
	6. PERFORMING ORG. REPORT NUMBER CU# 1533143
7. AUTHOR(s) Martin V. Goldman	8. CONTRACT OR GRANT NUMBER(s) AFOSR 80-0022
9. PERFORMING ORGANIZATION NAME AND ADDRESS University of Colorado Boulder, CO 80309	10. PROGRAM ELEMENT, PROJECT, TASK AREA & WORK UNIT NUMBERS 61102F 2301/A8
11. CONTROLLING OFFICE NAME AND ADDRESS Air Force Office of Scientific Research/NP Buidling 410 Bolling AFB DC 20332	12. REPORT DATE May 82 13. NUMBER OF PAGES 272
14. MONITORING AGENCY NAME & ADDRESS(if different from Controlling Office)	15. SECURITY CLASS. (of this report) UNCLASSIFIED 15a. DECLASSIFICATION DOWNGRADING SCHEDULE

16. DISTRIBUTION STATEMENT (of this Report)

Approved for public release;
distribution unlimited.

17. DISTRIBUTION STATEMENT (of the abstract entered in Block 20, if different from Report)

18. SUPPLEMENTARY NOTES

19. KEY WORDS (Continue on reverse side if necessary and identify by block number)

20. ABSTRACT (Continue on reverse side if necessary and identify by block number)

This interim report covers research performed from October 1, 1980 through September 30, 1981 on electron-beam excited plasma turbulence and electromagnetic emission, on propagation of intense electromagnetic radiation in the earth's ionosphere, on plasma diagnostics, and on experiments to accelarate ions and excite low frequency turbulence in the laboratory.

82 08 03 017

DD FORM 1 JAN 73 1473

LIST OF APPENDICES

A. "Breakup and Reconstitution of Langmuir Wavepackets", T. Tajima, M.V. Goldman, J. Leboeuf, and J. Dawson, Phys. Fluids 24, 182-183 (January, 1981).

B. "Harmonic Emission from Adiabatically Collapsing Langmuir Solitons", B. Hafizi and M.V. Goldman, Phys. Fluids 24, 145-150 (January, 1981).

C. "Self-focusing of Radio Waves in an Underdense Ionosphere", F. Perkins and M.V. Goldman, J. Geophys. Res. 86, No. A2, 600-608 (February, 1981).

D. "Langmuir Collapse in a Weak Magnetic Field", M.V. Goldman, J.C. Weatherall, and D.R. Nicholson, Phys. Fluids 24, 668-672 (April, 1981).

E. "Parametric Instabilities in Weakly Magnetized Plasmas", J.C. Weatherall, M.V. Goldman, and D. Nicholson, Astrophys. J. 246, 306-313 (May, 1981).

F. "Scattering and Collapse of Langmuir Waves Driven by a Weak Electron Beam", B. Hafizi, J.C. Weatherall, M.V. Goldman, and D. Nicholson, Phys. Fluids 25, 392-401 (1982)

G. "Nonlinear Evolution Equations, Recurrence, and Stochasticity", B. Hafizi, Phys. Fluids 24, 1791-1798 (1981).

H. "Chaotic (Strange) and Periodic Behavior in Instability Saturation by the Oscillating Two-Stream Instability", D.A. Russell and E. Ott, Phys. Fluids 24, 1976-1988 (1981).

AIR FORCE OFFICE OF SCIENTIFIC RESEARCH (AFSC)
NOTICE OF TRANSMITTAL TO DTIC
This technical report has been reviewed and is approved for public release IAW AFR 190-12.
Distribution is unlimited.
MATTHEW J. KELLY
Chief, Technical Information Division

I. "Solitons and Ionospheric Heating" J.C. Weatherall, J. Sheerin, D. Nicholson, G. Payne, M.V. Goldman, J. Geophys. Res. A 87, 823-842 (1982).

J. "Azimuthal Coherent Ion-Ring--Beam Generation in Unstable Magnetized Plasmas", R.A. Stern, D.N. Hill, and N. Rynn, Phys. Rev. Lett. 47, 792-795 (1981).

K. "Modulational Interaction of Non-linear Waves and Recurrence", B. Hafizi, submitted to Physics of Fluids, June, 1981.

L. "Modulational Interaction of Langmuir Waves in One Dimension", B. Hafizi, submitted to Physics of Fluids, March, 1981.

M. "Ion Trajectories in a Space Charge Wave on a Relativistic Electron Beam", D.A. Russell and E. Ott, submitted to Physics of Fluids, 1981.

N. "Summary of Simulations Relevant to the Benford Beam Emission Experiment", J.C. Weatherall and M.V. Goldman, Private Research Note, May, 1981.

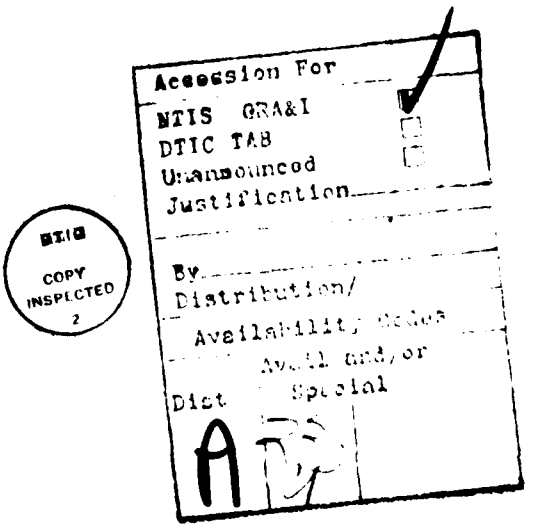

ABSTRACT

This interim report covers research performed from October 1, 1980 through September 30, 1981 on electron-beam excited plasma turbulence and electromagnetic emission, on propagation of intense electromagnetic radiation in the earth's ionosphere, on plasma diagnostics, and on experiments to accelerate ions and excite low frequency turbulence in the laboratory.

TABLE OF CONTENTS

I. Introduction

This interim report describes work performed under AFOSR grant #80-0022 during the period October 1, 1980 to September 30, 1981. The subject of research has been the theory of "Plasma Wave Turbulence and Particle Heating Caused by Electron Beams, Radiation, and Pinches". The period covered is the third stage of a comprehensive research program concerned with the nonlinear behavior of plasma subjected to intensely energetic sources.

One of the significant developments in plasma physics over the past decade has been the theoretical and experimental progress made in our understanding of nonlinear plasma wave evolution in response to external sources: A wide variety of radiation sources such as lasers,[1,2] microwaves,[3,4] and radar,[5,6] and of electron beam sources, such as solar electron streams[7,8] and laboratory beams[9] can excite plasma wave instabilities in target plasmas. The waves saturate into a turbulent spectrum,[10] and may heat the plasma, accelerate plasma particles, and/or emit their own radiation. Such processes have been linked to inertial[11] and magnetic[12] controlled thermonuclear fusion schemes, radar communications in the earth's ionosphere, and Type III solar radio bursts.[7,8] The phenomena also bear heavily on certain fundamental questions of plasma turbulence, such as wave collapse in phase space, electric-field envelope-soliton evolution,[13,14] and the nature of the so-called "strong turbulence".[13]

II. Summary of Accomplishments

In the following summary, we include accomplishments of our program from October 1980 to September 1981. The foundations for this work were laid during earlier sponsorship, under AFOSR #F49620-76-C-0005 from August 1976 through September 1979. Reference should be made to the November 1979 final report for this project, as well as the January 1981 interim report covering the period October 1979 through September 1980 in order to get a full picture of the underlying motivation and total perspective.

Our research has been divided into three main areas:

Beam-Plasma Interaction

Radiation-Plasma Interaction

Laboratory Research on Ion Beams

We shall summarize recent accomplishments in each of these areas separately. The details can be found in the Appendices, which are ordered as follows: Appendices A-E represent published versions of preprints included in the last interim report; Appendices F-J are publications of (new) work performed during the period covered by this report; Appendices H-M are preprints of submitted articles, and Appendix N is a research report.

A. Beam-Plasma Interaction

Our research has centered upon the nonlinear evolution of electron-beam excited Langmuir waves, and the electromagnetic emission from such waves. In new extension of previous numerical studies in two dimension, we have found that spatial self-focusing of Langmuir wave packets is invariably preceded by a

stage of linear instability. In the case of the weak electron streams which propagate through the solar wind, this linear instability is stimulated scattering off ions into low momentum regions of phase space (see Appendix F). In the case of the more intense relativistic electron beams studied in the laboratory by Benford, et al.,[15] the linear instability is modulational instability which causes break-up of beam-resonant wave packets into smaller packets whose size is determined by the wavelength of the fastest-growing unstable mode (see Appendix N). Spatial collapse follows the stage of linear instability. For the case of weak electron beams, the integrated energy in small-scale-size structures is a small fraction of the total wave energy, in agreement with the predictions of self-similar solutions (Appendix B). In work to be reported in detail in the next interim report, it is shown that non-thermal Landau damping in the vicinity of the beam velocity can lead to a steady state turbulence in which most of the energy resides at scale sizes longer than the beam-mode wavelength. It is likely that these long wavelength waves are responsible for emission near the plasma frequency (by parametric instability in a highly homogeneous plasma, and by conversion off density fluctuations in a plasma with low frequency turbulence present).

We have also explored the foundations of any statistical theory based on the dynamical (Zakharov) equations of beam-driven plasma turbulence, by studying intrinsically chaotic behavior of the solutions to the dynamical equations, as a

function of the beam growth rate. A postdoctoral research associate, Dr. D. Russell, has studied the transition to turbulence under assumed conditions of adiabatic ions, and with truncation to a few Fourier modes. With a beam mode, and two (degenerate) modulationally unstable modes, strange attractors and limit cycles were observed in phase space (Appendix H). A program of increasing the number of modes is now underway.

In further numerical work performed by another post-doctoral research associate, Dr. B. Hafizi, recurrent behavior was observed in nonlinear dynamical systems such as those described by the cubic Schroedinger and Kortweg de-Vries equations (Appendix G). In Appendices K and L, modulational interaction of nonlinear waves was modeled using three-, five-, seven-, nine-, and sixty-four-wave truncations of the nonlinear Schroedinger equation. A detailed description was given of the phase space for the three-wave system, and compared to that for the five-mode system analytically. It was shown computationally that the recurrence time for all the truncations was almost the same, and that the distribution of energy over the modes rapidly reached an asymptotic form as the number of modes was increased.

In Appendix M, single ion trajectories in an axis-symmetric space-charge wave on an electron beam were studied. The beam was assumed to move parallel to a strong uniform magnetic field. It was found that wave amplitudes too small to trap

beam electrons were also too small to engender stochastic motion of an ion initially trapped in the wave, and the ion remains trapped.

B. Radiation-Plasma Interaction

Appendix I is a reprint of a new theoretical paper on modification of the ionosphere by HF radar. For parameters characterizing the Platteville, Colorado, ionospheric heating facility, the HF radar excites Langmuir waves at its exact reflection point by the so-called oscillating two-stream instability.[5] The subsequent evolution of this instability is studied numerically, and found to involve spatial self-focusing and collapse of Langmuir wave packets. Comparisons are made with experiment.

Our paper on thermal self-focusing of HF radar and/or microwave beams in the ionosphere has been published and is included as Appendix C.

C. Laboratory Research on Ion Beams and Acceleration - R.A. Stern

The goal of the on-going program is to develop and enhance the efficiency with which large-amplitude waves in plasmas can accelerate ions. Two general directions were identified at the outset. First, the acceleration of ions in segments by means of ion-acoustic waves, in unmagnetized as well as magnetized plasma. Here the ion

beam ends up with its momentum directed along the direction of propagation of the wave, which is--in magnetized plasmas --parallel to the magnetic field. Second, the acceleration of ions across strong magnetic fields, by beams of cross-field instabilities. This totally new process has fundamental consequences of importance to other aspects of plasma physics such as ionospheric particle transport, and isotope separation.

i) Instrumentation Development and Testing

a) To study the acceleration of ions by ion-acoustic waves in unmagnetized plasmas, a surface-magnetic structure confined plasma device was assembled and tested. The basic configuration (Figure 1) consists of a gas discharge inside a large metal chamber of about 40 cm diameter and 50 cm length, surrounded on all sides by permanent magnets with about 1 kg field strength. In this chamber, it proved possible to operate a plasma at a background pressure of 10^{-5} Torr, more than one order of magnitude below that of previous studies. As a result, charge-exchange degradation of ion waves, which limited the amplitude of ion-accelerating waves in previous experiments, is avoided. Figure 2 shows ion-acoustic shocks (i.e., fully steepened ion-acoustic waves) propagating in this plasma. As seen, the waves are not at all degraded in amplitude. In contrast, similar waves at the higher pressures degrade by an order of magnitude. In conclusion, we have established that the surface-magnetic structure device operates as expected.

The size of the test metal chamber (contributed by Prof. N. Hershkowtiz of the University of Iowa who spent the academic year 1980-1981 with our group), is currently a limiting factor in the excitation of strong ion beam segments. Because the distances from control grids to walls are limited, and the strong magnetic confinement field occupy a sizeable fraction of these distances, calculations show that the relatively low-energy beams we can excite end up in curved rather than straight-line trajectories. To avoid complications resulting from these effects, a doubling of the chamber dimensions is under consideration. We have designed and requested independent support for the construction of a mating chamber of equal volume.

b) To minimize the scattering of ion beam segments by off-axis ion-acoustic waves--one of the principle limiting factors in ion beam generation--we have put together an experimental configuration involving a strong magnetic field. Here the unstable spectrum is narrower, and can be expected to have a correspondingly reduced effect on the ion beam. This device, a plasma column generated by microwave breakdown of a noble gas inside a solenoidal magnetic field, was contributed by Bell Laboratories. It was assembled and tested, and fully instrumented with motorized axial and radial Langmuir probes. Optical measurements have been delayed, pending resolution of a major technical problem: the presence of parasite radio noise from an as-yet undetermined source.

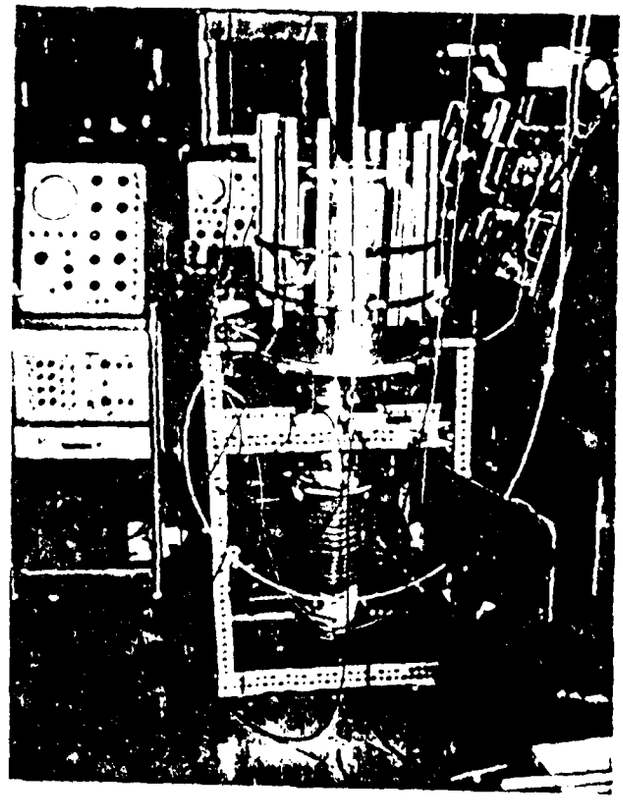

FIGURE 1

OF Plasma Machine Assembly

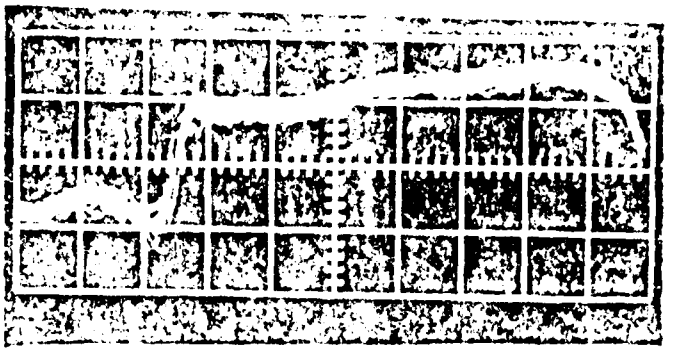

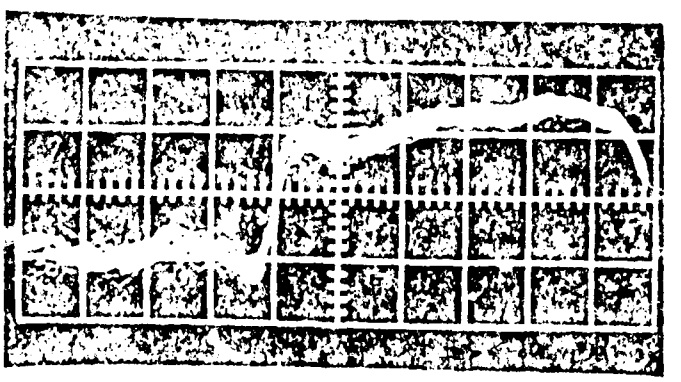

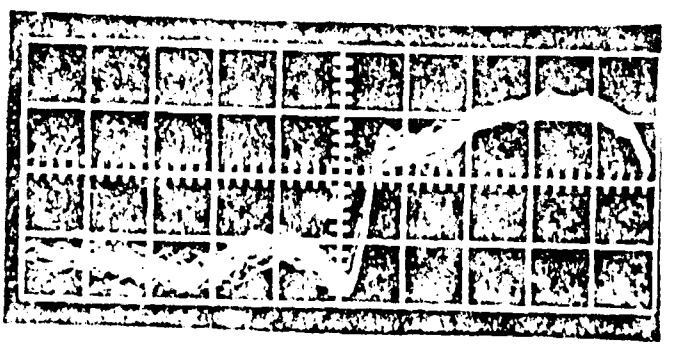

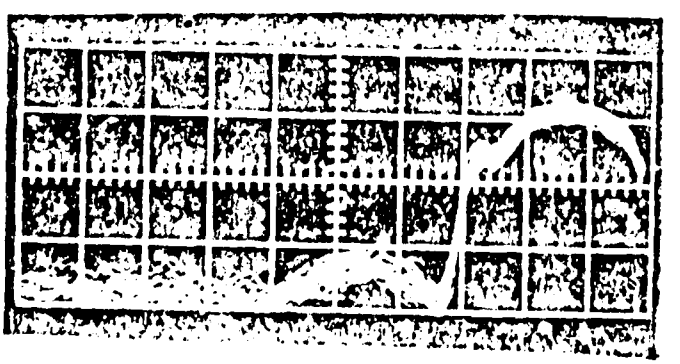

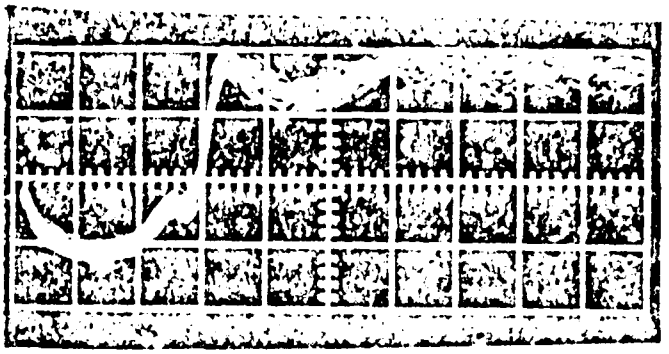

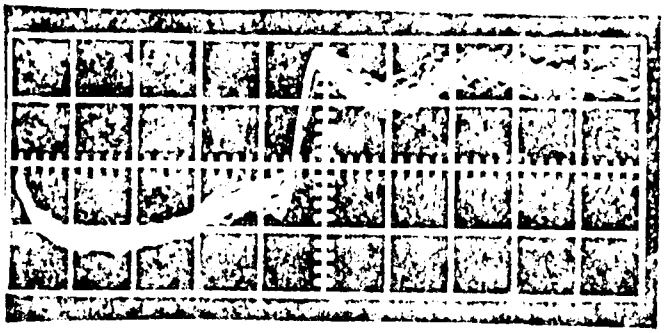

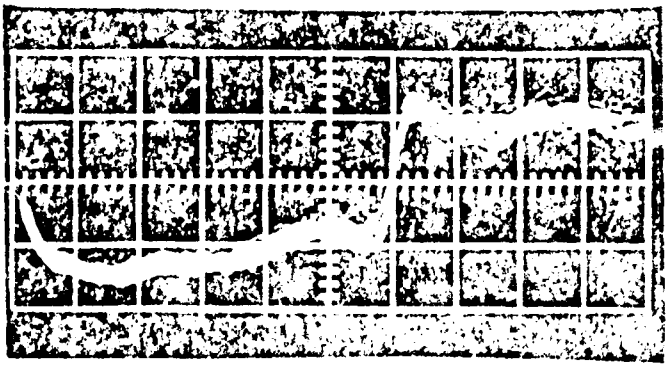

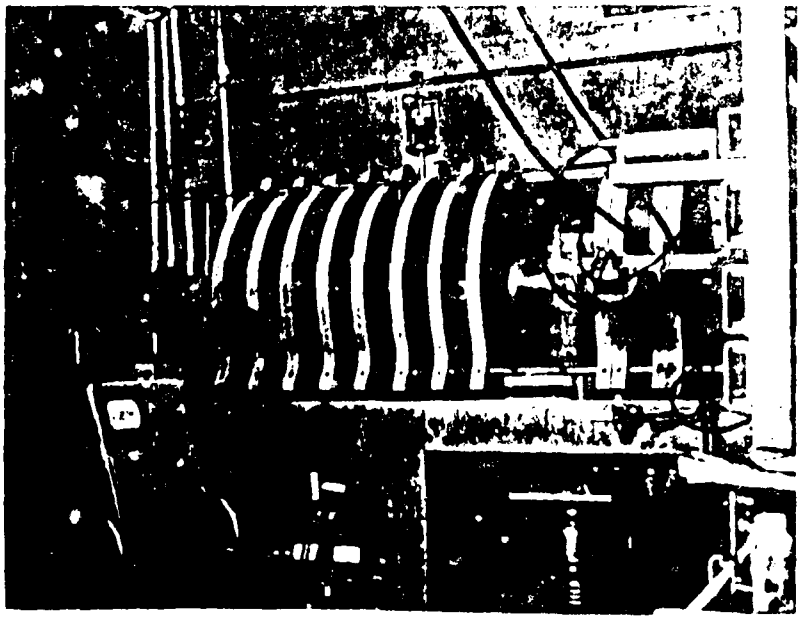

Preliminary measurements of wave excitation reveal that large-amplitude waves launched in this device are indeed free of degradation by off-axis ion-acoustic turbulence. An interesting new observation has emerged: it appears that some coupling from the on-axis ion-acoustic wave to cross- field ion-cyclotron modes is occurring. We are studying this interaction theoretically.

ii) Cross-Field Ion Acceleration in Magnetized Plasmas

As indicated in the proposal for this contract period, a principal new development of our work is the observation that ion beam segments can be driven across strong magnetic fields by electrostatic ion-cyclotron waves (EICW). We intended to quantify the process by measuring the relationship between beam speed, magnetic field and beam radius. We have successfully carried out these studies, using the Q-machine facility at the University of California, Irvine, and have obtained a firm model for the underlying physical process. To summarize, the radial electric field component of EICW imparts radial momentum to ions, which end up in large-diameter Larmor orbits convolved around the source region. The envelope of the ion circulation adds up to an aximuthal ion beam. Ion bunching occurs at the apogee of the orbits, as in magnetron motion, leading to the formation of beam segments.

A full report, included here as Appendix J has been published as a Physical Review Letter.

Based on this understanding, further technological developments are indicated. First, the process itself basically alters

our picture of transport processes in unstable plasmas, including the ionosphere. Specifically, the long-range ion transport demonstrated here indicates that multi-stage ion motion can occur, with scale lengths totally unrelated to density or temperature gradients, as in ordinary diffusion. Secondly, isotope separation processes now under development may be able to utilize our results to enhance spatial separation of particles with differing mass (for reference, see Appendix J).

III. Publications and Presentations during this grant period

A. Published versions of preprints included in last interim report (October, 1979 - September, 1980)

"Breakup and Reconstitution of Langmuir Wavepackets", T. Tajima, M.V. Goldman, J. Leboeuf, J. Dawson, Phys. Fluids 24, 182-183 (January, 1981).

"Harmonic Emission from Adiabatically Collapsing Langmuir Solitons", B. Hafizi and M.V. Goldman, Phys. Fluids 24, 145-150 (January, 1981).

"Self-focusing of Radio Waves in an Underdense Ionosphere", F. Perkins and M.V. Goldman, J. Geophys. Res. 86, 600-608 (February, 1981).

"Langmuir Collapse in a Weak Magnetic Field", M.V. Goldman, J.C. Weatherall, and D. Nicholson, Phys. Fluids 24, 668-672 (April, 1981).

"Parametric Instabilities in Weakly Magnetized Plasmas", J.C. Weatherall, M.V. Goldman, and D. Nicholson, Astrophys. J. 246, 306-313 (May, 1981).

B. Publications of (new) work performed during period covered by this report (October, 1980 - September, 1981)

"Azimuthal Coherent Ion Ring--Beam Generation in Unstable Magnetized Plasmas", R.A. Stern, D.N. Hill, and N. Rynn, Phys. Rev. Lett. 47, 792 (1981.

"Nonlinear Evolution Equations, Recurrence, and Stochasticity", B. Hafizi, Phys. Fluids 24, 1791-1798 (1981).

"Solitons and Ionospheric Heating", J.C. Weatherall, J. Sheerin, D. Nicholson, G. Payne, M.V. Goldman, J. Geophys. Res. A 87, 823-842 (1981).

"Chaotic (Strange) and Periodic Behavior in Instability Saturation by the Oscillating Two-Stream Instability", D.A. Russell and E. Ott, Phys. Fluids 24, 1976-1988 (1981).

"Scattering and Collapse of Langmuir Waves Driven by a Weak Electron Beam", B. Hafizi, J.C. Weatherall, M.V. Goldman, and D. Nicholson, Phys. Fluids 25, 392-401 (1982).

C. Papers submitted for publication during period of this report

"Modulational Interaction of Non-linear Waves and Recurrence", B. Hafizi, submitted to Physics of Fluids, June, 1981.

"Modulational Interaction of Langmuir Waves in One Dimension", B. Hafizi, submitted to Physics of Fluids, March, 1981.

"Ion Trajectories in a Space Charge Wave on a Relativistic Electron Beam", D.A. Russell and E. Ott, submitted to Physics of Fluids, 1981.

"Progress and Problems in the Theory of Type III Solar Radio Emission", Martin V. Goldman, submitted to Solar Physics, 1981.

D. Invited Talks presented between October, 1980 and September, 1981

"Soliton Collapse and Electromagnetic Emission", M.V. Goldman, invited one-hour lecture given, at the invitation of the Soviet Academy of Sciences, in Telavi, Georgia U.S.S.R., at a Workshop of Plasma Physics and Controlled Thermonuclear Physics, October, 1981.

"Langmuir Turbulence", M.V. Goldman, invited paper at Workshop on Stochasticity and Turbulence, Los Alamos Center for Nonlinear Studies, June, 1981.

"A Review of Solar Radio Wave Emission", M.V. Goldman, invited talk: Radiophysics Laboratory, CSIRO, Epping, Australia, March, 1981.

"Strange Attractors", M.V. Goldman, invited talk: University of Australia, March, 1981.

"Solitary Waves and Solar Radio Wave Emission", M.V. Goldman, invited colloquium, University of New South Wales, Sydney, Australia, March, 1981.

"Coherence and Chaos in Nonlinear Systems", D.A. Russell, Workshop on Stochasticity, Center for Nonlinear Studies, Los Alamos, June, 1981.

Invited Seminar, Los Alamos Scientific Laboratory, R. Stern, April, 1981.

H. Contributed Talks at Scientific Meetings

"Thermal Self-focusing of Radio Waves in an Underdense Ionosphere", M.V. Goldman, F.W. Perkins, APS Plasma Physics Meeting, San Diego, November, 1980 [Bull. Am. Phys. Soc. 25, 914 (1980)].

"Harmonic Emission by Adiabatically Collapsing Langmuir Solitons", B. Hafizi and M.V. Goldman, APS Plasma Physics Division Meeting, San Diego, November, 1980 [Bull. Am. Phys. Soc. 25, 914 (1980)].

"Langmuir Collapse in a Weak Magnetic Field", J.C. Weatherall, M.V. Goldman, and D.R. Nicholson, APS Plasma Physics Division Meeting, San Diego, November, 1980 [Bull. Am. Phys. Soc. 25, 984 (1980)].

"Ten-Channel Optical Polychromator for Doppler Ion Temperature Measurements on the Dodecapole Surmac", K.L. Lam, R.W. Schumacher, and R.A. Stern, APS Plasma Physics Division Meeting, San Diego, November, 1980 [Bull. Am. Phys. Soc. 25, 959 (1980)].

"Azimuthal Ion Ring Beam Generation in Unstable Magnetized Plasmas", R.A. Stern, D. Hill, and N. Rynn, APS Plasma Physics Division Meeting, San Diego, November, 1980 [Bull. Am. Phys. Soc. 25, 985 (1980)].

"Solitons and Ionospheric Modification", D.R. Nicholson, P.J. Hansen, G.L. Payne, J.C. Weatherall, M.V. Goldman, and J.P. Sheerin, URSI XXth General Assembly, Washington, D.C., August 10-19, 1981, Symposium on Active Experiments, Ionospheric Modification Session.

I. Ph.D. Thesis Completed

"Nonlinear Langmuir Waves in a Weak Magnetic Field", J.C. Weatherall, December, 1980.

J. Conferences Organized

Martin V. Goldman was organizer of an International Workshop on Plasma Physics, at the Aspen Center for Physics, June, 1980.

IV. References

1. S. Jackel, B. Perry, and M. Lubin, Phys. Rev. Lett. 37, 95 (1976).
2. M.J. Forrest, P.D. Morgan, N.J. Peacock, K. Kuriki, M.V. Goldman, and T. Rudolph, Phys. Rev. Lett. 37, 1681 (1976).
3. R.P.H. Chang, M. Porkolab, and B. Grek, Phys. Rev. Lett. 28, 206 (1972).
4. R. Stenzel and A.Y. Young, Phys. Rev. Lett. 28, 274 (1972).
5. F.W. Perkins and P.K. Kaw, J. Geophys. Res. 76. 282 (1971).
6. H.C. Carlson, W.E. Gordon, and R.L. Showen, J. Geophys. Res. 77, 1242 (1972).
7. K. Papadopoulos, G.L. Goldstein, and R. Smith, Astrophys. J. 190, 1242 (1972).

8. S. Bardwell and M.V. Goldman, Astrophys. J. 209, 912 (1976).

9. A.Y. Wong and B.H. Quon, Phys. Rev. Lett. 34, 1499 (1975).

10. D.F. DuBois and M.V. Goldman, Phys. Rev. Lett. 28, 218 (1972).

11. P.K. Kaw and J.M. Dawson, Phys. Fluids 12, 2585 (1969); D.W. Forslund, et al., Phys. Rev. Lett. 36, 35 (1975).

12. W.M. Hooke and S. Barnabei, Phys. Rev. Lett. 29, 1218 (1972).

13. V.E. Zakharov, Sov. Phys. JETP 35, 908 (1972).

14. G.J. Morales and Y.C. Lee, Phys. Fluids 19, 690 (1976).

15. C. Benford, D. Tzach, K. Kato, and D.F. Smith, Phys. Rev. Lett. 45, 1182 (1980).

APPENDIX A

A. "Breakup and Reconstitution of Langmuir Wavepackets"

T. Tajima, M.V. Goldman, J. Leboeuf, and J. Dawson,
Physics of Fluids 24, 182-183 (January, 1981).

Breakup and reconstitution of Langmuir wave packets

CU 1040

T. Tajima, Martin V. Goldman,[a)] J. N. Leboeuf, and J. M. Dawson

Physics Department, University of California, Los Angeles, California 90024
(Received 25 January 1980; accepted 17 September 1980)

Recursive behavior has been observed in a two-dimensional electrostatic particle simulation of a coherent intense Langmuir wave packet. The recursion may be associated with the fact that the plasma frequency has a spatial variation in the density depression created by the ponderomotive force.

The behavior of intense Langmuir waves involves many possible processes, solitons,[1] wave packet collapse,[2] cascading,[3] stimulated scattering, nonlinear Landau damping, explosive instabilities,[4] and modulational instabilities,[5] are only a few. Competition between some of these effects is only just beginning to be studied. Effects seen in a two-dimensional electrostatic particle simulation including ion and electron dynamics are reported here. An initial wave packet undergoes virtually complete reconstitution following its initial break-up.

Use is made of a standard finite-sized particle code. The initial condition consists of a Langmuir wave packet which has a Gaussian intensity profile in wavenumber space with average wavenumber $\mathbf{k}_0 = k_0\hat{x}$ and half-width $\Delta k_x = \Delta k_y = k_0$. The Langmuir waves are turned on in an initially uniform unmagnetized plasma over the time interval $t = 0$ to $t = 1\omega_p^{-1}$. The waves have approximately constant energy after the initial transients subside. Typical parameters in our study are: number of electrons (ions) $N_e(N_i) = 32768$; number of grids in the $x(y)$ direction $L_x = 128$ ($L = 32$) in this doubly periodic system; electron (ion) Debye length $\lambda_{De}(\lambda_{Di}) = 1\Delta$; $k_0 = 12\pi/128\Delta$ (in the x direction); $\Delta k_x = \Delta k_y = 2\pi/32\Delta$, the mass ratio $M/m = 5$, and particle size $a_x = a_y = \Delta$, where Δ is the grid spacing in both the x and y directions. In such a system, the electron collision frequency is $5 \times 10^{-4}\omega_p$ and the electron Landau damping decrement for the k_0 mode is $3 \times 10^{-7}\omega_p$. The plasma is therefore fairly dissipationless over the period of $10\omega_p^{-1}$.

Figure 1 shows three snapshots of equi-energy contours of the electrostatic wave energy density for a case with the initial wave amplitude for the $k = k_0$ mode of $E_{x0} = eE_{x_0}/m\omega_p^2\Delta = 0.6$ and the average wave energy $W = \langle E^2 \rangle/2\pi nT_e = 0.5$ over the period of $t = 5{,}100)\omega_p^{-1}$. Here, the angular brackets denote spatial averaging. The peak of the wave packet is located at $x = 64\Delta$ at $t = 0$. It travels in the positive x direction with the group velocity $v_g \simeq 0.6\Delta\omega_p$ until $t \simeq 10\omega_p^{-1}$. Linear theory predicts $v_g \cong 0.47\Delta\omega_p$. Figure 1(b) illustrates a slightly later stage $t = 20\omega_p^{-1}$. The coherent wave packet has broken into many seemingly random subpackets all over the space. The break-up occurs not only in the x direction, but also in the y direction. The behavior of the wave intensity in wave vector space (not shown here) indicates that the peak of the wave energy has shifted from $k = k_0$ to roughly $k = \frac{1}{2}k_0$ at $t = 20\omega_p^{-1}$. The assemblage of subpackets continues to change its structure until $t \simeq 50\omega_p^{-1}$, when a somewhat more organized structure begins to emerge. Figure 1(c) at $t = 70\omega_p^{-1}$ shows that the process of reconstitution of the subpacket has been completed and the wave packet profile is close to the one at $t = 0$, although at a somewhat shifted position. Also, in k space we see that the energy has oscillated back to around $\mathbf{k} = \mathbf{k}_0$ in the $\mathbf{k}$ space. When we made $L_x = 256$, the packet first propagated forward, then backward, and became many subpackets, it eventually came back to the original shape at the same place in about the same time. The size of the plasma does not appear to be a factor in the results. The density depression associated with the packet became shallower and wider as time elapsed. Although Fermi *et al.*[7] found nonlinear recursion in a computer simulation of the vibrations of a nonlinear string some two decades ago, there are few works in fluid or plasma physics dealing with the recursive process until the recent work of Yuen *et al.*[8] who solved a model nonlinear Schrödinger equation in one dimension, numerically.

To determine the physical process responsible for the wave packet recursion, we have made runs with several different wave packet energy densities. Figure 2 shows the recursion time vs the average wave packet energy density. All the cases shown in Fig. 2 produced recursion. All parameters except for the packet energy density are fixed at the same values as for the case $W = 0.5$. With W ranging from 0.25 to 0.75, the recursion time τ_r was found to be approximately inversely proportional to the wave energy density W as shown in Fig. 2. There were only minor differences in the wave packet evolution during the various recursions.

The observed behavior of τ_r as a function of W is consistent with the theoretical observations made by Kaw *et al.*[6] who studied the effect of fixed, spatially periodic ion density fluctuations on Langmuir wave evolutions. The break-up and recursion of an original Langmuir plane wave is due to the density dependence of the plasma frequency, which causes the oscillations in different spatial regions of the plasma to go in and out of phase with each other. In Fourier space the wave vectors $\mathbf{k}_i$ of the ion density fluctuation mix in with $\mathbf{k}_0$, producing sidebands at $\mathbf{k}_0 \pm \mathbf{k}_i$. The original mode at $\mathbf{k}_0$ becomes smaller in amplitude at first, but then returns at the time when the Bessel function, J_1, has its next extremum. This gives an approximate recursion time of

$$\tau_r = \frac{7.7\omega_p^{-1}}{\sqrt{5m_e/m_i}W^{1/2}}, \qquad (1)$$

0031-9171/81/010182-03$00.90
© 1981 American Institute of Physics

where δn_{max} is the maximum of the density ripple.

In our problem, the density perturbation is self-consistently generated by the ponderomotive force of the Langmuir wave packet. If the ions are roughly adiabatic, then balancing the plasma pressure against the ponderomotive force gives the relation between the density perturbation and the Langmuir field: $\delta n_{max}/n_0 \approx -W/4$. This predicts a scaling

$$\tau_r = 31/W, \tag{2}$$

which shows good agreement with the results of simulation, as given in Fig. 2. [Also, the numerically obtained δn_{max} measurements were in good agreement with Eq. (1).] The argument in Ref. 8 predicts a temporally periodic migration to both higher and lower wavenumbers in the Fourier-space evolution of the packet. We do not observe the generation of higher Fourier modes. Their absence is probably due to Landau damping, so we see only oscillation in the direction of lower wavenumbers and back.

Since the submission of this manuscript we have found some recent theoretical results which appear relevant

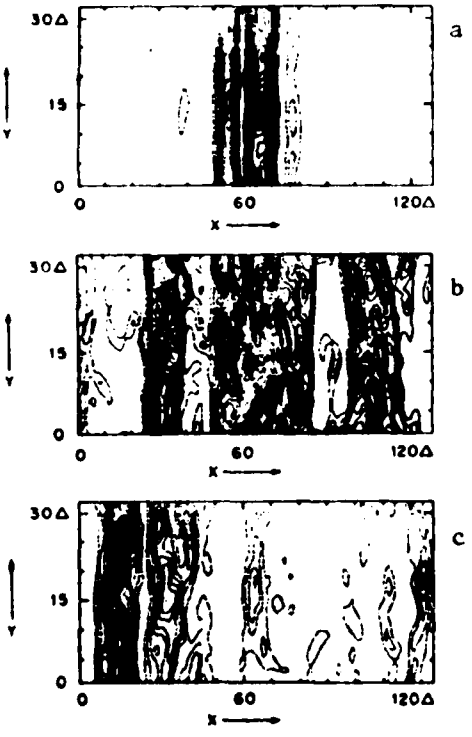

FIG. 1. Time sequence of contours of electric-field energy density $E^2/4\pi$ in x-y space. (a) at $t = 10\omega_p^{-1}$, (b) at $t = 20\omega_p^{-1}$, and (c) at $t = 70\omega_p^{-1}$. Real lines represent high-energy contours and dotted ones low contours.

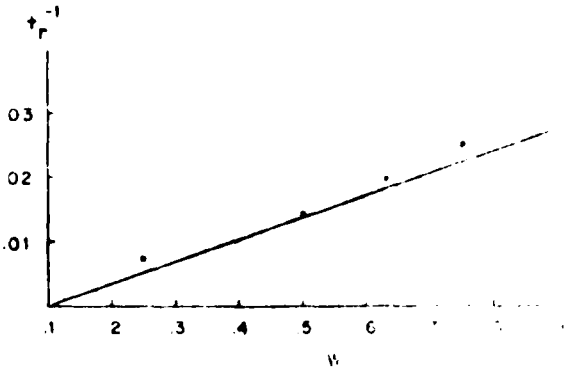

FIG. 2. Inverse of the wave packet recursion time vs [illegible] malized wave-energy density W, obtained by simulation.

to our numerical studies. Thyragaraja[9] has also noted recurrence can be expected in one-dimensional wave phenomena describable by a cubic Schrödinger [illegible] and has pointed out[10] that, in two dimensions, such systems will either collapse or recur. The wave packets we have studied should be roughly adiabatic, and therefore be describable by a simple cubic Schrödinger equation[2] to the extent that damping is negligible.

This work was supported by National Science Foundation Grants PHY79-01319 at the University of California and ATM76-14275 at the University of Colorado, and Air Force Office of Scientific Research Contract No. F49620-76-C-0005. Two of us (T.T. and M.V.G.) appreciate the hospitality of the Aspen Center for Physics where a part of this work was done. One of us (M.V.G.) would like to thank the Guggenheim Foundation for a fellowship held during part of this research.

[a]Permanent address: Department of Astro-Geophysics, University of Colorado, Boulder, Colorado 80309.

[1]V. E. Zakharov, Zh. Eksp. Teor. Fiz. 62, 1745 (1972) [Sov. Phys.-JETP 35, 908 (1972)].
[2]M. V. Goldman and D. R. Nicholson, Phys. Rev. Lett. [illegible] (1978).
[3]D. R. Nicholson and M. V. Goldman, Phys. Fluids 21, [illegible] (1978).
[4]M. Jones and J. Fukai, Phys. Fluids 22, 132 (1979).
[5]A. A. Vedenov and L. I. Rudakov, Dokl. Akad. Nauk [illegible] 767 (1964) [Sov. Phys.-Dokl. 9, 1073 (1965)].
[6]E. Fermi, J. Pasta, and S. Ulam, *Collected Papers of Fermi* (University of Chicago Press, Chicago, 1965), Vol. II, p. 977.
[7]H. C. Yuen and W. E. Ferguson, Phys. Fluids 21, [illegible]
[8]P. Kaw, A. T. Lin, and J. M. Dawson, Phys. Fluids 16, [illegible] (1973).
[9]A. Thyragaraja, Phys. Fluids 22, 2093 (1979).
[10]A. Thyragaraja (private communication).

APPENDIX B

B. "Harmonic Emission from Adiabatically Collapsing Langmuir Solitons"

B. Hafizi and M.V. Goldman
Physics of Fluids 24, 145-150 (January, 1981)

Harmonic emission from adiabatically collapsing Langmuir solitons

B. Hafizi and Martin V. Goldman

Department of Astro-Geophysics, University of Colorado, Boulder, Colorado 80309
(Received 19 May 1980; accepted 17 September 1980)

Numerical studies of radiation at $2\omega_p$ from a Langmuir envelope collapsing adiabatically in three dimensions show that the emissivity is higher than expected. A volume emissivity obtained from an approximate density of collapsing packets leads to favorable comparisons with measurements of type-III solar radio bursts.

I. INTRODUCTION

It is now believed that a type-III solar radio burst is associated with an electron beam launched into the solar wind during a solar flare, leading to electromagnetic emission at the fundamental and harmonics of the local plasma frequency. Gurnett and Anderson[1] have measured the volume emissivity of harmonic emission at $\frac{1}{2}$ a.u.

Recently, Goldman *et al.*[2] proposed a model for the emission based on the following model: An energetic beam of electrons launched into the solar wind excites Langmuir waves. Computations[3] indicate that a Langmuir wave packet grows up to a point where the spatially-averaged energy density W (normalized to the thermal energy) in the packet exceeds the threshold, W_{th}, for direct collapse.[4,5] The collapse time is infinite at threshold and decreases rapidly as W increases above W_{th}.[5] It is found that, typically, a packet continues to grow in strength up to about twice the threshold energy density before there is noticeable evidence of spatial collapse (and broadening in wave vector space). Once the packet becomes broad enough in k space, it should be kinematically possible to couple two Langmuir waves into a photon at twice the local plasma frequency.

The physics of Langmuir collapse is described by the Zakharov equations.[4] The general solution of these equations is unknown, however, it is known that they possess certain invariants.[4-6] It is also known[4,7,8] that in some cases the solutions approach a self-similar form over a region of space. There are two distinct stages of early collapse, the subsonic or adiabatic stage (described by a cubic Schrödinger equation), and the supersonic stage. In the subsonic stage, the ions respond to the ponderomotive force adiabatically, while, in the supersonic stage, ion inertia plays an important role.

In Ref. 2, using the plasmon number invariant, an upper bound, and using a supersonic self-similar solution, a much lower estimate of the emissivity of a bunch of collapsing packets was obtained. It was argued that most of the harmonic emission would occur in the supersonic stage.

In the present work, we examine the adiabatic stage numerically. We find that an adiabatically collapsing wave packet can lead to emission in the subsonic stage which is significantly higher than was thought possible. Owing to subtle stationary phase effects, this can occur for packets whose width Δk is still smaller than ω_p/v_e. With reasonable choices for the number density of collapsing wave packets, we find levels of emission consistent with the experimental estimate[1] for the volume emissivity.

II. EMISSIVITY OF A LANGMUIR WAVE PACKET

The emissivity is given by

$$\frac{d\mathbf{P}}{d\Omega} = \frac{cr^2}{4\pi} \lim_{T\to\infty} \frac{1}{T} \int_{-T/2}^{T/2} dt\, \mathbf{E}\times\mathbf{B},$$

where c is the speed of light, $\mathbf{E}(\mathbf{B})$ is the electric (magnetic) field, and r is the distance between the point of observation (where $\mathbf{E}\times\mathbf{B}$ is evaluated) and the origin. In terms of the current, $\mathbf{J}_{2\omega_p}$, at twice the (local) plasma frequency ω_p, the emissivity is,

$$\frac{d\mathbf{P}}{d\Omega} = \frac{\hat{\mathbf{r}}}{4\pi c^3} \lim_{T\to\infty} \frac{1}{T} \int_{-\infty}^{\infty} \frac{d\omega}{2\pi} \omega K |\mathbf{J}_{2\omega_p}(K\hat{\mathbf{r}},\omega)|^2 \sin^2\theta, \qquad (1)$$

where $\hat{\mathbf{r}}$ is the unit vector directed toward the point of observation, ω is the frequency variable in the temporal Fourier transform of the current, $K = |\omega^2 - \omega_p^2(r)|^{1/2}/c$, and θ is the angle between $\mathbf{J}_{2\omega_p}(K\hat{\mathbf{r}},\omega)$ and $\hat{\mathbf{r}}$, i.e.,

$$\sin\theta = |\hat{\mathbf{J}}_{2\omega_p}(K\hat{\mathbf{r}},\omega)\times\hat{\mathbf{r}}|.$$

We now make use of Zakharov's fundamental simplification[4] by expressing the current as a slowly varying envelope $\mathbf{j}_{2\omega_p}$ and a rapidly oscillating phase:

$$\mathbf{J}_{2\omega_p}(K\hat{\mathbf{r}},\omega_0) = \tfrac{1}{2}\mathbf{j}_{2\omega_p} \exp(-i\omega_0 t) + \text{c.c.},$$

where ω_0 is the photon frequency. The emissivity can then be expressed as[2]

$$\frac{d\mathbf{P}}{d\Omega} = \frac{K_0\omega_0\sin^2\theta_0}{8\pi c} \lim_{T\to\infty} \frac{1}{T} \int_{-T/2}^{T/2} dt\, |\mathbf{j}_{2\omega_p}(K_0\hat{\mathbf{r}},t)|^2, \qquad (2)$$

where Eq. (1) has been simplified by taking an "average" angle θ_0, wavenumber K_0, and frequency ω_0 out of the integral, where

$$K_0 = [\omega_0^2 - \omega_p^2(r)]^{1/2}/c. \qquad (3)$$

This procedure should be valid as long as the direction of $\mathbf{J}_{2\omega_p}(K\hat{r},\omega)$ does not vary significantly over values of the integrand in Eq. (1) for which $\mathbf{J}_{2\omega_p}$ is large.

III. DYNAMICS OF A LANGMUIR WAVE PACKET

We describe the nonlinear wave packet by a Schrödinger equation with cubic nonlinearity

 0031 9171/81/010145-06$00.90 1981 American Institute of Physics

$$\left(i\partial_t + \frac{3T_e}{2m_e\omega_p}\nabla'^2 + \frac{e^2}{8m_e\omega_p\bar{T}}|\mathbf{E}|^2\right)\mathbf{E} = 0,$$

where $\nabla' \equiv \partial/\partial\mathbf{r}'$; $\bar{T} \equiv \gamma_e T_e + \gamma_i T_i$; $T_e(T_i)$ is the electron (ion) temperature, with $\gamma_e(\gamma_i)$ being the associated adiabaticity index; m_e, e are the mass and charge of the electron, respectively; $\mathbf{E}$ is the envelope of the electric field $\mathbf{E}$:

$$\mathbf{E}(\mathbf{r}', t) = \tfrac{1}{2}\mathbf{E}(\mathbf{r}', t)\exp(-i\omega_p t) + \text{c.c.}$$

Under the following substitutions:

$$\mathbf{E} \to (32\pi n_e \bar{T})^{1/2}\mathbf{E}, \quad t \to \omega_p t, \quad \mathbf{r}' \to \sqrt{3}\,\lambda_D \mathbf{r}', \tag{4}$$

where n_e is the background number density and $\lambda_D = (T_e/4\pi n_e e^2)^{1/2}$ is the Debye length, the dimensionless form of Schrödinger's equation is obtained:

$$(i\partial_t + \tfrac{1}{2}\nabla'^2 + |\mathbf{E}|^2)\mathbf{E} = 0 \tag{5}$$

We note that the use of the Schrödinger equation is valid only in the subsonic stage, where the ions are adiabatic.[4,5] In the Appendix, this is justified for the time scale over which we calculate the emissivity.

The electrostatic field envelope $\mathbf{E}$ can be written as

$$\mathbf{E}(\mathbf{r}, t) = -\nabla[i\psi(\mathbf{r}, t)\exp(i\mathbf{k}_0\cdot\mathbf{r}/k_0)]. \tag{6}$$

Here, $\mathbf{k}_0 = \omega_p\hat{\mathbf{v}}_b/v_b$ is the wave vector of the most unstable beam mode. At $t = 0$, $\psi(\mathbf{r}, t = 0)$ is a real function which is localized around $\mathbf{r} = 0$ and has spatial widths parallel and perpendicular to $\mathbf{k}_0$. These initial widths are set by the k-space contours of the beam instability.[2] Roughly, $|\nabla_\parallel\psi| \approx \Delta k_\parallel|\psi|$ and $|\nabla_\perp\psi| \approx \Delta k_\perp|\psi|$ where $\Delta k_\parallel$ and $\Delta k_\perp$ are the parallel and perpendicular widths associated[2] with the beam instability; initially, $\Delta k_{\parallel,\perp} \ll k_0$.

Our central approximation will be to take ψ to be spherically symmetric at the initial and later times, so there will only be a symmetric width measure which changes with time. Throughout the calculation, the inequality $|\nabla\psi| \ll k_0|\psi|$ will be satisfied, so that the wave packet will remain relatively narrow in k space. This enables us to write Eq. (6) approximately as

$$\mathbf{E}(\mathbf{r}', t) \approx \hat{\mathbf{k}}_0\psi(r', t)\exp(i\mathbf{k}_0\cdot\mathbf{r}'). \tag{6'}$$

This field still has the phase factor $\exp(i\mathbf{k}\cdot\mathbf{r}')$ and is thus not spherically symmetric. However, the momentum $\mathbf{k}_0$ can be transformed away by the following gauge-frame transformation[7]:

$$\psi(\mathbf{r}', t) = \phi(r, t)\exp(-ik_0^2 t/2), \qquad \mathbf{r} = \mathbf{r}' - \mathbf{k}_0 t. \tag{7}$$

Using Eqs. (5)–(7), we find that the spherically symmetric scalar $\phi(r, t)$ satisfies

$$(i\partial_t + \tfrac{1}{2}\nabla^2 + |\phi|^2)\phi = 0. \tag{8}$$

We have studied this equation in Ref. 7. It was shown there that the condition for the electrostatic approximation is

$$|\nabla\psi| \ll |k_0\psi|,$$

which is well satisfied for most times of interest. This differs substantially from the so-called head-on approximation often made[8] to calculate harmonic emission. In addition, conditions were found for the adiabatic approximation. These can be expressed as

$$|\phi|^2, \quad k_0^2 \ll m/M.$$

In the Appendix, we shall consider the validity of these inequalities for the parameters of the present calculation.

In terms of ϕ, the current density $\mathbf{j}_{2\omega_p}$ can be written as [see Eq. (33) of Ref. 2]:

$$\mathbf{j}_{2\omega_p}(K_0\hat{\mathbf{r}}, t) = \frac{-3\sqrt{8}\,\omega_p\lambda_D^2\bar{T}}{\pi e}K_0 \times\left(\frac{\hat{\mathbf{r}}}{2} - \hat{\mathbf{r}}\cdot\hat{\mathbf{k}}_0\hat{\mathbf{k}}_0\right)\exp(-i\hat{\mathbf{k}}_0\cdot K_0\hat{\mathbf{r}}) \times\int d^3\mathbf{r}\,\phi^2(r)\exp[-i(K_0\hat{\mathbf{r}} - 2\mathbf{k}_0)\cdot\mathbf{r}].$$

The angular part of the integral can easily be evaluated, leading to

$$|\mathbf{j}_{2\omega_p}(K_0\hat{\mathbf{r}}, t)|^2 = \left(\frac{\sqrt{24}\,6\bar{T}\omega_p\lambda_D}{e(19 - 8\sqrt{3}\,\mu)^{1/2}}\right)^2 \times\left|\int_0^\infty r\phi^2\sin(Sr)\,dr\right|^2, \tag{9}$$

where

$$S = |K_0\hat{\mathbf{r}} - 2\mathbf{k}_0| = \sqrt{3}\,(v_{th}/c)(19 - 8\sqrt{3}\,\mu)^{1/2}, \quad \mu \equiv \hat{\mathbf{k}}_0\cdot\hat{\mathbf{r}}. \tag{10}$$

The quantity S is the momentum mismatch between the harmonic photon and two plasmons; also, v_{th} is the electron thermal speed. Use has been made of the fact that for emission at twice the local plasma frequency, Eq. (3) gives $K_0 = \sqrt{3}\,(\omega_p/c)$; moreover, $|\mathbf{k}_0| = 2(\omega_p/c)$. [Note that in Eq. (10) the dimensionless forms of K_0 and k_0 appear in accord with Eq. (4).]

Substituting Eq. (9) for the modulus square of the $2\omega_p$ current into Eq. (2), we have the following expression for the emissivity of a single wave packet

$$\frac{d\mathbf{P}}{d\Omega} = \hat{\mathbf{r}}\sin^2\theta_0\frac{\sqrt{6}\,(6\bar{T})^2K_0\omega_0}{\pi(19 - 8\sqrt{3}\,\mu)e^2}\left(\frac{v_{th}}{c}\right)^2 v_{th}\lim_{T\to\infty}\frac{1}{T} \times\int_{-T/2}^{T/2}dt\left|\int_0^\infty dr\,r\phi^2\sin(Sr)\right|^2. \tag{11}$$

IV. NUMERICS AND SCALING

Equation (8) is solved in the Hilbert space of ϕ by an implicit finite difference method in spherical geometry. The following invariants can easily be derived from this equation[6,9]:

$$I_1 = \int_0^\infty |\phi|^2 r^2 dr, \quad I_2 = \int_0^\infty (|\partial_r\phi|^2 - |\phi|^4)dr, \tag{12}$$

where I_1 is proportional to the boson number and I_2 is proportional to the Hamiltonian. The accuracy and stability of the numerical scheme is checked by the (semi) invariance of the discrete forms of the functionals I_1 and I_2 on the Hilbert space.

The computations are started by choosing a Gaussian for the initial potential

$$\phi(r, t=0) = \phi_0 \exp(-2r^2/l^2). \tag{13}$$

For the particular mesh size chosen, we take $l = 5.66$. From Eq. (9b) of Ref. 2, the parallel half-width of the packet is found to be

$$\Delta k_\parallel / k_0 = \tfrac{1}{4} \Delta v_b / v_b,$$

[Eq. (9b), Ref. 2], where v_b is the beam speed and Δv_b is the spread in this speed. From the values quoted in Ref. 2 we find

$$\frac{\Delta k_\parallel}{k_D} \equiv \frac{\Delta k_\parallel}{1/\lambda_D} = \tfrac{1}{4} \frac{\Delta v_b}{v_b} \frac{k_0}{k_D} \cong \tfrac{1}{4} \times 10^{-3}.$$

Note that the Schrödinger equation (5) is invariant under a stretching of $\mathbf{r}'$ by a factor A, provided the time t is stretched by A^2, and E is reduced by A. With $A = 300$, our choice of $l = 5.66$ can be made to correspond to the above value of $\Delta k_\parallel$. We therefore arrive at the following approximate scaling from type-III values (subscript "III") to computational values (subscript "c"):

$$\begin{aligned} (\phi)_{\rm III} &= (300)^{-1} (\phi)_c, \\ (t)_{\rm III} &= (300)^2 (t)_c, \\ (r)_{\rm III} &= 300 (r)_c. \end{aligned} \tag{14}$$

We choose $(\phi_0)_c$ to be 1.18, corresponding to an average energy density $(W)_c$, at twice the threshold value.[2,7] Using the scaling of Eq. (14), this leads to a value for $(W)_{III} \cong 10^{-4}$, which is in agreement with the value used in Ref. 2. Further, from Eqs. (4), (10), and (14) we find that

$$(S)_c = 300 (S)_{III} = 300 \sqrt{3} (v_{\rm th}/c)(19 - 8\sqrt{3}\mu)^{1/2}. \tag{15}$$

With $(v_{\rm th}/c) \sim 4.5 \times 10^{-4}$ in Eq. (15), S is sufficiently large for all ϕ, so that the spatial integral in Eq. (11) is seen to be practically zero for an initial ϕ of the form of Eq. (13). Thus, the scaling implied by $\Delta k_\parallel$ [Eq. (9b) of Ref. 2] leads to a negligible emissivity initially. The interesting feature that emerges from our computations is that the modulus and phase of ϕ change sufficiently in the subsonic regime to enable substantial emission to occur.

V. RESULTS AND DISCUSSION

Figures 1 (a) and (b) show the time development of the emissivity of a single packet, i.e., the expression given in Eq. (11) before performing a time average. The emission grows in an approximately exponential manner for most of the time development of the packet, reaching a maximum and decreasing thereafter until the collapse point. In this calculation θ_0 has been taken as 45° [see the remark following Eq. (2)] and $\mu = \hat{\mathbf{k}}_0 \cdot \hat{\mathbf{r}}$ has been taken as $\sqrt{3}/2$ ($\hat{k}_0$ making an angle of 30° with $\hat{r}$).

We note that the emissivity climbs from an initially negligible value to a peak many orders of magnitude larger, and then begins to decay. The peak occurs at $0.994 t_c$, where t_c is the adiabatic collapse time. In order to understand this behavior, we note that $dP/d\Omega$ in Eq. (11) is proportional to the absolute square of the following integral over ϕ:

$$I = \int_0^\infty dr\, r \phi^2 \sin Sr. \tag{16}$$

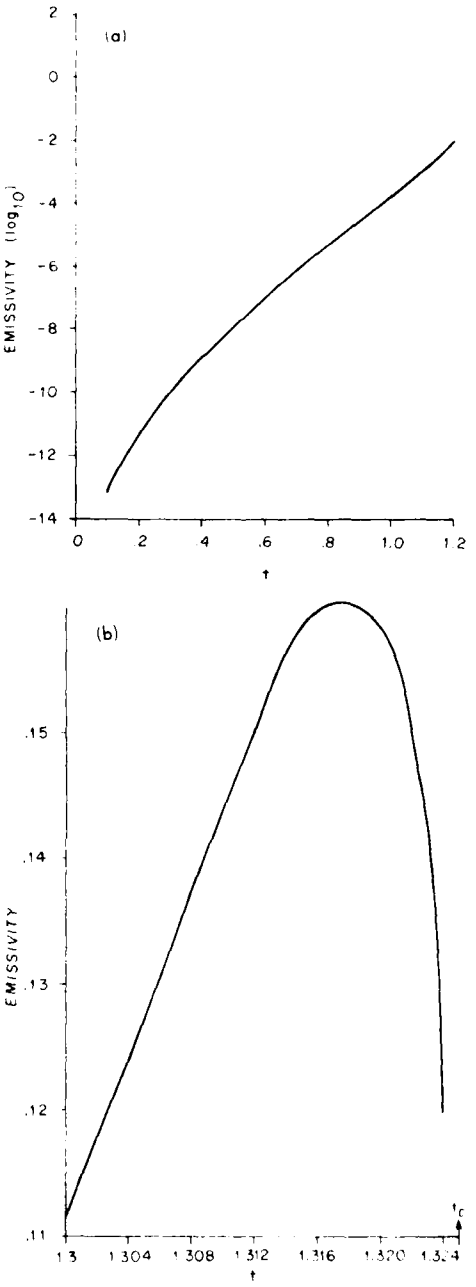

FIG. 1. Temporal development of emissivity from a collapsing wave packet. Note the logarithmic scale in (a) for the early stage, and the linear scale in (b), close to the collapse time. The scale on the time axis is in ω_p^{-1} and the computational scaling [see Eqs. (14) in text]. Collapse time is 1.3265.

Let us now write $\phi = A \exp(i\alpha)$, where $A(r)$ is a real modulus, and $\alpha(r)$ a real phase, and both are spherically symmetric. The integrand will be largest around the peak of rA^2, provided the phase factors $\exp[i(2\alpha + Sr)]$ do not produce severe phase mixing.

For our initial ϕ of Gaussian form, α is zero and the quantity $rA^2 \propto r \exp(-2r^2/l^2)$ peaks at $r_A = 2$, and has a width of $\Delta r_A \cong 2$. However, $\sin Sr$ oscillates with a half-wavelength $\pi/S = 0.5$. Hence, there is strong

phase mixing of the emissivity. This corresponds physically to the failure to conserve momentum in the coalescence of two plasmons to produce a photon.

At later times, the packet has collapsed considerably, so the rA^2 can peak at smaller r values with a smaller half-width, which is therefore less susceptible to phase mixing. In Fig. 2(a), we have plotted A^2 as a function of r at $t=0$ and at $t=1.312$. The half-width of A^2 has decreased by a factor of 6. In addition, the quantity rA^2 now peaks at $r_A \simeq 0.25$ with a half-width $\Delta r_A \approx 0.25$. This peak and half-width coincide with the peak and half-width of the first maximum of $\sin rS$, which would seem to indicate reduced phase mixing. However, effects associated with the phase α of the field are also beginning to come into play at this time. A region of stationary phase in the integrand of Eq. (16) corresponds to a range of points where $|S \pm (\partial\alpha/\partial r)|$ becomes significantly smaller than S. Such a region of stationary phase is beginning to occur at $t=1.312$ and is seen to overlap the peak of rA^2. This also contributes to the reduction of phase mixing. The normalized gradient of α, $(\partial\alpha/\partial r)/S$, is plotted as a function of r in Fig. 2(b) for the time $t=1.312$, and is seen to reach a maximum absolute value of about $\frac{1}{2}$.

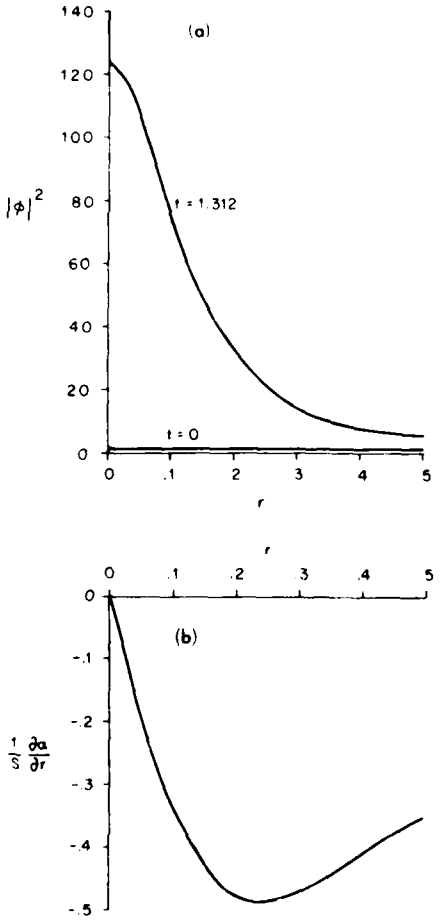

FIG. 2. Langmuir packet evolution. (a) Square modulus of Langmuir field, $|\phi|^2$ as a function of r at $t=0$ and at $t=1.32$. Note the Gaussian at $t=0$ appears flat because of limited range of r plotted. (b) Gradient of intrinsic phase of Langmuir envelope in units of momentum mismatch S, as a function of r, for $t=1.312$.

The phase α is also responsible for the eventual reduction of emissivity at later times. In Fig. 3, we have plotted $(\partial\alpha/\partial r)/S$ as a function of r at the later time $t=1.324$, corresponding to a reduced emissivity [see Fig. 1(b)]. The emissivity is reduced at this time because of the positive and negative oscillations in the gradient of α which once more lead to phase mixing. The reduction can also be viewed as a cancellation of the integrals over $\exp[i(2\alpha + Sr)]$ and $\exp[+i(2\alpha - Sr)]$, which have slightly different narrow regions of stationary phase.

A word is in order concerning the physical significance of the phase α. The momentum density carried by the Langmuir field is[7] $\mathbf{p} \cong (1/2i)(E_i^* \nabla E_i - E_i \nabla E_i^*)$. In our case, this reduces to

$$\mathbf{p} = [\mathbf{k}_0 + \nabla\alpha(r)]|\mathbf{E}|^2 .$$

Hence, $\nabla\alpha$ is a local plasmon momentum, which arises from the nonlinear dynamics of collapse, and adds to $\mathbf{k}_0 = \omega_p \tilde{\mathbf{v}}_b / v_b$. (We should bear in mind, however, that *average* plasmon momentum is conserved[7] and equal to $\mathbf{k}_0$ in the adiabatic stage of collapse so $\langle\nabla\alpha\rangle \equiv \int d^3r \times |E|^2 \nabla\alpha / \int d^3r |E|^2 = 0$.) The momentum conservation in the coalescence of two plasmons to produce a photon thus becomes $2\mathbf{k}_0 - \mathbf{K}_0 - 2\nabla\alpha \simeq 0$, which is essentially the stationary phase condition in the integral in Eq. (16). *Since the square modulus A^2 narrows spatially,* the failure of this phase matching condition is less serious. The gradient of A is $|\nabla A/A|$, which we may identify as a spread of wavenumbers Δk. Its maximum value

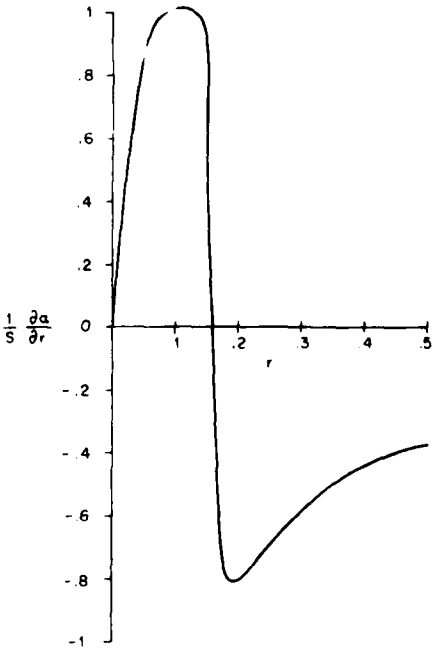

FIG. 3. Gradient of intrinsic phase of Langmuir envelope in units of momentum mismatch S, as a function of r for $t=1.324$.

of $\Delta k \approx (\Delta r_A)^{-1}$ becomes broader as real-space collapse progresses (as Δr_A tends to zero). At $t = 0$, we find $\Delta k_\parallel k_\parallel \approx 10^{-2}$, whereas at time $t = 1.316$, $\Delta k_\parallel k_\parallel \approx 60^{-2}$. Thus, stationary phase becomes less important as collapse proceeds. The exception is the late stages in which the phase oscillated rapidly, causing the resumption of phase mixing.

It is important to note the role of coherent phase in this calculation. Past estimates[8] of the volume emissivity have been based on Fourier space expansions of the second-order current in terms of Langmuir fields. In the resulting current-current correlation function, the decorrelation of four fields is performed by assuming the random phase approximation. Our calculations are in real space, rather than Fourier space. The existence of an assembly of wave packets in real space is due to random k-space phases, which cause constructive and destructive interference. However, once a real-space packet begins to collapse, there is a phase coherence which is preserved even for the increasingly widely separated k-space components in the spectrum of each collapsing packet. In this respect, the coherence of each collapsing packet is taken into account in our calculations, although the contribution from *different* packets are incoherent with respect to each other. Statistical assumptions underlie only our treatment of the density of collapsing packets, which yields the volume emissivity.

Another difference between the present calculation and past work[8] on the emissivity concerns the relative size of the average plasmon momentum $K_\parallel$. In the "head-on" approximation,[8] the plasmon momentum spectrum is assumed to extend over a region of k space much greater than $K_\parallel$, and containing "head-on," or oppositely directed, plasmons whose momenta are much greater than $K_\parallel$. This is not true for our initial spectrum, but in the late stages of adiabatic collapse where we find the greatest emission, the spread of momentum components $\nabla\omega$ in the packet is on the same order as $K_\parallel$, so our approximations are of marginal validity (see the Appendix).

In order to compute the volume emissivity, we need to know the density of collapsing packets n_c in the beam. We just quote the estimate made in Ref. 2,

$$n_c = \gamma_g \tau_c F n_o ,$$

[Eq. (59), in Ref. 2], where γ_g is the beam growth rate, τ_c is the collapse time, n_o is the density of wave packets, given by

$$n_o \simeq \Delta k_\parallel (\Delta k_\perp)^2/8$$

[Eq. (56), Ref. 2] in terms of the parallel $\Delta k_\parallel$ and perpendicular $\Delta k_\perp$ width of a single packet, and F is a dimensionless unknown parameter in our model that essentially measures the fraction of energy transferred from the beam to *collapsing* packets.

In order to work out the time averaging implied in Eq. (11), we follow Ref. 2 and compute the fractional time that the emissivity is within a half-width of its peak value. From Fig. 1, this fraction is roughly $0.025/1.325$. Thus, we write,

$$\left\langle \frac{dP}{d\Omega} \right\rangle_t \simeq \frac{0.025}{1.325} \times 0.16 \simeq 0.003 \text{ ergs sec}^{-1} \text{ sr}^{-1} ,$$

and obtain for the time-average volume emissivity the following result

$$J_{\omega_p} = n_e \left\langle \frac{dP}{d\Omega} \right\rangle ,$$

$$= \frac{\gamma_g}{8} \tau_c F \Delta k (\Delta k_\perp)^2 \times 0.003 ,$$

$$= \frac{1}{8} \left(\frac{\pi}{8e} \right)^{1/2} \frac{n_b}{n_e} \left(\frac{v_b}{\Delta v_b} \right)^2 \times 1.3265 \times 300 \times F$$

$$\times \frac{1}{4} \frac{\Delta v_b}{v_b} \frac{\omega_p}{v_b} \left(\frac{1}{4} \right)^2 \left(\frac{\omega_p}{v_b} \right)^2 \times 0.003 ,$$

where $1.3265 \times 300/\omega_p$ is the numerically determined[8] collapse time, and

$$\frac{\gamma_g}{\omega_p} = \left(\frac{\pi}{8e} \right)^{1/2} \frac{n_b}{n_e} \left(\frac{v_b}{\Delta v_b} \right)^2 ,$$

following Eq. (62) of Ref. 2: n_e is the background density, 40 cm^{-3}, n_b is the beam density, $10^{-3} n_e$, v_b and Δv_b are the beam speed and spread in speed, with $\Delta v_b / v_b \sim \frac{1}{3}$, $\Delta k_\perp k_\parallel \sim \frac{1}{4}$, Eq. (9a) of Ref. 2, and $\Delta k_\parallel k_\parallel = \frac{1}{4}(\Delta v_b / v_b)^2$, Eq. (9b) of Ref. 2. The quantity F is a factor (described in Ref. 2) which relates to the depletion of beam modes according to two different evolution scenarios. The final answer for the volume emissivity is therefore

$$J_{\omega_p} \sim 1 \times 10^{-10} F \text{ ergs cm}^{-3} \text{ sec}^{-1} \text{ sr}^{-1} . \quad (17)$$

This is compared with the measured value of 2×10^{-7} [see also Eq. (1) of Ref. 2]. We see that in order to reconcile the two values, F has to be around 10^{-3}. Considering the arguments presented in Ref. 2 concerning the magnitude of F, we see that a value of 10^{-3} is not unreasonable.

VI. CONCLUSION

Our calculations for a group of collapsing Langmuir wave packets account quite reasonably for the observed emissivity associated with type-III solar radio bursts. These results are encouraging enough to merit further elaboration; in particular, there is a clear need for a better estimate of the density of "collapsons."

ACKNOWLEDGMENTS

This work was supported by the Atmospheric Sciences Section of the National Science Foundation under Grants ATM 76-14275 and 7916837 to the University of Colorado. The work of M. V. Goldman was also supported by the Air Force Office of Scientific Research through Contract #AFF49620-76-C-0005 and Grant 80-0022, also awarded to the University of Colorado.

APPENDIX: VALIDITY OF ADIABATIC AND ELECTROSTATIC APPROXIMATIONS

Our calculations have been based on the cubic Schrödinger Eq. (5). The validity of this equation requires that the wave field be predominately electrostatic, and the low-frequency (ion) motions be adiabatic. The

conditions for both approximations are set forth in the Appendix of Ref. 7.

For the waves to be electrostatic, we must satisfy

$$\Delta k / k_0 \ll 1,$$

where $\Delta k \approx |\Delta| \phi|/\phi|$ is a measure of the gradient of ϕ. Our wave packets satisfy this criterion up until the very latest times of $t = 1.324$, where $\Delta k/k_0 \approx 60\%$.

The adiabatic ion approximation requires that

$$k_0^2, \quad |E|^2 < m/M = 5.4 \times 10^{-4}.$$

The condition on k_0 means that the mean wave packet group velocity is slow enough for the ions to follow the ambipolar field adiabatically. Since $k_0 = 10^{-2}$ in our calculations, it is always satisfied. The second condition essentially requires that the collapse speed remain subsonic. Taking into account the scaling of ϕ in Eq. (14), we may rewrite this condition as

$$|\phi_c|^2 \ll 50.$$

This condition breaks down at $r = 0$ near the time of peak emissivity at $t = 1.312$. However, only the peak of $r|\phi_c|^2$ is significant for the emissivity in Eq. (16). At this peak, we find from Fig. 2 that $|\phi_c|^2$ is of order 50, so the adiabatic approximation is marginal. At later times, it would appear to be violated. However, we have found the emissivity to go down at these times [see Fig. 1 (b)], so our calculation probably does not overestimate the emissivity.

[1] D. A. Gurnett and R. R. Anderson, Science **194**, 1159 (1976); J. Geophys. Res. **82**, 632 (1977).

[2] M. V. Goldman, G. F. Reiter, and D. R. Nicholson, Phys. Fluids **23**, 388 (1980).

[3] D. R. Nicholson, M. V. Goldman, P. Hoyng, and J. C. Weatherall, Astrophys. J. **223**, 605 (1978).

[4] V. E. Zakharov, Zh. Eksp. Teor. Fiz. **62**, 1745 (1972) [Sov. Phys.-JETP **35**, 908 (1972)].

[5] M. V. Goldman and D. R. Nicholson, Phys. Rev. Lett. **41**, 406 (1978).

[6] J. Gibbons, S. G. Thornhill, M. J. Wordrop, and D. ter Haar, J. Plasma Phys. **17**, 153 (1977).

[7] M. V. Goldman, K. Rypdal, and B. Hafizi, Phys. Fluids **23**, 945 (1980).

[8] D. B. Melrose and J. E. Stenhouse, Astron. Astrophys. **73**, 151 (1979).

[9] P. B. Budneva, V. E. Zakharov, and V. S. Synakh, Fiz. Plazmy **1**, 606 (1975) [Sov. J. Plasma Phys. **1**, 335 (1975)].

APPENDIX C

C. "Self-focusing of Radio Waves in an Underdense Ionosphere"

F. Perkins and M.V. Goldman
Journal of Geophysics Research 86, 600-608 (February, 1981)

JOURNAL OF GEOPHYSICAL RESEARCH, VOL. 86, NO. A2, PAGES 600-608, FEBRUARY 1, 1981

Self-Focusing of Radio Waves in an Underdense Ionosphere

F. W. PERKINS

Plasma Physics Laboratory, Princeton University, Princeton, New Jersey 08544

M. V. GOLDMAN

Department of Astro Geophysics, University of Colorado, Boulder, Colorado 80309

The theory of self-focusing instabilities in the ionosphere is developed emphasizing the critical parameters required to obtain sufficiently fast temporal and spatial growth rates so that the instability may be observed. It is shown that self-focusing will not occur unless $2\omega^2/\omega_{pi}^2 l < 1$, where ω is the radio wave frequency, ω_{pi} a typical ionospheric plasma frequency, and l the spatial growth length. (In the F region, $l \approx 25$ km is used, while in the E region $l \approx 1$ km.) In the F region, the threshold power flux P_t is $P_{tF} \approx (1.5\ \mu W\ m^{-2})(\omega/15\ MHz)^3 (T_e/1000\ °K)^4 \times (10^6\ cm^{-3}/n_e)^4 C_F$, where n_e and T_e are typical electron densities and temperatures, and $C_F \sim 1$ depends on spatial and temporal growth rates. In the E region, the result is $P_{tE} \approx (1\ mW\ m^{-2})(\omega/15\ MHz)^3 (10^6\ cm^{-3}/n_e) C_E$, where $C_E \approx 1$ again depends on growth rates. Dimensional analysis indicates nonlinear saturation will set in when variations of order unity occur in the radio wave intensity. The corresponding relative electron density fluctuations are given by $\delta n/n \sim \pi c^2/\omega_{pi}^2 l$. Applications to planned ionospheric heating experiments and ionospheric modification by the microwave beam from a satellite power station are discussed.

1. INTRODUCTION

Self-focusing of radio waves in the F region of the ionosphere has occurred in many overdense ionosphere modification experiments [*Thome and Perkins*, 1974; *Duncan and Behnke*, 1978] and its principles are well understood in terms of theory [*Vas'kov and Gurevich*, 1976; *Cragin and Fejer*, 1974; *Gurevich*, 1978; *Perkins and Valeo*, 1974]. These theories all indicate that self-focusing should occur in underdense ionospheric conditions as well, and recent observations [*Novozhilov and Savel'ev*, 1978] are qualitatively in accord with this prediction. The improved ionospheric heating facilities now nearing completion at Arecibo and Tromsø will permit scientific investigation of underdense self-focusing both in the E and F regions. Furthermore, there is current interest in what effect the 2.4 GHz microwave beam from a proposed Satellite Power Station (SPS) [*Brown*, 1973; *Glaser*, 1977; *Vanke et al.*, 1978] would have on the ionosphere. It will be shown that self-focusing of the SPS microwave beam may well occur, but not under all ionospheric conditions.

It is important to state clearly what the word underdense means. We take it to mean that the radiowave frequency f exceeds the maximum ionospheric plasma frequency $f_{p\,max}$ so that resonant interactions, such as parametric decay instabilities [*Fejer and Kuo*, 1973; *Das and Fejer*, 1980; *Perkins et al.*, 1974; *DuBois and Goldman*, 1972; *Vas'kov and Gurevich*, 1977*a*], which require the frequency matching condition $\omega = \omega_{pi}$ to be satisfied somewhere in the ionosphere, cannot occur. With this definition, a radiowave with frequency $\omega/2\pi$ by several times the maximum ionospheric plasma frequency can be reflected obliquely from the ionosphere and still be considered as underdense, as indeed was the case for the diagnostic wave in the *Novozhilov and Savel'ev* [1978] experiment. We will consider only cases with $\omega > \omega_{pi,\,max}$ so that just the self-focusing instability operates and parametric decay processes are not allowed.

The book by *Gurevich* [1978] provides an excellent summary of the physics governing the E region self-focusing instability. In particular, the instability exhibits exponential growth both in time and in space, along the direction of the radiowave beam. The goal of this work is to use this understanding to calculate the threshold radiowave power flux P_t required to induce the self-focusing instability in cases of practical interest. The key considerations beyond the basic physical principles derive from the finite extent of the ionosphere (which means that the spatial amplification must be sufficiently rapid) and the finite width of the radiowave beam. In particular, the temporal growth time must be a small fraction of the time it takes the ambient $\mathbf{E} \times \mathbf{B}$ drift to convect the ionospheric plasma through the beam. These two conditions set the practical threshold power flux. In contrast, according to equation (6.31) of *Gurevich* [1978], there is no threshold power flux for the self-focusing instability!

There are some interesting new physics points as well. First we shall show that there is an upper limit to the radiowave frequency above which self-focusing will not occur for a medium of finite extent. Secondly, in the E region, the ion-neutral collision frequency ν_{in} exceeds the ion gyrofrequency Ω_i, $\nu_{in} >> \Omega_i$, which means the ion motion across the magnetic field line is allowed. As a consequence, ion motion can be sufficiently rapid so that recombination does not suppress the self-focusing instability as predicted by Gurevich.

The question of whether the SPS microwave beam will introduce structure into the ionosphere via the self-focusing instability is best addressed by a combination of theory and experiment. As is the case with Ohmic heating [*Perkins and Roble*, 1978], experiments done at a frequency of 15 MHz using the improved Arecibo heating facility will both simulate the geometry of the SPS beam-ionosphere and be clearly in the underdense regime. Results of these experiments can be utilized to validate and refine the theory developed below, before it is extrapolated to the SPS parameters. But this extrapolation involves very large factors (~ 160 in frequency, $\sim 4 \times 10^4$ in threshold power flux) and should be taken as indicative rather than quantitative.

Section 2 of this paper sets forth the model. Section 3 derives the expressions for the critical power flux in the F and E

Copyright © 1981 by the American Geophysical Union.

Paper number 80A1127.
0148-0227/81/080A-1127$01.00

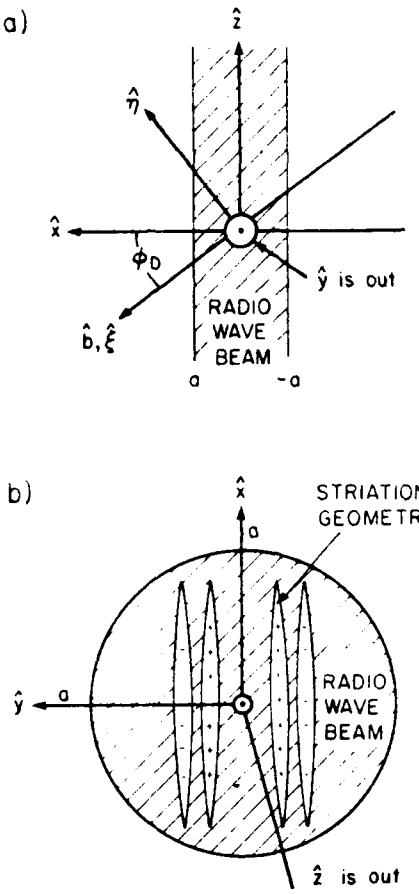

Fig. 1. Geometry of the self-focusing instability. (*a*) The radiowave beam is propagating in the **z** direction. The actual orientation of **z** in space depends on the application (see text). The magnetic field lies in the **b** direction which is taken to be in the **x** − **z** plane. The finite dimensions of the radiowave beam in the **x** − **z** plane are indicated. (*b*) Geometry of the self-focusing striations as viewed along the radiowave beam. The striations are elongated along the magnetic field and grow slowly in the direction of the radiowave beam, but they have a rapid spatial variation the **z** × **b** direction (i.e., the $\hat{y}$ direction).

regions. Section 4 applies these formulas to planned ionospheric heating experiments and to the SPS microwave beam. The paper concludes with a discussion and summary. Certain aspects of the eigenvalue problem associated with the finite beam width are discussed in the appendix.

2. Model and Equations

The basis for our model is the recognition that the transverse dimensions of ionospheric modification radiowave beams are substantially smaller than the characteristic lengths associated with the ionospheric plasma. We shall therefore adopt the model of a plasma with spatially uniform properties but containing a radiowave beam of finite transverse dimensions, $2a$, propagating in the **z** direction. The plasma contains a uniform magnetic field B in the **b** direction which we take to lie in the **x** − **z** plane. The principal spatial variation of the striations associated with the self-focusing instability can then be shown to be in the **z** × **b** direction (i.e., the $\hat{y}$ direction). Figure 1 portrays the geometry.

The actual orientation of the **z** direction in space depends on the application: For most ionospheric modification experiments **z** is vertically upward; for SPS beams, **z** is inclined downward, for powerful HF transmissions, **z** is almost horizontal [*Novozhilov and Savel'yev*, 1978].

The previous work [*Perkins and Valeo*, 1974; *Gurevich*, 1978] has shown that self-focusing striations do not propagate relative to the plasma. But the ambient **E** × **B** drifts will convect the plasma through the radiowave beam which is stationary. Typical convection velocities v_D range from 20–60 m s^{-1} [*Blanc and Amayenc*, 1979], yielding interaction times T given by

$$T \approx \frac{2a}{v_D} = (300\ \text{s})\left(\frac{a}{5\ \text{km}}\right)\left(\frac{30\ \text{m s}^{-1}}{v_D}\right) \tag{1}$$

In order for instability to fully develop, we require that the growth rate γ satisfy

$$\gamma T \geqq 10 \tag{2}$$

In practical units, (1) and (2) combine to give

$$\gamma > \left(\frac{1}{30\ \text{s}}\right)\left(\frac{5\ \text{km}}{a}\right)\left(\frac{v_D}{30\ \text{m/s}}\right) \tag{3}$$

Our model takes into account the finite size of the microwave beam by requiring that the growth rate be sufficiently fast. Apart from this, it is a good approximation to assume that the initial microwave beam intensity is independent of the y coordinate, so that in a linear stability analysis one can employ plane wave structures in the y direction. Quantitatively, this approximation requires that the beam intensity change by a negligible amount over the scale size of a striation. One can easily check a posteriori that this approximation is well satisfied.

In the F region, a plane wave approximation is not appropriate in the **x** direction because electron thermal conduction and plasma ambipolar diffusion along the magnetic field play an important role in determining the threshold power flux. Following the previous work, we shall assume that the perturbations grow exponentially along the center of the beam as $e^{z/l}$. Hence, the self-focusing instability is a spatial amplifier, requiring seed perturbations to get it started. The growth length l must be sufficiently short so that the total spatial amplification e^A is large ($A \approx 7$). For the F region, we shall adopt a nominal value of $l = 25$ km while for the E region $l = 1$ km. It is important to keep in mind that l represents the exponentiation distance along the radiowave beam. Beams propagating obliquely through the ionosphere clearly have a longer path length available for amplification than do vertically incident beams.

The calculations below constitute linear stability analysis which yields a generalized dispersion relation, i.e., a function which relates the temporal growth and the spatial amplification lengths to the power flux in the beam and the wavenumber in the y direction. This dispersion relation will form the basis of our application discussions.

Our model incorporates the following physics: (1) Radiowave propagation is adequately described by an isotropic, parabolic approximation to the wave equation [*Fock*, 1965]. An isotropic index of refraction is a valid assumption because the radiowave frequency is large compared to the electron gyrofrequency $\omega >> \Omega_e$. (2) The calculations are done in a frame in which the ambient electron drifts vanish. (3) Ion motion is controlled by ambipolar diffusion through the neutral gas. In

the E region, the ions have an ambient drift relative to the electrons in the range 20–100 m s^{-1} [*Harper et al.*, 1976]. (4) Electron motion and thermal conductivity is along the magnetic field and controlled by diffusion through ions and neutrals. The $\mathbf{E} \times \mathbf{B}$ velocity does not generate density fluctuations because it represents incompressible motion. For simplicity, the ambient electron temperature is assumed equal to the ambient ion temperature. (5) Recombination takes place in the E region. (It will be shown to be of moderate importance.) (6) No ion temperature perturbations occur because of their good thermal contact with neutrals. (7) Ohmic heating by the beam provides a heat source in the electron equation. Electrons lose energy by exchange with ions (in the F region) or with neutral molecules (in the E region). We have neglected electron cooling by excitation of $O(^1P)$ levels in the F region, as it is generally less than electron-ion cooling at and above the peak of the F region [*Perkins and Roble*, 1978, Figure 7]. Furthermore, the comment following (52) makes it clear that our F region results are not sensitive to the electron cooling process.

Let us first turn to the equation governing radiowave propagation in a medium with weak density fluctuations. Since we can safely assume that the ionosphere is an isotropic medium, the equation governing linearized wave propagation is

$$\left(\nabla^2 + \frac{\omega_0^2 - \omega_p^2(\mathbf{x})}{c^2}\right)\mathbf{E} = 0 \tag{4}$$

which is solved by

$$\mathbf{E}(\mathbf{x}, t) = \{\mathbf{E}_0 + \mathbf{E}_1(x, z)e^{\gamma t}\cos(ky - \omega t)\}\, e^{i(k_0 z - \omega_0 t)} + \{\mathbf{E}_0 + \mathbf{E}_1^*(x, z)e^{\gamma t}\cos(ky - \omega t)\}e^{-i(k_0 z - \omega_0 t)} \tag{5}$$

The justification for steady state in (4) is the condition $\gamma l\omega_0/c^2 k_0 \ll 1$, where l is the scale length, $|E_1/\partial_z E_1|$. The plasma frequency $\omega_p^2(\mathbf{x})$ is given by

$$\omega_p^2(\mathbf{x}) = \omega_p^2(1 + \delta n/n_0) \tag{6}$$

in terms of the relative density fluctuations

$$\delta n/n_0 = \Delta(x, z)e^{\gamma t}\cos(ky - \omega t) \tag{7}$$

Our notation is straightforward. k is the wavenumber of the plasma density striation in the y direction, ω and γ denote the frequency and growth rate of these striations, ω_0 and $k_0 = (\omega_0^2 - \omega_p^2)^{1/2}c^{-1}$ the frequency and wavenumber of the intense radiowave in the absence of striations. The Poynting flux P_0 of this wave is

$$P_0 = \frac{E_0^2 c}{2\pi}\left(\frac{ck_0}{\omega_0}\right)$$

where the last factor is effectively unity because the plasma is underdense: $\omega^2 \gg \omega_p^2$. Let us substitute (5) into (4), retain only terms linear in δn and $\mathbf{E}_1$, and make the assumption

$$k_0 \frac{\partial}{\partial z} \gg \frac{\partial^2}{\partial z^2}$$

which leads to the linearized parabolic wave equations

$$2ik_0 \frac{\partial}{\partial z} E_1 + \left(\frac{\partial^2}{\partial x^2} - k^2\right)E_1 - \frac{\omega_p^2}{c^2}\Delta E_0 = 0$$
$$-2ik_0 \frac{\partial}{\partial z} E_1^* + \left(\frac{\partial^2}{\partial x^2} - k^2\right)E_1^* - \frac{\omega_p^2}{c^2}\Delta E_0 = 0 \tag{8}$$

The overall lensing effect associated with ΔE_0 has been ignored. Since the first order field, E_1, propagates almost parallel to E_0 (i.e., $k \ll k_0$), we have taken their polarizations to be parallel and used scalar fields E_1 and E_0 in (8). A further simplification results by noting that the plasma density striations will vary much more rapidly in the y direction than the x direction, so that the x derivatives can be ignored in (8). This simplification is based on the recognition that variations in the x direction imply variations along the magnetic field (see Figure 1). The high electron thermal conductivity combined with rapid x variations supresses instabilities. Hence equations (8) become

$$2ik_0 \frac{\partial}{\partial z} E_1 - k^2 E_1 = \frac{\omega_p^2}{c^2}\Delta E_0$$
$$-2ik_0 \frac{\partial}{\partial z} E_1^* - k^2 E_1^* = \frac{\omega_p^2}{c^2}\Delta E_0 \tag{9}$$

The self-focusing instability is driven by spatially dependent ohmic heating Q which enters through the steady state electron heat equation

$$0 = \frac{\partial}{\partial \xi}\kappa \frac{\partial}{\partial \xi} T_e + Q - \nu_R n(T_e - T_0) \tag{10}$$

where

$$Q = \frac{\omega_p^2 \nu}{\omega_0^2 2\pi}\{E_0^2 + E_0(E_1 + E_1^*)e^{\gamma t}\cos(k_y - \omega t) + \cdots\} \tag{11}$$

and ξ is a coordinate parallel to the magnetic field (see Figure 1*a*). Here, ν_R denotes the electron energy relaxation frequency, ν the electron momentum collision frequency, and κ the electron thermal conductivity. One can easily check a posteriori that the temporal growth rate for self-focusing instabilities is small compared to the faster of two rates (1) the rate of electron heat diffusion across the radio beam (F region) or (2) the electron thermal relaxation frequency ν_R (E region). Hence the steady state heat equation is appropriate.

The electron heat equation is best discussed separately for the E and F regions. Let us first consider the F region where electron-ion collisions dominate the physics. The appropriate collision frequencies and thermal conductivity are [*Braginskii*, 1965]

$$\kappa = \frac{3.16 T_e n}{\nu m} \qquad \nu_R = 3\left(\frac{m}{M}\right)\nu$$
$$\nu = \frac{4(2\pi)^{1/2}}{3}\frac{ne^4 \ln \Lambda}{m^{1/2}T_e^{3/2}} \tag{12}$$

where m and M denote the electron and ion (taken to be O^+) mass, respectively. Both a zero-order and a first-order solution to (10) and (11) are required. Let us write this as

$$T_e = \delta T_e^{(0)} + \delta T_e^{(1)} + T_0$$

where T_0 is the ambient temperature, $\delta T_e^{(0)}$ is the heating correction produced by E_0^2 and $\delta T_e^{(1)}$ is due to $E_0 E_1$. We assume that departures from the ambient electron temperature T_0 are small:

$$\delta T_e^{(0)} \ll T_0 \qquad \delta T_e^{(1)} \ll \delta T_e^{(0)}$$

The electron heat conductivity equation can then be written as

$$0 = \frac{2}{7}C_1\frac{\partial^2}{\partial\xi^2}\theta + \frac{C_2(n/n_0)^2}{\theta^{3.7}}[E_0^2 + E_0(E_1 + E_1^*)] - C_3\frac{(n/n_0)^2}{\theta^{3.7}}(\theta^{2.7} - 1) \quad (13)$$

where

$$\theta = (T_e/T_0)^{1/2} \quad (14)$$

and

$$C_1 = \frac{3.16T_0^2n_0}{m\nu_0}$$

$$C_2 = \omega_{pi}^2\nu_0/2\pi\omega_0^2 \quad (15)$$

$$C_3 = 3T_0n_0\nu_0(m/M)$$

Let us expand θ as

$$\theta = 1 + \delta\theta^{(0)} + \delta\theta^{(1)} \quad (16)$$

where $\delta\theta^{(0)}$ satisfies the linearized equilibrium equation with constant density

$$0 = \frac{2}{7}C_1\frac{\partial^2}{\partial\xi^2}\delta\theta^{(0)} + C_2E_0^2 - C_3\frac{2}{7}\delta\theta^{(0)} \quad (17)$$

The equation governing the linearized response to the self-focusing ohmic heating term is

$$0 = \frac{2}{7}C_1\frac{\partial^2}{\partial\xi^2}\delta\theta^{(1)} + C_2E_0^2\left(\frac{2\delta n}{n_0} - \frac{3}{7}\delta\theta^{(1)} + \frac{E_1 + E_1^*}{E_0}\right) - C_3\frac{2}{7}\delta\theta^{(1)} \quad (18)$$

where we have neglected the small cross terms $\delta\theta^{(0)}\,\delta\theta^{(1)}$, etc. Let the temperature perturbation associated with the self-focusing instability be denoted by

$$\frac{\delta T_e^{(1)}}{T_0} = \frac{2}{7}\delta\theta^{(1)} \equiv \tau(x, z)e^{\gamma t}\cos(ky - \omega t) \quad (19)$$

Then, in terms of the power flux P_0, the equation governing τ reads

$$\frac{\partial^2}{\partial\xi^2}\tau - \frac{\tau}{L_t^2}\left(1 + \frac{3}{2}\frac{P_0}{P_1}\right) + \frac{1}{L_t^2}\frac{P_0}{P_1}\left(2\Delta + \frac{E_1 + E_1^*}{E_0}\right) = 0 \quad (20)$$

where

$$L_t^2 = \frac{C_1}{C_3} = \frac{1.05T_0}{m\nu_0^2}\left(\frac{M}{m}\right) \quad (21)$$

$$P_1 = \frac{cC_3}{2\pi C_2} = \frac{3cT_0\omega_0^2m^2}{4\pi e^2M} \quad (22)$$

and Δ is defined in (7). In practical units, the formulas for P_1 and L_t are

$$P_1 = \left(600\ \frac{\mu W}{m^2}\right)\left(\frac{T_0}{1000°K}\right)\left(\frac{\nu}{15\ MHz}\right)^2 \quad (23)$$

$$L_t = (13\ km)\left(\frac{T_0}{1000°K}\right)^{1/2}\left(\frac{10^6\ cm^{-3}}{n}\right) \quad (24)$$

The last term on the left-hand side of (20) brings out the competition between the stabilizing effects of density fluctuations (caused by the density dependence of the collision frequency) and the destabilizing contribution from self-focusing.

In the E region, electron-neutral collisions play the principal role. Furthermore, the ohmic heating may be sufficiently intense so that the electron temperature in the radiowave beam considerably exceeds the ambient electron temperature [*Perkins and Roble*, 1978]. The principal electron temperature dependence of electron-neutral collision processes is adequately represented by considering only electron-N_2 collisions. Thus, in (10) and (11), we can use [*Banks and Kockarts*, 1973]

$$\nu = \nu_{en} = 2.3 \times 10^{-8}\left(\frac{T_e}{1000°K}\right)n_n$$

$$K = \frac{8}{\pi}\frac{n_0T_e}{m\nu_{en}} = C_4\frac{n_0}{n_n} \quad (25)$$

The electron-neutral energy relaxation frequency ν_K is generally much smaller than the momentum collision frequency ν_{en} but has important variations with temperature. For energy loss by excitation of rotational levels, one can take [*Banks and Kockarts*, 1973]

$$\nu_K = 1.1 \times 10^{-11}\left(\frac{1000°K}{T_e}\right)^{1/2}n_n \quad (26)$$

while for excitation of vibrational levels of N_2 the appropriate formula is

$$\nu_K = 8.6 \times 10^{-11}\left(\frac{1000°K}{T_e}\right)e^{3353°K/T_e}n_n \quad (27)$$

According to (26) and (27), the transition between rotational and vibrational cooling occurs near $T_e = 1500°K$. A lower transition temperature would result had vibrational excitations of O_2 been included, but this will not be important to our arguments.

The next question to answer is: Will thermal conduction or local cooling control the electron temperature perturbations in the E region? Let us introduce a characteristic length L_t which makes the rate of cooling by thermal conduction (estimated by $(K/n_0)(L_t^{-2})$) equal to the local cooling rate. The formula for L_t reads

$$L_t = \left(\frac{K}{n_0\nu_K}\right)^{1/2} = (1\ km)\left(\frac{3.9 \times 10^{11}}{n_n}\right)\left(\frac{T_e}{1000°K}\right)^{1/2} \quad (28)$$

where we used the rotational cooling rate (26). The Cira (1972) atmosphere gives $n_n \simeq 5 \times 10^{11}$ at 120 km. Hence throughout the E region, electron thermal conduction will not play a major role, provided the self-focusing striations have a parallel wavenumber satisfying $k\,L_t < 1$. On the other hand, the characteristic scale sizes for radiowave beams and typical variations in E region parameters are at least several kilometers. It follows that in the E region a plane wave model with $k\,L_t \lesssim 1$ can be used in the direction along the magnetic field.

To reiterate, our arguments show the importance of thermal conductivity is different in the E and F regions. Because L_t is comparable to or larger in the F region than the size of the radiowave beam, in the F region we must treat a nonlocal thermal diffusion problem. In the E region, the radiowave intensity does not vary over the characteristic scale L_t, permitting a plane wave approximation.

As was the case in the F region, the solution to the electron temperature equation in the E region is composed of an equilibrium part T_{e0} which can be taken as spatially uniform and a perturbed part. The equilibrium part is the solution of

$$\frac{\omega_p^2 E_0^2}{2\pi\omega_0^2 n_0} = \frac{\nu_R}{\nu_{en}}(T_{e0} - T_0) \tag{29}$$

where the right-hand side is just a function of T_{e0}. The perturbed part satisfies the equation

$$0 = L_{e0}^2 \frac{\partial^2}{\partial\xi^2}\tau + \frac{\omega_p^2 \nu_0 E_0^2}{\omega_0^2 2\pi n_0 T_{e0}\nu_{R0}}\left(\frac{E_1 + E_1^*}{E_0}\right) - \beta\tau \tag{30}$$

where

$$\beta = 1 + \frac{\omega_p^2 \nu_0 E_0^2}{2\pi\omega_0^2 n_0 \nu_{R0} T_{e0}}\left(\frac{T}{\nu_R}\frac{\partial \nu_R}{\partial T}\right)_{T_{e0}} - 1 \tag{31a}$$

$$\beta = 1 + \left(1 - \frac{T_0}{T_{e0}}\right)\left(\frac{T}{\nu_R}\frac{\partial \nu_R}{\partial T}\right)_{T_{e0}} - 1 \tag{31b}$$

Here $\tau = \delta T_e/T_{e0}$ and the subscript 0 on collision frequencies and temperatures denotes evaluation at the equilibrium electron temperature T_{e0}. In (30) we have retained the thermal conduction term. For a thermally stable equilibrium solution to exist, one must have $\beta > 0$.

In the case of HF ionospheric modification experiments, the second term in β will be small near threshold and T_{e0} will be close to T_0. Under conditions where the equilibrium electron temperature is well above the ambient temperature $T_{e0} \gg T_0$ [*Perkins and Roble*, 1978], (31*b*) shows that $\beta \simeq (T/\nu_R)(\partial\nu_R/\partial T) \simeq 4$ because of the rapid increase of vibrational cooling with electron temperature.

3. Self-Focusing Instabilities

The equations governing plasma motion also differ in the E and F regions, because in the F region the ion-neutral collision frequency ν_{in} is much less than ion gyrofrequency Ω, and plasma motion can proceed only along magnetic field lines. In the E region, $\nu_{in} \gg \Omega$, and ion motion across the field is important.

Let us turn first to the F region, where the formula for ν_{in} is [*Banks and Kockarts*, 1973]

$$\nu_{in} \simeq 7 \times 10^{-10} n_n \tag{32}$$

At an altitude of 300 km, the Cira (1972) atmosphere yields $\nu_{in} \simeq 1$ Hz.

Upon elimination of the ambipolar electric field, the momentum and continuity equations governing plasma motion yield

$$0 = -2T_0\frac{\partial\Delta}{\partial\xi} - T_0\frac{\partial\tau}{\partial\xi} - M\nu_{in}v_{i\parallel} \tag{33a}$$

$$\frac{\partial\Delta}{\partial t} + \frac{\partial v_{i\parallel}}{\partial\xi} = 0 \tag{33b}$$

where Δ and τ are the relative electron density and temperature fluctuations defined in (7) and (19) respectively. Equations (9), (20), and (33) form a closed set which govern the linear stability of self-focusing striations.

These equations are most easily solved in the (ξ, η) coordinate system of Figure 1. It is clear that the dependent variables should depend on the distance along the magnetic field from beam center, $\xi - \xi_0$, where $\xi_0 = -\eta(\sin\phi_D/\cos\phi_D)$, and should show spatial exponential growth along the direction of the beam. In other words the functional dependence will be

$$\Delta(\xi, \eta) = \Delta(\xi - \xi_0)\exp(\eta/l\cos\phi_D) \tag{34a}$$

$$\Delta(\xi, \eta) = \Delta\left(\xi + \frac{\eta\sin\phi_D}{\cos\phi_D}\right)\exp\left(\frac{\eta}{l\cos\phi_D}\right) \tag{34b}$$

where l is the real spatial growth length along the direction of the beam, and ϕ_D is the magnetic dip angle (see Figure 1*a*). All other dependent variables will have the same functional form. A standard coordinate rotation yields

$$\frac{\partial}{\partial z} = \cos\phi_D\frac{\partial}{\partial\eta} - \sin\phi_D\frac{\partial}{\partial\xi} \tag{35}$$

with the consequence that

$$\frac{\partial}{\partial z}(\xi - \xi_0) = \frac{\partial}{\partial z}\left(\xi + \frac{\eta\sin\phi_D}{\cos\phi_D}\right) = 0 \tag{36}$$

Using the functional form (34*b*) for E_1, E_1^* and Δ and (35), we can solve equations (9) to obtain

$$\frac{E_1 + E_1^*}{E_0} = -\Delta\frac{\omega_p^2 l}{2k_0 c^2}\left(\frac{2\alpha}{\alpha^2 + 1}\right) \tag{37}$$

where

$$\alpha = k^2 l/2k_0 \tag{38}$$

The dependence of (37) on α is characteristic of modulational instabilities [*Bardwell and Goldman*, 1976]. Two interesting observations can be made at this point. First, the term evaluated in (37) is the destabilizing term in (20). The most unstable modes will occur when (37) has its maximally negative value. Since l is fixed by the requirement of a particular rate of spatial growth, the most unstable mode will occur when the function $2\alpha/(\alpha^2 + 1)$ has its maximum value. This occurs when

$$\alpha = k^2 l/2k_0 = 1 \tag{39}$$

In practical units, the perpendicular wavelength $\lambda_\perp$ of this mode is

$$\lambda_\perp = \frac{2\pi}{k} = \left(\frac{\pi l c}{f}\right)^{1/2} = (1.2\text{ km})\left(\frac{l}{25\text{ km}}\right)^{1/2}\left(\frac{15\text{ MHz}}{f}\right)^{1/2} \tag{40}$$

where f is the radiowave frequency.

The second observation concerns the competition between the destabilizing (37) and stabilizing terms (2Δ) in (20). Thus for a self-focusing instability to occur, in the F region, the inequality

$$\frac{\omega_p^2 l}{4k_0 c^2} \equiv \frac{l}{\epsilon} = 700\left(\frac{n_0}{10^6\text{ cm}^{-3}}\right)\left(\frac{l}{25\text{ km}}\right)\left(\frac{15\text{ MHz}}{f}\right)^2 > 1 \tag{41}$$

must be satisfied. Clearly, there is no question that this inequality will be strongly satisfied for HF ionospheric modification experiments. But the SPS application is a close call. We can recast inequality (41) into the form

$$4.4\left(\frac{n_0}{10^6\text{ cm}^{-3}}\right)\left(\frac{l}{25\text{ km}}\right)\left(\frac{2.4\text{ GHz}}{f}\right)^2 > 1 \tag{42}$$

which shows the ionosphere is ordinarily just dense enough to permit self-focusing at the SPS frequency. Inequality (41) has physical significance: it says that a 100% density modulation

should produce a phase shift of at least 2π between two ray paths in a distance l. It is evident that unless the ionosphere is sufficiently dense to produce significant phase shifts, self-focusing could not take place.

Let us return to the calculation of the threshold value for F region self-focusing. It will turn out that the threshold flux is substantially less than P_t. Thus, combining (20), (37) and (41), we obtain the equation

$$\frac{\partial^2}{\partial \xi^2}\tau - \frac{\tau}{L_r^2} = \frac{P_0(\xi - \xi_0)}{L_r^2 P_2}\Delta\left(\frac{2a}{a^2+1} - \epsilon\right) \tag{43}$$

where

$$P_2 = n_0 T_0 c\left(\frac{6m\omega_0^3 c}{M\omega_p^4 l}\right) \tag{44}$$

and we have explicitly indicated that the power flux in the radiowave beam varies as a function of $\xi - \xi_0$. Combining (33*a*) and (33*b*), one obtains the plasma ambipolar diffusion equation

$$\frac{\partial \Delta}{\partial t} = 2D\frac{\partial^2}{\partial \xi^2}\Delta + D\frac{\partial^2}{\partial \xi^2}\tau \tag{45}$$

where

$$D = T_0/M\nu_{in} \tag{46}$$

Substitution of forms (7) and (19) into (45) shows that $\omega = 0$ and

$$\gamma\Delta = 2D\frac{\partial^2}{\partial \xi^2}\Delta + D\frac{\partial^2}{\partial \xi^2}\tau \tag{47}$$

The coupled set (43), (47) can be simplified when the variation of $P_0(\xi - \xi_0)$ occurs on a much faster spatial scale than L_r. Indeed, this is our basic approximation. Hence in regions where P_0 is appreciable, we can ignore the term involving L_r^2 on the left-hand side of (43). This permits an elimination of $\partial^2\tau/\partial\xi^2$ and the eigenvalue equation becomes

$$\frac{\gamma}{D}\Delta - 2\frac{\partial^2\Delta}{\partial \xi^2} = \frac{P_0(\xi - \xi_0)}{L_r^2 P_2}\Delta\left(\frac{2a}{a^2+1} - \epsilon\right) \tag{48}$$

and the boundary conditions are

$$\Delta \sim \Delta_0 \exp\left[-|\xi - \xi_0|\left(\frac{\gamma}{2D}\right)^{1/2}\right] \tag{49}$$

as $|\xi - \xi_0| \to \infty$. For definiteness, we shall assume that the radiowave beam has a Gaussian dependence in the x direction

$$P_0(\xi - \xi_0) = P_0 e^{-x^2/a^2} = P_0 e^{-[(\xi - \xi_0)^2\cos^2\phi_D/a^2]} \tag{50}$$

where ϕ_D is the magnetic dip angle (see Figure 1*a*). We make the change of variable

$$u = (\xi - \xi_0)/L_\gamma \tag{51}$$

$$L_\gamma = \left(\frac{2D}{\gamma}\right)^{1/2} = (3.3\text{ km})\left(\frac{T_0}{1000°\text{K}}\right)^{1/2}\left(\frac{1\text{ Hz}}{\nu_{in}}\right)^{1/2}\left(\frac{10^{-1}\text{ s}}{\gamma}\right)^{1/2} \tag{52}$$

(The neglect of the L_r^{-2} term on the left side of (43) is justified by the inequality $L_\gamma^2 \ll L_r^2$.) This change of variables leads to the nondimensional eigenvalue equation

$$\Delta - \frac{\partial^2}{\partial u^2}\Delta = \Lambda e^{-u^2\cos^2\phi_D/a^2}\Delta \tag{53}$$

where

$$u_0 = (a/L_\gamma\cos\phi_D) \tag{54}$$

$$\Lambda = \frac{DP_0}{\gamma L_r^2 P_2}\left(\frac{2a}{a^2+1} - \epsilon\right) \tag{55}$$

The next step is to find the eigenvalue Λ in terms of the parameter u_0. In general an analytic solution of (53) is not possible. However, we can obtain solutions when $u_0 \gg 1$ and when $u_0 \ll 1$. For the case $u_0 \gg 1$, we expand the exponential and obtain the harmonic oscillator equation of quantum mechanics

$$\frac{\partial^2}{\partial u^2}\Delta + (\Lambda - 1) - \frac{\Lambda u^2}{u_0^2}\Delta = 0 \tag{56}$$

whose fundamental solution is accurately given by

$$\Delta = \exp\left[-\frac{u^2}{2u_0}\left(1 + \frac{1}{u_0}\right)^{1/2}\right] \tag{57}$$

$$\Lambda \approx 1 + \frac{1}{u_0} \tag{58}$$

When u_0 is large, Δ becomes small before u/u_0 reaches unity, justifying our expansion.

When $u_0 \ll 1$, the exponential term varies rapidly compared to Δ and we can integrate (53) assuming Δ is constant (but $\partial\Delta/\partial u$ varies) to obtain the eigenvalue equation

$$\frac{1}{\Delta}\frac{\partial\Delta}{\partial u} = -1 = -\Lambda\int_0^\infty e^{-u^2/u_0^2}du = -\frac{\Lambda\pi^{1/2}}{2}u_0 \tag{59}$$

An adequate interpolation formula which combines (58) and (59) is

$$\Lambda = 1 + \frac{2}{\pi^{1/2}u_0} \tag{60}$$

Most self-focusing experiments have $u_0 \gtrsim 1$. In the appendix it is shown by a variational principle that the interpolation formula (60) is likely to be accurate in the vicinity of $u_0 \simeq 1$.

Our key result, the generalized dispersion relation, is

$$P_0 = P_{r,t}\frac{\left(1 + \frac{2}{\pi^{1/2}u_0}\right)}{\left(\frac{2a}{1+a^2} - \frac{\epsilon}{2}\right)} \tag{61}$$

where

$$P_{r,t} = \frac{\gamma L_r^2 P_2}{2D} = 3.15(n_0 T_0 c)\left(\frac{c\omega_0^3}{l\omega_p^4}\right)\left(\frac{\gamma\nu_{in}}{\nu_0^2}\right)\left(\frac{M}{m}\right) \tag{62}$$

In practical units, the formula for $P_{r,t}$ is

$$P_{r,t} = \left(1.5\frac{\mu\text{W}}{\text{m}^2}\right)\left(\frac{10^6\text{ cm}^{-3}}{n}\right)^3\left(\frac{T_0}{1000°\text{K}}\right)^4\left(\frac{f}{15\text{ MHz}}\right)^3 C_t \tag{63}$$

with the definition

$$C_t = \left(\frac{\gamma}{10^{-1}\text{ s}^{-1}}\right)\left(\frac{25\text{ km}}{l}\right)\left(\frac{\nu_{in}}{1\text{ Hz}}\right) \tag{64}$$

We note that the critical power flux is quite sensitive to temperature and density, principally because of the density and temperature dependence of the electron-ion collision frequency ν_0. The requirement for a rapid growth rate limits the self-focusing perturbation to the center of the radiowave beam, because otherwise plasma ambipolar diffusion would not be fast enough. This is in contrast to the results of *Gurevich* [1978] and *Vas'kov and Gurevich* [1977*a*, *b*], who ignore the fact that ambipolar diffusion proceeds at a finite rate and that only a limited interaction time is available because of ambient $\mathbf{E} \times \mathbf{B}$ drifts (see (1)).

The plasma dynamics of the *E* region requires separate consideration of ions and electrons. The ion motion is governed by the *E* region ion-neutral collision frequency [*Banks and Kockarts*, 1973]

$$\nu_{in} = 7.5 \times 10^{-10} n_n \tag{65}$$

Using the Cira (1972) atmosphere, we find $\nu_{in} \simeq 1.4 \times 10^4$ at 110 km. Since $\nu_{in} \gg \Omega_i$, the ion motion is unmagnetized ambipolar diffusion and governed by

$$\left(\frac{\partial}{\partial t} + \mathbf{v}_D \cdot \nabla\mathbf{V}\right)\Delta + \nabla \cdot \mathbf{v}_i = -\Gamma\Delta \tag{66}$$

$$\mathbf{v}_i = -\frac{T_{e0}}{M\nu_{in}} \nabla\left(\psi + \frac{T_0}{T_{e0}}\Delta\right) \tag{67}$$

$$\psi = e\phi/T_{e0} \qquad \Gamma = 2\alpha n_0 \tag{68}$$

where ϕ is the electrostatic potential, and $\alpha = 3 \times 10^{-7}$ cm^3 s^{-1} is a typical *E* region recombination coefficient. Equation (66) takes account of the relative electron-ion drift $\mathbf{v}_D$. The corresponding electron equations are

$$\frac{\partial}{\partial t}\Delta + \nabla \cdot \mathbf{v}_e = -\Gamma\Delta \tag{69}$$

$$\mathbf{v}_{e\perp} = \frac{-T_{e0}c}{eB_0} \nabla\psi \times \hat{b} \tag{70}$$

$$v_{e\parallel} = \frac{-T_{e0}}{m\nu_0} \nabla(\Delta - \psi + \tau) \tag{71}$$

where ν_0 denotes the electron-neutral collision frequency (25) evaluated at temperature T_{e0}.

The appropriate form for the dependent variables is

$$\begin{aligned} \Delta &\propto g(t, \xi, \eta)\ \mathrm{Re}\ \Delta_0\, e^{i(k_y y - \omega t)} \\ \psi &\propto g(t, \xi, \eta)\ \mathrm{Re}\ \psi_0\, e^{i(k_y y - \omega t)} \\ \tau &\propto g(t, \xi, \eta)\ \mathrm{Re}\ \tau_0\, e^{i(k_y y - \omega t)} \end{aligned} \tag{72}$$

where

$$g(t, \xi, \eta) = e^{\gamma t} \cos[k_x(\xi - \xi_0)] \exp[\eta/l \cos\phi_D] \tag{73}$$

and Δ_0 is real. Hence Δ has exactly the same form (7), (34) as the *F* region calculations. It follows that we can use (37) in (30) to obtain

$$0 = L_t^2 \frac{\partial^2}{\partial\xi^2}\tau - \alpha\tau - \frac{\omega_p^4 \nu_0 l E_0^2}{4\pi\omega_0^3 c \nu_{R0} n_0 T_{e0}} \Delta\left(\frac{2\alpha}{\alpha^2 + 1}\right) \tag{74}$$

Equation (74) can be recast into

$$\tau_0 = \frac{-\Delta_0 P_0}{P_1} \tag{75}$$

where

$$P_1 = (n_0 T_{e0} c)\frac{2c\omega_0^3 \nu_{R0}}{l\omega_p^4 \nu_0}\left(\frac{\alpha^2 + 1}{2\alpha}\right)(1 + k_\perp^2 L_t^2) \tag{76}$$

Next, we make use of (75) and of the fact that the most rapid spatial variation comes from the exp $[i(ky - \omega t)]$ dependence to evaluate (66) (71):

$$\gamma + \Gamma + i(\mathbf{k} \cdot \mathbf{v}_D - \omega) + \frac{k^2 T_0}{M\nu_{in}}\Delta_0 = -\frac{k^2 T_{e0}}{M\nu_{in}}\psi_0 \tag{77}$$

$$\gamma + \Gamma - i\omega + \frac{k_\parallel^2 T_{e0}}{m\nu_0}\left(1 - \frac{P_0}{P_1}\right)\Delta_0 = \frac{k_\parallel^2 T_{e0}}{m\nu_0}\psi_0 \tag{78}$$

The solution of (77), (78) is

$$\omega = k v_D \cdot \hat{y}\left(1 + \frac{k^2 m\nu_0}{k_\parallel^2 M\nu_{in}}\right)^{-1} \tag{79}$$

$$P_0 = P_1\left(1 + \frac{T_0}{T_{e0}} + \frac{(\gamma + \Gamma)M\nu_{in}}{k^2 T_{e0}}\left(1 + \frac{k^2 m\nu_0}{k_\parallel^2 M\nu_{in}}\right)\right)^{-1} \tag{80}$$

Let us discuss the result of (80). First, for nominal *E* region densities $n_0 \sim 10^5$ cm^{-3}, the recombination rate $\Gamma = 2n_0\alpha \sim 6 \times 10^{-2}$ s^{-1} is comparable to the growth rates we envision. Second, for values of $\alpha = k^2 l/2k_0$ near unity, the ion diffusion rate γ_D, is

$$\gamma_D = \frac{k^2(T_{e0} + T_0)}{M\nu_{in}} = \alpha\frac{2k_0(T_{e0} + T_0)}{lM\nu_{in}} = (0.1\ \mathrm{s}^{-1})\alpha\left(\frac{1\ \mathrm{km}}{l}\right) \cdot \left(\frac{1500\ \mathrm{s}^{-1}}{\nu_{in}}\right)\left(\frac{T_{e0} + T_0}{1000^\circ\mathrm{K}}\right)\left(\frac{f}{15\ \mathrm{MHz}}\right) \tag{81}$$

which is also comparable to growth rates. We can, however, satisfy the double inequality

$$\frac{1}{L_t^2} \gg k_\parallel^2 \gg k^2 \frac{m\nu_0}{M\nu_{in}} \tag{82}$$

because

$$k^2 L_t^2 \frac{m\nu_0}{M\nu_{in}} = \frac{8}{\pi}\frac{\gamma_{Di}}{\nu_{R0}} \ll 1 \tag{83}$$

The first part of the inequality (82) justifies our assertion that thermal conduction is small relative to local cooling in the *E* region. As a result, we can choose $k_\parallel^2$ so that terms involving $k_\parallel^2$ in (76), (79) and (80) are ignorable. This choice minimizes the threshold flux and leads to the generalized dispersion relation

$$P_0 = P_{c,E}\left(\frac{\alpha^2 + 1}{2\alpha}\right)\left(1 + \frac{(\gamma + \Gamma)}{\alpha\gamma_{Di}}\right) \tag{84}$$

where

$$P_{c,E} = n_0(T_{e0} + T_0)c\left(\frac{2c\omega_0^3 \nu_{R0}}{l\omega_p^4 \nu_0}\right) \tag{85}$$

In practical units, the formula for $P_{c,E}$ is

$$P_{c,E} = \left(1\ \frac{\mathrm{mW}}{\mathrm{m}^2}\right)\left(\frac{f}{15\ \mathrm{MHz}}\right)^3\left(\frac{10^5\ \mathrm{cm}^{-3}}{n_0}\right)C_t \tag{86}$$

where

$$C_t = \left(\frac{T_{e0} + T_0}{T_{e0}}\right)\left(\frac{1000^\circ\mathrm{K}}{T_{e0}}\right)^{1/2}\left(\frac{1\ \mathrm{km}}{l}\right) \tag{87}$$

The temperature and density dependence are not so strong in the E region because neutral rather than charged particle collisions are involved. The strong dependence on radiowave frequency remains. Formula (40) shows that the perpendicular wavelength of the striations will be close to 300 m for E region self-focusing. The next generation of ionospheric modification experiments will easily exceed this threshold value for self-focusing, especially if the frequency is near $f = 5$ MHz.

4. Applications and Discussion

Our central results are the threshold power fluxes for the onset of self-focusing instabilities: (63) for the F region and (86) for the E region. For comparison, the European ionospheric heating facility nearing completion at Tromsø, will have an effective radiated power of 360 MW, yielding an E region flux at 2 mW/m^2 and an F region flux of 300 μW/m^2. These fluxes will exceed the respective threshold fluxes, even when $f = 15$ MHz. The question then arises, what are the consequences of self-focusing instabilities and how do we detect them?

Dimensional analysis of linear theory provides estimates for the nonlinear consequences. We can interpret (37) as giving the fluctuations δP in the power flux

$$\frac{\delta P}{P_0} = -2\frac{\delta n}{n}\left(\frac{\omega_e^2 l}{4k_0c^2}\right)\left(\frac{2\alpha}{\alpha^2+1}\right) \tag{88}$$

while (41) shows that the coefficient of $\delta n/n$ is very large. Consequently, nonlinearities will develop first in the wave propagation equation and the self-focusing instability will cause intensity fluctuations of order unity to develop. Equation (88) provides an estimate of the magnitude of the concomitant density fluctuations when $\delta P/P_0 \simeq 1$. The expected wavelength of the density fluctuations is given by (40) and Figure 1 portrays their geometry. *Vas'kov and Gurevich* [1977*b*] discuss a mathematical model for the nonlinear saturation.

It is important to recognize that the self-focusing instability generates density fluctuations with just the correct magnitude and orientation to produce intensity scintillations in the driving beam. Hence, in order for these fluctuations to produce significant intensity scintillations in a diagnostic wave, that wave should be propagating parallel (or antiparallel) to the driving wave and should have a frequency which differs from the driving frequency by no more than a factor of 3. In particular, the diagnostic wave should not have a component of its wave vector in the $\hat{z} \times \hat{b}$ direction, which would result in its propagating across the density maxima and minima, thereby averaging out their effect. The geometry of *Novozhilov and Savel'yev* [1978] was ideal from this point of view with the diagnostic wave propagating antiparallel to the driving wave and closely matched in frequency. Radio-stars are another possible source of diagnostic waves. In this case, the driving wave would be launched in the direction of the radio-star, and scintillations of the radio-star signal should be observed up to frequencies several times the driving frequency. As (88) and (41) show, the density fluctuations associated with HF-driven self-focusing instabilities have a magnitude $\delta n/n \sim 10^{-4}$ and are probably not directly observable. The characteristic exponentiation times of roughly 10 s imply delay times of roughly a minute after transmitter turn-on before scintillations become observable. The *Novozhilov and Savel'yev* [1978] experiment agrees with this prediction. Although high-peak-power radars can exceed the threshold power flux, the long growth times show that the self-focusing instability is driven by the average, not peak, power of a radar system.

There is a distinct possibility that the 2.4 GHz microwave beam from a proposed Satellite Power Station could produce self-focusing. Recasting (63) into a form appropriate to the SPS, we find

$$P_{sf} = \left(6\frac{\mathrm{W}}{\mathrm{m}^2}\right)\left(\frac{10^6}{n}\right)^4\left(\frac{T_e}{1000^\circ\mathrm{K}}\right)^4\left(\frac{f}{2.4\ \mathrm{GHz}}\right)^2 C_f$$

where C_f is given by (64) and is roughly unity. Although planned power fluxes for the SPS are in the range 250 W m^{-2}, natural variations in ionospheric density and temperature can raise the threshold flux to this value. Furthermore, the ohmic heating of the ionosphere by the SPS microwave beam itself [*Perkins and Roble*, 1978] can raise the electron temperature above 2000°K, which works toward stabilizing the instability. Hence one cannot make an unequivocal prediction regarding whether the SPS beam will generate self-focusing. Our best estimate is that at times the ionosphere could be sufficiently cold and dense so that self-focusing would occur. According to (40), the wavelength of striations created by SPS self-focusing will be $\lambda_\perp \simeq 100$ m. By (88) and (42), the density fluctuations would be quite large: $\delta n/n \sim 10^{-1}$. A scaled HF test of self-focusing at $f = 15$ MHz could validate predictions for the threshold flux, but would have a much smaller effect on telecommunications than SPS self-focusing because of the much weaker density fluctuations at HF combined with the larger scale size. Ten percent density fluctuations with scale sizes of 100 m can seriously effect ionospherically propagated shortwave broadcast signals. If the striations were steepened by $\mathbf{E} \times \mathbf{B}$ drifts as in the case with artificial plasma clouds [*Scannapieco et al.*, 1976], then higher frequency telecommunications systems could be affected as well. A quantitative investigation of this question awaits future work. It is also evident that if the SPS generates self-focusing, then intensity fluctuations of order unity could be expected on the rectenna.

In closing, we can remark that thermal self-focusing is under investigation in the laboratory (J. Drummond and W. B. Thompson, private communication, 1980) and in laser-fusion applications [*Langdon*, 1979]. The details differ from the ionospheric theory.

Appendix: Variational Principle Approximation to Eigenvalue Problem

In the eigenvalue problem of (53), namely,

$$(\partial_u^2 - 1)\Delta = -\Lambda e^{-u^2/2}\Delta \tag{A1}$$

the lowest eigenvalue Λ may be found approximately by the following variational principle [*Morse and Feshbach*, 1953, p. 1108]:

$$\Lambda = \int_{-\infty}^{+\infty} du[\Delta_u^2 + \Delta^2]\Big/\int_{-\infty}^{+\infty} du\Delta^2 e^{-u^2/2} \tag{A2}$$

The eigenvalues are not terribly sensitive to the precise shape of the trial function. We use the trial function,

$$\Delta = e^{-\alpha|u|} \tag{A3}$$

to find

$$\Lambda = (1 + 1/\alpha u_0)^2(1 + \alpha/2) \tag{A4}$$

Differentiating with respect to α gives the minimum eigenvalue, Λ_{min}, at

$$\alpha = [(1 + 16u_0^2)^{1/2} - 1]/4u_0^2 \tag{A5}$$

From (A4) and (A5), we find the asymptotic behavior

$$\lim_{u_0 \to 0} \Lambda_{min} = \frac{2^{1/2}}{u_0}$$
$$\lim_{u_0 \to \infty} \Lambda_{min} = 1 + \frac{1}{u_0} \tag{A6}$$

These agree quite well with the exact asymptotic solutions (58) and (59). (Note, the exact coefficient $2/\pi^{1/2} = 1.13$ is slightly smaller than $2^{1/2}$.) Moreover, when $u_0 = 1$, (A4) and (A5) yield $\Lambda_{min} = 2.10$, whereas the interpolation formula (60) gives $\Lambda = 2.13$.

Acknowledgments. Discussions with Gerald Meltz and Charles Rush contributed substantially to this work. Comments by A. V. Gurevich on the preprint manuscript were appreciated. Financial support came from U.S. Department of Energy contract DE-AT03-76ER10100 with SRI International, from U.S. Air Force Office of Scientific Research contract 80-0022 with the University of Colorado, and from U.S. Air Force Office of Science Research contract 80-00656 with Princeton University.

The Editor thanks J. A. Fejer and H. P. Freund for their assistance in evaluating this paper.

REFERENCES

Banks, P. M., and G. Kockarts, *Aeronomy*, Academic, New York, 1973.

Bardwell, S., and M. V. Goldman, Three-dimensional Langmuir wave instabilities in type III solar radio bursts, *Astrophys. J., 209*, 912-926, 1976.

Blanc, M., and P. Amayenc, Seasonal variations of the ionosphere $E \times B$ drifts along Saint Santin on quiet days, *J. Geophys. Res., 84*, 2691-2704, 1979.

Braginskii, S. I., Transport processes in a plasma, in *Reviews of Plasma Physics*, edited by M. A. Leontovich, vol. 1, p. 205, Consultants Bureau, New York, 1965.

Brown, W. C., Satellite power stations: A new source of energy?, *IEEE Spectrum, 10*, 38-47, 1973.

Cragin, B. L., and J. A. Fejer, Generation of large-scale field-aligned irregularities in ionospheric modification experiments, *Radio Sci., 9*, 1071-1075, 1974.

Das, A. C., and J. A. Fejer, Generation of small-scale field-aligned irregularities in heating experiments, *J. Geophys. Res.*, in press, 1980.

DuBois, D. F., and M. V. Goldman, Spectrum and anomalous resistivity for the saturated parametric instability, *Phys. Rev. Lett., 28*, 218-221, 1972.

Duncan, L. M., and R. A. Behnke, Observations of self-focusing electromagnetic waves in the ionosphere, *Phys. Rev. Lett., 41*, 998-1001, 1978.

Fejer, J. A., and Y. Y. Kuo, Structure in the nonlinear saturation spectrum of parametric instabilities, *Phys. Fluids, 16*, 1490, 1973.

Fock, V. A., *Electromagnetic Diffraction and Propagation Problems*, p. 213, Pergamon, New York, 1965.

Glaser, P. E., Solar power from satellites, *Phys. Today, 30*(2), 30, 1977.

Gurevich, A. V., *Nonlinear Phenomena in the Ionosphere*, pp. 282-298, Springer, New York, 1978.

Harper, R. M., R. H. Ward, C. J. Zamlatti, and D. T. Farley, *E* region ion drifts and winds from incoherent scatter measurements at Arecibo, *J. Geophys. Res., 81*, 25-35, 1976.

Langdon, A. B., Filamentation in collisional ICF plasmas, *Bull. Am. Phys. Soc., 24*, 1105, 1979.

Morse, P. M., and H. Feshbach, *Methods of Theoretical Physics*, McGraw-Hill, New York, 1953.

Novozhilov, V. I., and S. M. Savel'yev, Irregular structure of the ionosphere in the field of a strong obliquely incident radio wave, *Geomagn. Aeron., 18*, 145-147, 1978.

Perkins, F. W., and R. G. Roble, Ionospheric heating by radiowaves: Predictions for Arecibo and the satellite power station, *J. Geophys. Res., 83*, 1611-1624, 1978.

Perkins, F. W., and E. J. Valeo, Thermal self-focusing of electromagnetic waves in plasmas, *Phys. Rev. Lett., 32*, 1234-1237, 1974.

Perkins, F. W., C. Oberman, and E. J. Valeo, Parametric instabilities and ionospheric modification, *J. Geophys. Res., 79*, 1478-1496, 1974.

Scannapieco, A. J., S. L. Ossakow, S. R. Goldman, and J. M. Pierre, Plasma cloud late time spectra, *J. Geophys. Res., 81*, 6037, 1976.

Thome, G. D., and F. W. Perkins, Production of ionospheric striations by self-focusing of intense radiowaves, *Phys. Rev. Lett., 32*, 1238-1240, 1974.

Vanke, V. A., V. M. Lopukhim, and V. L. Savin, Satellite solar power stations, *Sov. Phys. Usp. Engl. Transl., 20*, 989-1001, 1977.

Vas'kov, V. V., and A. V. Gurevich, Modulational instability of radiowaves in upper ionosphere, *Geomagn. Aeron. Engl. Transl., 16*, 141-144, 1976.

Vas'kov, V. V., and A. V. Gurevich, Resonance instability of small-scale plasma perturbations, *Sov. Phys. JETP Engl. Transl., 46*, 487, 1977*a*.

Vas'kov, V. V., and A. V. Gurevich, Saturation of the modulation instability of narrow radiobeams in a magnetized plasma, *Sov. J. Plasma Phys. Engl. Transl., 3*, 185-190, 1977*b*.

(Received April 22, 1980;
revised August 6, 1980;
accepted August 7, 1980.)

APPENDIX D

D. "Langmuir Collapse in a Weak Magnetic Field"

M.V. Goldman, J.C. Weatherall, and D.R. Nicholson
Physics of Fluids 24, 668-672 (April, 1981)

Langmuir collapse in a weak magnetic field

Martin V. Goldman and J. C. Weatherall

Department of Astro-Geophysics, University of Colorado, Boulder, Colorado 80309

D. R. Nicholson

Department of Physics and Astronomy, University of Iowa, Iowa City, Iowa 52242

(Received 18 June 1980; accepted 29 December 1980)

With magnetic fields that are not too weak, Langmuir collapse times can be prolonged and the packet geometry significantly distorted

I. INTRODUCTION

Within the last few years there have been great theoretical strides in the understanding of "self-focusing mechanisms for the nonlinear saturation of certain Langmuir wave instabilities."[1-5] In particular, it has been shown[4] for a class of weak "bump-on-tail" instabilities that direct spatial collapse can occur due to the self-ponderomotive force of intense Langmuir wave packets. This may have important implications for type-III solar radio bursts,[1-6] for the radar-modified ionosphere,[7] and for laboratory and space beam-plasma systems.

In physical problems a weak background magnetic field is often present pointing parallel to the direction of propagation of the driven Langmuir wave packet. Linear stability analyses have recently been performed[8,9] for monochromatic Langmuir waves in the presence of a weak magnetic field.

There has been little work on the effects of a magnetic field on collapse. One theory[7] claims to have found stable pancake-shaped Langmuir solitons pumped by radio waves in the ionosphere. Other studies[10,11] have shown Langmuir collapse in magnetic fields, but only for special symmetries and in parameter regimes apparently unrelated to experiment. Our work differs from these in terms of parameter regime, geometry, phenomena observed, and physical explanation.

First, we shall demonstrate, numerically, that weak magnetic fields can significantly prolong the time for collapse of a broadband Langmuir wave packet, and alter its geometry into a more dipolar form, but cannot render it one dimensional. Second, we prove analytically a magnetic virial theorem which gives sufficient conditions for collapse, and helps explain its retardation. Third, we demonstrate that measured *mean* solar magnetic fields might affect the Langmuir collapse associated with type-III bursts at 0.5 a.u., although only for relatively low wave energies.

II. LANGMUIR WAVE COLLAPSE IN A MAGNETIC FIELD

The Langmuir field envelope $\mathcal{E}$ obeys a generalized nonlinear Schrödinger equation

$$i\partial_t \mathcal{E} + \tfrac{1}{2}\nabla\nabla\cdot\mathcal{E} - \tfrac{1}{2}C^2\nabla\times\nabla\times\mathcal{E} - \tfrac{1}{2}\Omega^2 \mathsf{P}\cdot\mathcal{E} - \delta n\,\mathcal{E} = 0, \qquad (1)$$

where the units of time are ω_p^{-1}, length is measured in units of $\sqrt{3}$ times the Debye length, $|\mathcal{E}|^2$ has the units of $64\pi n\theta$, where θ is the common electron and ion temperature, and

$$C^2 \equiv c^2/3v_e^2 \gg 1, \quad \Omega^2 = \omega_{ce}^2/\omega_p^2 < 1.$$

The magnetic dispersive term, $(-\Omega^2/2)(\mathsf{P}\cdot\mathcal{E})$, arises from an expansion in the magnetic field. The operator $\mathsf{P}_{ij} = \delta_{ij} - \hat{\mathbf{b}}_i\hat{\mathbf{b}}_j$ projects out vector components perpendicular to the magnetic field direction $\hat{\mathbf{b}}$. In the linear limit, Eq. (1) gives the quasi-longitudinal dispersion relation for an oblique Langmuir-wave envelope

$$\omega = \tfrac{1}{2}k^2 + \tfrac{1}{2}\Omega^2\sin^2\theta \qquad (2a)$$

where θ is the angle between $\mathbf{k}$ and $\hat{\mathbf{b}}$. The condition for neglect of the transverse part of the field is

$$\Omega\sin\theta \ll C^2k^2, \qquad (2b)$$

which we shall assume is well satisfied. If we restrict the electric field to two dimensions, the condition which must be satisfied is weaker: $\Omega^2\sin^2\theta \ll C^2k^2$.

The density deviation δn is in units of $2n_0$, where n_0 is the average background density. It obeys a hydrodynamic equation driven by the ponderomotive force

$$(C_s^{-2}\partial_t^2 + \hat{\nu}\partial_t - \nabla^2)\delta n = \nabla^2|\mathcal{E}|^2, \qquad (3)$$

where C_s is the ion-acoustic speed in units of $(3\theta/m_i)^{1/2}$ and $\hat{\nu}$ is an operator representing the effect of Landau damping of ion-acoustic waves in an equal temperature plasma. We have also briefly studied[8] magnetic field contributions to Eq. (3), but find no effect on the nonlinear evolution of a broadband packet (only a small volume in k space is affected).

Our numerical work assumes $\mathcal{E} = -\nabla\phi$, and generates solutions to Eq. (3), together with the divergence of Eq. (1), namely,

$$i\partial_t\nabla^2\phi + \tfrac{1}{2}\nabla^4\phi - \tfrac{1}{2}\Omega^2\nabla\cdot\mathsf{P}\cdot\nabla\phi - \nabla\cdot(\delta n\nabla\phi) = 0. \qquad (4)$$

In k space we take an initial packet of randomly phased modes with a shape characteristic of a prior, slow bump-on-tail instability.[5] In real space this appears as an initial pattern of wave packets oriented along the direction of the beam [see Fig. 1(a)]. The initial wave amplitudes are centered about a k-space wavenumber of $k_0 = 0.011\,k_D$. The parallel and perpendicular widths are $\Delta k_\parallel = 0.25\,k_0$, $\Delta k_\perp = 0.17\,k_0$. The choice of these parameters is motivated by the application to type-III solar radio burst phenomena at 1–2 a.u. The initial energy density is $\langle W\rangle = 16\langle|E|^2\rangle = 1.3\times10^{-4}$. This value assures that $\langle W\rangle$ far exceeds the threshold[4,5] for adiabatic col-

 0031 9171/81/040668 05$00.90 ©1981 American Institute of Physics

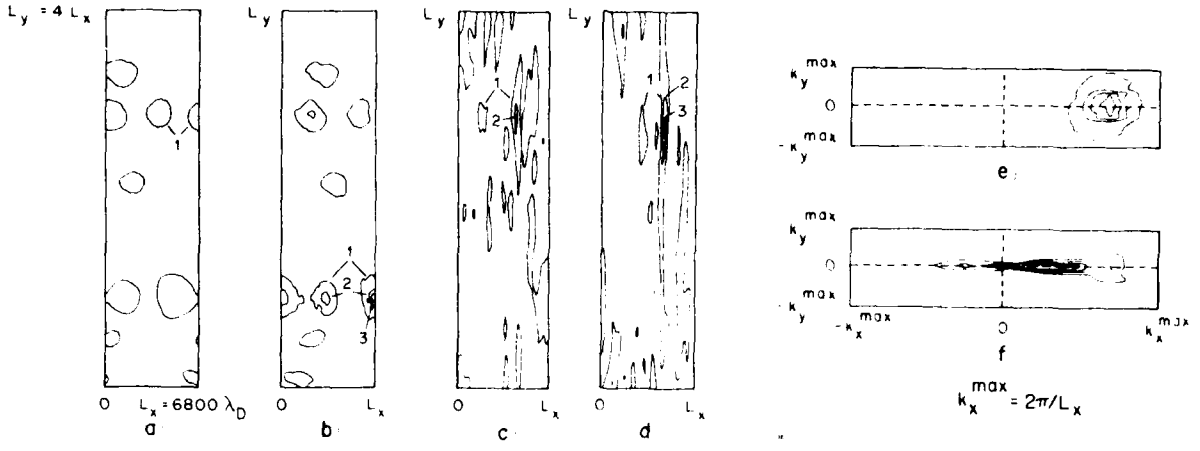

FIG. 1. Evolution of Langmuir waves. In (a), (b), (c), and (d), we plot contours of equal Langmuir field modulus in real space. The spacing in the 64×64 grid is four times finer in x than in y. Contours 1, 2, and 3 correspond to $W = 1.8 \times 10^{-4}$, 7.3×10^{-4}, and 1.6×10^{-3}. (a) is at $t = 0$; (b) is at $\omega_{pe}t = 0.76 \times 10^5$ with $B = 0$; (c) and (d) represent the evolution from (a) (at times $\omega_{pe}t = 3.6 \times 10^5$ and 4.1×10^5) for the case $\omega_{ce}/\omega_{pe} = 0.1$; (e) and (f) show field contours in k space for the nonmagnetic case (e) and the magnetic case (f) at times corresponding to (b) and (d), respectively.

lapse, although it is not necessarily the only choice for the type-III problem (see Sec. V). The real space packets collapse as shown in Fig. 1(b).

Next, with the same initial conditions, we introduce a small magnetic field in the $\mathbf{k}_0$ direction, such that $\Omega = 0.1$. The collapse is slowed down by a factor of 5, as shown in Figs. 1(c) and 1(d). The packets now tend toward a pancake shape, but are not one dimensional.

We shall argue that the effect of the small magnetic field when $\Omega = 0.1$ is to retard direct adiabatic collapse. In the magnetized case, induced scattering of Langmuir waves off (dynamic) ions[8,12] seems to occur before substantial steepening of the wave packets, whereas in the nonmagnetic case it occurs later. For our parameters, the scattered waves are in the forward direction,[6] with wavenumbers on the order of $k_0/3$. The evidence for this is shown in the k-space picture in Fig. 1(f) for the $\Omega = 0.1$ case, compared with Fig. 1(e) in the nonmagnetic case, $\Omega = 0$. The geometry and time scale for the configuration shown in Fig. 1(f) are similar to what we obtain for a *monochromatic* initial packet, with B set equal to zero (not shown here). For a monochromatic initial packet, direct collapse cannot occur, because there is no ponderomotive force, and the linear induced scatter instability dominates at early times. This enables a fairly positive identification of Fig. 1(f) as resulting from induced scatter off ions. A more one-dimensional configuration in k-space results, followed by collapse.

In Fig. 2 we plot, as a function of Ω, the time for the peak energy density in a collapsing packet to increase by a factor of ten. Significant slowing requires $\Omega \geq 0.1$.

III. VIRIAL THEOREM FOR MAGNETIC COLLAPSE

We now offer a theoretical explanation for why the direct collapse is slowed down by a magnetic field. The results shown in Fig. 1 all occur in the regime of adiabatic ions, where Eq. (3) reduces to

$$\delta n = -|\mathcal{E}|^2. \tag{5}$$

We now derive a virial theorem for Eqs. (4) and (5) (with $\mathcal{E} = -\nabla\phi$). This derivation represents an improvement over the derivation of Ref. 4, even in the limit $\mathbf{B} = 0$, because the electromagnetic terms are treated more directly. That is, the $\nabla \times \nabla \times \mathcal{E}$ term in the full vector field Eq. (1) is explicitly eliminated when the divergence is taken to obtain Eq. (4) for the scalar potential ϕ. The Lagrangian density for Eq. (4) with δn given by Eq. (5) is

$$\mathcal{L} = \tfrac{1}{2}i(\dot{\phi}^*\nabla^2\phi - \dot{\phi}\nabla^2\phi^*) - \tfrac{1}{2}|\nabla^2\phi|^2 - \tfrac{1}{2}\Omega^2(\nabla\phi \cdot \mathbf{p} \cdot \nabla\phi^*) + \tfrac{1}{2}|\nabla\phi|^4. \tag{6}$$

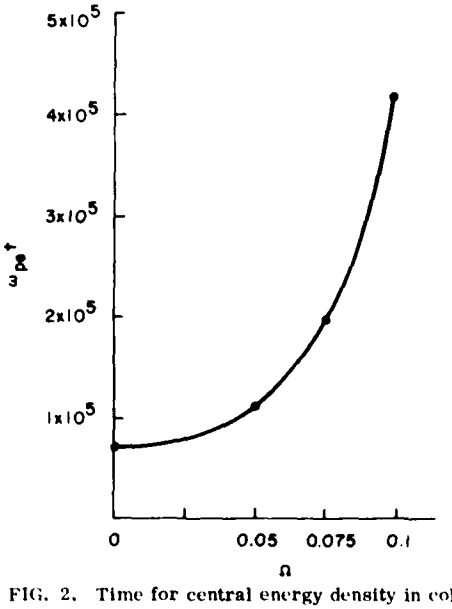

FIG. 2. Time for central energy density in collapsing wave packet to reach ten times initial value for different values of Ω, as determined numerically from the initial conditions given in Fig. 1(a).

The dependence on $\nabla^2\phi$ requires a generalization of Lagrange's equation.[13] Hence, the equation of motion [Eq. (4)], is obtained from

$$\partial_t \mathcal{L}_{\phi_t^*} + \nabla \cdot \mathcal{L}_{\nabla\phi^*} - \{(\partial^2/\partial \mathbf{x}_i^2)[\partial \mathcal{L}/\partial(\partial^2\phi^*/\partial \mathbf{x}_i^2)]\} = 0 ,$$

where a subscript of $\mathcal{L}$ indicates differentiation with respect to that variable.

From the Lagrangian density we derive[13,14] a momentum equation

$$\partial_t \mathbf{p} + \nabla \cdot \mathbf{T} = 0 , \tag{7}$$

where the momentum density is $\mathbf{p} = (\mathcal{S}_L^* \cdot \nabla \mathcal{S}_L - \mathcal{S}_L \cdot \nabla \mathcal{S}_L^*)/2i$, with $\mathcal{S}_L \equiv -\nabla\phi$. The stress tensor[13,14] for a Lagrangian with higher order derivatives is

$$T_{ij} = \frac{\delta_{ij}\mathcal{L}}{2} - \phi_j^* \mathcal{L}_{\phi_i^*} - \left(\phi_{ij}^* - \phi_j^* \frac{\partial}{\partial \mathbf{x}_i}\right)\frac{\partial \mathcal{L}}{\partial(\partial^2\phi^*/\partial \mathbf{x}_i^2)} + \text{c.c.} ,$$

where c.c. stands for the complex conjugate. A subscript i on ϕ or ϕ^* indicates a derivative with respect to $\mathbf{x}_i$, and there is no sum over i.

The total momentum, $\mathbf{P} \equiv \int d\mathbf{r}\, \mathbf{p}$ is conserved for fields which fall to zero fast enough at infinity in the (unbounded) plasma. Another conserved quantity is

$$H \equiv \tfrac{1}{2}\int d\mathbf{r}[|\nabla \cdot \mathcal{S}_L|^2 - |\mathcal{S}_L|^4] + H_B , \tag{8a}$$

where

$$H_B \equiv \frac{\Omega^2}{2}\int d\mathbf{r}\,|\mathcal{S}_L \cdot \mathbf{P}|^2 . \tag{8b}$$

The final equation needed to generate a virial theorem is obtained from the longitudinal part of Eq. (1) rather than from Eq. (4). For an initially longitudinal wave packet, the transverse part of the field $\mathcal{S}_T$ will remain small as long as inequality (2b) is satisfied, and as long as $\Delta k \ll k_0$. Then, $|\mathcal{S}_T| = \sigma(|\mathcal{S}_L|\Omega/k^2C^2) \ll |\mathcal{S}_L|$. We take the scalar product of Eq. (1) with $\mathcal{S}_L^*$ and subtract the complex conjugate to obtain the approximate result

$$\partial_t |\mathcal{S}_L|^2 + \nabla \cdot \mathbf{p} = 0 . \tag{9}$$

From Eqs. (7) and (9) we derive a virial theorem[4] for the mean packet width, $\langle \delta r^2 \rangle \equiv \int d\mathbf{r}\, \delta r^2 |\mathcal{S}_L|^2/N$, where $N \equiv \int d\mathbf{r}\,|\mathcal{S}_L|^2$ is the conserved quantity which follows from (9). The virial theorem involves the trace of the stress tensor.[4] The result is

$$\partial_t^2 \langle \delta r^2 \rangle = 2[A - 2(H_B/N)] + (2 - D)\langle |\mathcal{S}_L|^2 \rangle , \tag{10a}$$

$$A \equiv 2H/N - (\mathbf{P}/N)^2 . \tag{10b}$$

Here, D is the dimensionality of coordinate space ($D = 2$ for the numerical simulations).

What can this theory tell us about the magnetic field strength necessary to affect collapse? Let us consider a two-dimensional Gaussian wave packet

$$\mathcal{S} = i(E_0/k_0)\nabla \exp[ik_0 x - \tfrac{1}{2}(\Delta k_\parallel^2 x^2) - \tfrac{1}{2}(\Delta k_\perp^2 y^2)] . \tag{11}$$

We find that

$$A = \tfrac{1}{2}\left(\frac{\Delta k_\parallel^2}{k_D^2} + \frac{\Delta k_\perp^2}{k_D^2} + \frac{\Delta k_\perp^2}{3k_0^2}\Omega^2 - \frac{W}{24}\right). \tag{12}$$

When there is no magnetic field, the condition for collapse is $D > 2$ and $A < 0$. For the two-dimensional wave packet, the collapse threshold condition can then be written

$$W/24 > (\Delta k_\parallel^2 + \Delta k_\perp^2)/k_D^2 . \tag{13}$$

In two dimensions, the rate of collapse is a constant because A is invariant.

With a nonzero magnetic field, the threshold condition for collapse to begin is still (13), but the rate of collapse [$A - 2H_B N$, in (10a)] can change sign because although A is invariant, H_B can decrease with time! Therefore, collapse is not assured even if initially $A - 2H_B/N$ is negative. We find in the numerical simulations that H_B can decrease with time. As H_B gets smaller and A remains constant, the collapse rate will go from a large negative number (fast collapse) to a smaller negative number (slower collapse). The collapse rate, $A - 2H_B/N$, can even change sign, thus leading to inhibition of collapse due to magnetic dispersion, provided

$$\frac{\Delta k_\perp^2}{3k_0^2}\Omega^2 > \frac{\Delta k_\parallel^2}{k_D^2} + \frac{\Delta k_\perp^2}{k_D^2} - \frac{W}{24} . \tag{14}$$

Close to the collapse threshold, the right side of (14) can be near zero. This implies that an infinitesimal magnetic field can alter a marginally stable collapse.

While (14) is necessary, it is not a sufficient condition for an effect of the B field on collapse. This is because we have assumed that H_B decreases with time, although this is not always true. The condition for H_B *to decrease cannot be derived from theory*, but is discovered empirically from numerical simulation to require that the magnetic dispersion be larger than the nonlinear refraction contribution to the invariant A [see Eq. (12)]

$$(\Delta k_\perp^2/3k_0^2)\Omega^2 > W/24 . \tag{15}$$

When the inequality (13) is satisfied, so that collapse can begin, then the ordering implied by (15) yields the following easily interpreted criterion for an effect of the magnetic field on collapse

$$\Omega^2 > 3k_0^2/k_D^2 . \tag{16}$$

This just means that the magnetic dispersion in the wave packet exceeds the thermal dispersion. This condition is independent of the packet width $\Delta k_\perp$.

For type-III parameters at 0.5 a.u., $k_0 = 0.01\ k_D$, and $\Omega = 0.01$, so that the terms in (16) are roughly equal.

IV. DISCUSSION

In the previous section we maintained that a magnetic field can cause a wave packet to evolve toward smaller perpendicular wavenumbers and cause H_B to decrease. When H_B gets smaller, the collapse rate can change sign, which means collapse may be prevented. When this occurs, our numerical solutions show that other nonadiabatic wave interactions, such as parametric instability, take place, and the virial theorem no longer applies. These interactions seem to lead ultimately to a geometry in which collapse can occur (for example, by cascade down to a "condensate").

These points are well demonstrated in the initial val-

ue simulations. In the case of no magnetic field, the evaluation of A gives

$$A \simeq -0.6\times10^{-5}. \tag{17}$$

This rate of collapse remains constant as long as the collapse is abiabatic. In the other case, when the magnetic field is such that $\Omega = 0.1$, the magnetic term is

$$2H_B/N \simeq 8\times10^{-5}. \tag{18a}$$

The rate of collapse is proportional to

$$A - 2H_B/N = -0.6\times10^{-5}. \tag{18b}$$

This has the same numerical value as (17) because the H_B term contained in A is explicitly subtracted out. Therefore, collapse can begin, even when the magnetic pressure is relatively large. Numerical simulation shows that subsequently $2H_B/N$ gets smaller. We show the behavior of $2H_B/N$ during adiabatic collapse for different values of the magnetic field in Table I. For some cases (in particular, when $\Omega = 0.1$) there is a significant decrease in $2H_B/N$, enough to make $A - 2H_B/N$ positive. This effect is observed empirically to occur when the magnetic energy is greater than the nonlinear interaction energy, as given in Eq. (15) for a Gaussian wave packet.

We can construct the following scenario for magnetic collapse of Langmuir waves. When the condition (15) is satisfied, the collapse transverse to the B field is inhibited. The transverse dimensions of the packets remain the same. However, the longitudinal dimension becomes smaller because nonlinear self-focusing still occurs along the direction of B_0. The collapse rate is slower than the case $\Omega = 0$. Eventually, parametric instability (induced scatter off ions) occurs to produce a new k-space configuration. Such instabilities will be very intense because the background level of the unstable modes is enhanced during the longitudinal contraction of the wave packets. Since the k-space scatter is principally in the B_0 direction, the real space wave packets become increasingly elongated in the transverse direction. The new configuration produces pancake-shaped wave packets which can collapse in both directions. Although our simulations cannot continue beyond this point, the results of Krasnosel'skikh and Sotnikov[10] show that as collapse proceeds to dimensions such that $\Delta k_\parallel/k_D \lesssim \Omega$, the wave packet tends to become symmetric.

The magnetic effects on parametric instability do not depend on pump energy, but occur when the magnetic dispersion of an unstable wave exceeds the thermal dispersion

$$\Omega \sin\theta \gtrsim k. \tag{19}$$

These effects are geometric.[9-10,15]

The new behavior we have just described also depends upon the energy W, according to Eq. (15). The fact that magnetic effects scale with W is important to the type-III problem, as we discuss in the next section.

TABLE I. $2H_B/N$ vs time for different values of Ω.

$\omega_{pe}t$	$\Omega = 0.01$	$\Omega = 0.05$	$\Omega = 0.075$	$\Omega = 0.10$
0.14×10^5	0.84×10^{-5}	2.7×10^{-5}	6.1×10^{-5}	8.3×10^{-5}
0.27	0.85	2.7	5.9	8.1
0.41	0.89	2.6	5.7	8.0
0.55	0.99	2.6	5.3	7.5
0.69	1.4	2.7	4.8	7.2
0.83		2.8	4.2	7.1
0.96			3.8	7.0
1.1				6.7
2.1				5.6

V. EFFECT OF MAGNETIC FIELD IN TYPE-III BURST LANGMUIR TURBULENCE

The connection between the initial value problem we have solved here and the beam-driven type-III problem has been stated in our previous work.[6] The role of the beam is to "prepare" the Langmuir wave packets into a state (given by our initial value data) which then passes over into a collapse, and decouples from the beam. Recent dynamic models[16] in which the broadband pump is allowed to grow exponentially due to the interaction with a type-III electron stream at the rate $\gamma \sim \omega_{pe} = 10^{-4}$, show that the pump saturates at a level where $\langle W\rangle = 10^{-5}$. Also, an experimental upper bound on the mean solar magnetic field at 0.5 a.u. is found to be $\Omega = 0.01$.[17] To make contact with the discussion given here and the type-III problem, we repeat the initial value simulations for $\Omega = 0.01$ and two values of $\langle W\rangle$, 1.0×10^{-4} and 1.0×10^{-5}. The resulting collapsing wave packets are shown in Figs. 3(a) and 3(b). When $\langle W\rangle = 1.0\times10^{-4}$ [Fig. 3(a)], there is no distortion of the collapsing wave packet. Magnetic effects are observable for this $\langle W\rangle$ only when $\Omega \lesssim 0.03$. In the case when $\langle W\rangle = 1.0\times10^{-5}$, which is perhaps more relevant to the type-III problem [Fig. 3(b)], the collapsing wave packets are elongated because of the magnetic field.

The result is consistent with the empirical scaling of

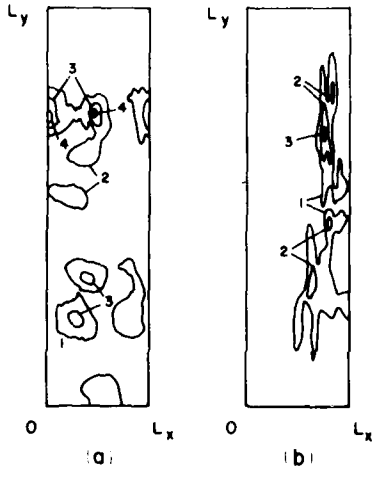

FIG. 3. Contours of equal Langmuir field modulus when $\Omega = 0.01$ for two values of initial energy: (a) $\langle W\rangle = 1.0\times10^{-4}$ (as in Fig. 1) at time $\omega_{pe}t = 0.78\times10^5$ and (b) $\langle W\rangle = 1.0\times10^{-5}$ at time $\omega_{pe}t = 5.7\times10^5$. The magnetic field has more effect on case (b). Contours, 1, 2, 3, and 4 correspond to $W = 0.3\times10^{-4}$, 1.0×10^{-4}, 5.0×10^{-4}, and 10.0×10^{-4}.

Eq. (15). When the electrostatic energy is less by a factor of 1/10, the magnetic effects can be expected to occur when Ω^2 is also smaller by 1/10.

Hence, we find that magnetic effects may have some significance in type-III plasma wave evolution. However, these effects are only marginally evident when $\Omega = 0.01$ and $\langle W \rangle = 10^{-5}$.

VI. CONCLUSION

In numerical simulations of collapse we have identified two effects due to the magnetic field; a change in the shape of the collapsing wave packet and a slowing in the collapse rate. These effects seem to be related. The virial theorem shows that the rate of collapse is slowed because of a decrease in magnetic energy H_B, which is brought about by a decrease in perpendicular wavenumbers. This occurs because nonlinear wave transitions favor modes with smaller perpendicular wavenumbers when the magnetic energy is larger than the interaction energy.[16]

In the examples given here, the magnetic field does not prevent collapse. Even in cases where the initial wave packet does not itself collapse, wave interactions seem to eventually create a pancake shaped wave packet which does.

When this theory is applied to growing beam problems, the slow down results in an overshoot of the beam saturation levels and introduces more electrostatic energy into the system.[16] In the type-III problem, this effect might enhance the wave energy, and produce increased electromagnetic emission for realistic values of the magnetic field. The altered packet shapes would also be expected to affect the pattern of electromagnetic emission and its polarization characteristics.

ACKNOWLEDGMENTS

We would like to acknowledge important conversations with A. Barut and G. Dulk.

This work was supported by the Atmospheric Research Section, National Science Foundation, Grant No. ATM 76-14275, by the Air Force Office of Scientific Research (M.V.G. and J.C.W. only), Grant No. F49620-76-C-0005, and by the National Aeronautics and Space Administration, Grant No. NAGW-91. One of us (D.R.N.) was also supported by the Atmospheric Research Section, National Science Foundation, Grants Nos. ATM 76-22487 and ATM 79-18778, and by S.U.D.O.E. Grant No. EY-76-5-01-2059. We thank the National Center for Atmospheric Research, supported by the National Science Foundation, for computer time used in this study.

[1]V. E. Zakharov, Zh. Eksp. Teor. Fiz. **62**, 1745 (1972) [Sov. Phys.-JETP 35, 908 (1972)].
[2]R. N. Sudan, in *Proceedings of the Sixth European Conference on Controlled Fusion and Plasma Physics*, Moscow (Joint Institute for Nuclear Research, Moscow, USSR, 1973), Vol. 2, p. 185.
[3]N. R. Pereira, R. N. Sudan, and J. Denavit, Phys. Fluids **20**, 936 (1977).
[4]M. V. Goldman and D. R. Nicholson, Phys. Rev. Lett. 41, 406 (1978).
[5]M. V. Goldman, G. F. Reiter, and D. R. Nicholson, Phys. Fluids 23, 388 (1980).
[6]D. R. Nicholson, M. V. Goldman, P. Hoyng, and J. C. Weatherall, Astrophys. J. 223, 605 (1978).
[7]V. I. Petviashvili, Fiz. Plazmy 2, 450 (1976) [Sov. J. Plasma Phys. 2, 247 (1976)].
[8]J. C. Weatherall, M. V. Goldman, and D. R. Nicholson, Astrophys. J. (to be published).
[9]H. P. Freund and K. Papadopoulos, Phys. Fluids **23**, 139 (1980).
[10]V. V. Krasnosel'skikh and V. I. Sotnikov, Fiz. Plazmy 3, 872 (1977) [Sov. J. Plasma Phys. 3, 491 (1978)].
[11]A. S. Lipatov, Zh. Eksp. Teor. Fiz. Pis'ma Red. **26**, 516 (1977) [JETP Lett. **26**, 337 (1977)].
[12]D. R. Nicholson and M. V. Goldman, Phys. Fluids 21, 1766 (1978).
[13]A. Barut and G. H. Mullen, Ann. Phys. **20**, 203 (1962).
[14]L. D. Landau and E. M. Lifshitz, *Classical Theory of Fields* (Addison Wesley, Reading, Mass., 1971), p. 77.
[15]D. F. Smith and V. N. Tsytovich (private communication).
[16]J. Weatherall, Ph.D. thesis, University of Colorado (1980).
[17]G. A. Dulk and D. J. McLean, Solar Phys. **57**, 279 (1978).

APPENDIX E

E. "Parametric Instabilities in Weakly Magnetized Plasmas"

J.C. Weatherall, M.V. Goldman, and D. Nicholson
Astrophysical Journal 246, 306-313 (May, 1981)

THE ASTROPHYSICAL JOURNAL, 246:306–313, 1981 May 15
© 1981. The American Astronomical Society. All rights reserved. Printed in U.S.A.

PARAMETRIC INSTABILITIES IN WEAKLY MAGNETIZED PLASMA

J. C. WEATHERALL AND M. V. GOLDMAN
Department of Astro-Geophysics, University of Colorado

AND

D. R. NICHOLSON
Department of Physics and Astronomy, University of Iowa
Received 1979 November 13; accepted 1980 November 19

ABSTRACT

Parametric instabilities in a weakly magnetized plasma are discussed. The results are applied to waves excited by electron streams which travel outward from the Sun along solar-wind magnetic field lines, as in a type III solar radio burst.

Subject headings: hydromagnetics — instabilities — plasmas — Sun: radio radiation

I. INTRODUCTION

Intense waves in plasmas are known to cause parametric instabilities, resulting in the transfer of energy from the intense wave to other waves; for a review see Nishikawa *et al.* (1976). An important astrophysical phenomenon involving such intense waves is the type III solar radio burst, involving a stream of electrons which travels outward from the Sun along solar wind magnetic field lines; for reviews, see Nicholson *et al.* (1978), Smith and Nicholson (1980), and Goldstein, Smith, and Papadopoulos (1980). There has been a great deal of work involving the application of parametric instability theory to type III solar radio bursts; see Papadopoulos, Goldstein, and Smith (1974), Bardwell and Goldman (1976), Smith, Goldstein, and Papadopoulos (1976, 1979), Nicholson *et al.* (1978), Goldman and Nicholson (1978), Nicholson and Goldman (1978), and references therein.

There is a substantial body of literature concerning parametric instabilities in a magnetized plasma; see, e.g., Kaw (1976), Porkolab and Goldman (1976), Kaufman and Stenflo (1975), Sanuki and Schmidt (1977), and Dysthe and Pécseli (1978). Nevertheless, previous applications of parametric instability theory to type III bursts have not treated magnetic field effects systematically. (See, however, a qualitative discussion in Nicholson *et al.* 1978. Also see Freund and Papadopoulos 1980 for a treatment of some, but not all, magnetic field effects.) This paper represents a step in the direction of a proper inclusion of the effects of magnetic field on wave evolution during type III bursts. It is a direct generalization of the earlier work of Bardwell and Goldman (1976).

II. PARAMETRIC INSTABILITIES

An electron stream traveling through a background plasma gives rise to Langmuir waves (high frequency electron plasma waves with frequency near the local electron plasma frequency) through the well known beam-plasma instability. As a first approximation, the spectrum of stream-excited Langmuir waves can be represented by a single large-amplitude monochromatic wave. As discussed in detail by Bardwell and Goldman (1976), this is in many respects not a very good approximation, but it allows analytic progress, the results of which may have important implications for the true situation.

Our theoretical model thus consists of an intense single monochromatic Langmuir wave (the "pump" wave) traveling along a uniform background magnetic field $\boldsymbol{B}_0$ in an infinite, homogeneous plasma. The electric field of this intense wave is given by

$$\boldsymbol{E}(\boldsymbol{r}, t) = \mathcal{E}_0 \hat{x} \cos(k_0 x - \omega_0 t), \tag{1}$$

where $\mathcal{E}_0$ is a real constant, and $\hat{x}$ is the magnetic field direction. Even though $\boldsymbol{E}$ is an intense wave, we assume that it is still weak enough that it propagates as a linear wave and satisfies the linear Langmuir dispersion relation

$$\omega_0^2 = \omega_e^2 + 3k_0^2 v_e^2, \tag{2}$$

where ω_e is the electron plasma frequency, $\omega_e^2 = 4\pi n_0 e^2 / m_e$; the average electron density is n_0; the electronic charge

has magnitude e; the electron mass is m_e; the thermal speed $v_e \equiv (T_e/m_e)^{1/2}$; and the electron temperature T_e has units of energy so that Boltzmann's constant does not appear explicitly.

In accordance with standard parametric instability theory, we suppose that high frequency and low frequency fluctuations in the plasma are coupled together by the pump wave and grow exponentially. In general, the coupling involves the pump wave, a low frequency wave characterized by a complex frequency ω and wavenumber $\boldsymbol{k}$, and two high frequency waves characterized by the frequencies and wavenumbers $(\omega_0+\omega, \boldsymbol{k}_0+\boldsymbol{k})$ and $(\omega_0-\omega^*, \boldsymbol{k}_0-\boldsymbol{k})$. For simplicity, we assume throughout this paper that all waves are longitudinal, having electric fields parallel to their wavenumbers. The possibility of electromagnetic decay waves is briefly discussed in § IV. The low frequency wave is therefore characterized by an electric field $\boldsymbol{E}_1$ of the form

$$\boldsymbol{E}_1(\boldsymbol{r},t) = \tfrac{1}{2}\mathcal{E}_1\hat{k}\exp(-i\omega t + i\boldsymbol{k}\cdot\boldsymbol{r}) + \tfrac{1}{2}\mathcal{E}_1^*\hat{k}\exp(i\omega^* t - i\boldsymbol{k}\cdot\boldsymbol{r}), \tag{3}$$

while the high frequency electric fields are

$$\boldsymbol{E}_+(\boldsymbol{r},t) = \tfrac{1}{2}\mathcal{E}_+\hat{k}_+\exp\left[-i(\omega_0+\omega)t + i(\boldsymbol{k}_0+\boldsymbol{k})\cdot\boldsymbol{r}\right] + \tfrac{1}{2}\mathcal{E}_+^*\hat{k}_+\exp\left[i(\omega_0+\omega^*)t - i(\boldsymbol{k}_0+\boldsymbol{k})\cdot\boldsymbol{r}\right], \tag{4}$$

and

$$\boldsymbol{E}_-(\boldsymbol{r},t) = \tfrac{1}{2}\mathcal{E}_-\hat{k}_-\exp\left[-i(\omega_0-\omega^*)t + i(\boldsymbol{k}_0-\boldsymbol{k})\cdot\boldsymbol{r}\right] + \tfrac{1}{2}\mathcal{E}_-^*\hat{k}_-\exp\left[i(\omega_0-\omega)t - i(\boldsymbol{k}_0-\boldsymbol{k})\boldsymbol{r}\right], \tag{5}$$

where $\hat{k}_\pm$ are unit vectors in the $\boldsymbol{k}_0 \pm \boldsymbol{k}$ directions. The relation among the four different wave vectors is shown in Figure 1. While Figure 1 is drawn in the k_x-k_y plane, all figures in this paper can be rotated around the k_x axis to obtain a fully three-dimensional picture.

The high frequency and low frequency modes couple together to produce new normal modes described by the dispersion relation:

$$\frac{1}{\chi_e(\omega,\boldsymbol{k})} + \frac{1}{\chi_i(\omega,\boldsymbol{k})} = -k^2\lambda_e^2\frac{W_0}{4}\left[\frac{\mu_+^2}{\epsilon(\omega_0+\omega,\boldsymbol{k}_0+\boldsymbol{k})} + \frac{\mu_-^2}{\epsilon(\omega_0-\omega,\boldsymbol{k}_0-\boldsymbol{k})}\right], \tag{6}$$

where the angular factors are

$$\mu_\pm \equiv \hat{k}_0\cdot\hat{k}_\pm, \tag{7}$$

the electron Debye length $\lambda_e \equiv v_e/\omega_e$, and the dimensionless energy density

$$W_0 \equiv \frac{\mathcal{E}^2}{4\pi n_0 T_e}. \tag{8}$$

Kaw (1976) uses an equation similar to (6) to study instabilities of electrostatic waves in a magnetized plasma, but with a dipole pump. [The reader may recall that in studying linear longitudinal waves, one writes Poisson's equation $\nabla\cdot\boldsymbol{E} = 4\pi\rho$ as $ik(1+\chi_e+\chi_i)E = 0$, where the electron susceptibility χ_e is proportional to that portion of the charge density ρ due to electron motion and where the ion (in this paper, proton) susceptibility χ_i is proportional to that

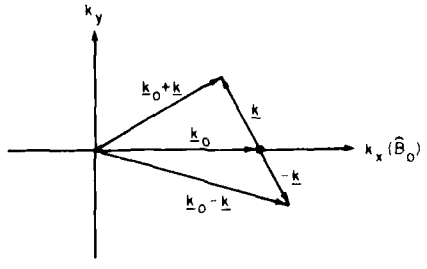

FIG. 1 Relation among the four wavevectors involved in a parametric instability

portion of the charge density ρ due to ion motion. The combination $\epsilon = 1 + \chi_e + \chi_i$ is called the linear dielectric function, and the dispersion relation for the wave involved is contained in the expression $\epsilon = 0$. It is this dielectric function ϵ which appears twice on the right side of (6).] In the next two sections we evaluate the dispersion relation (6) in the unmagnetized case.

III. UNMAGNETIZED CASE

We first solve the dispersion relation (6) neglecting the background magnetic field, with parameters roughly corresponding to a typical type III solar radio burst at a position one-third of a solar radius above the Sun's surface. These are (Bardwell and Goldman 1976): $n_e = 10^8$ cm^{-3}, $T_e = T_i = 140$ eV, $k_0\lambda_e = 0.05$, and $W_e = 10^{-4}$. In the unmagnetized limit, we take the dielectric function needed on the right side of (6) from fluid theory (Krall and Trivelpiece 1972)

$$\epsilon(\omega_0 \pm \omega, \boldsymbol{k}_0 \pm \boldsymbol{k}) = \pm 2\frac{\omega}{\omega_e} - 3k^2\lambda_e^2 \mp 6\boldsymbol{k}\cdot\boldsymbol{k}_0\lambda_e^2, \tag{9}$$

where throughout this paper $\omega_i \ll \omega_e$, ω_0 and $\omega_0 \gtrsim \omega_e$.

For the low frequency susceptibilities needed on the left-hand side of (6), we use the results of kinetic theory, as has previously been done by Bardwell (1976). This is somewhat more accurate than the fluid model employed by Bardwell and Goldman (1976) especially in the present case of equal electron and ion temperatures. The results of the fluid and kinetic approaches are in quite good qualitative agreement, and differ quantitatively only by factors of less than 2. The kinetic susceptibilities for species s are (Montgomery 1971)

$$\chi_s(\omega, \boldsymbol{k}) = -\frac{1}{k^2\lambda_s^2}\left[1 + \zeta_s Z(\zeta_s)\right], \tag{10}$$

where

$$\zeta_s \equiv \frac{\omega}{2^{1/2}kv_s}, \tag{11}$$

with v_s the thermal speed of species s and Z the plasma dispersion function (Fried and Conti 1961) which arises because the background electron and ion distribution functions have been taken to be Maxwellian.

The dielectric function (9) and the susceptibilities (10) are inserted in the dispersion relation (6) which is then solved numerically to yield the complex frequency $\omega(\boldsymbol{k})$. The imaginary part of this frequency is then plotted as a function not of $\boldsymbol{k}$, but rather as a function of the Langmuir wave vector, $\boldsymbol{k}^1 \equiv \boldsymbol{k}_0 - \boldsymbol{k}$. Figure 2 shows the resulting contours of constant growth rate. This two-dimensional contour plot can be rotated about the $\hat{k}_y(\hat{B}_0)$ axis to yield a fully three-dimensional contour plot. Figure 2 is in agreement with the corresponding figure in Bardwell and Goldman (1976). As discussed in detail by Bardwell and Goldman (1976), there are three distinct regimes of instability; these are

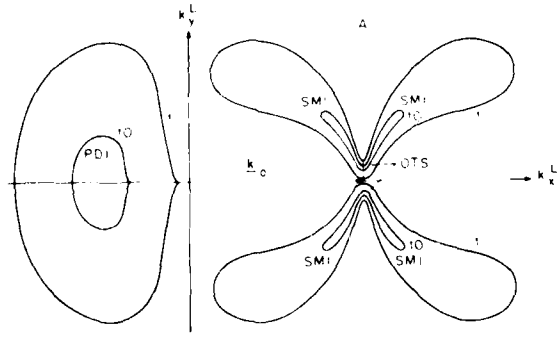

FIG. 2.—Solution to the dispersion relation (6) in the unmagnetized case; the contours represent the imaginary part of the frequency (the growth rate) as a function of two-dimensional Langmuir wavenumber $\boldsymbol{k}^1 \equiv \boldsymbol{k}_0 - \boldsymbol{k}$. This figure can be rotated about the k_y^1 axis to obtain a fully three-dimensional picture. The contour labeled 1 represents a growth rate $\omega_i/\omega_e = 10^{-6}$, while the contour labeled 10 represents a growth rate $\omega_i/\omega_e = 10^{-5}$. The parameters are those of § III.

labeled PDI (parametric decay instability), SMI (stimulated modulational instability), and OTS (oscillating two-stream instability). The purely growing modes we identify as the OTS are confined to the small region of k-space with $\boldsymbol{k} \perp \boldsymbol{k}_0$ and $\boldsymbol{k} \ll \boldsymbol{k}_0$. This should not be confused with the OTS described in Papadopoulos, Goldstein, and Smith (1974) and Smith, Goldstein, and Papadopoulos (1979), which occurs in the large amplitude limit such that $W_0 \gg 10(k_0\lambda_e)^2$ (see discussion in § V of this paper). The maximum growth rate ω_i in each of the three regimes is close to $\omega_i/\omega_e \approx 1.3 \times 10^{-2}$ in the present case. The properties of these three regimes in the unmagnetized case have been reviewed by Bardwell and Goldman (1976). In the next section we consider the modification of these three regimes in the weakly magnetized situation.

IV. WEAKLY MAGNETIZED CASE

In this section we consider the modification of the previous results in the presence of a weak magnetic field. In this paper "weak" means that the electron gyrofrequency $\Omega_e \equiv eB_0/m_e c$ (c is the speed of light) is much less than the electron plasma frequency ω_e. For example, with the solar corona parameters of the previous section and a reasonable magnetic field strength of 2.5 gauss, we have $\Omega_e/\omega_e = 0.1$. Note that while the magnetic field is weak in the sense we have described, the magnetic field energy density for the present parameters exceeds the kinetic energy density of the background electrons (i.e., this is a low-β plasma).

The magnetic field affects both the high frequency and the low frequency wave motions. For the high frequency longitudinal waves, the electrons feel a $\boldsymbol{v}\times\boldsymbol{B}$ force in addition to an electric field force, and the dielectric function becomes (Ginzburg 1964)

$$\epsilon(\omega_0 \pm \omega, \boldsymbol{k}_0 \pm \boldsymbol{k}) = 1 - 2\frac{\omega_e^2}{\omega_0^2}\left[3k^2\lambda_e^2 \mp 6\boldsymbol{k}\cdot\boldsymbol{k}_0\lambda_e^2 + (\mu_e^2 - 1)\frac{\Omega_e^2}{\omega_0^2}\right], \tag{12}$$

which must be used on the right-hand side of the dispersion relation (6).

There are also magnetic field effects on the low frequency wave motions. For heuristic purposes, suppose we ignore the strong ion Landau damping of ion acoustic waves in an equal temperature plasma and use the dispersion relation $\omega = kc_s$ to estimate a typical ion-acoustic frequency. With the sound speed $c_s \approx (T_e/m_i)^{1/2}$ and a typical low frequency wavenumber $k\lambda_e \sim 0.02$, we have $\omega/\omega_e \sim 4 \times 10^{-4}$. The ion gyrofrequency $\Omega_i \sim 5 \times 10^{-5}\omega_e$, and the ion (proton) plasma frequency is $\omega_{pi} \sim 0.02\omega_e$. Thus, the frequency ordering of interest is $\Omega_i \ll \omega \ll \omega_{pi} < \Omega_e \ll \omega_e$.

For most of the wavenumbers k^{-1} in Figure 2, the product of the ion gyroradius ρ_i, with the low-frequency wavenumber, $k = |\boldsymbol{k}_0 - \boldsymbol{k}|$, is substantially greater than unity. We find that the modification of the low-frequency ion susceptibility due to a magnetic field is insignificant for most of the wavenumbers in this problem. The exception is the OTS. Along the dashed line labeled A in Figure 2, ω is purely imaginary, and at maximum growth rate $\omega_i/\omega_e = 1.0 \times 10^{-5} < \Omega_i/\omega_e$ and $k\rho_i \sim 1$. We shall find that the OTS branch is substantially suppressed, but we attribute this to the low frequency effects on the electrons, not to $k\rho_i \sim 1$. The magnetic effects on the low-frequency ion motion do not seem to be important because the results are the same whether they are included in the calculation or not.

As for the electrons, the fact that $|\omega| \ll \Omega_e$ (and typically $k_\perp\rho_e \ll 1$, where ρ_e is the electron gyroradius) means that the low-frequency electron motion is indeed strongly magnetized. In other words, electrons are not free to follow low frequency motions across the field lines, but rather they begin an $\boldsymbol{E}\times\boldsymbol{B}_0$ drift when subjected to low-frequency electric fields perpendicular to the field lines. Along the magnetic field lines the electrons are perfectly free to move, like beads on a wire. As discussed in somewhat more detail by Nicholson *et al.* (1978), the net result of these parallel and perpendicular effects is that for angles ($\sim k_\perp/k_\parallel$) which are greater than $(m_e/m_i)^{1/2}$ from perpendicular to $\hat{\boldsymbol{B}}_0$, there is no effect of the magnetic field on the low frequency wave motions (m_i is the proton mass). Only in the small range of angles $|k_\parallel/k_\perp| < (m_e/m_i)^{1/2}$ are the electron motions inhibited greatly and the low frequency wave properties modified. As we shall see, the instability growth rates in this small range of angles can be severely reduced because of the inhibition of electron motion across field lines.

Let us perform a simple analytic calculation to illustrate one case of a reduction in growth rate due to the magnetic field. We focus our attention on the dashed line labeled A in Figure 2. Along this line where $\boldsymbol{k}\cdot\boldsymbol{k}_0 = 0$, the instability is purely growing with $\omega = i\omega_i$. Now suppose we have a plasma with cold ions and a growth rate whose magnitude is small. The unmagnetized fluid susceptibility for species s is $\chi_s = -\omega_s^2/(\omega^2 - k^2v_s^2)$, which means we can ignore the ion susceptibility term on the left-hand side of the dispersion relation (6). Inserting the electron susceptibility $\chi_e \approx 1/k^2\lambda_e^2$, the unmagnetized dielectric function (9), and the assumption $\omega = i\omega_i$ into the dispersion relation (6), we find

$$\frac{\omega_i}{\omega_e} = \left(\frac{3}{8}W_0k_\perp^2\lambda_e^2 - \frac{9}{4}k_\perp^4\lambda_e^4\right)^{1/2}. \tag{13}$$

whereupon the highest growth rate is

$$\omega_i/\omega_r = W_0^2/8, \tag{14}$$

which occurs at

$$k_y\lambda_e = (W_0^2/12)^{1/2}. \tag{15}$$

Now, how is this result modified when the magnetic field is included? Continuing to ignore the ions in the low frequency susceptibilities on the left-hand side of (6), there are two places where magnetic field effects enter. The first is in the high frequency dielectric function, where (12) replaces (9). One may think of the change as replacing $-3k^2\lambda_e^2$ in (9) by $-3k^2\lambda_e^2+(\mu_\perp^2-1)\Omega_e^2/\omega_r^2$ in (12). As both terms are negative, this effect is as if the wavenumber in (9) were increased; the result is merely a shift in the growth rate curve to smaller wavenumbers with no change in the maximum growth rate obtainable. This effect was first suggested to us by Smith and Tsytovich (1977).

The second place where the magnetic field effect enters is in the low frequency electron susceptibility. For the case under discussion with $\boldsymbol{k}\cdot\hat{\boldsymbol{B}}_0=0$, the unmagnetized electron susceptibility, $(k\lambda_e)^{-2}$, is replaced by $\chi_e\approx\omega_r^2/\Omega_e^2$, corresponding to polarization drift; and, neglecting for simplicity the high frequency magnetic effect of the previous paragraph, the dispersion relation (6) yields (without assuming ω purely imaginary)

$$\frac{\omega^2}{\omega_r^2}=\frac{9}{4}k^4\lambda_e^4-\frac{3}{8}\frac{W_0^2k^4\lambda_e^4\omega_r^2}{\Omega_e^2}=\frac{9}{4}k^4\lambda_e^4\left(1-\frac{W_0^2}{6}\frac{\omega_r^2}{\Omega_e^2}\right), \tag{16}$$

which does not predict instability at all for the parameters of the present paper. This crude calculation exhibits the reduction in the growth rate when the low frequency mode propagates within an angle of $(m_e/m_i)^{1/2}$ with the perpendicular to the magnetic field.

We emphasize that this great reduction in growth rate occurs only for the branch marked OTS in Figure 2. For the other branches marked PDI and SMI in Figure 2, the low frequency mode has an angle greater than $(m_e/m_i)^{1/2}$ to the perpendicular to the magnetic field, and propagates as if the medium were unmagnetized.

To make these remarks rigorous, we numerically solve the dispersion relation (6) with the parameters already mentioned ($\Omega_e/\omega_r=0.1$). For the low frequency electron and ion susceptibilities we use the magnetized kinetic version which is given by (Bekefi 1966)

$$\chi_s(\omega,\boldsymbol{k})=\frac{1}{k^2\lambda_s^2}\left[1+\zeta_s\exp(-a_s)\sum_n^{\infty}{}_{-\infty}I_n(a_s)Z\left(\zeta_s-n\frac{\Omega_s}{2^{1/2}k_z v_s}\right)\right], \tag{17}$$

where $\zeta_s\equiv\omega/2^{1/2}k_z v_s$, $a_s\equiv k_y^2\rho_s^2$, and the I_n are modified Bessel functions. For the high frequency dielectric functions we use the fluid versions (12). The solution of the instability dispersion relation (6) is shown in Figure 3. Comparing this figure to Figure 2, we notice several effects of the magnetic field. The most dramatic effect is the disappearance of the OTS branch, in agreement with the crude analytic calculation. The other dramatic effect is a squeezing of the contours in the $\hat{y}$-direction for both the PDI and SMI branches. We ascribe this effect almost totally to the magnetic term in the high frequency dielectric function (12).

It is important to note that despite the squeezing of the contours in the direction perpendicular to the magnetic field, the vertical extent of the region of fastest growth (the contours labeled 10) is only slightly affected by the magnetic

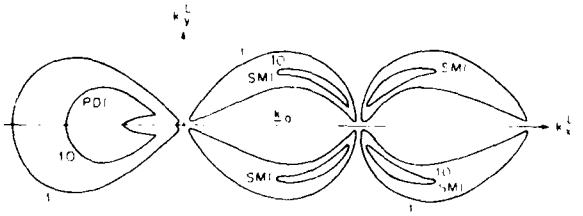

FIG. 3.—Solution of the dispersion relation (6) in the weakly magnetized case. All parameters and contour labels are the same as in Fig. 2, with $\Omega_e/\omega_r=0.1$.

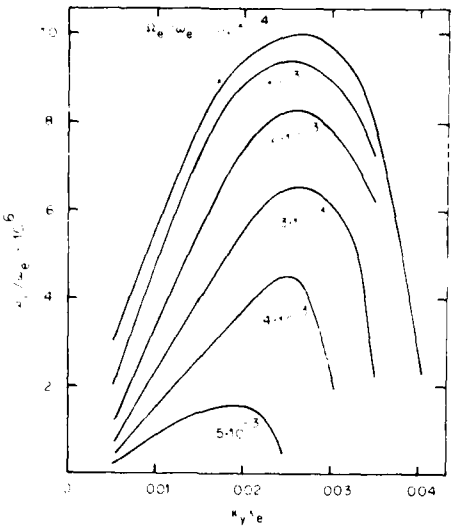

FIG. 4.—Curves of growth rate versus wavenumber for the OTS branch of Fig. 2, for different values of Ω_e/ω_e; all other parameters are the same as in Fig. 2. The horizontal axis of this figure should be thought of as the dashed line labeled A in Fig. 2.

field. This is true for both the SMI and the PDI branches; the maximum perpendicular extent of the "10" contour is reduced by only 10% of its unmagnetized value in each case.

Returning to the OTS branch, we have seen in Figure 2 that in the unmagnetized case it has as large a growth rate as any other branch, while when $\Omega_e/\omega_e = 0.1$ (Fig. 3) it has completely disappeared. In order to explore the nature of this transition, we show in Figure 4 curves of growth rate versus perpendicular wavenumber $k_\perp\lambda_e$ for various values of Ω_e/ω_e, with $k_\parallel = 0$. The horizontal axis of this figure should be identified with the dashed line labeled A in Figure 2. We see that even for the small value $\Omega_e/\omega_e = 0.005$, the instability has almost disappeared. The OTS branch is very sensitive to the presence of a weak magnetic field; the main reason for this is the resistance of the magnetic field to motion of electrons across field lines.

In this paper we have considered only longitudinal decay waves. There also exists a host of potential electromagnetic decay products. Although we have not performed a systematic numerical study of the electromagnetic decay possibilities, we have considered many specific examples within the context of the present parameters. In every case, we find growth rates far lower than the maximum growth rates of the SMI and PDI branches. Of course, in a particular region of wavenumber space, an electromagnetic instability can have the largest growth rate. For example, when the OTS instability is reduced to zero growth rate by the weak magnetic field, the region of wavenumber space which formerly contained the OTS can now support a parametric instability involving a magnetosonic wave. Whereas the low-frequency electron motion across field lines is inhibited by the magnetic field, a magnetosonic wave moves the field lines, thus allowing the electrons to move and enhancing the tendency toward instability. Our calculations indicate, however, that the resulting growth rate is very much smaller than the growth rates of the PDI and SMI branches in the weakly magnetized case. Thus, we feel that there is no indication that electromagnetic effects would change the overall growth rate picture in the weakly magnetized case. The effort required to produce a comprehensive contour plot such as Figures 2 and 3 including all electromagnetic effects does not seem to be warranted.

This concludes our detailed calculations. All of the results of this section agree with the qualitative predictions of Nicholson *et al.* (1978).[1] In the next section we discuss the implications of these results for parametric instabilities and soliton collapse associated with type III solar radio bursts.

[1] In § IV of this reference, the expression $k\rho_i \approx 800$ in the sixth paragraph should be replaced by the expression $k\rho_i \approx 20$. Equation (13) should read

$$\omega^2 - k^2c_s^2 - \frac{\Omega_i\Omega_e}{1 + (k_\perp/k_\parallel)^2(\Omega_e^2/\omega^2 - 1)} = 0$$

V. SUMMARY AND DISCUSSION

In this section we summarize the preceding results and discuss the implications of these results for the theory of type III solar radio bursts.

In the unmagnetized version, the parametric instabilities to which an intense monochromatic Langmuir wave is subject consist of three kinds: the OTS, PDI, and SMI. The maximum growth rates in each branch are comparable. One of these branches, the OTS, is very sensitive to the addition of a weak magnetic field. For the parameters of the present paper, this branch is virtually wiped out for a magnetic field such that $\Omega_e/\omega_{pe} \approx 0.005$. The other two branches, the PDI and the SMI, are very insensitive to the addition of a weak magnetic field. This is true both for the maximum growth rate in each branch, and for the extent of each branch in the wavenumber direction perpendicular to the direction of the magnetic field.

We conclude that to the extent that the stream-excited Langmuir waves of a type III burst are monochromatic, the linear parametric instabilities to which these waves are subject are not one-dimensional in nature. The presence of a weak magnetic field does not change the overall growth rate picture. The detailed type III Langmuir wave scenarios of earlier work (Bardwell and Goldman 1976; Nicholson *et al.* 1978) need not be modified.

This strong conclusion must, of course, be tempered by repeating the observation that the Type III stream-excited Langmuir waves are not monochromatic, but have a spread of wavenumbers along the magnetic field and across the magnetic field. No satisfactory general theory of parametric instabilities due to a broad-band pump wave presently exists even in the unmagnetized case, although some results have been obtained (Bardwell and Goldman 1976; Thomson and Karush 1974; Smith, Goldstein, and Papadopoulos 1979). The frequency spread in a broad-band pump will tend to disorder the coherent growth of the modes in Figures 2 or 3. However, in a statistical sense, those modes may still experience instability. In numerical simulations, parametric wave growth is still observed with a broad-band pump (Nicholson *et al.* 1978).

Broad-band effects can often speed the nonlinear processes, as in the case that the regions of constructive interference of Langmuir waves in real space undergo a direct collapse. In the low solar corona, where $k_0 > (m_i/m_e)^{1/2}$, the wave packets have a group speed larger than the ion-acoustic speed, and collapse cannot occur without some scattering, perhaps by the instabilities considered in this paper. For $\frac{1}{3}$ AU, when $k_0\lambda_e \approx 0.01$, the wave packets can collapse directly, thus bypassing the stage of parametric instability (Nicholson *et al.* 1978).

In recent papers putting forth a theory of type III radio bursts, Smith, Goldstein, and Papadopoulos (1979), and Goldstein, Smith, and Papadopoulos (1979) study rate equations in which a linear instability plays a central role in the transfer of energy out of resonance with the type III electron stream. That instability, which they refer to as the oscillating two-stream instability (OTSI), is supposed to occur for $k \gg k_0$. The fact that we do not find such an instability in our analysis deserves further comment.

The geometry of the purely growing instability is determined by the values of the pump energy and wavenumber, W_0 and k_0. If $W_0 \ll 10(k_0\lambda_e)^2$, as in the present paper, then the instability will have $k \ll k_0$, and have a maximum growth rate perpendicular to the pump wave vector. On the other hand, with $W_0 \gg 10(k_0\lambda_e)^2$ then $k \gg k_0$, and the instability has maximum growth rate along the direction of the pump wavenumber k_0 as in Smith *et al.* Nonetheless, both instabilities rightly have been called oscillating two-stream instabilities, and the failure to distinguish between these two cases has undoubtedly caused some confusion.

In either case, the OTSI involves two Langmuir daughter waves, with wavenumber $\boldsymbol{k}_0 \pm \boldsymbol{k}$ shifted up and down relative to the pump wavenumber, $\boldsymbol{k}_0$. The instability occurs when the upshifted and downshifted waves beat with the pump wave at nearly the same frequency. The frequency mismatch, or the beat frequency, δ_-, for the two waves is

$$\delta_- = -\tfrac{3}{2}(k^2\lambda_e^2)\omega_{pe} + 3(\boldsymbol{k}\cdot\boldsymbol{k}_0\lambda_e^2)\omega_{pe}.$$

In the dipole limit (a), $k \gg k_0$, both daughter waves have nearly the same mismatch because of the small wavenumber of the pump wave, k_0. The threshold for instability is $W_0 > 3(k\lambda_e)^2$ (Smith, Goldstein, and Papadopoulos 1979). Because $k \gg k_0$, this threshold condition implies $W_0 \gg 3(k_0\lambda_e)^2$. In the other limit ($b$), $k \ll k_0$, the mismatch frequencies are made equal when $\boldsymbol{k} \perp \boldsymbol{k}_0$ (Bardwell and Goldman 1976). The fastest growing wavenumber for this instability is given by equation (15). Since the wavenumber k is assumed to be much less than k_0, this requires $W_0 \ll 12(k_0\lambda_e)^2$.

Hence we arrive at the important conclusion that as the pump strength W_0 increases, the OTSI goes from case (b) to case (a). The character of this instability is described in detail in Bardwell's Ph.D. thesis (1976). Although the effect of the magnetic field is to suppress completely the OTSI in the small k limit, in the other limit, $k \gg k_0$, the magnetic field has important, but less drastic effects (Freund and Papadopoulos 1980).

After the completion of this work (Weatherall, Goldman, and Nicholson 1978), we became aware of the related work by Freund and Papadopoulos (1980) which examines magnetic field effects on type III generated parametric instability

at $\frac{1}{3}$ AU for large values of pump energy ($W_0 = 10^{-3}, 10^{-2}$). Because $W_0 \gtrsim (k_0\lambda_e)^2$, they study a regime complementary to ours. However, they ignore the effect of the magnetic field on the low frequency motions. This is not likely to affect their results, since they do not consider waves perpendicular to the magnetic field where we find the effect important. Generally, their work agrees with ours in finding the decay branch to be quite insensitive to a weak magnetic field, except for a shift of unstable wave vectors to smaller perpendicular wavenumbers.

To conclude, the results of the present paper are applicable in the regime [case (*b*)] of relatively low pump energies ($W_0 = 10^{-4}$ and parameters appropriate to a distance of one-third of a solar radius above the Sun's surface). The complementary regime [case (*a*)] of relatively high pump energies has been considered in the work of Smith, Goldstein, and Papadopoulos (1979), Goldstein, Smith, and Papadopoulos (1979), and Freund and Papadopoulos (1980). Which of these regimes is more appropriate will depend upon the detailed parameters of an individual type III solar radio burst. As pointed out by Smith, Goldstein, and Papadopoulos (1979), these parameters can vary over wide ranges from burst to burst.

This work was supported by the National Science Foundation, Atmospheric Research Section under ATM 76-14275 and by the Air Force Office of Scientific Research (M.V.G. and J.C.W.) under contract F49620-76-C-0005. We also thank the National Center for Atmospheric Research, supported by the National Science Foundation, for computer time used in this research. One of us (D.R.N.) was supported by the Atmospheric Research Section, National Science Foundation, grants ATM 78-22487 and ATM 79-18778, and by U.S.D.O.E. grant EY-76-5-02-2059.

REFERENCES

Bardwell, S. 1976, Ph.D. thesis, University of Colorado at Boulder.
Bardwell, S., and Goldman, M. V. 1976, *Ap. J.*, **209**, 912.
Bekefi, G. 1966, *Radiation Processes in Plasmas* (New York: Wiley), p. 236.
Dysthe, K. B., and Pécseli, H. L. 1978, *Plasma Phys.*, **20**, 971.
Freund, H. P., and Papadopoulos, K. 1980, *Phys. Fluids*, **23**, 139.
Fried, B. D., and Conti, S. D. 1961, *The Plasma Dispersion Function* (New York: Academic).
Ginzburg, V. L. 1964, *The Propagation of Electromagnetic Waves in Plasmas* (Reading: Addison-Wesley), p. 120.
Goldman, M. V., and Nicholson, D. R. 1978, *Phys. Rev. Letters*, **41**, 406.
Goldstein, M. L., Smith, R. A., and Papadopoulos, K. 1979, *Ap. J.*, **234**, 683.
———. 1980, *Proc. Symp. Nonlinear Effects in Space Plasmas* (Dordrecht: Reidel).
Kaufman, A. N., and Stenflo, L. 1975, *Phys. Scripta*, **11**, 269.
Kaw, P. K. 1976 in *Advances in Plasma Physics*, Vol. **6** (New York: Wiley).
Krall, N. A., and Trivelpiece, A. W. 1973, *Principles of Plasma Physics* (New York: McGraw-Hill), p. 144.
Montgomery, D. C. 1971, *Theory of the Unmagnetized Plasma* (New York: Gordon & Breach), p. 68.
Nicholson, D. R., and Goldman, M. V. 1978, *Phys. Fluids*, **21**, 1766.
Nicholson, D. R., Goldman, M. V., Hoyng, P., and Weatherall, J. C. 1978, *Ap. J.*, **223**, 605.
Nishikawa, K., Liu, C. S., Kaw, P. K., and Kruer, W. L. 1976, in *Advances in Plasma Physics*, Vol. **6** (New York: Wiley).
Papadopoulos, K., Goldstein, M. L., and Smith, R. A. 1974, *Ap. J.*, **190**, 175.
Porkolab, M., and Goldman, M. V. 1976, *Phys. Fluids*, **19**, 872.
Sanuki, H., and Schmidt, G. 1977, *J. Phys. Soc. Japan*, **42**, 664.
Smith, D. F., and Nicholson, D. R. 1980, in *Proc. Symposium on Nonlinear Effects in Space Plasmas* (Dordrecht: Reidel).
Smith, D. F., and Tsytovich, V. N. 1977, private communication.
Smith, R. A., Goldstein, M. L., and Papadopoulos, K. 1976, *Solar Phys.*, **46**, 515.
———. 1979, *Ap. J.*, **234**, 348.
Thomson, J. J., and Karush, J. I. 1974, *Phys. Fluids*, **17**, 1608.
Weatherall, J., Goldman, M. V., and Nicholson, D. R. 1978, *Bull. A.P.S.*, **23**, 787.

M. V. GOLDMAN and J. C. WEATHERALL: Department of Astro-Geophysics, University of Colorado, Boulder, CO 80309

D. R. NICHOLSON: Department of Physics and Astronomy, University of Iowa, Iowa City, IA 52242

APPENDIX F

F. "Scattering and Collapse of Langmuir Waves Driven by a Weak Electron Beam"

B. Hafizi, J.C. Weatherall, M.V. Goldman, and D. Nicholson
Physics of Fluids 25, 392-401 (1982)

Scattering and collapse of Langmuir waves driven by a weak electron beam

B. Hafizi, J. C. Weatherall, and Martin V. Goldman

Department of Astro-Geophysics, University of Colorado, Boulder, Colorado 80309

Dwight R. Nicholson

Department of Physics and Astronomy, University of Iowa, Iowa City, Iowa 52242
(Received 26 March 1981; accepted 20 November 1981)

The evolution of Langmuir waves predicted by the beam-driven Zakharov equations is studied numerically with high resolution in one and two dimensions, for parameters appropriate to type III solar radio bursts at 0.5 a.u. It is found that collapse is preceded by momentum transfer to ion-acoustic quasimodes even in the absence of a weak solar magnetic field. The early evolution is similar in one and two dimensions. A zero momentum condensate forms in both cases, but its subsequent behavior differs in one dimension and two dimensions. The corresponding real-space wave packets collapse rapidly in two dimensions, but evolve as slowly growing solitons in one dimension. Detailed comparisons are made with other one-dimensional models of "strong" Langmuir turbulence associated with type III bursts.

I. INTRODUCTION

In principle, there are two classes of nonlinear phenomena which can saturate Langmuir waves driven unstable by a warm ("bump-on-tail") electron beam; wave-particle interactions and wave-wave interactions. In the former, the back reaction of the resonant "beam-modes" on the beam electrons can lead to plateau formation. This is treated by various versions of quasilinear theory. In the case of wave-wave interactions, energy is spread from the resonant beam modes to nonresonant modes by stimulated scattering off background ions[1] or ion-acoustic waves,[2] and by nonlinear self-focusing effects such as modulational instability[2-4] and collapse.[5-7] The so-called Zakharov equations[3] can be used to treat all of these wave-wave interactions simultaneously.[2] In the present paper, we shall be concerned with the interplay between the various wave-wave interactions, and its significance for the Langmuir turbulence associated with type III solar radio emissions.[8-12]

In the Zakharov equations, low-frequency ion-acoustic waves are driven by the ponderomotive force associated with Langmuir waves. This is described by a hydrodynamic equation for the low-frequency density, in which the ponderomotive force acts as a source term. The resulting modulations in the density cause nonlinear refraction in the Langmuir waves. This is described by a nonlinear Langmuir wave equation, in which we also employ the approximation of a purely electrostatic high-frequency field having a slowly varying envelope. For our purposes, therefore, the Zakharov equations are two coupled nonlinear partial differential equations for the low-frequency (ion) density and for the Langmuir envelope.

In the cases of interest to us, the electron and ion temperatures are assumed to be equal. This means ion-acoustic waves are heavily damped by ion Landau damping, and should, more properly, be called ion-acoustic quasimode. We therefore insert a strong phenomenological damping into the ion-acoustic equation. One of the nonlinear effects then contained in the Zakharov equations is the induced scattering of a Langmuir wave off such an ion-acoustic quasimode into another wave.[2] The scattered wave may be backward or forward in relation to the first, but it always loses momentum to the quasimode in the process. It can be shown that scattering off such ion-acoustic quasimodes is roughly equivalent[2] to scattering off discrete ions (which requires a kinetic equation for the ion distribution function). Another name for the latter phenomenon is "nonlinear Landau damping off ions," while the former is sometimes called a parametric decay instability. We shall use all these terms interchangeably, since we have assumed equal electron and ion temperatures.

Induced scattering off ions forms the basis for what is sometimes called "weak turbulence" theory. A group of unstable or large amplitude waves, centered narrowly around a wave vector, k_0, undergoes a cascade of scatters toward lower wavenumbers $k < k_0$. If there is enough linear dissipation, the cascade stops, a steady state develops, and the instability saturates. When the phases of the various modes are random, this is an example of saturation by a weak turbulence process.

If there is not enough linear dissipation, energy accumulates at very small wavenumbers into a "condensate."[5] When the condensate has enough energy (relative to its square width, Δk^2), it can spill out to higher wavenumbers by means of modulational interaction (which is the basis for "strong turbulence" theory). This process has a simple interpretation in coordinate space. The wave packets associated with the condensate cause density cavities to develope due to ponderomotive force. The resulting self-focusing leads to the spatial collapse[5-7] of the packets to dimensions which may be on the order of several Debye lengths. The Fourier components of such a narrow wave packet now see heavy Landau damping, because k is on the order of the Debye wavenumber k_D. Hence, by this circuitous route, a steady-state saturation of the original instability may be possible.

 0031-9171/82/020392-10$01.90 © 1982 American Institute of Physics

Many aspects of this sequence of processes are still quite controversial. However, the cascade-collapse sequence has been confirmed[13] by two-dimensional numerical solutions to the Zakharov equations, for the case when the "pump" waves around k_0 are assumed to have initial amplitudes much larger than the noise level of other modes. In these studies, the pump waves were not driven by any linear instability, such as beam instability. We shall refer to such cases as "undriven." In the undriven cases studied, k_0 was chosen to be large enough so that many (back and forth) scatterings were possible in the cascade. The condition for this is $k_0 \gg (m/M)^{1/2} k_D$, where m/M is the electron to ion mass ratio. This condition is equivalent to the requirement that the group velocity of the pump waves be much larger than the ion-sound speed.

In other[5] two-dimensional numerical studies with the Zakharov equations, a different mode of behavior was observed for an undriven group of pump waves around $k_0 \sim (m/M)^{1/2} k_D$. When the initial energy density in the undriven pump waves was made sufficiently large, a direct collapse of the associated real space wave packets occurred. Such direct collapse was enabled, in principle, because the group velocity of the pump wave packets was less than the ion-acoustic speed, so the nonlinearly refracting cavity of density could keep pace with the packet. Direct collapse occurred even though one final induced-scatter off ions was still kinematically possible (in the forward direction, due to the low value of k_0).

A theory for direct collapse of an initial undriven broadband pump was developed,[6] using the approximation of adiabatic ions, in which particle pressure is assumed to be balanced by ponderomotive force. The theory predicted the collapse threshold pump energy density, $W = |E|^2/4\pi n\theta$ (in units of the background electron energy density $n\theta$), in terms of the pump bandwidth, Δk: $W_{th} = 48(\Delta k)^2$. This threshold condition is approximately satisfied for the numerical studies which showed undriven direct collapse (e.g., Fig. 1 of Ref. 6), although the adiabatic approximation is not strictly satisfied, due to momentum transfer to ions.

The further claim was made[8,6] that direct collapse also occurs when beam-modes (centered about $k_0/k_D = 0.01$) are driven by the weak electron beams associated with type III bursts at 0.5 a.u. The argument was based on numerical integration of the Zakharov equations which seemed to show[8] that the weakly driven beam modes grew to an energy density two or three times the collapse threshold, and that afterward direct collapse occurred exactly as in the undriven problem. However, subsequent studies[14] included a weak background solar magnetic field, and showed that direct collapse was slowed down sufficiently by magnetic effects so that substantial induced scatter off ions did have time to occur, and prevented direct collapse. The relevance of direct collapse for the physical conditions of the type III problem was therefore significantly diminished.

We seek to establish in this paper that even for nonmagnetic conditions under which a driven direct collapse was thought to be possible, a substantial buildup of scattered waves occurs at small wavenumbers. The observed collapse is associated with this "condensate" of wave modes, rather than the beam-resonant modes. The interpretation is more in line with earlier[5,13] pictures of cascade followed by collapse. However, there are additional unexpected nonlinear effects present, such as long-time phase coherence of wave packets and a continual loss of momentum to ions. In addition, the final condensate is centered around zero k, rather than the wavenumber associated with induced scatter (a result also found in Ref. 13).

We begin with a two-dimensional numerical solution to the beam driven Zakharov equations for a case when $k_0 \gg k_D < (m_e/m_i)^{1/2}$. The choice of physical parameters is motivated by the type III problem at 0.5 a.u. The qualitative behavior in this simulation is not different from previous studies,[8] but the improved time and spatial resolution make it possible to follow the collapse of the wave packets for longer times than before, and identify a migration of the Langmuir spectrum toward smaller wavenumbers. The major point of this paper is that the depletion of the beam-resonant (pump) waves is due to scattering off ions, rather than collapse.

In order to support the interpretation of the results we solve the same Zakharov equations in one dimension. The time scales and energy densities in one dimension are found to be comparable to the two-dimensional case during the early time evolution, even though collapse is not seen. This means that the scattering instabilities (which occur predominantly in one dimension) must have a significant role in the saturation of the beam-plasma instability.

We give another solution in one dimension, representing the limit of adiabatic ions for which the Zakharov equations reduce to a nonlinear Schrödinger equation. The purpose of this example is to demonstrate the role of ions in the scattering of the Langmuir pump waves to smaller k modes.

After the condensate has formed, there appears to be a difference between the further time development in one and two dimensions. In one dimension we see real space solitons intensifying on the time scale of the beam growth rate, whereas in two dimensions the solitons are collapsing unstably at a rate which is an order of magnitude faster, for as long as we are able to follow them. There are theoretical reasons[11,15] to expect collapse to depend strongly on dimensionality in certain limits, but this problem requires further numerical study.

The plan of this paper is as follows: In Sec. II we set up the basic equations and describe the initial conditions and boundary conditions, which are appropriate in the type III problem at 0.5 a.u. In Sec. III, we present a two-dimensional numerical solution of the Zakharov equation. Section IV is devoted to the one-dimensional Zakharov equation for both the adiabatic and nonadiabatic cases. These examples serve to clarify the roles of the various nonlinear processes identified in the two-dimensional solution. In Sec. V we elaborate on the limitations of one-dimensional

solutions to the Zakharov equations. The implications of our results for various aspects of type III theory are described in Sec. IV. Finally, in Sec. VII, we discuss how our work and conclusions differ from the one-dimensional statistical theory of Smith, Goldstein, and Papadopoulos[16,17] in the context of the type III emission problem.

II. EVOLUTION OF NONLINEAR LANGMUIR WAVES

The starting point in studying nonlinear Langmuir waves is Zakharov's equations

$$(i\partial_t + i\nu_e + \nabla^2)\nabla\cdot\mathbf{E} = \nabla\cdot n\mathbf{E}\,, \tag{1}$$

$$(\partial_t^2 + \nu_i\partial_t - \nabla^2)n = \nabla^2|\mathbf{E}|^2\,, \tag{2}$$

where $\mathbf{E}(\mathbf{x},t) = -\nabla\phi$ is the low frequency envelope of the assumed longitudinal Langmuir field: $\mathbf{E}_L(\mathbf{x},t) = \mathbf{E}(\mathbf{x},t) \times \exp(-i\omega_{pe}t) + \text{c.c.}$, and n is the perturbation on the background ion density, n_0. The units of time, length, density, and electric field in our dimensionless notation are

$$[t] = \frac{3}{2}\frac{1}{\eta}\frac{m_i}{m_e}\omega_{pe}^{-1}\,,$$

$$[x,y] = \frac{3}{2}\left(\frac{1}{\eta}\frac{m_i}{m_e}\right)^{1/2}\lambda_e\,,$$

$$[n] = \tfrac{4}{3}\eta(m_e/m_i)n_0\,,$$

$$[E] = \eta\left(\frac{m_e}{m_i}\right)^{1/2}\left(\frac{16\pi n_0 T_e}{3}\right)^{1/2}\,,$$

where the plasma frequency is given by $\omega_{pe} = 4\pi n_0 e^2/m_e$, the electron Debye length is $\lambda_e = (T_e/m_e\omega_{pe}^2)$, and the dimensionless ratio $\eta = (\gamma_e T_e + \gamma_i T_i)/T_e$. The ratio of ion- to-electron mass is $m_i/m_e = 1836$; T_e and T_i are the temperatures and γ_e and γ_i are the ratios of specific heats for the electron and ion gas. Although these equations describe complicated wave-wave behavior, they do not include particle-wave effects except in the phenomenological damping terms, ν_e and ν_i.

In order to simulate Langmuir wave phenomena during type III solar radio bursts at 0.5 a.u., we solve Eqs. (1) and (2) by the split-step Fourier method on a finite grid.[8,18,19] The computation is set up as follows. The beam unstable modes are centered at $k_0\lambda_e = 0.011$, with a finite bandwidth Δk_x and Δk_y (x is parallel to the beam and k_0; y is in the transverse direction). The beam plasma instability is simulated by transforming Eq. (1) into k space and using a negative damping rate,[8,20] $-\nu_e/\omega_{pe} = 10^{-6}$, for the appropriate k modes. Other relevant parameters are: $T_e \sim T_i = 20$ eV, $\omega_{pe} = 4\times10^5$ sec^{-1}, $n_0 = 50$ cm^{-3}, $\lambda_e = 470$ cm, $\eta = 2$. Except for the beam unstable modes, the plasma wave damping is $\nu_e = 0$; $\nu_i = 2kc_s$, corresponding to heavily damped ion-acoustic modes. Initially, all of the plasma wave modes are given some small, randomly phased amplitude (noise).

III. SIMULATION IN TWO DIMENSIONS

In our two-dimensional calculation, we use a 64×64 point grid, with $\Delta k_x = (1/6)k_0$ and $\Delta k_y = (1/2)k_0$. First, we present the history of the wave energy density during the simulation which shows that the wave processes contained in Eqs. (1) and (2) can effectively decouple the system from the beam. In Fig. 1 we plot two curves which show the total energy density in the system and the energy density in the beam-driven modes. W is a dimensionless ratio, $\langle W\rangle = \langle|E(x)|^2\rangle/4\pi n_0 T_e$, where $\langle|E|^2\rangle$ denotes a spatial average of $|E(x)|^2$. Remember that the beam modes are being pumped throughout the run at a constant rate. These modes grow linearly at early times until they saturate at energy $\langle W\rangle_p \sim 10^{-5}$. At later times these pump modes experience a drastic loss of energy due to nonlinear wave processes. The rate of energy transfer to the plasma waves depends upon the term $\nu_e E$. With the pump modes severely depleted the energy input into all waves is practically cut off, leading to the saturation of the total energy in Langmuir waves. We are still not seeing a fully-developed steady-state turbulence, because we have not included Langmuir wave dissipation. (Note that the total wave energy has a slight positive slope.) A major unanswered question is whether, given enough time and accuracy, the energy grows to a significantly higher level.

Let us examine, in detail, the wave behavior at three times t_1, t_2, and t_3, as indicated in Fig. 1. The behavior at these times is representative of the variety of nonlinear phenomena observed in the simulation.

At time t_1, we observe wave packets propagating at $0.025c_e$, slightly less than the group velocity of the beam resonant waves, $v_{gr} = 3(k_0\lambda_e)v_e = 0.033v_e$, as shown in the sequence of pictures in Fig. 2(a). The time between frames is $0.07\times10^6\,\omega_{pe}^{-1}$, and the spatial width of the frame is $3.7\times10^3\,\lambda_e$. Therefore, a thermal electron traveling at speed v_e will traverse the horizontal length of the frame 18.5 times in the interval between frames. Because the grid is periodic, a wave which exits one side of the grid will reappear on the opposite side.

The wave packet in Fig. 2(a) does not behave accord-

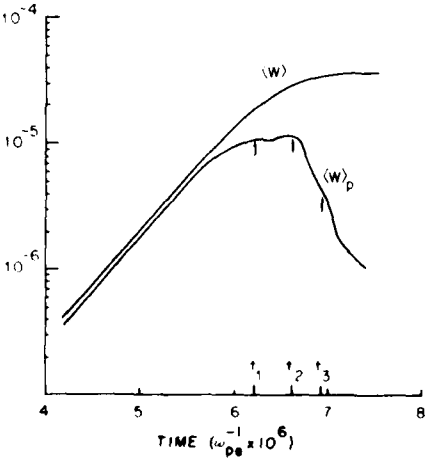

FIG. 1. Energy density in the pump resonant modes, $\langle W\rangle_p$, and total energy density $\langle W\rangle$ during the two dimensional simulation of a type III burst at 0.5 a.u.

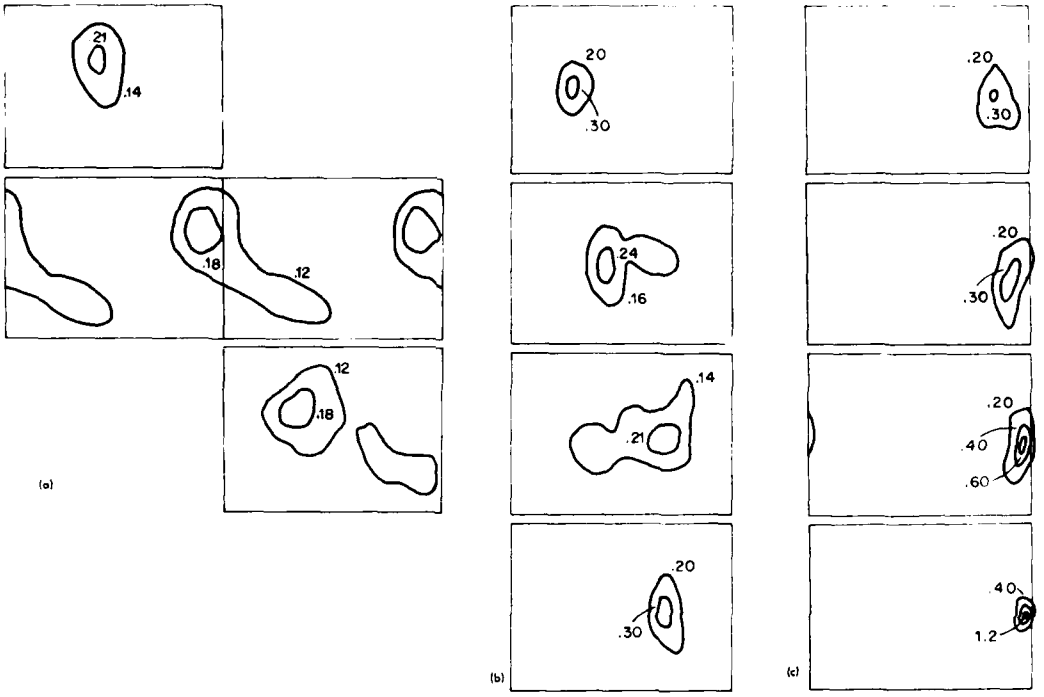

FIG. 2. Successive time snapshots of contours of constant electric field amplitude $|E|$ in real $(x\text{-}y)$ space during nonlinear phases of type III Langmuir wave interaction. (a) coherent wave propagation near time t_1; (b) decay instability near time t_2; (c) Langmuir collapse near time t_3. Amplitude labels are in dimensionless units $[E]$.

ing to the rules of linear waves. Because of thermal dispersion, this wave packet should "disperse" on time scales of

$$\tau \sim \left(\frac{2}{L^2}\frac{d^2\omega_0}{dk_0^2}\right)^{-1} \sim \frac{1}{3}\frac{L^2}{\lambda_e^2}\,\omega_{pe}^{-1} = 8\times 10^4\omega_{pe}^{-1}\,, \tag{3}$$

where the width of the wave packet is about $L = 500\,\lambda_e$. Clearly, it persists longer than this time. The reason is that nonlinear forces are very important. A calculation shows that this wave packet, with central amplitude, E_0, is just at the threshold for collapse[6] (for adiabatic ions in an infinite plasma):

$$\frac{|E|_{th}^2}{2\pi n_0(T_e + T_i)} = 48\left(\frac{L^2}{\lambda_e^2}\right) = 1.5\times 10^{-4}\,, \tag{4}$$

whereas

$$|E_0|^2\ 2\pi n_0(T_e + T_i) = 1.7\times 10^{-4}\,. \tag{5}$$

For energy values near threshold, the collapse time[6] can be very long

$$\tau_c = \frac{1}{2}\frac{\lambda_e}{L}\left[\left(\frac{|E|^2 - |E|_{th}^2}{2\pi n_0(T_e + T_i)}\right)\right]^{-1}\omega_{pe}^{-1} = 3\times 10^5\omega_{pe}^{-1}\,. \tag{6}$$

The k-space distribution of wave amplitude at time t_1, shown in Fig. 3(a), indicates that wave energy is being transferred from the pump modes into neighboring modes in k space. This broadening in k space can correspond to the nonlinear steepening of wave packets in real space. Although we may be seeing the beginning of a direct collapse, it is relatively slow, and does not have time to develop. Part of the reason is the instability which affects the packets by the time t_2.

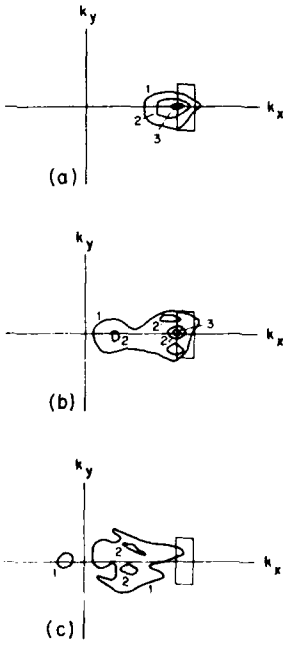

FIG. 3. Contours of electric field amplitude in k space at times (a) t_1, showing collapse broadening, (b) t_2, showing the parametric excitation of particular wave modes, and (c) t_3, showing the formation of a condensate. Contour labels indicate relative amplitude. The rectangular box shows the pump (beam unstable) modes centered at $k_0\lambda_e = 0.011$.

At time t_2, which marks the precipitous depletion of the pump waves, there are discrete modes which have enhanced amplitudes [see Fig. 3(b)]. These are identified with modulational and scattering instabilities. For example, induced scattering off ion-acoustic quasimodes is known[2,3] to occur for waves with Langmuir wavenumber and maximum growth rate

$$k_L\lambda_e = -k_0\lambda_e + (4\eta m_e/27m_i)^{1/2},$$
$$\gamma = 3^{3/2}W_0/16\eta\omega_{pe}. \tag{7}$$

(These formulas assume a monochromatic pump.) The feature we see in Fig. 3(b) at $k_L\lambda_e = 0.002$ is due to this instability. The observed growth rate of this mode, approximately $5\times10^{-6}\,\omega_{pe}$, is consistent with the theoretical growth rate γ when $W_0 \sim \langle W\rangle_p = 10^{-5}$. The instability growth time is comparable to the collapse time given in Eq. (6).

The two contours which are off the x axis in Fig. 3(b), appear to be the modulationally unstable waves studied by Bardwell and Goldman.[2] We note that the beam-modes pump these waves in a forward cone, rather than at high backward and forward wave vectors in one dimension, as suggested by Smith, Goldstein, and Papadopoulos.[16] The forward cone geometry of the modulational instability is only transformed into the backward-forward geometry at much smaller pump wavenumbers (where the "dipole" approximation is valid), or much larger pump energy densities. In this limit, another pseudonym for the modulational instability becomes appropriate; the "oscillating two-stream instability."[3,4,16] Theory[2] predicts the same growth rates for the modulationally unstable waves as for the waves which have undergone induced scattering. This is in accord with Fig. 3(b). The modulationally unstable waves are predicted[2] to occur at $k_L\lambda_e \sim (W_0/12)^{1/2} \sim 1.6\times10^{-3}$, also in rough agreement with Fig. 3(b). Although this is the first time the forward cone modulational instability has been found to be excited by a broadband spectrum of beam-driven pump modes, the immediate subsequent evolution of the Langmuir waves appears to be dominated by the induced scatter (decay) instability.

A sequence of wave packet configurations in real space at this same time t_2 is shown in Fig. 2(b). The wave packet is now traveling with a mean group velocity which is much slower than before. This corresponds to the lower centroid of wavenumbers if we make the identification $v_g \sim 3(k\lambda_e)v_e$. The wave packet suffers some distortion, which may be associated with the instabilities, but then appears intact again in the final frame. The coherence of the packet is rather remarkable. The location of a packet in real space depends on a particular set of (random) phase of the modes in k space, whose interference pattern produces the real space packet. The tendency of the packet to stay together may be evidence that there is no phase shift associated with the scattering process.

Subsequent to time t_2, and up to the time t_3, we see a catastrophic collapse [Fig. 2(c)] until the length scale becomes too small for the grid. The collapsed wave packet continues to lose momentum until it appears nearly stationary. Wave energy is distributed in a very large region of k space, including backward traveling waves, as shown in Fig. 3(c).

From the example given here, we can conclude that the collapse of growing broadband pump waves does not occur fast enough compared with the secondary parametric instabilities excited. In fact, the scattering (decay) instability seems to be very important in depleting the pump modes. While the inclusion of collapse has been a principal motivation for doing the calculation in two dimensions, the scattering instability is predominantly one-dimensional. To find out how well a simpler, one-dimensional model can do in this problem, we repeat the simulation in one dimension.

IV. SIMULATION IN ONE DIMENSION

For the same parameters, the one-dimensional calculation uses a discrete system of 128 modes, with three pump modes and $\Delta k \sim k_0/3$. The results allow a similar interpretation as in the previous case. During the linear growth phase, the pump waves are enhanced in amplitude, as shown in the k space spectrum in Fig. 4(a). At a later time, the k space spectrum has evolved into that of Fig. 4(b). First, we note that the pump modes, instead of being of equal amplitudes, have developed a peak on the lower wavenumber side. Second, the pump modes have caused the amplitude in adjacent modes to grow. This is similar to the collapse-like broadening also observed in two dimensions. Finally, the broad feature near the origin of k space is apparent, and is due to the scattering (decay) instability.

At the time that the decay instability becomes prevalent, the pump modes deplete rapidly, as shown in Fig. 5. The saturation of total energy is at about twice the level given in Fig. 1 for the two-dimensional case.

Figure 6(a) shows the envelope waves in real space at the time corresponding to the depletion of the pump waves. Collapse is not occurring as it did in two dimensions, but a modulational interaction[1,2,11,12] is beginning to produce shorter length scales. The condition for this process is $W \sim \xi(\Delta k\lambda_e)^2$, where Δk is the wavenumber spread in the Langmuir waves and ξ is a number of order unity. At the time of Fig. 6(a), this inequality is marginally satisfied with $W \sim 6\times10^{-5}$ and $(\Delta k\lambda_e)^2 \sim 5\times10^{-5}$ (the scattering instability has broadened the k-space spectrum to such an extent that the bandwidth of the beam-modes is irrelevant). Therefore, the formation of caverns is energetically possible. Still, we expect the transfer of energy to short wavelengths to proceed rather slowly since the condition for the modulational instability is only marginally satisfied. At a much later time, soliton-like structures have formed as in Fig. 6(b).

Is the rapid depletion of the pump truly due to the scattering (decay) instability of the Langmuir pump waves? One way to approach this question is to use a version of the wave equations (1) and (2) which assures that no momentum be lost to the ions. A nonlinear Schrödinger equation,

$$i\partial_t E + i\nu_e E + \nabla^2 E + E^2 E = 0, \tag{8}$$

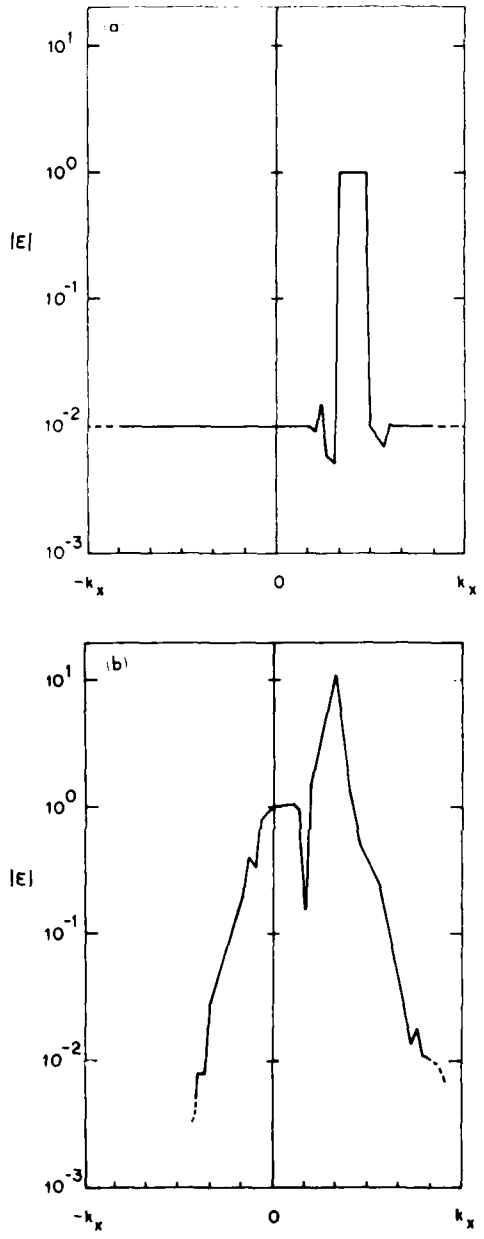

FIG. 4. Electric field amplitude in k space during the one-dimensional simulation at times (a) $T = 4.6 \times 10^6\ \omega_{pe}^{-1}$, showing the enhancement of the pump modes, and (b) $T = 6.7 \times 10^6\ \omega_{pe}^{-1}$, showing many of the same features seen in Fig. 3(b). The amplitudes of 60 wave modes centered at zero are shown. The largest wavenumber k_x is $0.025\ \lambda_e^{-1}$.

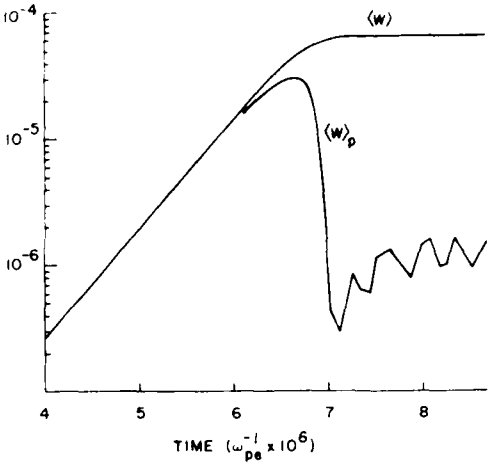

FIG. 5. Energy density in the pump resonant modes, $\langle W \rangle_p$, and total energy density $\langle W \rangle$ during the one-dimensional simulation.

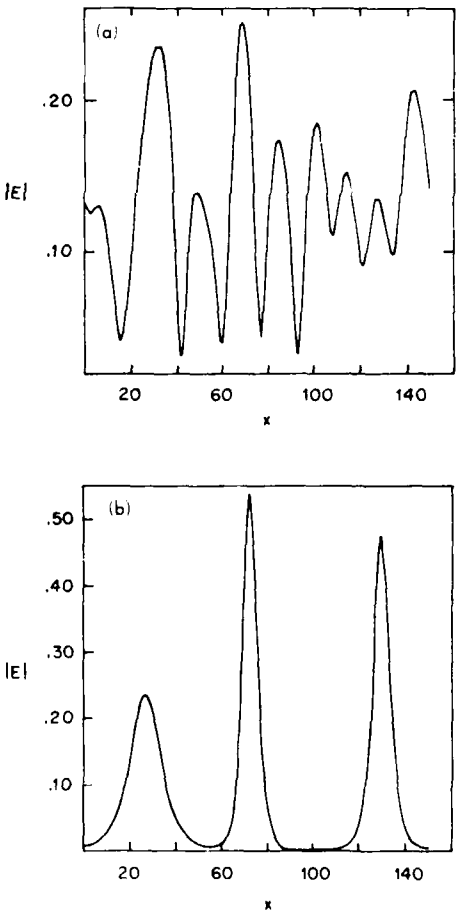

FIG. 6. Electric field amplitude in real space during the one-dimensional stimulation at times (a) $T = 6.9 \times 10^5\ \omega_p^{-1}$ and (b) $T = 9.9 \times 10^5\ \omega_{pe}^{-1}$, spanning several beam growth time scales. Labels are in the dimensionless units [E], [x]. In dimensional units, $x = 100$ corresponds to $4500\ \lambda_e$.

is obtained from Eqs. (1) and (2) by neglecting the time derivatives in the ion mode equation (the adiabatic approximation), and therefore it excludes the scattering (decay) instability. Analytic work[6,14] on direct collapse has been in the context of this equation. By solving Eq. (8) in one dimension for our choice of parameters at 0.5 a.u., we find that with the transfer of energy from pump modes into neighboring k-space modes, the pump energy saturates, but does not deplete (see Fig. 7).

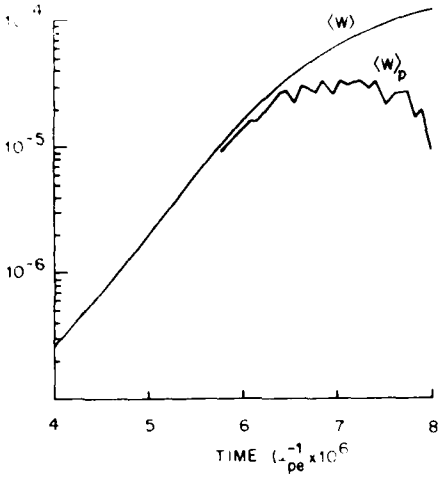

FIG. 7. Energy density in the pump resonant modes, $\langle W\rangle_p$, and total energy density $\langle W\rangle$ during a one-dimensional simulation using Eq. (8) instead of Eqs. (1) and (2).

Therefore, the depletion of the pump modes must be associated with the scattering (decay) instability.

V. DISCUSSION

The interpretation of the role of parametric instability given here derives from more detailed two-dimensional numerical simulations than were previously available, and is reinforced by a direct comparison of one- and two-dimensional models. As was explicitly pointed out, the earlier two-dimensional models[8] of direct collapse were limited by the eventual breakdown of energy conservation; the loss of energy in the system was attributed to the loss of wave energy into parts of the grid where it was subtracted by aliasing.[23] Those runs were also done on a 32×32 grid. A more efficient algorithm now available enables the more accurate (smaller time step) simulation on a 64×64 grid presented here. The results are very similar up to the point where the earlier runs become limited by numerical errors. Our present simulations are not limited by the accumulation of errors, but the finite number of modes available in the grid. Collapse does not proceed past the last frame in Fig. 2(c), because it has already reached the size of the grid spacing. However, there are no evident losses in energy. Because of these these facts, the simulation in this paper must have more value in interpreting the wave behavior at later times when collapse, scattering instability, and numerical limitations occur in short order. In particular, we can now conclude that the distortion of a wave packet such as seen in Fig. 2(b) is due to the scattering (decay) instability, and not a change in the physics of direct collapse due to an artificial numerical damping.

Our interpretation is also facilitated by the choice of $\Delta k_x = (1/2)\Delta k_y$. This is about half the bandwidth of the previous work,[8] and is designed to model the beam unstable modes more accurately. As it turns out, the evolution of the pump modes experiences a more prolonged "saturation," as exhibited by the plateau of W_p in Fig. 1, in comparison with the case $\Delta k_x = \Delta k_y$ studied previously.[8] This enables the identification of a saturation and depletion phase as a distinct physical process. Nonetheless, it appears that the inhibition of direct collapse and the final level of total energy saturation are not sensitive to the bandwidth of the pump. (We have verified this for the case previously studied,[8] in which $\Delta k_x = \Delta k_y = k_0/6$.)

Although the one-dimensional model was adequate to describe the decay instability and the subsequent depletion of the pump waves, the behavior during the "collapse" is markedly different from the two-dimensional model. For example, the localized structures appearing in Fig. 6 slowly steepen on the time scale of the beam growth, involving some 10^3 plasma periods. The two-dimensional collapse shown in Fig. 2(c) is much faster in comparison, occurring in 10^2 plasma periods. The problem with the one-dimensional calculation is that it allows wave packets to evolve into "solitons." Solitons are exact solutions to the wave equation with the form

$$E = [(1-V^2/2)]^{1/2}\sqrt{\nu}\,\mathrm{sech}\,\sqrt{\nu}\xi\,\exp[i(k_0 x - \omega_0 t)],$$
$$\xi = x - Vt, \quad \nu = (k_0^2 - \omega_0), \quad V = 2k_0. \tag{9}$$

For instance, with the choice of $\sqrt{\nu} = 0.37$ and $V = 0$, this solution describes the central spike in Fig. 6(b) very well. These one-dimensional soliton solutions are not physical, because they are not stable in higher dimensions.[15,24,25] They continue to steepen here because energy is being added to the system by means of the beam instability. The time scale for their evolution is related to the beam growth rate γ by

$$\tau^{-1} \sim \gamma\,(W/W_p), \tag{10}$$

where W_p is the energy in the pump modes, and W is the total energy in the soliton. This time is longer than the collapse time scale given by Eq. (6) and demonstrated by the two-dimensional simulation. Therefore, beyond the depletion of the pump by the scattering instability, the one-dimensional calculation becomes physically inaccurate. A two- or three-dimensional model is necessary to include the dissipation of energy through Landau damping of collapsing waves. Such a process may be relevant to the establishment of a fully developed turbulent state.

The two-dimensional simulation described here have also been done with a background magnetic field.[13,26] The magnetic field cannot justify a one-dimensional treatment because it does not prevent collapse transverse to the field.[27] However, up to the point when collapse occurs, the magnetic simulations appear almost one-dimensional because of the effect on the collapse time and on the scattering instability.[26,28] In this problem, there can be magnetic effects even when the electron cyclotron frequency is as small as $\omega_{ce} = 0.01\,\omega_{pe}$, which is a realistic value at 0.5 a.u. For $\omega_{ce} = 0.03\,\omega_{pe}$, the saturation level of electrostatic energy is similar to the one-dimensional value.

VI. EFFECTS ON TYPE III EMISSION

The fact that scattering of beam-modes into a low-k condensate precedes collapse may have important

consequences for the type III solar burst problem.

First, we note that the beam-driven modes are remote from the condensate, and the rate of injection of energy into the condensate is, therefore, very slow once the beam modes are depleted. In fact, the region of k space where the scattered waves accumulate is the negative slope region of a realistic type III burst bump-on-tail beam. In this region the beam should absorb Langmuir waves rather than emit them.

Second, the waves at the plasma frequency cannot remain predominantly electrostatic, unless the spread in wavenumber Δk is much less than k_0, the mean wavenumber.[6] Since this is not the case for the condensate, a large electromagnetic component near ω_p may develop. Such a mechanism could be responsible for type III burst emission near the plasma frequency.

Third, calculations[10,12,30] of electromagnetic emission which involve beam parameters must be viewed critically if collapsing wave packets are decoupled from the beam as a result of their low group velocity. For example, Hafizi and Goldman,[12] taking as their premise the earlier work[6,3,10] on direct collapse, represent the electric field by a scalar function $\varphi(r,t)$, by writing

$$E(r,t) \sim \hat{k}_1 \varphi(r,t) \exp(ik_0 \cdot r) . \tag{11}$$

This requires that the spatial variation of φ be small compared with the phase term. If wavenumbers tend to zero as a result of decay and modulational processes before the collapse occurs, then not only does the use of the beam resonant wavenumber k_0 seem inappropriate, but the electrostatic approximation breaks down, and the use of a scalar field cannot be justified directly. We do not know how these changes will affect the results of the emission calculation.

Finally, it is possible that the background solar magnetic field plays a prominent role during the early time evolution of the condensate. This is because, at such low wavenumbers, magnetic dispersion is much larger than thermal dispersion in the Langmuir wave dispersion relation, even for the very weak solar magnetic field at 0.5 a.u.

All of these effects are currently under study.

VII. COMPARISONS WITH OTHER MODELS OF "STRONG" LANGMUIR TURBULENCE IN TYPE III BURSTS

Smith and his co-workers[4,16,17] have studied the type III problem in one dimension, extensively. Their approach is to use phenomenological rate equations for the average spectral energy density W_k in one-dimensional k space. This is different from our method of solving the Zakharov equations. In both cases the saturated energy density in Langmuir waves occurs at similar levels, $\langle W \rangle \sim 10^{-4}$, despite the difference in parameters, spectral shapes, and physical mechanisms. This may be the results of comparable roles of parametric instability on the evolution of the pump waves.

In the work of Smith *et al.*,[16,17] the following physical processes are represented by rates in one dimension: growth of beam modes by a beam distribution based on *in situ* observations at 1 a.u., the oscillating two-stream instability, anomalous absorption of Langmuir waves by ion density fluctuations, and Landau damping by solar wind electrons.

An example of a type III burst simulation at 0.5 a.u. is given in Figs. 4(a)–(c) of Ref. 17, although the value of beam number density is $n_b/n = 5\times10^{-6}$, which is much larger than our choice of $n_b/n = 10^{-6}$. (Generally, their values of n_b/n are 5 to 100 times larger than ours.) The beam resonant modes grow up around $k_0\lambda_e \sim 0.01$, and have a width $\Delta k/k_0$ of about 10%. When the energy density $\langle W \rangle_p$ exceeds 3×10^{-5}, there is a transfer to higher wavenumbers (more than five times larger than the pump wavenumber) by the oscillating two-stream instability. This spectrum is stabilized by anomalous absorption of Langmuir waves due to ion density fluctuations, and Landau damping by solar wind electrons.

We have the following comments regarding these results:

(1) The induced scatter off ions, or decay instability, which we find dominates the early time evolution of Langmuir waves, is explicitly neglected. This neglect is based on an estimate (Ref. 16, p. 354) for the threshold of the decay instability. Nonetheless, our numerical experiments in one and two dimensions of the beam-driven Zakharov equations consistently support the appearance of this instability, and at the same time do not exclude *a priori* oscillating two-stream instabilities [see, for example, our Fig. 3(b)] and the associated explanation]. This discrepancy in the nature of the parametric instability has been addressed over a period of many years by both groups.[2,4,14,16] We believe that the decay instability occurs for relatively weak beams ($n_b/n \lesssim 10^{-6}$) and low pump wave energy. The dipole limit of the oscillating two-stream instability seems to be appropriate only for strongly pumped waves.

To some extent, the saturation of the beam driven waves does not appear to be sensitive to the nature of these instabilities. It turns out that the threshold used for the oscillating two-stream instability is of the same order as the threshold we observe for the decay instability. The transfer of energy out of the beam modes when $\langle W \rangle_p \sim 3\times10^{-5}$ is common to both models. The difference is that while the oscillating two-stream instability transfers energy directly to larger wavenumbers, the decay instability precipitates the formation of a condensate, which then collapses to produce large wavenumbers. Although it may appear that after the condensate forms at early times the two models effectively approach the same state, we are concerned that the following differences between the oscillating two-stream instability and the collapse of the condensate may be important: first because of the momentum transfer to ions or ion-acoustic quasimodes, the

condensate has zero momentum, not the momentum of the beam modes; second, the beam modes are driven locally, whereas the condensate is driven nonlocally (in k space).

(2) We have shown the limitation of a one-dimensional treatment of the condensate, and found the time scale for k-space broadening to be characteristic of the beam growth rate. This is an order of magnitude slower than the evolution of the condensate which we observe in two dimensions and associate with Langmuir collapse in real space. This limitation of a one-dimensional treatment has been recognized by other workers[31,32]; the usefulness of one-dimensional simulation has nonetheless been demonstrated in some cases, particularly for strongly pumped turbulence. For the example in this paper, the one-dimensional treatment is adequate only for the initial stages of the wave evolution.

(3) Smith *et al.*[16] are able to fully stabilize the beam instability by a combination of anomalous absorption and Landau damping, after the Langmuir spectrum has spread to higher wavenumbers. Our calculations are stopped at much lower wavenumbers because of expected inaccuracies in the numerical technique (even with the improvements that have been built into the present codes). Thus, we have only studied the early, and perhaps transient, phase of what may or may not be an eventual steady state. Landau damping at large wavenumbers, not included in our code, will undoubtedly play an important role. We point out that the anomalous absorption considered by Smith *et al.* is fully contained in the Zakharov equations with no additional terms needed. In fact, it is possible to derive the anomalous absorption term formally from the Zakharov equations by assuming that there exists a mean Langmuir field and ion density which are coherent over long times and distances, and by averaging over short wavelength, fast fluctuations.

(4) The kind of coherence that we find to be occurring in Langmuir wave packet collapse, and even in the scattering (decay) instability, cannot be found with a statistical theory, and may not be consistent with assumptions such as the random phase approximation. Real space wave packets cannot be constructed without phase information, nor can collapse be inferred unambiguously from the spectral information yielded by a statistical theory. We therefore believe there is particular value in performing the kind of detailed analysis of the dynamical wave equations studied in this paper.

The most relevant systematic statistical treatment to date is that of DuBois and Rose,[33,34] who apply the direct interaction approximation directly to the one-dimensional Zakharov equations, and address problems such as the self-consistent renormalizations of response functions and correlation functions, closure (the handling of higher order correlation functions), intermittency, and the existence of mean fields. They stress the importance of the behavior of a zero wavenumber condensate, and show that only a fully renormalized statistical theory can treat the highly nonlinear behavior of the condensate.

ACKNOWLEDGMENTS

We would like to acknowledge helpful conversations with D. F. Smith and D. F. DuBois.

This work was supported by the National Aeronautics and Space Administration Grant No. NAGW-91, the Air Force Office of Scientific Research Grant No. 80-0022, and by the National Science Foundation, Atmospheric Sciences Section Grant No. 7916837 of the University of Colorado. The work of D.R.N. was supported by the National Science Foundation, Atmospheric Research Section Grant No. ATM76-22487 and Grant No. ATM79-18778, and by the United States Department of Energy Grant No. EY-76-S-02-2059. Computer time for this research was provided by the National Center for Atmospheric Research (supported by the National Science Foundation).

[1]S. A. Kaplan and V. N. Tsytovich, Astron. Zh. 44, 1036 (1967)[Sov. Astron.-A. J. 11, 956 (1968)]; V. V. Zheleznyakov and V. G. Zaitzev, Astron. Zh. 45, 19 (1968)[Sov. Astron.-A. J. 14, 47 (1970)].
[2]S. Bardwell and M. V. Goldman, Astrophys. J. 209, 912 (1976).
[3]K. Nishikawa, J. Phys. Soc. Jpn. 24, 916, 1152 (1968).
[4]K. Papadopoulos, M. L. Goldstein, and R. A. Smith, Astrophys. J. 190, 175 (1974).
[5]V. E. Zakharov, Zh. Eksp. Teor. Fiz. 62, 1745 (1972) [Sov. Phys.-JETP 35, 908 (1972)].
[6]M. V. Goldman and D. R. Nicholson, Phys. Rev. Lett. 41, 406 (1978).
[7]A. A. Galeev, R. Z. Sagdeev, Y. S. Sigov, V. D. Shapiro, and V. I. Shevchenko, Fiz. Plazmy 1, 10 (1975)[Sov. J. Plasma Phys. 1, 5 (1975)].
[8]D. R. Nicholson, M. V. Goldman, P. Hoyng, and J. Weatherall, Astrophys. J. 223, 605 (1978).
[9]D. F. Smith and D. R. Nicholson, in *Wave Instabilities in Space Plasmas* (D. Reidel, Dordrecht, 1979), p. 225.
[10]M. V. Goldman, G. F. Reiter, and D. R. Nicholson, Phys. Fluids 23, 388 (1980).
[11]M. V. Goldman, K. Rypdal, and B. Hafizi, Phys. Fluids 23, 945 (1980).
[12]B. Hafizi and M. V. Goldman, Phys. Fluids 24, 145 (1981).
[13]D. R. Nicholson and M. V. Goldman, Phys. Fluids 21, 1766 (1978).
[14]M. V. Goldman, J. Weatherall, and D. R. Nicholson, Phys. Fluids 24, 668 (1981).
[15]A. A. Galeev, R. Z. Sagdeev, V. D. Shapiro, and V. I. Shevchenko, Zh. Eksp. Teor. Fiz. 73, 1352 (1977)[Sov. Phys.-JETP 46, 711 (1977)].
[16]R. A. Smith, M. L. Goldstein, and K. Papadopoulos, Solar Phys. 46, 515 (1976); Astrophys. J. 234, 348 (1979).
[17]M. L. Goldstein, R. A. Smith, and K. Papadopoulos, Astrophys. J. 234, 683 (1979).
[18]A. J. Chorin, J. Fluid Mech. 57, 785 (1973).
[19]N. Pereira, R. Sudan, and J. Denavit, Phys. Fluids 20, 936 (1977).
[20]G. R. Magelssen and D. F. Smith, Solar Phys. 38, 205 (1977).
[21]A. A. Vedenov, and L. I. Rudakov, Dok. Akad. Nauk SSSR 159, 767 (1965)[Sov. Phys.-Dokl. 9, 1073 (1965)].
[22]L. I. Rudakov and V. N. Tsytovich, Phys. Reports C40, 1 (1978).
[23]S. A. Orszag, Phys. Fluids Suppl. 12, II 250 (1969).
[24]V. E. Zakharov and A. M. Rubenchik, Zh. Eksp. Teor. Fiz. 65, 997 (1973)[Sov. Phys.-JETP 38, 494 (1974)].
[25]G. Schmidt, Phys. Rev. Lett. 34, 724 (1975).
[26]J. Weatherall, Ph.D. thesis, University of Colorado (1980).

[27]V. V. Krasnosel'skikh and V. I. Sotnikov, Fiz. Plazmy 3, 872 (1977)[Sov. J. Plasma Phys. 3, 491 (1977)].
[28]H. P. Freund and K. Papadopoulos, Phys. Fluids 23, 139 (1980).
[29]J. Weatherall, D. R. Nicholson, and M. V. Goldman, Astrophys. J. 246, 306 (1981).
[30]K. Papadopoulos and H. P. Freund, Geophys. Res. Lett. 5, 881 (1978).
[31]H. L. Rowland, J. G. Lyon, and K. Papadopoulos, Phys. Rev. Lett. 46, 346 (1981).
[32]L. M. Degtyarev, R. Z. Sagdeev, G. I. Solov'ev, V. D. Shapiro, and V. I. Shevchenko, Fiz. Plasmy 6, 485 (1980) [Sov. J. Plasma Phys. 6, 263 (1980)].
[33]D. F. DuBois and H. A. Rose (to be published).
[34]D. F. DuBois, H. A. Rose, and M. V. Goldman, J. Phys. Suppl. (Paris) C7-601 (1979).

APPENDIX G

G. "Nonlinear Evolution Equations, Recurrence, and Stochasticity"

B. Hafizi
Physics of Fluids 24, 1976-1988 (1981)

PF 12307

Nonlinear evolution equations, recurrence and stochasticity

B. Hafizi

Department of Astro-Geophysics, University of Colorado,
Boulder, Colorado 80309

(Received February 2, 1981)

Revised May 1981

Perturbative, spatially-periodic solutions of the Korteweg-deVries, the modified Korteweg-deVries, and the nonlinear Schrödinger equations are shown to be recurrent and non-stochastic, densely covering parts of the phase-space bounded by level surfaces of the constants of motion. The connection of this result with the numerical phenomena of recurrences and the slow randomization of nonlinear systems is discussed.

I. INTRODUCTION

The nonlinear Schrödinger and the modified Korteweg-deVries equations describe a number of physical effects in the regime where the linear approximation to collective disturbances ceases to be valid.[1] For example, these equations have been derived in studies of the modulational instability and propagation of hydromagnetic waves in cold, collision-free plasmas,[2,3] and the modulational instability of Langmuir waves in warm, collision-free plasmas.[4] The importance of these (and certain other) equations is not only their ubiquity but also the fact that they are solvable by the method of the inverse scattering problem.[1,5-7] Basically, the Cauchy problem for these equations is solved for the class of rapidly decreasing functions (on the real line) by means of the scattering theory of an auxiliary linear operator, L. An equation of the form

$$\partial_t u = S[u] \ ,$$

where S is a nonlinear operator, can be solved provided it admits the "Lax representation"[8]

$$\partial_t L = i[L,A]$$

for some operator, A. Here $[\cdot,\cdot]$ denotes the usual commutator. For the nonlinear Schrödinger equation,

$$i\partial_t u + \partial_x^2 u + \kappa |u|^2 u = 0 \ , \qquad \text{(for complex } u\text{)} \tag{1}$$

the operators are[6]

$$L = i\begin{bmatrix} 1+p & 0 \\ 0 & 1-p \end{bmatrix}\partial_x + \begin{bmatrix} 0 & u^* \\ u & 0 \end{bmatrix} ,$$

$$A = -p\begin{bmatrix} 1 & 0 \\ 0 & 1 \end{bmatrix}\partial_x^2 + \begin{bmatrix} |u|^2/(1+p) & i\partial_x u^* \\ -i\partial_x u & -|u|^2/(1-p) \end{bmatrix} ,$$

where $K = 2/(1-p^2)$.

For the modified Korteweg-deVries equation

$$\partial_t u + 6u^2\partial_x u + \partial_x^3 u = 0 , \qquad \text{(for real } u\text{)} \qquad (7)$$

the operators are[7]

$$L = -i\begin{bmatrix} 0 & 1 \\ -1 & 0 \end{bmatrix}\partial_x + \begin{bmatrix} 0 & u \\ u & 0 \end{bmatrix},$$

$$A = -4i\begin{bmatrix} 1 & 0 \\ 0 & 1 \end{bmatrix}\partial_x^3 - i\partial_x\begin{bmatrix} 3(u^2-i\partial_x u) & 0 \\ 0 & 3(u^2+i\partial_x u) \end{bmatrix}$$

$$-i\begin{bmatrix} 3(u^2-i\partial_x u) & 0 \\ 0 & 3(u^2+i\partial_x u) \end{bmatrix}\partial_x .$$

It is natural to consider the eigenvalue problem

$$L\psi = \lambda\psi ,$$

where ψ is an eigenvector belonging to the eigenvalue λ. If one insists that the time evolution of ψ be governed by

$$i\partial_t\psi = A\psi ,$$

it is readily shown that the spectrum of the operator L does not vary with time. It is then possible to reconstruct the

operator L [and hence the solution u(x,t) appearing in L] from its spectrum by well-known methods[5] using only the asymptotic behavior of its eigenvectors. The crucial point here is that for rapidly decreasing functions u(x,t) (as $|x| \to \infty$), the spatial and temporal behavior of ψ for large |x| is independent of the desired function u(x,t). This method has been used to investigate the time-asymptotic behavior of solutions of Eqs. (1) and (2) and also some important particular solutions describing the interaction of a finite number of solitons, the multi-soliton solutions.

In a number of cases, the solutions of Eqs. (1) and (2) under spatially-periodic boundary conditions are required. Thus, a large number of very interesting and illuminating computational studies, where the use of periodic boundary conditions is natural, have revealed that the propagation of Langmuir waves in plasmas, etc., have an apparently recurrent temporal behavior.[4,9] An example of this recurrent behavior for the case of Langmuir waves is presented in Sec. II of the present paper. One would naturally like to study this process in order to understand the underlying mechanism(s). In attempting to examine this phenomenon, one finds that the power of the inverse scattering method is lost for functions u(x,t) periodic in x.[5,10-12] However, there have been some interesting studies for this case, too. Such studies have been concerned with certain exact analytical solutions that are the analogs of the multi-soliton solutions in the case of rapidly decreasing functions.[10,11,13] In fact, the problem turns out to be similar to that in the band theory of solids. Thus, at

any instant in time, the operator L is a function of u(x), which in turn is a periodic function of x. The spectrum of L is then characterized by the presence of allowed and forbidden zones, with eigenvectors of the Bloch form. For the Korteweg-deVries equation,

$$\partial_t u + 6u\partial_x u + \partial_x^3 u = 0 \quad , \qquad \text{(for real u)}$$

for example, which describes nonlinear magnetohydrodynamic waves in warm, collisionless plasmas,[14] L is the usual Stürm-Liouville operator, $-\partial_x^2 + u(x,t)$.[8] It has been shown that the analog of the n-soliton (multi-soliton) solution is the manifold of solutions u(x), such that the spectrum of L has exactly n forbidden zones.[13] Further, it has been shown that the dynamical behavior of these special solutions is almost-periodic in time. (For the definition of an almost-periodic function, see Eq. (19).) The special nature of these solutions is made apparent by noting that a typical periodic function u(x) has infinitely many band-gaps. Further, the stability of these special solutions to small perturbations has not been considered.

Our investigation of the nonlinear Schrödinger and of the modified Korteweg-deVries equations was motivated by the desire to understand the anomalously slow randomization of one-dimensional nonlinear systems, originally studied by Fermi, Pasta, and Ulam.[9,15,16] It is observed numerically that a given distribution of energy amongst the modes for either the nonlinear Schrödinger equation, the modified Korteweg-deVries equation, or an anharmonic lattice periodically recurs with apparently little thermalization (or equilibriation).

The slow randomization of nonlinear systems has also been examined from a different point of view.[17] This is based on the rigorous perturbation theorem of Kolmogoroff, Arnol'd, and Moser.[18] According to this theorem, under certain circumstances (Hamiltonian) perturbations of a Hamiltonian system merely lead to a distortion of the linear-solution manifolds, thus retaining the almost-periodic character of the linear solutions.

Our purpose here is to present an approximate solution of the nonlinear Schrödinger and of the modified Korteweg-deVries equations in the spirit of the Kolmogoroff-Arnol'd-Moser theorem. It turns out that the mode-mode interactions are such that the Kolmogoroff-Arnol'd-Moser theorem cannot guarantee the preservation of the linear manifolds; in fact, our perturbation solution shows this. Even so, the (approximate) solutions turn out to be almost-periodic in time. The almost-periodicity of the solutions was suggested by the numerical solutions of the nonlinear Schrödinger equation, described in this paper.

According to a well-known theorem of Liouville,[19] a Hamiltonian system of N degrees of freedom and N commuting integrals of motion is completely integrable, thus allowing separation of variables and introduction of action-angle variables. This rules out the possibility of complete randomization.[16] When the number of degrees of freedom is not finite, the existence of (an "equal" number of) constants of motion is necessary but not sufficient for integrability. For the class of rapidly decreasing functions, both the Korteweg-deVries

and the nonlinear Schrödinger equations have been shown to be integrable by explicit transformations to action-angle variables, furnished by the scattering data of the inverse method.[20,21] However, the non-integrability of a very general version of the nonlinear Schrödinger equation for periodic functions u(x,t) has already been suggested using the superconvergent method proposed by Kolmogoroff.[22]

Attention must be drawn to the following. The discovery of solitons in one of the early computations of the Korteweg-deVries equation[9] has led some to believe that the recurrence phenomenon observed there is due to the solitons, which interact elastically. It must be noted that this is not so. In fact, it has been conjectured by Lax[11] that all spatially-periodic solutions of the Korteweg-deVries equation have recurrent behavior. This has been proved for the special multi-soliton solutions mentioned earlier; it is true for the zero-order (i.e., non-soliton) solutions of the nonlinear Schrödinger, modified Korteweg-deVries, and Korteweg-deVries equations [cf., discussion following Eq. (8)]; it is also true for the perturbative solutions given in this paper. The true explanation of the recurrence phenomenon seems to lie in the boundary conditions and the existence of (perhaps an infinite number of) constants of motion.

II. NUMERICAL RESULTS

Our investigations were in large part directed by numerical solutions of the nonlinear Schrödinger equation with periodic boundary conditions. We assume that u(x) is periodic with period L and has continuous derivatives of all orders. Then u(x)

can be represented in terms of its Fourier coefficients u_k:

$$u(x,t) = \frac{1}{\sqrt{L}} \sum_{\ell=-\infty}^{\infty} u_k \exp(ikx) \ , \qquad (3)$$

where $k = \frac{2\pi}{L} \ell$ (ℓ is an integer)

The particular nonlinear Schrödinger equation of interest has the form

$$i\partial_t u + \partial_x^2 u + (|u|^2 - \langle |u|^2 \rangle)u = 0 \ , \qquad (4)$$

where $\langle \ \rangle$ denotes a spatial average. The subtraction term in Eq. (4) is a peculiarity of wave-wave interactions in a plasma. (It must be emphasized that the nature of the solution given ... not an artifact of this term.)

Eq. (4) can be considered as a set of ordinary differential equations in the space

$$V \left[u(x) = \frac{1}{\sqrt{L}} \sum_{\ell=-\infty}^{\infty} u_k \exp(ikx) : \sum_k |u_k|^2 < \infty \right]$$

with the usual norm $\|u(x)\| = \sum_{\ell=-\infty}^{\infty} |u_k|$.

By direct substitution of Eq. (3) into Eq. (4), one has

$$i \frac{du_k}{dt} - k^2 u_k + \frac{1}{L} \sum_{k',k''}{}' u_{k'} u_{k''}^* u_{k-k'+k''} = 0 \ , \qquad (5)$$

where $\sum_{k',k''}{}'$ indicates that $k' \neq k$, this being due to the subtraction term in Eq. (4).

It is well-known that the nonlinear Schrödinger equation has infinitely many commuting integrals of motion.[6] The ones associated with the invariance group of the Lagrangian density of Eq. (4) are[23]

$$H = \sum_k k^2 |u_k|^2 - \frac{1}{2L} \sum_{k,k',k''}' u_k\, u_{k'}^*\, u_{k''}\, u_{k-k'+k''}^* \quad ,$$

$$P = \sum_k k |u_k|^2 \quad ,$$

$$B = \sum_k |u_k|^2 \quad ,$$

representing the Hamiltonian, the momentum, and the boson number respectively.

$\sum_{k,k',k''}'$ indicates that $k' \neq k$.

The computations were performed by the Galerkin method of using a finite number (32) of Fourier modes spanning the desired solution space. The integration of the ordinary differential equation, Eq. (5), was carried out by splitting the evolution operator into its linear and nonlinear parts. The linear part of the integration was performed exactly and the nonlinear part by implicit methods in x space. Aliasing errors were avoided by the usual method.[24] The errors sustained in H, P, and B were less than 1% in the computations.

The evolution of a group of electrostatic (Langmuir) waves

having initially a Gaussian distribution in k space was examined for several values of the boson number B. Following our comments in the Introduction, the ubiquity of the nonlinear Schrödinger equation ensures that by suitable rescaling, the evolution of this packet may be regarded as typical for many different, real physical problems; for example, traveling waves of finite amplitude on deep water (Stokes waves).[25] In all cases, the wave packet was observed to break up (in x space) into several local maxima and minima and to approximately reconstitute the original after a long time. Figure 1 shows the trajectories for the second and the sixth modes over a period of approximately three recurrences of the initial Gaussian packet. (We note that the initial Gaussian packet was centered on the sixth-mode in k space.) To render the figure clearer, a barely empty circular area centered on the origin of the coordinate axes has been removed, thus expanding the orbit structure considerably. If this is not done, an orbit appears as a circle whose circumference is a thick line.

The approximate recurrence of the wave packet and the orbit structures suggest that the solutions are almost-periodic in time, as is the case for the special, finite-zone potentials noted earlier. It must be borne in mind, though, that due to inaccuracies and the finite magnitude of the time step, it can never be proved whether an orbit is simply-periodic and closes on itself or that it is almost-periodic and does not quite close on itself.[4,9]

III. PERTURBATION ANALYSIS

In this section we present an analysis of the computations which is not based on the special, exact results of the method for finite-zone potentials. However, our results are special also in that they are approximate and assume a convergent perturbation expansion. Further, in what follows, we assume that the Fourier series expansion in Eq. (3) is absolutely and uniformly convergent so that all the manipulations are rigorously valid.

In the linear approximation, Eq. (5) becomes

$$i\frac{du_k}{dt} - k^2 u_k \simeq 0 \quad , \qquad \text{for all } k \tag{6}$$

representing a countably infinite set of uncoupled harmonic oscillators, $u_k(t) = u_k(t=0)\exp(-ik^2t)$, for all k, with countably infinite constants of motion, $|u_k(t)|$ (for all k), and whose integrability is shown explicitly. Clearly, any solution lies on an infinite-dimensional torus whose cross-sections are circles of radius $r = |u_k(t)| = |u_k(t=0)|$ (for every k). Further, Eq. (6) shows that the flow on the torus is characterized by a frequency vector ω:

$$\omega = \left(\cdots, \ -2^2, \ -1^2, \ 0^2, \ 1^2, \cdots \right) \tag{7}$$

with

$$\ell^2 = \left(\frac{2\pi}{L}\ell\right)^2 \qquad (\ell \text{ is an integer}) \tag{8}$$

Since the frequency components are rationally dependent, being integer multiples of one another, it follows that the flow on the torus is simply-periodic with period (recurrence time)

$$T_r = \frac{2\pi}{\omega_1} = \frac{L^2}{2\pi}$$

The constancy of the frequency vector ω, Eq. (7), on the constant energy manifolds implies that the system is degenerate.[18]

In order to apply the Kolmogoroff-Arnol'd-Moser stability theorem, we proceed as follows. As a functional of u(x), the Hamiltonian of the nonlinear Schrödinger equation is

$$H = \int_{-L/2}^{L/2} dx \left[|\partial_x u|^2 - \frac{1}{2} |u|^2 \left(|u|^2 - \langle |u|^2 \rangle \right) \right] . \qquad (9)$$

Defining real-valued functions q(x) and p(x) through

$$u(x) = q(x) + ip(x) \quad ,$$

Eq. (9) takes the form

$$H = \int_{-L/2}^{L/2} dx \left\{ (\partial_x q)^2 + (\partial_x p)^2 - \frac{1}{2} (q^2+p^2) \left[(q^2+p^2) - \langle (q^2+p^2) \right] \right\}$$

which becomes, on using

$$(q,p)(x) = \frac{1}{\sqrt{L}} \sum_{\ell=-\infty}^{\infty} (q_k, p_k) \exp(ikx) , \qquad \left(k = \frac{2\pi}{L} \ell \right) ,$$

the following

$$H = + \sum_k k^2 \left(q_k^2 + p_k^2 \right) - \frac{1}{2L} \sum_{k,k',k''}' \left(q_k q_{k'} q_{k''} q_{-k'+k''}^* + \right.$$

$$\left. p_k p_{k'}^* p_{k''} p_{k-k'+k''}^* + 2 q_k q_{k'}^* p_{k''} p_{k-k'+k''}^* \right) , \qquad (12)$$

where use has been made of

$$(q_k^* , p_k^*) = (q_{-k}, p_{-k}) ,$$

which follows from the reality of $q(x)$ and $p(x)$.

Introducing (zeroth-order) real-valued action-angle variables $\left[(J,\phi), (I,\psi)\right]$ through

$$q_k = \sqrt{J_k} \exp (i \phi_k) ,$$

$$p_k = \sqrt{I_k} \exp (i \psi_k) ,$$

the Hamiltonian, Eq. (10), becomes

$$H = + \sum_k k^2 (J_k + I_k) - \frac{1}{2L} \sum_{k,k',k''}' \left\{ \left(J_k J_{k'} J_{k''} J_{k-k'+k''} \right)^{1/2} \exp \left[i \left(\phi_k - \phi_{k'} + \phi_{k''} - \phi_{k-k'+k''} \right) \right] \right.$$

$$+ \left(I_k I_{k'} I_{k''} I_{k-k'+k''} \right)^{1/2} \exp \left[i \left(\psi_k - \psi_{k'} + \psi_{k''} - \psi_{k-k'+k''} \right) \right]$$

$$\left. + 2 \left(J_k J_{k'} I_{k''} I_{k-k'+k''} \right)^{1/2} \exp \left[i \left(\phi_k - \phi_{k'} + \psi_{k''} - \psi_{k-k'+k''} \right) \right] \right\} \qquad (11)$$

All perturbation theories of the stability of linear flow for Hamiltonian systems are based on the idea of a sequence of canonical transformations $\left[(J,\phi);\ (I,\psi)\right] \rightarrow \left[(J',\phi');\ (I',\psi')\right] \rightarrow \ldots$ such that the final Hamiltonian is a function only of the action variables, thus reducing the solution to one of simple quadrature. This is the well-known process of transformation to a Birkhoff normal form.[18] However, there are certain requirements for the convergence of this process. These requirements are also necessary for the preservation of the invariant of the linear flow as embodied in the Kolmogoroff-Arnol'd-Moser theorem. In particular, it is necessary that there be no low-order resonances between independent degrees of freedom of the linear flow. However, we see from Eqs. (11) and (8) that the frequencies of J_k and I_k are identical for every k. Thus, whenever there is a coupling between two such modes, there is the possibility of resonant energy exchange. Such a coupling is manifest in the first term in the braces in Eq. (11). Under these circumstances, the Kolmogoroff-Arnol'd-Moser theorem cannot guarantee the preservation of the tori of the linear flow and, in fact, the destruction of these tori is possible.

Since the same method of solution is used, the details of the calculation for Eq. (1) only will be given, and the solution of Eq. (2) will be quoted at the end.

A naive perturbation calculation of Eq. (5) ends up with a "small divisor" problem.[18] To avoid this secular behavior, several time scales are introduced via the following expansions[20,22]

$$u_k(t) = u_k^{(0)}\left(\tau_0, \tau_1, \tau_2, \ldots\right) + \epsilon u_k^{(1)}\left(\tau_0, \tau_1, \tau_2, \ldots\right) + \ldots \quad (12)$$

$$\frac{d}{dt} = \partial_{\tau_0} + \epsilon \partial_{\tau_1} + \epsilon^2 \partial_{\tau_2} + \ldots \quad (13)$$

where ϵ is a small parameter and $\tau_0, \tau_1, \tau_2, \ldots$ are independent time variables.

An ϵ is appended to the nonlinear term in Eq. (5); Eqs. (12) and (13) substituted in to obtain, to order ϵ^0,

$$i\partial_{\tau_0} u_k^{(0)} - k^2 u_k^{(0)} = 0$$

with the general solution

$$u_k^{(0)}\left(\tau_0, \tau_1, \tau_2, \ldots\right) = u_k^{(0)}\left(\tau_1, \tau_2, \ldots\right) \exp\left(-ik^2 \tau_0\right), \quad (14)$$

where $u_k^{(0)}(\tau_1, \tau_2, \ldots)$, a function of the (slower) time-variables $\tau_1, \tau_2, \ldots$, is to be determined.

With the aid of Eq. (14), the perturbation expansion to order ϵ^1 is

$$i\partial_{\tau_0} u_k^{(1)} - k^2 u_k^{(1)} = -i\partial_{\tau_1} u_k^{(0)} \exp\left(-ik^2 \tau_0\right)$$

$$- \frac{1}{L} \sum_{k',k''}{}' u_{k'}^{(0)} u_{k''}^{(0)*} u_{k-k'+k''}^{(0)} \exp\left\{-i\left[k^2 + 2(k'-k)(k'-k'')\right]\tau_0\right\},$$

with the general solution

$$u_k^{(1)}(\tau_0,\tau_1,\ldots) = u_k^{(1)}(\tau_1,\ldots)\exp(-ik^2\tau_0)$$

$$-\tau_0\left[\frac{\partial}{\partial\tau_1}\dot{u}_k^{(0)} - \frac{i\dot{u}_k^{(0)}}{L}\sum_{k'}{}'\left|\dot{u}_{k'}^{(0)}\right|^2\right]\exp(-ik^2\tau_0)$$

$$-\frac{1}{2L}\sum_{k',k''}{}''\frac{\dot{u}_{k'}^{(0)}\dot{u}_{k''}^{(0)*}\dot{u}_{k-k'+k''}^{(0)}}{(k'-k)(k'-k'')}\exp\left\{-i\left[k^2+2(k'-k)(k'-k'')\right]\tau_0\right\},$$

where $u_k^{(1)}(\tau_1,\tau_2,\ldots)$ is to be determined, $\sum_{k'}{}'\left|\dot{u}_k^{(0)}\right|^2$ indi

that $k' \neq k$, and $\sum_{k',k''}{}''$ indicates that $k' \neq k$ and $k' \neq k''$. The

latter exclusion is precisely due to the mode-resonance phenom

mentioned earlier, which gives rise to the secular term

$$\tau_0\frac{iu_k^{(0)}}{L}\sum_{k'}{}'\left|u_{k'}^{(0)}\right|^2\exp(-ik^2\tau_0).$$

Non-secular behavior is ensured by choosing

$$\frac{\partial}{\partial\tau_1}u_k^{(0)} - \frac{iu_k^{(0)}}{L}\sum_{k'}{}'\left|\dot{u}_{k'}^{(0)}\right|^2 = 0.$$

This equation implies $\frac{\partial}{\partial\tau_1}\left|u_k^{(0)}\right|^2 = 0$, whence its solution is

$$\dot{u}_k^{(0)}(\tau_1,\tau_2,\ldots) = U_k(\tau_2,\ldots)\exp\left(\frac{i(N-\left|U_k\right|^2)\tau_1}{L}\right), \qquad (10)$$

where $U_k(\tau_2,\ldots)$ is to be determined and

$$N = \sum_k \left| U_k(\xi_2, \xi_3, \ldots) \right|^2 .$$

Using Eqs. (14) - (16) in Eq. (12), we finally have

$$u_k(t) = \exp\left[i\left(N - |U_k|^2 - k^2 L\right) t/L \right] \left[U_k - \frac{1}{2L} \sum_{k',k''}'' \frac{U_k, U_{k''}^* U_{k-k'+k''}}{(k'-k)(k'-k'')} \right.$$

$$\left. \times \left(\exp\left\{ i\left[|U_k|^2 - |U_{k'}|^2 + |U_{k''}|^2 - |U_{k-k'+k''}|^2 - 2(k'-k)(k'-k'')L \right] t/L \right\} - 1 \right) \right] ,$$

where ϵ has been set equal to 1 and $u_k^{(1)}$ has been chosen such that $u_k(t=0) = U_k$ and that Eq. (17) preserves the constants of motion H, P, and B to order (U^6) (see Appendix A).

An identical calculation leads to the following solution for the modified Korteweg-deVries equation

$$u_k(t) = \exp\left[ik\left(M - |U_k|^2 + k^2 L\right) t/L \right] \left[U_k + \frac{1}{3L} \sum_{k',k''}''' \frac{U_k, U_{k'} U_{k''} U_{k-k'-k''}}{(k'+k'')(k'-k)(k''-k)} \right.$$

$$\left(\exp\left\{ i\left[k|U_k|^2 - k'|U_{k'}|^2 - k''|U_{k''}|^2 - (k-k'-k'')|U_{k-k'-k''}|^2 - 3(k'+k'')(k'-k)(k''-k) \right] t/L \right\} \right.$$

$$\left. \left. - 1 \right) \right] + O(U^5) , \qquad (18)$$

where

$$M = \sum_k |U_k|^2 ,$$

$u_k(t=0) = U_k$ and $\sum_{k',k''}'''$ indicates that $k' \neq -k''$, $k' \neq k$, and $k'' \neq k$.

We note that by a remarkable nonlinear transformation[28], given by a Riccati equation, Eq. (18) gives also an explicit solution for the Korteweg-deVries equation.

IV. DISCUSSION

As they stand, the solutions given by Eqs. (17) and (18) are not particularly informative. In order to understand the behavior of these solutions, we need to consider the class of almost-periodic functions.

For illustrative purposes, take the simple case of a flow on the surface of a two-dimensional torus, Figure 2. Denote the geographical coordinates by q_1 (longitude) and q_2 (latitude), and take the flow given by

$$\frac{dq_1}{dt} = \omega_1 \ ,$$

$$\frac{dq_2}{dt} = \omega_2$$

If $\omega_1/\omega_2 = m/n$ (m and n being integers), then in a time $t = 2\pi m/\omega_1 = 2\pi n/\omega_2$ a point on the surface of the torus traces out a trajectory which closes on itself after winding on the surface m-times the long way around and n-times the short way around. This is an example of a periodic flow. If ω_1/ω_2 is irrational, i.e., not the quotient of two integers, then the moving point never quite

returns to its original position. In fact, the trajectory covers the surface of the torus densely and ergodically. This is an example of an almost-periodic flow.

Closely associated with an almost-periodic flow is an almost-periodic function, an example of which is $\phi(t) = \sin t + \sin \sqrt{5}\, t$. Since $\sqrt{5}$ is irrational, there is no (non-zero) time t such that $\phi(t) = \phi(0) = 0$, although it approaches zero infinitely many times to great accuracy. The subtleties of this behavior are embodied in the following definition.

DEFINITION:[29] $\phi(t)$ is an almost-periodic function of t if for every $\varepsilon > 0$, there exists a $\tau_0(\varepsilon) > 0$ and a $\tau < \tau_0$ in every interval of length τ_0, such that $|\phi(t) - \phi(t+\tau)| < \varepsilon$, for all t.

This essentially says that if we divide the t-axis into intervals of length τ_0, then in every one of these the function approximates a particular value that it has in each of the previous intervals.

Perhaps the character of an almost-periodic function is best captured by a theorem of H. Bohr[29] to the effect that such a function may be represented by a (generalized) Fourier series

$$\phi(t) = \sum_{j=-\infty}^{\infty} \phi_j \exp(i\omega_j t) \quad , \tag{19}$$

where the frequencies ω_j are not necessarily integer multiples of a given frequency ω_0.

Comparing Eqs. (17) and (18) with Eq. (19), we conclude (see Appendix B) that the solutions of the nonlinear Schrödinger, the

Korteweg-deVries, and the modified Korteweg-deVries equations are almost-periodic functions of time and come arbitrarily close to any point on their orbit in the course of their time evolution.

In the linear approximation, we saw that the frequencies of the modes were integer multiples of one another, leading to a simply-periodic time development. However, due to mode-mode interactions [cf., discussion following Eq. (11)] there arise resonant interactions between the linear modes, leading to the exchange of energy. One effect of this resonance interaction is to re-normalize the zero-order frequencies. The amplitude-dependent (renormalized) frequencies are no longer simple multiples of one another, in general, and so the trajectory of the system does not close on itself. In fact, the orbit will densely cover a region of phase space that is bounded by the level surfaces of the constants of motion P, P, and H (See Appendix A). To our knowledge, it is not known if, under periodic boundary conditions, the modified Korteweg-deVries or the nonlinear Schrödinger equations possess an infinite set of constants of motion associated with their hidden symmetries. We have only determined that the solutions given here preserve the obvious constants of motion related to the invariance group of the Lagrangian density.

What about stochastization? The original expectation in the computations of Fermi, Pasta, and Ulam[15] was that with the inclusion of nonlinearity an arbitrary distribution of energy amongst the modes would evolve irreversibly toward an asymptotically stationary equilibrium state. The negative results obtained by Fermi, et al., can be accounted for by an almost-periodic solution

for the nonlinear oscillators, such as those given in this paper. (In this connection, reference must also be made to the related work of Thyagaraja[30].) Although the almost-periodic character of these solutions is due to energy exchange amongst the modes, the system neither evolves irreversibly nor equilibriates. Thus, starting from an arbitrary distribution of energy amongst the modes, rather than evolving irreversibly towards a state in which there is a stationary distribution of energy over the modes, the energy oscillates back and forth over the modes (almost-)periodically, at least for the time-scale over which our perturbative solution is valid. For consider the two-time autocorrelation function R(T) of an almost-periodic solution $\zeta(t)$:

$$R(T) = \lim_{\cdot\cdot} \frac{1}{\cdot} \int_{-\cdot}^{\cdot\cdot} \zeta(t)\,\zeta(t+T)\,dt. \qquad (\cdot\cdot)$$

where ζ is, for example, the envelope of the free-surface [illegible] for Stokes waves on deep water, or the electric field envelope of Langmuir waves in a plasma. Since $\zeta(t)$ is almost periodic, it can be represented as

$$\zeta(t) = \sum_{n=-\cdot}^{\cdot} a_n \exp(i\omega_n t) \quad , \qquad (n \text{ is an integer}) \qquad (2\cdot)$$

where $\omega_n/\omega_m \neq$ rational number.

Substituting Eq. (21) into Eq. (20), we have

$$R(T) = \lim_{\cdots} \sum_{n,m} a_n a_m \exp\,(i\,\omega_m T) \frac{\sin(\omega_n+\omega_m)\,T/2}{(\omega_n+\omega_m)\,T/2} + \sum_n a_n a_{-n} \exp(i\,\omega_n T) \quad (22)$$

For a stochastic (or mixing) flow, the auto-correlation function must decay to zero (as $T \to \infty$). However, we see from Eq. (22) that R(T) oscillates as a function of T. It may be recalled that the Landau-Hopf model of fluid turbulence is no longer regarded as a viable theory for this same reason[31] (among other shortcomings).[32]

Ergodicity of the flows, which is a stronger condition than dense orbits but weaker than stochasticity, remains an open question. For ergodicity, one must show that the time spent by the trajectory of the system in a region of phase space is proportional to the area (or measure) of that region. For an infinite dimensional system, there are considerable technical difficulties involved in demonstrating this. In this connection, we note that the ergodicity of certain similar degenerate Hamiltonian systems has already been established.[33]

In closing, we must reiterate some of the main points of our study. As noted in the Introduction, the nonlinear equations which are the objects of this work are well-known for their common occurrence in many branches of physics. With such equations at hand, one often uses numerical methods of solution, with periodic boundary conditions. This is no doubt motivated in part by the fact that in the linear approximation, these equations possess the usual sinusoidal solutions. In this limit,

therefore, a collection of harmonic waves in a plasma, described by the nonlinear Schrödinger equation, or Stokes waves on deep water, described by the same equation,[34] would disperse and then reconstitute exactly the original wave-packet when the different harmonic components come under constructive interference. The result of this paper may be succinctly expressed by the statement that, for small nonlinearities, one can still expect (approximate) reconstitution of the original wave packet over and over again. As it stands, this statement may be of limited value for the person performing computational studies of, say, Stokes waves on deep water, since the small departures from the perfectly recurrent linear system may not amount to much over a limited computational time.[34] However, it must be noted that the almost-recurrent behavior predicted by the solutions given here may imply an ergodic temporal development, which would be of considerable import in the statistical theories of fluid turbulence.

The recent computational study by Yuen and Ferguson[31] of the modulational interaction of Stokes waves on deep water provides us with the basic clue as to how to modify the present calculations in order to describe the recurrence phenomena in regimes where the nonlinearities are not necessarily small. In a future article,[35] we will provide a detailed analytical study of the nonlinear Schrödinger equation with particular reference to the experiments[25] and computations.[34]

V. CONCLUSION

For small departures from linearity, we have determined that the spatially-periodic solutions of the Korteweg-deVries, the modified Korteweg-deVries, and the nonlinear Schrödinger equations are almost-periodic functions of time. This behavior is connected with the approximate recurrence phenomena observed in numerical computations of nonlinear systems and their associated anomalously slow stochastization.

The almost-periodicity of certain exact, special solutions of these equations has already been established. It is of interest to determine if this characteristic is shared by all the spatially-periodic solutions, as conjectured by Lax for the Korteweg-deVries equation. Our results hint at such a possibility. Finally, we note that in the same regime of validity, our calculations can be easily generalized to more than one dimension and to vector fields.

After completion of this work, we became aware of an interesting recent paper[36] addressing a related problem. Specifically, the authors of this paper consider the slow modulation of the exact finite-gap solutions[10,11,13] in space and in time under the influence of perturbations, using the method of multiple scales.

AD-A117 862 COLORADO UNIV AT BOULDER F/G 20/9
PLASMA WAVE TURBULENCE AND PARTICLE HEATING CAUSED BY ELECTRON --ETC(U)
MAY 82 M V GOLDMAN AFOSR-80-0022
UNCLASSIFIED CU-1533143 AFOSR-TR-82-0592 NL

2 OF 4
AD A
117862

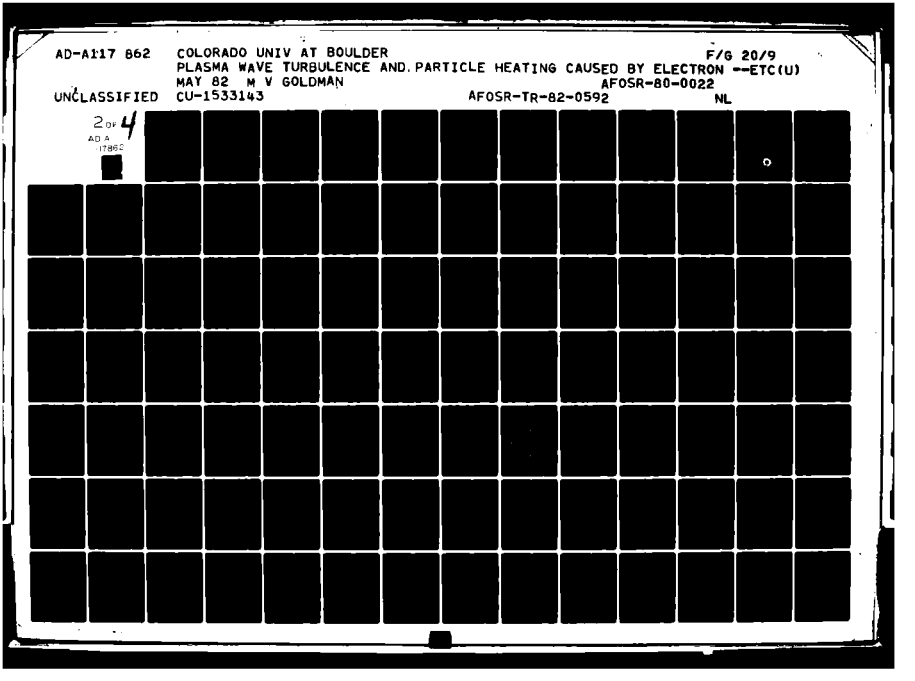

ACKNOWLEDGMENTS

Discussions with A. O. Barut, M. V. Goldman, C. F. Meyers, and D. A. Russell have greatly contributed to the final form of this paper.

This work was supported by the National Science Foundation under Grant ATM 7916837, the Air Force Office of Scientific Research under Contract F496.0-76-C-0005, the National Aeronautics and Space Administration under Contract NAGW-91, and the National Center for Atmospheric Research Computing Facility in Boulder, Colorado.

APPENDIX A

In this appendix, we show that the perturbation solution of the nonlinear Schrödinger equation preserves the boson number to appropriate order, i.e., $O(U^6)$. The conservation of the momentum and of the Hamiltonian can be similarly demonstrated.

The boson number is defined following Eq. (5):

$$B = \sum_k |u_k(t)|^2 \quad . \tag{A1}$$

From Eq. (17), the right-hand side of Eq. (A1) is given by

$$\sum_k |u_k(t)|^2 = \sum_k |U_k|^2 - \frac{1}{2T} \sum_{k,k',k''}'' \left[\frac{U_k U_{k'}^* U_{k''} U_{k-k'+k''}^*}{(k'-k)(k'-k'')} \right.$$

$$\times \left(\exp\left\{ -i \left[|U_k|^2 - |U_{k'}|^2 + |U_{k''}|^2 - |U_{k-k'+k''}|^2 - 2(k'-k)(k'-k'') \right] t/T \right\} - \right.$$

$$+ \frac{U_k^* U_{k'} U_{k''}^* U_{k-k'+k''}}{(k'-k)(k'-k'')}$$

$$\times \left(\exp\left\{ +i \left[|U_k|^2 - |U_{k'}|^2 + |U_{k''}|^2 - |U_{k-k'+k''}|^2 - 2(k'-k)(k'-k'') \right] t/T \right\} \right.$$

$$\left. \left. -1 \right) \right] + O(U^6) \tag{A2}$$

Under the following sequence of operations: $k \to k' \to k'' \to k'''$, $k \longleftrightarrow k'$, and $k''' \to k''$, the second exponential term in Eq. (A2) becomes

$$-\frac{U_{k'}^{*} U_{k}^{*} U_{k-k'+k''} U_{k'''}}{(k'-k)(k'-k'')}$$

$$\times \left(\exp \left\{ -i \left[|U_k|^2 - |U_{k'}|^2 + |U_{k''}|^2 - |U_{k-k'+k''}|^2 - 2(k'-k)(k'-k'') \right] t \right\} \right)$$

which cancels the first exponential term; whence

$$B = \sum_k |n_k(t)|^2 = \sum_k |U_k|^2 + O(U^6) \quad ,$$

expressing the invariance of the boson number $\sum_k |n_k|^2$ [illegible] its initial value.

APPENDIX B

The purpose of this appendix is to prove:

THEOREM: $u_k(t)$ as given by Eq. (17) or Eq. (18) is an almost-periodic function of time.

We remark that Eqs. (17) and (18), truncated to a finite number of terms, constitute, by definition, quasi-periodic functions of time.[29] By a well-known theorem, such functions are almost periodic. We, therefore, have to prove this property for the full set of terms in Eqs. (17) and (18). We give the details for Eq. (17) only.

PROOF: Consider

$$q_k(t) = \sum_{\substack{Lk'/2\pi = -\infty \\ Lk''/2\pi = -\infty}}^{\infty} \frac{U_{k'} U_{k''}^* U_{k-k'+k''}}{(k'-k)(k'-k'')} \exp(i\omega_{k,k',k''} t) \quad ,$$

where

$$\omega_{k,k',k''} = \left[|U_k|^2 - |U_{k'}|^2 + |U_{k''}|^2 - |U_{k-k'+k''}|^2 - 2(k'-k)(k'-k'')L \right] / L \qquad (B1)$$

We have assumed that $\sum_{Lk/2\pi = -\infty}^{\infty} |U_k|$ is absolutely and uniformly convergent (Sec. III); so, therefore, is $\sum_{k',k''} |U_{k'} U_{k''}^* U_{k-k'+k''}|$. Let

$$\sum_{k',k''} |U_{k'} U_{k''}^* U_{k-k'+k''}| \qquad (B2)$$

Suppose $\epsilon > 0$ is given and let

$$n = \left[\sqrt{\frac{3\rho}{\epsilon}} \frac{L}{2\pi} \right] + 1 \qquad (B2)$$

where [a] denotes the largest integer less than a.

By definition, the finite sum

$$S_k^{(n)}(t) = \sum_{k'-k,k'-k" = -2\pi n/L}^{2\pi n/L} \frac{U_{k'}U_{k"}^{*}U_{k-k'+k"}}{(k'-k)(k'-k")} \exp(i\omega_{k,k',k"}t)$$

is a quasi-periodic function of t.

Clearly,

$$q_k(t) - S_k^{(n)}(t) = \sum_{\substack{k'-k,k'-k" \geq 2\pi n/L \\ k'-k,k'-k" \leq -2\pi n/L}} \frac{U_{k'}U_{k"}^{*}U_{k-k'+k"}}{(k'-k)(k'-k")} \exp(i\omega_{k,k',k"}t)$$

Now, there exist a $t_0(\epsilon) > 0$ and a $\tau > 0$ in every interval of length t_0 such that

$$\left| S_k^{(n)}(t) - S_k^{(n)}(t+\tau) \right| < \epsilon/3 \quad , \text{ for all } t \qquad (B5)$$

by quasi-periodicity of $S_k^{(n)}$, and

$$\left| q_k(t) - S_k^{(n)}(t) \right| < \rho/(3\rho/\epsilon) = \epsilon/3 \quad , \text{ for all } t \qquad (B6)$$

by Eqs. (B2) and (B3).

Now,

$$q_k(t) - q_k(t+\tau) = \left[q_k(t) - S_k^{(n)}(t) + S_k^{(n)}(t)\right] - \left[q_k(t+\tau)\right.$$

$$\left. - S_k^{(n)}(t+\tau) + S_k^{(n)}(t+\tau)\right] = \left[q_k(t) - S_k^{(n)}(t)\right] - \left[q_k(t+\tau) - S_k^{(n)}(t+\tau)\right]$$

$$+ \left[S_k^{(n)}(t) - S_k^{(n)}(t+\tau)\right] \quad ;$$

whence, by the Cauchy-Schwartz inequality,

$$|q_k(t) - q_k(t+\tau)| \leq |q_k(t) - S_k^{(n)}(t)| + |q_k(t+\tau) - S_k^{(n)}(t+\tau)|$$

$$+ |S_k^{(n)}(t) - S_k^{(n)}(t+\tau)| < \epsilon/3 + \epsilon/3 + \epsilon/3 = \epsilon \text{ , for all } t$$

[by Eqs. (B5) and (B6)].

Thus $q_k(t)$ is an almost-periodic function of time. By standard theorems, therefore, so are $u_k(t)$ and $u(x, t)$.

REFERENCES

1. A. C. Scott, F. Y. F. Chu, and D. W. McLaughlin, Proc. IEEE 61, 1443 (1973).
2. T. Taniuti and H. Washimi, Phys. Rev. Lett. 21, 209 (1968).
3. T. Kakutani and H. Ono, J. Phys. Soc. Jpn. 26, 1305 (1969).
4. G. J. Morales, Y. C. Lee, and R. B. White, Phys. Rev. Lett. 32, 457 (1974).
5. M. J. Ablowitz, D. J. Kaup, A. C. Newell, and H. Segur, Stud. Appl. Math. 53, 249 (1974).
6. V. E. Zakharov and A. B. Shabat, Zh. Eksp. Teor. Fiz. 61, [illegible] (1971) [Sov. Phys.-JETP 34, 62 (1972)].
7. M. Wadati, J. Phys. Soc. Jpn. 34, 1289 (1973).
8. P. D. Lax, Commun. Pure Appl. Math. 21, 467 (1968).
9. N. J. Zabusky and M. D. Kruskal, Phys. Rev. Lett. 15, [illegible]
10. S. P. Novikov, Funkts. Anal. Prilozn. 8, 54 (1974) [Funct. Anal. Appl. 8, 236 (1974)].
11. P. D. Lax, Commun. Pure Appl. Math. 28, 141 (1975).
12. V. A. Marčenko, Mat. Sb. 95, 331 (1974) [Math USSR Sb. 24, 319 (1974)].
13. B. A. Dubrovin, V. B. Matveev, and S. P. Novikov, Usp. Mat. Nauk 31, 55 (1976) [Russian Math. Surveys 31, 59 (1976)].
14. H. Kever and G. K. Morikawa, Phys. Fluids 17, 2090 (1974).
15. E. Fermi, J. R. Pasta, and S. M. Ulam, in Collected Papers of Enrico Fermi, edited by E. Segre (University of Chicago Press, Chicago, 1965), Vol. 2, p. 978.
16. V. E. Zakharov, Zh. Eksp. Teor. Fiz. 65, 219 (1973) [Sov. Phys.-JETP 38, 108 (1974)].

17. J. Ford, in Lectures in Statistical Physics, edited by W. C. Schieve and J. S. Turner, in Lecture Notes in Physics 28 (Springer-Verlag, Berlin, New York, 1974). p. 204.

18. V. I. Arnol'd, Usp. Mat. Nauk 18, 91 (1963) [Russian Math. Surveys 18, 85 (1963)].

19. V. I. Arnol'd, Mathematical Methods of Classical Mechanics (Springer-Verlag, New York, 1978), p. 272.

20. V. E. Zakharov and L. D. Fadeev, Funkts. Anal. Prilozn. 5, 18 (1971) [Funct. Anal. Appl. 5, 280 (1971)].

21. V. E. Zakharov and S. V. Manakov, Teor. Mat. Fiz. 19, 332 (1974) [Theor. Math. Phys. 19, 551 (1974)].

22. N. V. Nikolenko, Funkts. Anal. Prilozn. 10, 55 (1976) [Funct. Anal. Appl. 10, 209 (1976)].

23. L. M. Degtyarev, V. G. Makhan'kov, and L. I. Rudakov, Zh. Eksp. Teor. Fiz. 67, 533 (1974) [Sov. Phys.-JETP 40 , 264 (1975)].

24. S. A. Orszag, Phys. Fluids Suppl. II 12, II-250 (1969).

25. B. M. Lake, H. C. Yuen, H. Rungaldier, and W. E. Ferguson, J. Fluid. Mech. 83, 49 (1977).

26. G. Sandri, Ann. Phys. 24, 332 (1963); 24, 380 (1963).

27. E. A. Frieman, J. Math. Phys. 4, 410 (1963).

28. R. N. Miura, J. Math. Phys. 9, 1202 (1968).

29. Y. Hagihara, Celestial Mechanics, Vol. 1 (The MIT Press, Cambridge, Mass., 1970), p. 149.

30. A. Thyagaraja, Phys. Fluids 22, 2095 (1979).

31. D. Ruelle and F. Takens, Commun. Math. Phys. 20, 167 (1971).

32. J. B. McLaughlin and P. C. Martin, Phys. Rev. A12, 186 (1975).

33. A. B. Katok, Izv. Akad. Nauk USSR 37 (1973) [Math. USSR Izv. 7, 535 (1973)].

34. H. C. Yuen and W. E. Ferguson, Jr., Phys. Fluids 21, 1275 (1978).

35. B. Hafizi; to be submitted to the Physics of Fluids.

36. H. Flaschka, M. G. Forest, and D. W. McLaughlin, Commun. Pure Appl. Math. 33, 739 (1980).

FIGURE CAPTIONS

Fig. 1. Trajectories of k space modes over a period of three recurrences of an initially-Gaussian wave-packet. (a) second mode, (b) sixth mode. At any instant in time t, the electric field is given by $r(t)\exp[i\theta(t)]$. If R is the minimum value of r(t) in the computations, the ordinate and the abscissa are the [illegible] and the real parts of $[r(t)-0.9R]\exp[i\theta(t)]$, respectively, and labeled Imaginary (E'_k) and Real (E'_k) on the figures. This transformation renders the orbit structures much clearer, but greatly exaggerates the angles of intersections in (b).

Fig. 2. Torus, representing the phase-space of a system with two degrees of freedom. Geographical coordinates are q_1 (longitude) and q_2 (latitude).

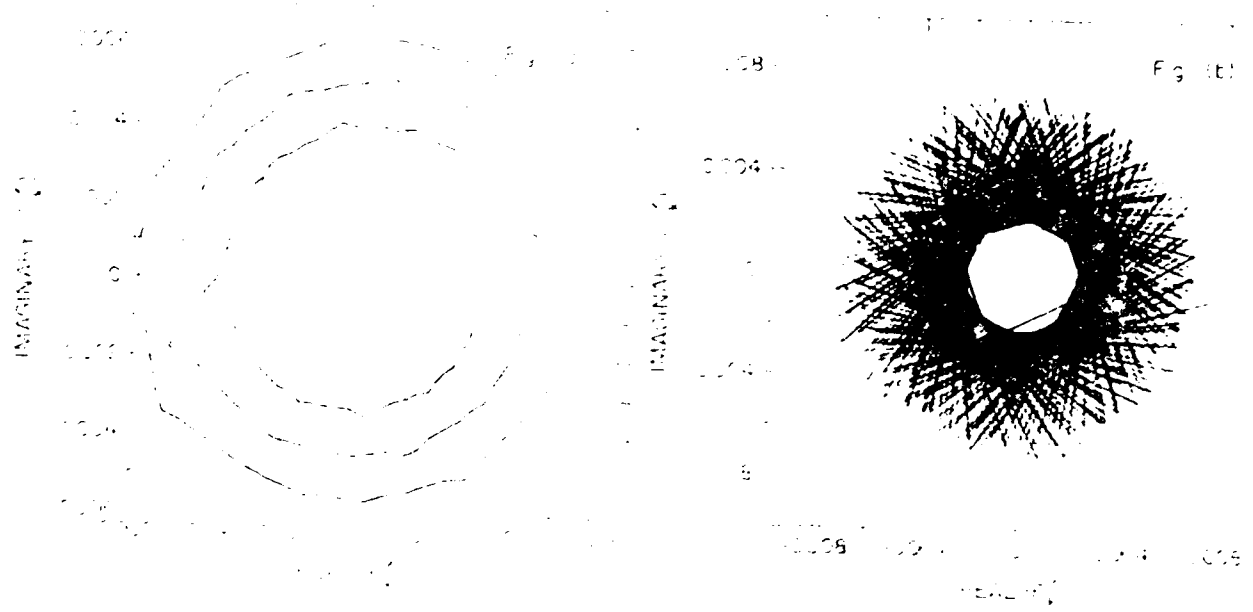

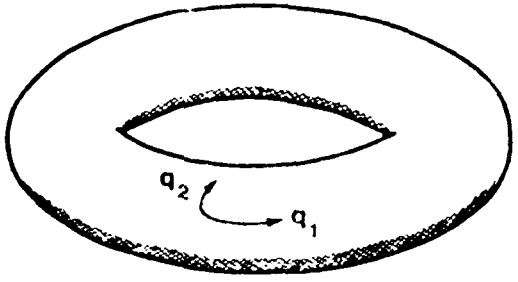

Fig. 2

APPENDIX II

II. "Chaotic (Strange) and Periodic Behavior in Instability Saturation by the Oscillating Two-Stream Instability"

D.A. Russell and E. Ott
Physics of Fluids 24, 1976-1988 (1981).

Chaotic (strange) and periodic behavior in instability saturation by the oscillating two-stream instability

David A. Russell[a)]

Department of Electrical Engineering, Cornell University, Ithaca, New York 14853

Edward Ott

Department of Physics and Astronomy, and Department of Electrical Engineering, University of Maryland, College Park, Maryland 20742

(Received 10 February 1981; accepted 29 July 1981)

The nonlinear Schrödinger equation with linear growth and damping is truncated to three waves. The resulting system of nonlinear ordinary differential equations describes the excitation of linearly damped waves by the oscillating two-stream instability driven by a linearly unstable pump wave. This system represents a simple model for the nonlinear saturation of a linearly unstable wave. The model is examined analytically and numerically as a function of the dimensionless parameters of the system. It is found that the model can exhibit a wealth of characteristic dynamical behavior including stationary equilibria, Hopf bifurcations to periodic orbits, period doubling bifurcations, chaotic solutions characteristic of a strange attractor, tangent bifurcations from chaotic to periodic solutions, transient chaos, and hysteresis. Many of these features are shown to be explainable on the basis of one-dimensional maps. In the case of chaotic solutions, evidence for the presence of a strange attractor is provided by demonstrating Cantor set-like structure (i.e., scale invariance in the surface of section).

I. INTRODUCTION

Recently, it has become clear that nonconservative dynamical systems can exhibit various types of characteristic dynamical behavior. Particular interest has centered on bifurcation phenomena and on the possibility of chaotic motions on a strange attractor (a definition of a strange attractor is given in Sec. IIID). It is probable that these concepts will have an impact on plasma physics, particularly in the area of plasma turbulence.

The present work considers a simple model for instability saturation of a linearly unstable wave: the growth of energy in the unstable wave is arrested when its amplitude is large enough to parametrically excite linearly damped waves. In a previous paper[1] this process was studied for the case in which the parametric excitation of the linearly damped waves was due to the resonant three wave decay instability process. In the present paper we consider the case in which the parametric excitation of linearly damped waves is due to the oscillating two-stream instability. (This problem has been studied elsewhere,[2] however, the present paper is a more thorough investigation of the problem and reveals a greater variety of dynamical behavior than was found in Ref. 2.)

In the case of the resonant three-wave decay instability, Ref. 1, it was reported that as a parameter of the system was increased a sequence of period doubling bifurcations leading to apparently chaotic solutions took place. It was also observed that periodic solutions reemerged from chaos (tangent bifurcations) and existed over narrow ranges of the varied parameter. These features were interpreted on the basis of a numerically obtained, smooth, one-dimensional map. In contrast with this previous work, in the present paper we are able to discern a richer variety of characteristic dynamical behavior. This behavior includes the previously discussed period doubling bifurcations, chaos and tangent bifurcations, in addition to phenomena not observed in the previous paper: transient chaos, hysteresis, and Cantor set-like structure. (It is possible that *hysteresis and transient chaos could also be found* in the three-wave problem but for different parameter ranges than those studied in Ref. 1. Cantor set-like structure is also almost certainly present but could not be computationally resolved.) Another difference from the model discussed in Ref. 1 is that, in the case of the oscillating two-stream instability, stationary final states occupy a comparatively large region of parameter space.

The starting point for obtaining the model equations studied here is the one-dimensional nonlinear Schrödinger equation with linear wave growth and damping included

$$i\left(\frac{\partial E}{\partial t}+\hat{\gamma}E\right)+\frac{\partial^2 E}{\partial x^2}+\left[|E|^2-\langle|E|^2\rangle\right]E=0, \tag{1}$$

where E is the complex amplitude coefficient of the x-directed electric field, $\langle|E|^2\rangle$ denotes the spatial average of $|E|^2$, and $\hat{\gamma}$ is a linear growth-damping operator defined so that the Fourier transform of $\hat{\gamma}E(x,t)$ is $\gamma(k)E_k(t)$, where E_k is the Fourier transform coefficient of E. In addition, normalizations have been introduced so as to absorb any parametric dependences of the coefficients of the various terms in Eq. (1). We now consider (and subsequently justify) an approximate solution of (1) for which E consists of three traveling waves

$$\begin{aligned}E(x,t)=&E_0(t)\exp[i(k_0x-\omega_0t)]\\&+E_1(t)\exp[i(k_1x-\omega_1t)]\\&+E_2(t)\exp[i(k_2x-\omega_2t)],\end{aligned} \tag{2}$$

where $2k_0=k_1+k_2$, $\omega_0=\omega_1^R+\omega_2^R$ ($\omega_j^R=\mathrm{Re}\,\omega_j$, $j=0,1,2$), and $\omega_{1,2}^I=\gamma$

a)Present address: Department of Astro-Geophysics, University of Colorado, Boulder, Colo. 80309.

 0031-9171/81/111976-13$00.90 © 1981 American Institute of Physics

$\omega_{1,2}$. Introducing (2) in (1) and taking the k_0, k_1, and k_2 components of (1) we obtain

$$\dot{E}_0 = -\gamma(k_0)E_0 + i\left[|E_1|^2E_0 + |E_2|^2E_0 + 2\bar{E}_0E_1E_2\exp(2i\delta t)\right], \tag{3a}$$

$$\dot{E}_1 = -\gamma(k_1)E_1 + i\left[|E_0|^2E_1 + |E_2|^2E_1 + E_0^2\bar{E}_2\exp(-2i\delta t)\right], \tag{3b}$$

$$\dot{E}_2 = -\gamma(k_2)E_2 + i\left[|E_0|^2E_2 + |E_1|^2E_2 + E_0^2\bar{E}_1\exp(-2i\delta t)\right], \tag{3c}$$

where $\delta = (\delta_1 + \delta_2)/2$, and $\dot{E}_\sigma = dE_\sigma/dt$. [These equations can be solved analytically[2] in the case $\gamma(k_{0,1,2}) = 0$.]

We now discuss our truncation of the nonlinear Schrödinger equation to just three terms. Consider a system which is periodic in x with period L; then, $k = 2\pi n/L$, $n = \pm1, \pm2, \ldots$. For example, we could take k_0 to be the wavenumber of the fundamental mode, $k_0 = 2\pi/L$, coupled resonantly to a pair of shorter wavelength sidebands, $k_1 = 2\pi n/L$ and $k_2 = 2\pi(2-n)/L$. Our use of only one set of daughter waves (i.e., one value of n) might be justified; for example, if other sets of daughter waves experience much stronger linear damping. More generally, in many physical situations described by Eq. (1), a proper model may require one to include additional daughter wave pairs in the decay process, thus resulting in a larger number of coupled ordinary differential equations. Nevertheless, we believe that, even in such situations, the present analysis may be of some use in that it illustrates, at least qualitatively, a type of behavior that may arise. Accepting the consideration of only one relevant linearly damped daughter-wave pair, we also need to consider the k components which are generated when (2) is substituted into the nonlinear term of (1) (i.e., the term $|E|^2E = E^2\bar{E}$, where $\bar{E}$ denotes the conjugate of E). These k components are just the original k components (k_0, k_1, k_2), plus four additional components:

$$2k_1 - k_0, \quad 2k_2 - k_0, \quad 3k_1 - 2k_0, \quad \text{and} \quad 3k_2 - 2k_0.$$

Equations (3) represent a self-consistent solution of (1) only if E_σ is negligibly small for these additional k values (i.e., the additional k components are strongly damped).

Introducing amplitude-phase variables $E_\sigma \equiv a_\sigma(t)\exp(i\psi_\sigma(t))$, $\sigma = 0, 1, 2$, where a_σ and ψ_σ are real, Eqs. (3) (which are three complex equations) reduce to four real equations,

$$\dot{a}_0 = \gamma_0 a_0 + 2a_0a_1a_2\sin\theta, \tag{4a}$$

$$\dot{a}_{1,2} = -\gamma_{1,2}a_{1,2} - a_0^2a_{2,1}\sin\theta, \tag{4b}$$

$$\dot{\theta} = -2\delta + (a_1^2 + a_2^2 - 2a_0^2) + \left[4a_1a_2 - a_0^2\left(\frac{a_2}{a_1} + \frac{a_1}{a_2}\right)\right]\cos\theta, \tag{4c}$$

where $\theta(t) \equiv 2\psi_0 - \psi_1 - \psi_2 - 2\delta t$, $\gamma_0 = \gamma(k_0)$, $\gamma_{1,2} = \gamma(k_{1,2})$, and we assume that $\gamma_0, \gamma_1, \gamma_2$ are all positive. With this choice of signs, wave 0 is linearly unstable and its nonlinear decay wave products (waves 1 and 2) are linearly damped. Furthermore, we may assume that the amplitudes a_0 and the time have been normalized so that $\gamma_0 = 1$. In this case $\gamma_{1,2}$ are dimensionless and become the decay wave damping rates divided by the pump wave growth rate. Likewise, δ becomes the frequency mismatch normalized to the pump growth rate. Henceforth, we take $\gamma_0 = 1$. In what follows we make a further simplifying restriction; we assume that $\gamma_2 = \gamma_1$ (e.g., consider Landau damping of the sidebands in the case of an even electron velocity distribution function with $k_1 = -k_2$, k_0). In this case Eqs. (4b), when multiplied by $a_{1,2}$ and subtracted from each other, yield

$$\frac{d}{dt}(a_1^2 - a_2^2) = -2\gamma(a_1^2 - a_2^2),$$

where $\gamma = \gamma_1 = \gamma_2$. Thus, $(a_1^2 - a_2^2)$ decays exponentially with time. Since we are particularly interested in the long-time behavior of Eqs. (4), we set $a_1 = a_2$ from the outset. In this case Eqs. (4) reduce from four equations to three equations:

$$\dot{a}_0 = a_0 + 2a_0a_1^2\sin\theta, \tag{5a}$$

$$\dot{a}_1 = -\gamma a_1 - a_0^2a_1\sin\theta, \tag{5b}$$

$$\dot{\theta} = -2\delta + 2(a_1^2 - a_0^2) + 2(2a_1^2 - a_0^2)\cos\theta. \tag{5c}$$

The rest of this paper will be devoted to a discussion of the properties of the solutions of Eqs. (5). Section II discusses analytical results which can be obtained from (5). Section III presents numerical results and discussion. Conclusions and summarizing remarks appear in Sec. IV.

II. PRELIMINARY ANALYTICAL RESULTS AND DISCUSSION

A. Phase space contraction

Let $b_0 = a_0^2$ and $b_1 = a_1^2$. Equations (5) then become

$$\dot{b}_0 = 2b_0 + 4b_0b_1\sin\theta, \tag{6a}$$

$$\dot{b}_1 = -2\gamma b_1 - 2b_0b_1\sin\theta, \tag{6b}$$

$$\dot{\theta} = 2(b_1 - b_0) + 2(2b_1 - b_0)\cos\theta - 2\delta. \tag{6c}$$

We view Eqs. (6) as generating a flow in a three-dimensional Cartesian phase space, (b_0, b_1, θ). By partial differentiation of Eqs. (6) we obtain the divergence of the "velocity" of this flow,

$$\frac{\partial\dot{b}_0}{\partial b_0} + \frac{\partial\dot{b}_1}{\partial b_1} + \frac{\partial\dot{\theta}}{\partial\theta} = -2(\gamma - 1). \tag{7}$$

Thus, the divergence of this flow is a constant and is negative if $\gamma > 1$ (i.e., if the damping rate exceeds the growth rate). Therefore, any volume in this phase space which evolves under the flow generated by Eqs. (6) varies in time as $V(t) = V(0)\exp[-2(\gamma - 1)t]$. Here, we shall only consider the case $\gamma > 1$. (Saturation of the instability was not found for $\gamma < 1$.) In this case volumes always contract exponentially with time. Thus, if the solutions remain bounded (i.e., the wave 0 is saturated), they are expected to eventually approach a confined subspace of the original three dimensional (b_0, b_1, θ) space which has zero volume. This conclusion has important implications, some of which are discussed in Secs. IIB and IIID.

B. Oscillating two-stream instability

Here, we show that Eqs. (5) yield the well-known linear parametric instability threshold condition on the pump amplitude. In particular, it will be shown that $\delta < 0$ is necessary for the oscillating two-stream instability to exist. Thus, only negative δ need be considered in our subsequent discussion. To obtain the linear parametric instability we consider $a_0 = a_1$, and neglect any time dependence of a_0 [i.e., disregard the self-consistent evolution of a_0 generated by Eq. (5a)]. In this case (5c) becomes

$$\dot{\theta} = -2[\delta + a_0^2(1 + \cos\theta)].$$

Focusing our attention on purely growing modes, we set $\dot{\theta} = 0$, and obtain an equation for $\cos\theta$,

$$\cos\theta = -[1 + (\delta/a_0^2)].$$

Thus, δ must be negative in order that $|\cos\theta| < 1$. From (5b) the instability growth rate is $-\gamma - a_0^2\sin\theta$. Thus, for the instability $\sin\theta < 0$ and $a_0^4\sin^2\theta = a_0^4(1 - \cos^2\theta) > \gamma^2$, which, when combined with the result for $\cos\theta$, yields the linear instability threshold conditions $a_0^2 > (\gamma^2 + \delta^2)^{1/2} - \delta$ and $\delta < 0$. While this analysis neglects the self-consistent evolution of a_0, it does provide considerable insight into the full evolution of Eqs. (5). If Eqs. (5) are initialized with small amplitudes, a_0 will start off growing exponentially at the rate one, and a_1 will damp exponentially at the rate γ. Eventually, a_0 will become large enough so that a_1 becomes unstable to the oscillating two-stream instability; a_1 then grows. We will find (Sec. III) that, depending on the parameters and initial conditions, several possibilities then exist for the subsequent evolution of the system: (a) the growth of a_1 may not be sufficiently strong to arrest the instability, and a_0 still grows without bound; (b) the system eventually settles down to a stationary state ($a_{0,1} = \dot{\theta} = 0$); (c) the system eventually settles into a limit cycle for which $a_{0,1}$ and θ are periodic functions of time; and (d) the final state of the system is one in which $a_{0,1}$, and θ vary chaotically with time and $a_{0,1}$ does not go to infinity. Such chaotic solutions are characterized by broad frequency power spectra and sensitive dependence of the solutions upon initial conditions.

In agreement with the conclusions reached in Sec. IIA, for cases (b) and (c) the solution is obviously asymptotic to a zero volume subspace of the original (b_0, b_1, θ) space. For (b) this subspace is simply a point (the stationary state); while for case (c), the subspace is a closed curve which the orbit of the system traces out on each period of its motion. These subsets to which the system orbit asymptotes are called attractors. In Sec. IIID we discuss the attracting set for the case (d), the case of chaotic motions.

C. Stationary equilibria and their stability

In order to investigate the possibility of stationary, time-independent solutions of (6), we set $\dot{b}_0 = \dot{b}_1 = \dot{\theta} = 0$ and obtain (cf. Appendix):

$$a_0^{*2} = -(2\sin\theta^*)^{-1}, \tag{8a}$$

$$b_0^* = -\gamma(\sin\theta^*)^{-1}, \tag{8b}$$

$$\sin\theta^* = \frac{\gamma(\gamma - \frac{1}{2}) \pm [(\gamma - 1)^2(\gamma^2 + \frac{1}{4} - \gamma)]^{1/2}}{\delta^2 + (\gamma - 1)^2}, \tag{8c}$$

where b_0^* and θ^* denote stationary values of b_0 and θ. If $\gamma^2 < (\gamma - \frac{1}{2})$, there are two possible stationary state solutions corresponding to the two signs possibilities in (8c). Both of these solutions satisfy $\sin\theta^* < 0$, so that $b_{0,1}^* > 0$. (This condition is necessary because $b_{0,1}^2 = a_{0,1}^2$.) If $\gamma^2 > (\gamma - \frac{1}{2})$, there are no stationary solutions to Eqs. (8) since (8c) then becomes complex. We now discuss the stability of these stationary solutions. To do this we linearize Eqs. (6) for perturbations about the stationary state:

$$b_{0,1} = b_{0,1}^* + \delta b_{0,1}\exp(st),$$

$$\theta = \theta^* + \delta\theta\exp(st).$$

A cubic equation for s results which can be analyzed to obtain the stability conditions for the stationary states (cf. Appendix). It is found that the solution corresponding to the choice of the plus sign in Eq. (8c) is always unstable. The stability of the remaining root is summarized in the $\delta - \gamma$ space diagram shown in Fig. 1.

III. NUMERICAL RESULTS AND DISCUSSION

In this section we present the result of integrating Eqs. (5) numerically. The frequency mismatch is held constant, $\delta = -6$, so that we are describing the behavior of a dynamical system that depends on a single parameter, γ. (The behavior to be described generalizes to other values of δ as well.) (See Fig. 2.) The discussion is divided into four parts. Part A gives a brief summary of our findings and demonstrates hysteresis. In B we analyze the periodic trajectories using power spectra and a one-dimensional map defined on the surface of section. In C we present some general features of the chaotic behavior as a function of γ. This behavior includes chaotic transients and tangent bifurcations. Our discussion of chaos is completed in D where we in-

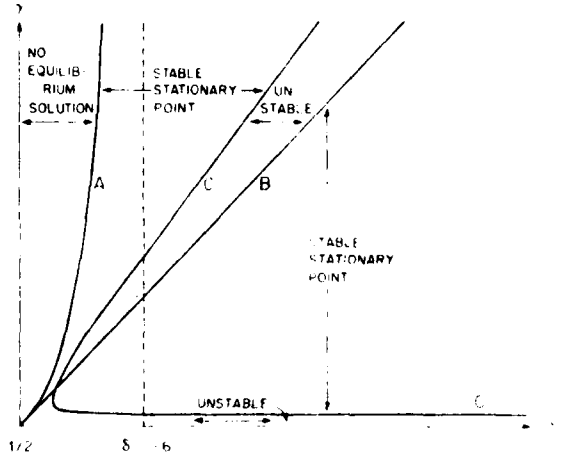

FIG. 1. Stability of the stationary point P^* corresponding to the minus sign choice in Eq. (8c). A: $\gamma < \gamma^2 + \frac{1}{4}$. B: $\gamma > 1/2 - \delta$. C: $\delta^2 < (\delta - 1)^2(\gamma + 1) - (\gamma^2 + \frac{1}{4} - \gamma)$.

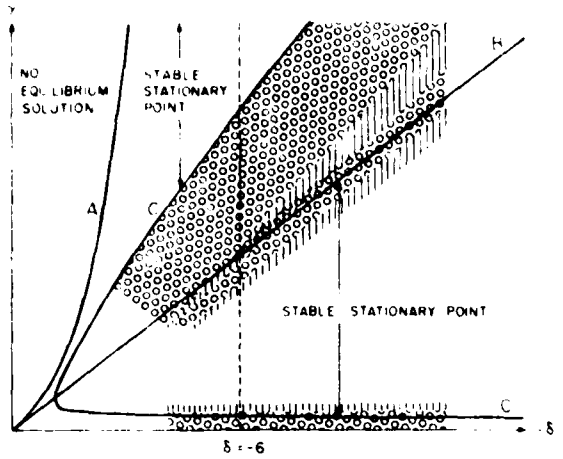

FIG. 2. Long-time asymptotic behavior of (5). ||||||| — chaotic behavior. °°°°° — limit cycles. Overlapping regions indicate the presence of two attractors. (The low γ region has been exaggerated for clarity. Curves A, B, and C are the same as in Fig. 1.)

vestigate a strange attractor. Examples of $a_1(t)$ versus t for typical cases for which the attractor is chaotic, a simple limit cycle, a stationary point, and a stationary point with a chaotic transient are shown in Figs. 3(a) to (d).

A. General remarks and hysteresis

Above curve A in Fig. 1, i.e., $\gamma = \delta^2 + 3$ (=36.75 here), it is observed that the pump wave amplitude, $a_0(t)$, eventually diverges exponentially in time. However, three types of saturated behavior are possible for $36.75 > \gamma > 1$. The trajectory may converge to a stable stationary point, a limit cycle, or a complicated "surface" on which the motion is chaotic (a strange attractor). Thus, we have isolated three types of attractors: points, closed curves, and strange attractors (cf. Table I).

The character of an attractor may change with γ. For example, when $36.75 > \gamma > 9.77$ (i.e., between curves A and C in Fig. 2) the stable stationary point is the only attractor present in phase space. At $\gamma = 9.77$ the system undergoes Hopf bifurcation (cf. the Appendix): the stationary point loses stability, and a stable limit cycle is born in its place. With decreasing γ, this orbit goes through a sequence of period doubling bifurcations that terminates in chaotic behavior at $\gamma = 6.7925$.

For two ranges of γ we observe two co-existing distinct attractors (cf. Table I). Which one a given orbit eventually is asymptotic to is determined by its initial conditions. Aside from their types and locations in phase space we distinguish between them using the long-time average of the pump wave intensity, $\langle a_0^2 \rangle$ (see Fig. 4). Consider the two attractors, labeled A1 and A2 in Fig. 4, that are present when γ is between 5.55 and 6.84. A1 has the larger $\langle a_0^2 \rangle$ value and changes from a limit cycle to a strange attractor as γ decreases from 6.84 to 5.55. A2 has the smaller $\langle a_0^2 \rangle$ value and chang-

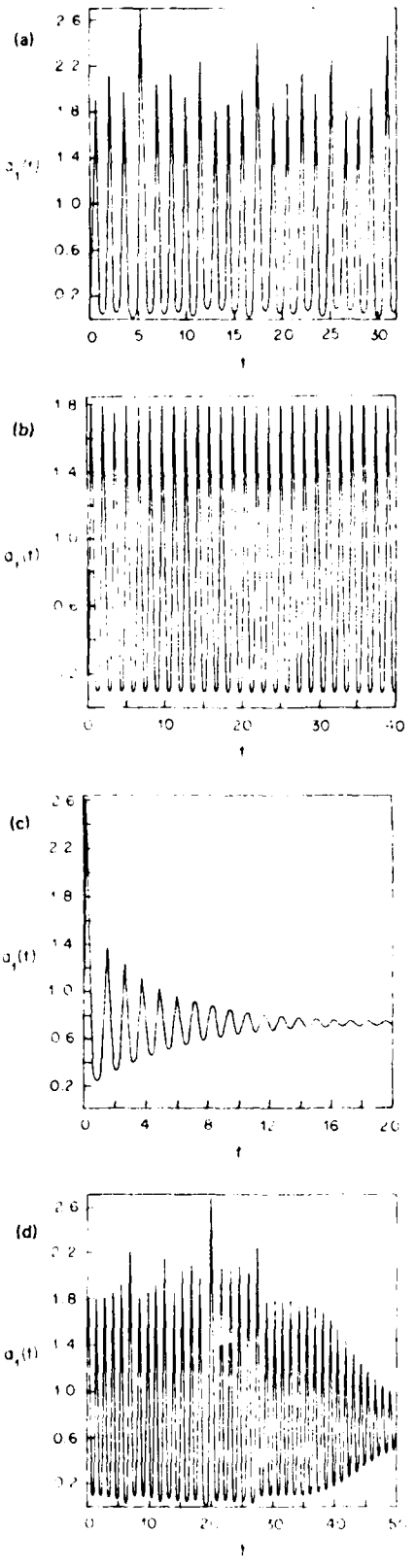

FIG. 3. $a_1(t)$ when (a) $\gamma = 5.6$, illustrating chaos, (b) $\gamma = 7.5$, a simple limit cycle, (c) $\gamma = 5.0$, convergence to the stable stationary point, and (d) $\gamma = 5.5$, a chaotic transient followed by convergence to the stable stationary point.

TABLE I. Saturated behavior of system (5). SSP—stable stationary point, SLC—simple limit cycle. If more than one type of behavior is listed then there are two attractors present for that range of gamma.

9.77	$\gamma <$	36.75		SSP
6.88	γ	9.77		SLC
6.82	γ	6.87	Sequence I	2-cycle or SLC (γ > 6.84)
6.7966	γ	6.81	Sequence I	4-cycle or SLC
6.7956	γ	6.7965	Sequence I	8-cycle or SLC
6.79295	γ	6.7935	Sequence I	16-cycle or SLC
	γ	6.79287	Sequence I	32-cycle or SLC
6.362	γ	6.79250		Chaos or SLC (γ > 6.5) or SSP (γ < 6.5)
6.17	γ	6.361		SLC or SSP
6.07	γ	6.16	Sequence II	2-cycle or SSP
6.05	γ	6.06	Sequence II	4-cycle or SSP
6.0356	γ	6.045	Sequence II	8-cycle or SSP
6.03482	γ	6.03555	Sequence II	16-cycle or SSP
6.034601	γ	6.03481	Sequence II	32-cycle or SSP
6.034556	γ	6.034600	Sequence II	64-cycle or SSP
	γ =	6.034555	Sequence II	128-cycle or SSP
5.55	γ	6.03454		Chaos or SSP
1.81	γ	5.50		SSP
	γ	1.805	Sequence III	Chaos or SSP
	γ =	1.80	Sequence III	8-cycle or SSP
	γ	1.75	Sequence III	2-cycle or SSP
1.05	γ	1.70	Sequence III	SLC or SSP (γ > 4.3)
				or SLC (Hopf, 1.3 < γ < 4.3)

es from a limit cycle (different from A1) to a stable fixed point as γ decreases through the same range. A1 is absent and A2 is a point if γ < 5.55. A2 is absent and A1 is a limit cycle if γ > 6.84.

Suppose we choose a value of γ for which both attractors A1 and A2 exist and pick initial conditions on A1. We allow the system to evolve in time and slowly decrease γ. The trajectory will remain on A1 until this attractor vanishes at γ = 5.55, then the trajectory will be drawn to A2. Apparently, this is because as γ approaches 5.55 from above, A2's neighborhood of attraction swells to intersect A1. Initial points that would be on or near the strange attractor, A1, for γ > 5.55 converge to A2 for γ < 5.55 along trajectories that wander chaotically for a while as though A1 were still present. (See Sec. IIIC for a discussion of such chaotic transients.) Increasing γ to its original value, we will have changed the state of the system from A1 to A2. By analogy to magnetostatics, the existence of two states of the system for a given choice of γ, or equivalently, the dependence of the global behavior on initial conditions, is called hysteresis.[3] [Notice that from (6) we have $\langle a_0^2\rangle/\langle a_1^2\rangle = 2\gamma$ for all saturated states of the system.]

B. Period doubling bifurcations

Figures 5(a) to (c) show $a_1(t)$ for three values of γ illustrating successive period doubling bifurcations. Three sequences of such bifurcations, beginning with a simple limit cycle, have been observed for $\delta = -6$ (see Table I). To study these bifurcations, we record the intersections of the trajectory with a $\dot{a}_1$ = constant plane. This plane is our surface of section. For definiteness, we keep only those points for which $\dot{a}_1 > 0$. Thus, we generate a sequence of points $\{[a_0(t_n), a_1(t_n)]\}$, where t_n is the time of the nth piercing of the surface of section. These points represent a cross section of the attractor in the long-time asymptotic limit.

$$P_\gamma[a_0(t_n), a_1(t_n)] = [a_0(t_{n+1}), a_1(t_{n+1})]$$

defines the Poincaré map of (5). This is a discrete two-dimensional map and is necessarily invertible because (5) is a system of first-order, ordinary differential equations.

It is often observed that the orbit trajectory intersects the surface of section on what appears (at least to a

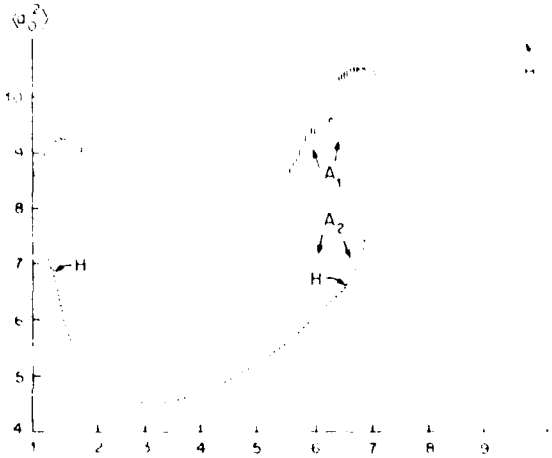

FIG. 4. Hysteresis: the long-time average of a_0^2 versus γ. ||||||—chaotic behavior, ∞∞∞∞∞—limit cycles, ... stable stationary point. *H* indicates a Hopf bifurcation (A1 and A2 are labels used in the text).

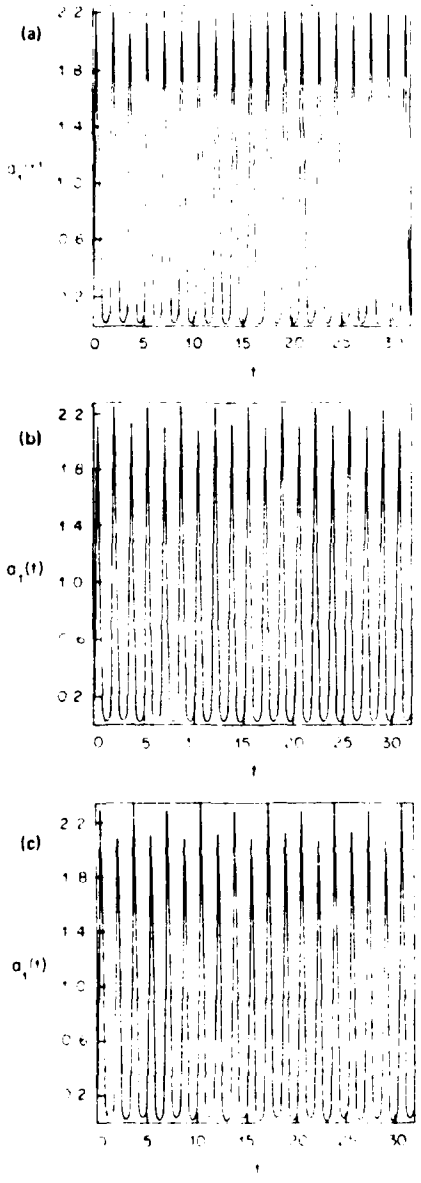

FIG. 5. $a_1(t)$, illustrating successive period-doubling bifurcations. (a) $\gamma = 6.25$, a simple limit cycle, (b) $\gamma = 6.12$, a 2-cycle, and (c) $\gamma = 6.055$, a 4-cycle.

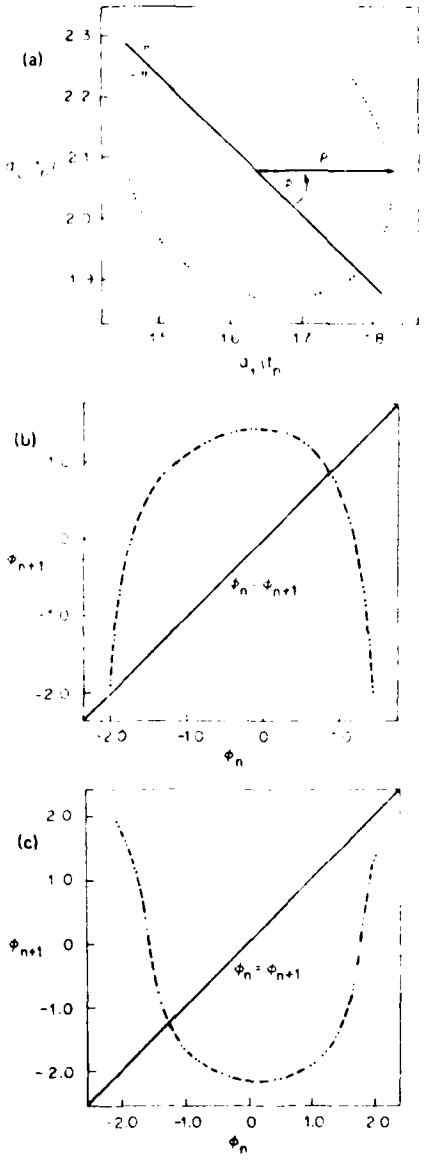

FIG. 6. Construction of the one-dimensional map, F_γ, from points in the surface of section. (a) surface of section and (b) one-dimensional map, F_γ, constructed from the 32-cycle ($n = 5$) at $\gamma = 6.03447$. (c) F_γ for the 32-cycle at $\gamma = 6.79287$.

first approximation) to be a simple smooth arc. In such cases it makes sense to construct a discrete one-dimensional map, F_γ, from the Poincaré map. (F_γ plays a fundamental role in our description of period doubling bifurcations in this section and is used to account for the tangent bifurcations from chaotic to periodic behavior described in Sec. IIIC.)

For many-times bifurcated periodic orbits, this arc has a roughly semicircular shape. We choose to adopt polar coordinates in the surface of section [cf. Fig. 6(a)]. This turns out to be a good choice for defining F_γ. I_γ may then be written as $I_\gamma(\rho_n, \phi_n) = (\rho_{n+1}, \phi_{n+1})$, where $(\rho_n, \phi_n) = [\rho(t_n), \phi(t_n)]$. Suppose we restrict our attention to the coordinate ϕ and graph ϕ_{n+1} versus ϕ_n for each trajectory in (a_0, a_1, v) phase space that we wish to study using F_γ. For all of the periodic orbits studied, this discrete graph appears to lie on a simple smooth curve in the (ϕ_n, ϕ_{n+1}) plane [cf. Fig. 6(b) and (c)]. Furthermore, this curve intersects any ϕ_n constant line in at most one point. Therefore, we define F_γ to be the simplest smooth interpolation of the discrete graph $[(\phi_n, \phi_{n+1})]$ such that

$$F_\gamma(\phi_n) = \phi_{n+1}.$$

This gives us a well-defined, i.e., single-valued, map for all trajectories observed to be asymptotic to a periodic orbit, provided that some of the early transient behavior is ignored. It is understood that there are

enough points in the discrete graph to make this interpolation reasonably unambiguous. For example, a twice-bifurcated simple limit cycle intersects the surface of section in only four points. Nevertheless, we will assume that the map, F_γ, at this "4-cycle" is similar to that which is more conveniently defined at higher bifurcations of the same cycle. This assumption is supported by the transient behavior of trajectories near the 4-cycle: the corresponding transient points in the discrete graph, $\{(\phi_n, \phi_{n+1})\}$, lie along arcs representing pieces of F_γ at higher bifurcations.

The construction of F_γ is illustrated in Fig. 6. We require only that $p > 0$ be "inside" the attracting arc in the surface of section and that $\theta = 0$ be chosen so as to permit construction of a well-defined F_γ. This was always possible for the cases studied. Otherwise, the choice of origins for p and θ does not affect the behavior of F_γ as is pertains to the bifurcation phenomena to be described.

The maps, F_γ, are not invertible: two different ϕ_n's are mapped into the same ϕ_{n+1}. In the chaotic regimes, where virtually no interpolation is required, this (combined with the necessary invertibility of P_γ) implies that the arc in the surface of section must have finite width: if

$$(\rho_n, \phi_n), (\rho_n, \phi_n) \xrightarrow{P_\gamma} (\rho'_n, \phi'_n), (\rho''_n, \phi''_n),$$

then $\rho'_n \neq \rho''_n$. The structure within the attracting arc in the case of chaotic motion is discussed in Sec. IIID. (Naturally, it is reasonable to reduce the two-dimensional Poincaré map to the one-dimensional map F_γ only if the transverse thickness of the arc containing this structure is thin.)

Iterates of the map are defined in an obvious way:

$$F_\gamma^{(2)}(\phi) \equiv F_\gamma[F_\gamma(\phi)], \quad F_\gamma^{(3)}(\phi) \equiv F_\gamma\{F_\gamma[F_\gamma(\phi)]\}, \quad \text{etc.}$$

The fixed points of $F_\gamma^{(k)}$ are the intersections of its graph, $\phi_{n+k} = F_\gamma^{(k)}(\phi_n)$, with the identity $\phi_{n+k} = \phi_n$. If ϕ_m^* is a fixed point of $F_\gamma^{(k)}$, then $\phi_{m+k}^* = \phi_m^*$. Linearizing $F_\gamma^{(k)}$ about the fixed point, it is easy to see that ϕ_m^* is stable if, and only if, $|DF_\gamma^{(k)}(\phi_m^*)| < 1$, where $DF_\gamma^{(k)}$ denotes the derivative of $F_\gamma^{(k)}$ with respect to its argument. By the chain rule

$$DF_\gamma^{(k)}(\phi_m^*) = F'_\gamma(\phi_{m+k-1}^*) F'_\gamma(\phi_{m+k-2}^*) \cdots F'_\gamma(\phi_m^*),$$

and the prime denotes differentiation with respect to the argument.

If ϕ_m^* is a fixed point of $F_\gamma^{(k)}$ but not of $F_\gamma^{(k/\nu)}$, $\nu = 1, 2, \ldots, k-1$, then so are the $k-1$ points $\phi_{m+k-1}^*, \phi_{m+k-2}^*, \ldots, \phi_{m+1}^*$. These k fixed points of $F_\gamma^{(k)}$ are cycled among themselves by F_γ and share the same stability because $DF_\gamma^{(k)}$ has the same value at each of them. Let us call these points the irreducible fixed points of $F_\gamma^{(k)}$; they may or may not exist, depending on γ.

A bifurcation sequence may be described as follows. A stable limit cycle exists for values of γ in one of the three intervals given in Table I. Each interval is partitioned by a sequence of critical values of γ, γ_j, $j = 1, 2, \ldots$). Between the γ_j's the period, T, of the cycle is a continuous function of γ but doubles discontinuously at each γ_j:

$$\lim_{\gamma \to \gamma_j} \frac{T(\gamma_j + \sigma)}{T(\gamma_j - \sigma)} = \begin{matrix} 1 \\ 2 \end{matrix}$$

(upper signs refer to sequences I and II in Table I, and lower signs refer to sequence III).

When γ is between γ_n and γ_{n+1}, the limit cycle intersects the surface of section in 2^n points, and $F_\gamma^{(2^n)}$ has 2^n stable irreducible fixed points, ϕ_m^*; these are the only stable fixed points that $F_\gamma^{(2^n)}$ has. (Therefore, a single trajectory is called a "2^n cycle".) As γ approaches γ_{n+1}, $DF_\gamma^{(2^n)}(\phi^*)$ approaches -1 from above, and transient points are observed to converge more slowly to, and to alternate about, the stable fixed points. As γ passes through γ_{n+1}, each irreducible fixed point of $F_\gamma^{(2^n)}$ loses stability, bifurcating into two of the 2^{n+1} new-born stable irreducible fixed points of $F_\gamma^{(2^{n+1})}$. This process is illustrated in Fig. 7.

Feigenbaum has conducted theoretical studies of a class of one-dimensional maps having a single extremum and depending on a single parameter.[3] Our maps apparently belong to this class. These maps generate an infinite sequence of period doubling bifurcations as the parameter approaches a critical value γ_∞, the limit point of the γ_j's, and in this limit show striking universal quantitative behavior. We now briefly describe this predicted behavior near $\gamma = \gamma_\infty$ and compare it with our numerical results.

The range of γ over which a stable 2^n cycle exists decreases geometrically fast with increasing n. Let

$$\Delta_n \equiv (\gamma_{n-1} - \gamma_{n-2})/(\gamma_n - \gamma_{n-1}).$$

For maps having a quadratic extremum, i.e.,

$$F_\gamma(\phi - \phi_0) \sim (\gamma/2)\phi^2$$

the theory determines that

$$\lim_{n \to \infty} \Delta_n = 4.6642016\ldots$$

We find that for sequence I

$$\Delta_n = 4.76 \pm 0.65$$

and for sequence II

$$\Delta_n = 4.77 \pm 0.18$$

($n = 5, 7$ is as far as we were able to pursue sequences I, II; sequence III was not systematically studied because of the comparatively slow time evolution of the transients).

Let ϕ_j^n, $j = 1, 2, \ldots, 2^n$, be the irreducible stable fixed points of $F_\gamma^{(2^n)}$, ordered so that ϕ_{2j-1}^n and ϕ_{2j}^n are born from ϕ_j^{n-1} by bifurcation. For definiteness, choose

$$d_j^n \equiv \phi_{2j-1}^n - \phi_{2j}^n \quad \text{when } DF_\gamma^{(2^n)}(\phi_j^n) < 0.$$

From Fig. 8(e) it is clear that d_1^n is a rapidly decreasing function of n. This is a reflection of the increased convolution of the map with increased iterates.

Suppose ϕ_1^n and ϕ_2^n are on some small neighborhood of the extremum of F_γ, ϕ_0. When γ is chosen so that $DF_\gamma^{(2^n)}(\phi_j^n) = 0$, $j = 1, 2, \ldots, 2^n$, ϕ_1^n and ϕ_2^n are separated by a distance of d_1^n. Upon bifurcation to the stable 2^{n+1} cycle, ϕ_1^n and ϕ_2^n split into $\phi_{1,2}^{n+1}$ and $\phi_{3,4}^{n+1}$, respectively,

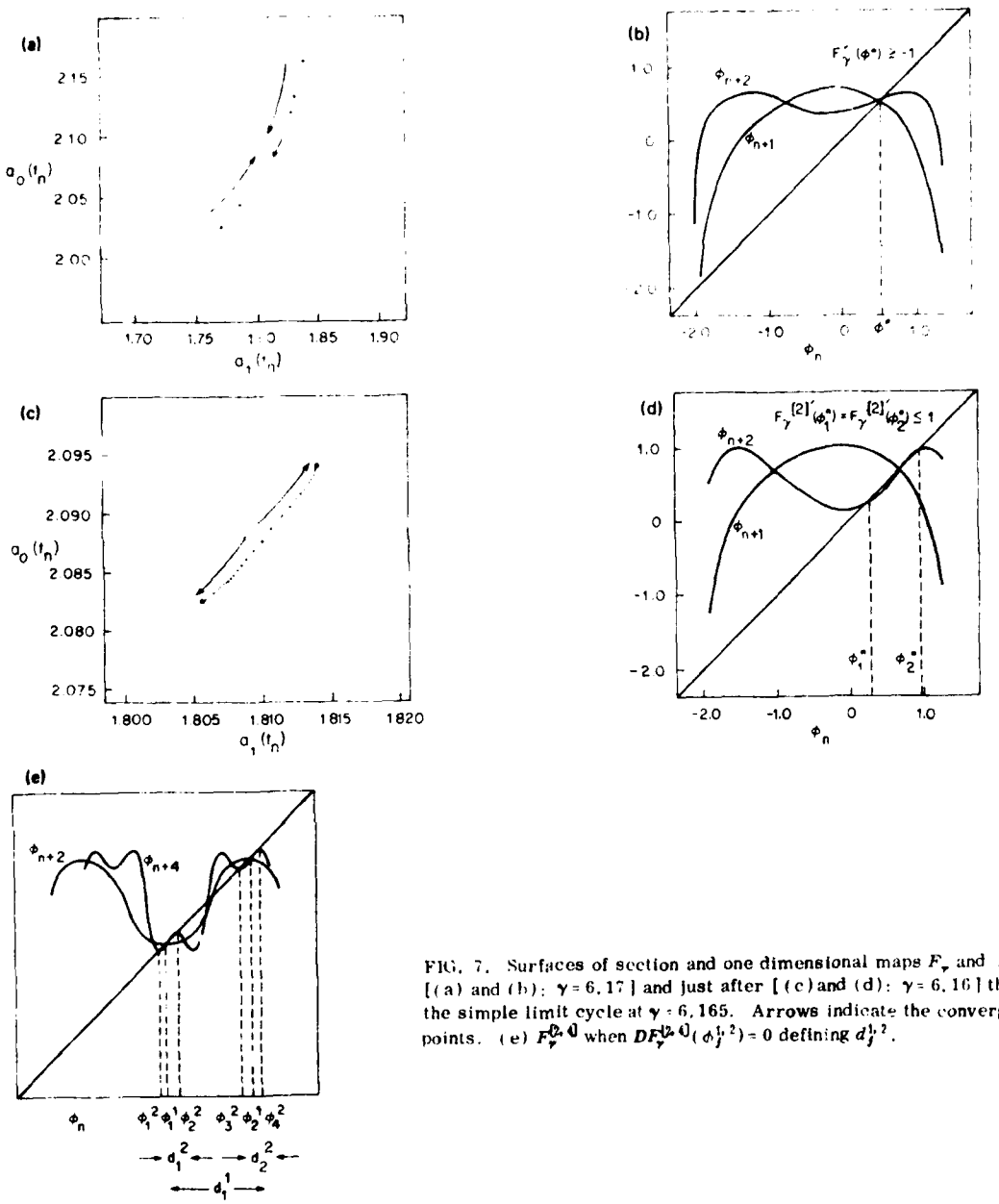

FIG. 7. Surfaces of section and one dimensional maps F_γ and $F_\gamma^{[2]}$, just before [(a) and (b): $\gamma = 6.17$] and just after [(c) and (d): $\gamma = 6.16$] the bifurcation of the simple limit cycle at $\gamma = 6.165$. Arrows indicate the convergence of transient points. (e) $F_\gamma^{[2,4]}$ when $DF_\gamma^{[2,4]}(\phi_j^{1,2}) = 0$ defining $d_j^{1,2}$.

For large n these two pairs are also in some small neighborhood of ϕ_0. When γ is chosen so that $DF_\gamma^{[2^{n-1}]}(\phi_j^{n-1}) = 0$, $j = 1, 2, \ldots, 2^{n-1}$, ϕ_1^{n-1} and ϕ_2^{n-1} (ϕ_3^{n-1} and ϕ_4^{n-1}) are separated by a distance d_1^{n-1} (d_2^{n-1}). Feigenbaum's theory determines that for large n, $d_1^n/d_{1,2}^{n-1} \sim$ a constant depending only on the order of the extremum ϕ_0. For those ϕ_j^n and ϕ_k^{n-1} nearest to ϕ_0 the theory predicts that

$$\lim_{n\to\infty} (d_j^n/d_k^{n-1}) = 2.5029\ldots \equiv \alpha$$

for maps with a quadratic extremum. In other words, the distances, d_j^n, between ϕ_j^n's near ϕ_0 are reduced by a factor of α upon bifurcation.

If F_γ has a quadratic extremum, then $|F_\gamma(\phi_1^n) - F_\gamma(\phi_2^n)| \sim |\phi_1^n - \phi_2^n|^2 \sim (d_1^n)^2$ and $|F_\gamma(\phi_1^{n-1}) - F_\gamma(\phi_2^{n-1})| \sim (d_1^{n-1})^2 \sim (d_1^n \alpha)^2$. But, $F_\gamma(\phi_1^{n-1})$ and $F_\gamma(\phi_2^{n-1})$ bifurcate from $F_\gamma(\phi_1^n)$. Therefore, the distances, d_j^n, between ϕ_k^n's near $F_\gamma(\phi_0)$ are reduced by a factor of α^2 upon bifurcation. In general, the d_j^n's rescale under bifurcation according to a complicated function of ϕ. However, for large n, a first approximation to this function has half of the d_j^n's rescaling by α and half by α^2 (cf. Ref. 5).

This rescaling has important implications for the spectrum of a highly bifurcated limit cycle. Let $A^n(\omega)$ be the frequency spectrum of a 2^n cycle. $\mathrm{Log}_{10}|A^n(\omega)|$ has pronounced peaks at $\omega_k = \omega_0(k\ 2^n)$, $k = 1, 2, \ldots, 2^n$,

for some $\omega_0(\gamma)$. Let $A_k^n \equiv A^n(\omega_k)$ denote these components of the spectrum. Feigenbaum shows[5] that for n asymptotically large,

$$|A_{2k-1}^{n+1}| = |A_{k-1/2}^n| \mu, \quad k = 1, 2, \ldots, 2^n.$$

Here, $A_{k-1/2}^n$ is obtained by smoothly interpolating the odd k components of $A^n(\omega)$ and $\mu \equiv 4\alpha[2(1+\nu^{-2})]^{-1/2} = 6.57\ldots$. Thus, in the limit of many bifurcations the odd subharmonics of the spectrum tend to be self-similarly reproduced. For sequences I and II we calculate an average odd subharmonic rescaling factor:

$$\log_{10}(\mu_n) \equiv \langle \log_{10}|A_k^n| - \tfrac{1}{2}\log_{10}|A_{2k-1}^{n+1}| - \tfrac{1}{2}\log_{10}|A_{2k+1}^{n+1}| \rangle_{\text{odd } k}$$

for $n = 2$ through 4 and 6, respectively. We offer the averaged values of $\log_{10}(\mu_n)$ over all bifurcations of the sequence for comparison with Feigenbaum's result, $\log_{10}(\mu) = 0.818\ldots$

$$\text{Sequence I: } \langle \log_{10}(\mu_n) \rangle_{n=2,3,4} = \begin{cases} 0.781, & \tilde{a}_0 \\ 0.832, & \tilde{a}_1 \end{cases}$$

$$\text{Sequence II: } \langle \log_{10}(\mu_n) \rangle_{n=2,\ldots,7} = \begin{cases} 0.834, & \tilde{a}_0 \\ 0.832, & \tilde{a}_1 . \end{cases}$$

[Here $\tilde{a}_{0,1}$ indicates the spectrum of $a_{0,1}(t)$.]

C. Chaotic behavior and tangent bifurcations

The long-time asymptotic behavior of (5) is said to be chaotic when the motion is not discernably periodic. Nonperiodic motion is observed to be stochastic: if two initial points in (a_0, a_1, θ) phase space are chosen very close to each other, but not on the same trajectory, then the distance between them, $\delta x(t)$, diverges exponentially fast immediately after they begin to move along their respective trajectories,

$$\delta x(t) \sim \delta x(0)\exp(\lambda_1 t), \quad \lambda_1 = \lambda_1(\gamma) > 0. \tag{9}$$

Eventually this exponential divergence saturates abruptly, and $\delta x(t)$ becomes an erratic function of time (see Fig. 8).

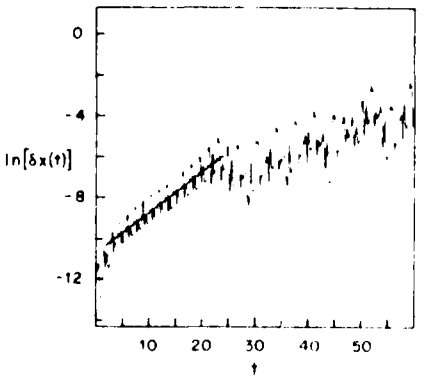

FIG. 8. Stochasticity: the natural logarithm of the distance, $\delta x(t)$, between two initially very close points when the long-time asymptotic behavior is chaotic. $\gamma = 6.729$. Initially, $\delta x(t)$ oscillates about an average value that diverges exponentially in time.

Each of the bifurcation sequences described above culminates in apparently chaotic behavior. In principle this chaos is a product of infinitely many period doublings as γ approaches the critical point Γ_c, and the period of the motion diverges. In fact, when γ is just beyond the critical point the power spectrum, $\log_{10}|A(\omega)|$, may be thought of as a superposition of two parts. One part is discrete and consists of a finite number of sharp spikes. The other part is continuous as a function of ω. The spikes achieve a height above the erratic, or "noisy," part of the power spectrum; they are evenly spaced and correspond closely to the taller spikes in the power spectrum of the periodic motion observed just before γ moves through Γ_c. This endurance of the stronger subharmonics of the periodic

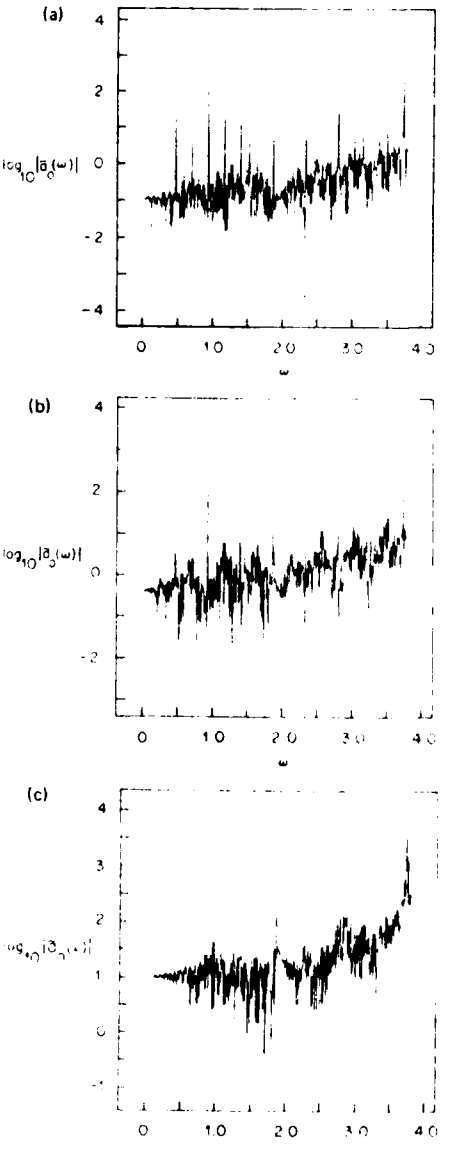

FIG. 9. Quasi-periodic chaotic behavior: the power spectrum, $\log_{10}|\tilde{a}_0(\omega)|$, of the pump wave amplitude at (a) $\gamma = 6.03460$, (b) $\gamma = 6.03425$, and (c) $\gamma = 6.029$. These values of gamma lie just beyond the critical point $\Gamma_c \simeq 6.03454$.

motion gives the onset of chaos a "quasi-periodic" character, as shown in Fig. 9. The average height of the noisy part of the power spectrum increases as γ moves away from Γ_c into the chaotic regime, but the heights of the sharp spikes remain approximately constant. Consequently, the smaller spikes are successively lost in the noisy part of the power spectrum as γ moves beyond the critical point.

The chaotic regimes are punctuated by sudden appearances of stable 3- and 5-cycles. These periodic orbits are born via "tangent bifurcations"[6] when $F_\gamma^{(3,5)}$ is tangent to the identity, $\phi_f = \phi_{f^{3,5}}$, as in Fig. 10(a). Period doubling to stable 3×2^n and 5×2^n cycles occurs as described in Sec. IIIB and eventually results in a return to chaotic behavior. However, it is observed that these 3×2^n and $5\cdot2^n$ cycles exist only over a very small interval in γ (e.g., the range in γ is less than $2\cdot10^{-3}$ for the 3×2^n cycles). In the chaotic regime following sequence I the map, F_γ, develops an inflection at its minimum. This new local maximum rises with decreasing γ to intersect the identity and terminate the chaotic regime. This is shown in Fig. 10(b). The simple limit cycle that begins sequence II is thus born by tangent bifurcation.

Suppose a tangent bifurcation to a stable k cycle occurs at γ_t such that the behavior is chaotic for $\gamma < \gamma_t$, when the attractor intersects the surface of section in some arc. Then for $\gamma < \gamma_t$, trajectories are observed to puncture the surface chaotically along the arc until the intersections fall within the attracting neighborhood of the stable fixed points of $F_\gamma^{(k)}$. The duration of these "chaotic transients"[7-9] depends sensitively on the initial point chosen and on γ. As γ approaches γ_t from below, the attracting neighborhood of the fixed points diminishes, and the transients tend to last longer.

Chaotic transients are also observed following the disappearance of the strange attractor (labeled A1 in Fig. 4) at $\gamma = 5.55$. For $\gamma < 5.55$ this attractor coexists with a stable stationary point (A2 in Fig. 4). As γ approaches 5.55 the neighborhood of attraction of the fixed point apparently intersects the strange attractor. If we choose an initial point in (a_0, a_1, γ) phase space that would lie on A1 for $\gamma < 5.55$ and evolve the system in time with $\gamma > 5.55$, so that A1 does not exist, the immediate subsequent behavior is as if A1 were still present. That is, for γ slightly less than 5.55, transient points are distributed along an arc in the surface of section that is nearly indistinguishable from the intersection of A1 with the surface of section observed when $\gamma < 5.55$. The duration of this chaotic transient depends strongly on where we choose the initial point on the "remnant" of A1. Eventually, the trajectory converges to the stable stationary point A2. Some examples of chaotic transients are illustrated in Fig. 11.

D. A strange attactor

Bifurcation sequence III converges in γ to chaotic behavior at $\gamma = 1.805$. The chaotic behavior is very

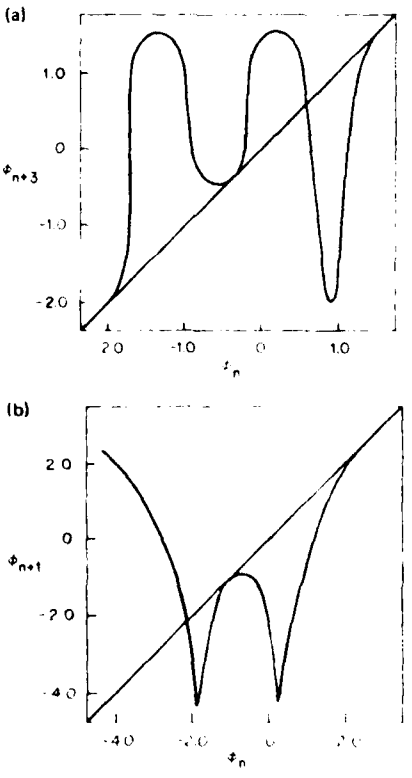

FIG. 10. Tangent bifurcations to (a) the 3-cycle at $\gamma = 5.9885$ and (b) the simple limit cycle at $\gamma = 6.361$.

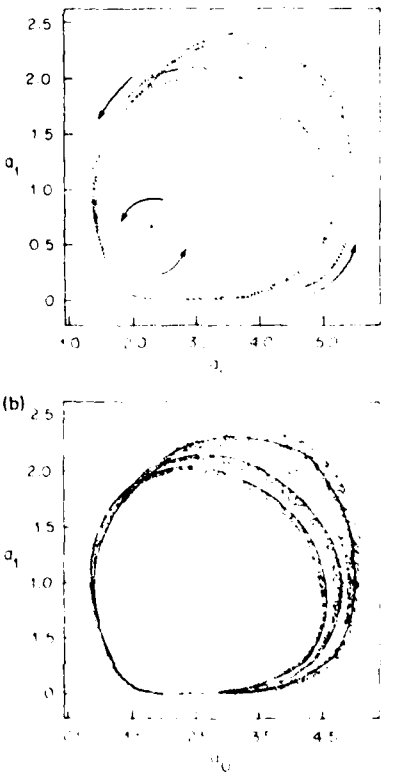

FIG. 11. Chaotic transients: projection of the motion onto the a_0–a_1 coordinate plane when convergence is to (a) the stationary point at $\gamma = 5.540$ (40 transient points in the surface of section) and (b) the 3-cycle at $\gamma = 5.9885$ (110 transient points in the surface of section).

short-lived in γ (cf. Table I). At these smaller values of γ the system evolves more slowly in time and is globally much more sensitive to initial conditions. Possibly due to the slower contraction of phase space volumes, the attractor intersects the surface of section in an arc of easily discernible thickness.

On magnification, the attracting arc is seen to be made up of several closely spaced lines some of which appear to be thicker than others. Higher magnification of one of the thick lines (cf. Fig. 12) reveals the same pattern of lines as was found by the first magnification. This repetition of a pattern under magnification, or "scale invariance," is also a property of the Cantor set. (See the Appendix for a definition of the Cantor set.)

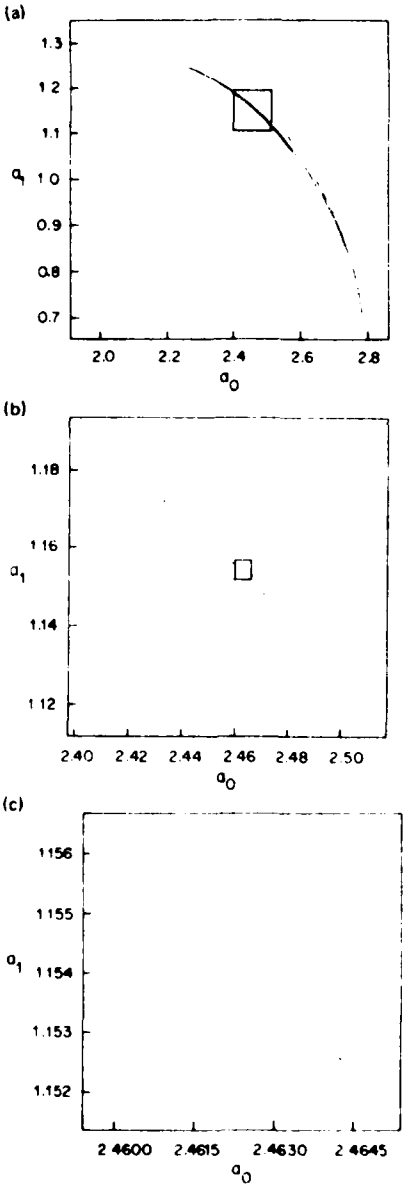

FIG. 12. Scale invariance of the strange attractor at $\gamma = 1.805$: (a) the attracting arc in the surface of section, (b) enlargement of the small box in (a), (c) enlargement of the small box in (b).

Attractors having Cantor set-like scale invariance are among the earliest theoretical examples of strange attractors.[10,11] This structure has since been observed numerically in the strange attractors of some two-dimensional maps used to model dynamical systems.[12,13]

To compare the structures of different attractors, we define a fractional dimension[14] as follows. Let $N(\epsilon)$ be the minimum number of cubes of side length ϵ required to cover the attractor. Then,

$$D = \lim_{\epsilon \to 0} \frac{\log N(\epsilon)}{\log(1/\epsilon)} \tag{10}$$

is the Hausdorff dimension of the attractor. To locate the attractor to within the precision ϵ we need $N(\epsilon)$ bits of information. For small ϵ, $N(\epsilon) \sim \epsilon^{-D}$. For example, the dimension of a point is zero $[N(\epsilon) = 1]$, that of a closed orbit is one $[N(\epsilon) \sim \epsilon^{-1}]$, and that of the surface of a three-dimensional sphere is two $[N(\epsilon) \sim \epsilon^{-2}]$.

For most purposes, an attractor will be said to be strange if its dimension is nonintegral. The dimension of the Cantor set defined in the Appendix is $\log(2)/\log(3) = 0.6309\ldots$. In an earlier paper[15] we used the definition, Eq. (10), to determine D numerically for the chaotic attractor at $\gamma = 1.805$:

$$D = 2.318 \pm 0.002 .$$

As an example of a set with dimension between two and three, consider the union of concentric spherical surfaces in 3-space whose radii are the elements of the Cantor set defined in the Appendix. The dimension of this set is $2.6309\ldots$.

The dimension may be related to the local stability of trajectories on the attractor. Let $\delta\mathbf{x}(t)$ denote the vector displacement of two points in phase space that are evolved by Eqs. (5). For $|\delta\mathbf{x}(0)|$ arbitrarily small, we may assume that subsequently

$$\delta\mathbf{x}(t) = \mathsf{A}(t) \cdot \delta\mathbf{x}(0) . \tag{11}$$

Writing (5) as $\dot{\mathbf{x}} = G(\mathbf{x})$, we find

$$\dot{\mathsf{A}} = \mathsf{DG}(\mathbf{x}) \cdot \mathsf{A} ,$$

where DG is the Jacobian of (5). Let $[\alpha_j(t),\ j = 1,2,3]$ be the eigenvalues of $\mathsf{A}(t)$. Then,

$$\lambda_j = \lim_{t \to \infty} \ln |\alpha_j(t)|^{1/t}, \quad j = 1,2,3 ,$$

defines the Lyapunov "type numbers"[16] of (5). One of these, λ_2 say, is necessarily zero. [To see this notice that the distance between two close points on the same trajectory varies as $|G(\mathbf{x})|$.] From (11), phase space volumes contract exponentially at the rate $-(\lambda_1 + \lambda_2 + \lambda_3)$, so that using (7) we have

$$\lambda_1 + \lambda_3 = -2(\gamma - 1) < 0 . \tag{12}$$

For stochastic trajectories one of these, λ_1 say, is greater than zero. [This is the same λ_1 as in (9).]

A conjecture has recently been made relating the Lyapunov numbers to the dimension of a strange attractor.[17] For n-dimensional phase space this conjecture is

$$D = k + \frac{\lambda_1 + \lambda_2 + \cdots + \lambda_k}{-\lambda_{k+1}} = D_L ,$$

where $\lambda_1 > \lambda_2 > \cdots > \lambda_n$ and k is the largest integer for which $\lambda_1 + \lambda_2 + \cdots + \lambda_k > 0$. For the present system $k = 2$. Aided by Eq. (12), we have found the Lyapunov numbers numerically[15]:

$$D_L = 2.317 \pm 0.001,$$

so that $D = D_L$ to within the obtained accuracy, consistent with the conjecture.

IV. CONCLUSION

We have modeled the nonlinear saturation of the oscillating two-stream instability using a three-dimensional dynamical system resulting from a truncation of the nonlinear Schrödinger equation to three modes. A discrete one-dimensional map constructed numerically from the trajectories describes much of the global behavior of the system in a way consistent with the general theory of such maps. In particular, we find bifurcation sequences of periodic orbits that are in good quantitative agreement with the theory.

Chaotic behavior is observed to take place on strange attractors having Cantor set-like structure. Our study of one of these attractors strongly suggests a relationship between their fractional dimension and the local stability of their trajectories. Such a relationship would be important for the theory of distribution functions on strange attractors.

ACKNOWLEDGMENTS

Helpful conversations with James Hanson, Jean-Marie Wersinger, and James Yorke are gratefully acknowledged.

This work was supported by the U.S. Department of Energy; and in part (D. A. R. only) by the National Aeronautics and Space Administration under Grant No. NAGW-91, the National Science Foundation, Atmospheric Research Section, Grant No. 7916837, and by the Air Force Office of Scientific Research Grant No. 80-0022.

APPENDIX

1. Stability analysis

The fixed points (b_1^*, b_2^*, θ^*) of (6) are given by

$$b_0^* = -\gamma \sin\theta^*, \quad b_1^* = -1 \pm (2\sin\theta^*),$$

where θ^* solves

$$(2\gamma - 1) + 2(\gamma - 1)\cos\theta^* - 2\delta\sin\theta^* = 0, \tag{A1}$$

with $\sin\theta^* \neq 0$ since $b_{0,1} \equiv a_{0,1}^2$. Let

$$\cos\theta_0 = -\delta\,[\delta^2 + (\gamma - 1)^2]^{-1/2}$$

and

$$\sin\theta_0 = \gamma - 1\,[\delta^2 + (\gamma - 1)^2]^{-1/2},$$

where $0 < \theta_0 < \pi/2$ since $\delta > 0$ and $\gamma > 1$. Then, (A1) becomes

$$\sin(\theta^* + \theta_0) = \frac{\frac{1}{2} - \gamma}{[\delta^2 + (\gamma - 1)^2]^{1/2}}. \tag{A2}$$

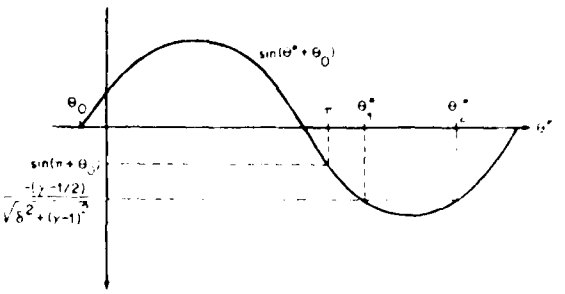

FIG. 13. $\sin(\theta_0 + \theta^*)$, identifying the two stationary points of (5) corresponding to $\theta_{1,2}^*$.

Equation (A2) can be solved provided

$$\gamma > \delta^2 + \tfrac{3}{4}. \tag{A3}$$

With (A3) enforced, we see from Fig. (13) that (A2) has two possible solutions, θ_1^* and θ_2^*. For $0 < \theta_0 < \pi/2$, $\sin\theta_2^* > 0$, so that θ_2^* is an admissible solution to (A2). θ_1^* is admissible provided

$$\sin(\pi + \theta_0) > \frac{\frac{1}{2} - \gamma}{[\delta^2 + (\gamma - 1)^2]^{1/2}}$$

which, on using the expression for $\sin\theta_0$ above, is easily seen to be satisfied for all γ. Therefore, $\theta_{1,2}^*$ are two stationary points of (6) for $\gamma > \delta^2 + \frac{3}{4}$. From (A1) we find

$$\cos\theta_{1,2}^* = \frac{-(\gamma - 1)(\gamma - \frac{1}{2}) \pm \delta[\delta^2(\delta^2 + \frac{1}{4} - \gamma)]^{1/2}}{\delta^2 + (\gamma - 1)^2},$$

$$\sin\theta_{1,2}^* = \frac{\delta(\gamma - \frac{1}{2}) \pm [(\gamma - 1)^2(\delta^2 + \frac{1}{4} - \gamma)]^{1/2}}{\delta^2 + (\gamma - 1)^2}.$$

Label the two stationary points $(b_0^*, b_1^*, \theta_{1,2}^*)$, $P_{1,2}^*$, respectively.

Assuming a solution to (6) of the form

$$b_{0,1} = b_{0,1}^* + \delta b_{0,1} \exp(st), \quad \theta = \theta^* + \delta\theta \exp(st)$$

and linearizing the resulting equations in $\delta b_{0,1}$ and $\delta\theta$, we obtain a homogeneous system of algebraic equations which is solvable provided

$$F(s) = s^3 + C_2 s^2 + C_1 s + C_0 = 0, \tag{A4a}$$

where

$$C_2 = 2(\gamma - 1),$$

$$C_1 = (2\gamma - \sin^2\theta^*)(2 + 3\cos\theta^* + 2\cos^2\theta^*),$$

and

$$C_0 = (8\gamma - \sin^2\theta^*)[(\gamma - 1) + (\gamma - \tfrac{1}{2})\cos\theta^*],$$

(θ^* stands for $\theta_{1,2}^*$). Let us write (A4a) as

$$F(s) = (s - \alpha)(s - \alpha^*)(s - \beta)$$
$$= s^3 - s^2[\alpha + \alpha^* + \beta] + s[\beta(\alpha + \alpha^*) + |\alpha|^2] - |\alpha|^2\beta, \tag{A4b}$$

where α^* is the complex conjugate of α, and β is real. A stationary point is stable only if $\beta < 0$ and $\alpha + \alpha^* < 0$.

For both $P_{1,2}^*$ it is straightforward to show that $\beta = -C_0$ ($= -C_0$) is zero only at $\gamma = \delta^2 + \frac{3}{4}$ and is positive for $\gamma > \delta^2 + \frac{3}{4}$.

tive) for σ_1^* (σ_2^*) if $\gamma > \delta^2 + \frac{1}{4}$. Therefore, the stationary point P_1^* is unstable.

The stability of P_2^* is determined entirely by $\alpha + \bar{\alpha}$ because $\det = 0$ for this point. From (A4), $\alpha + \bar{\alpha} = 0$ if, and only if, (remember, $\gamma > 1$)

$$\cos\sigma_2^* = 0, \quad (\gamma - \tfrac{1}{2})\ (\gamma - 1) = \tfrac{1}{2}, \tag{A5}$$

i.e.,

$$\gamma = \tfrac{1}{2} - \delta \quad \text{and} \quad \delta^2 = (\gamma - 1)^2(\gamma + 1)^2\ 3\gamma(\gamma - \tfrac{1}{3}), \quad \delta < 0.$$

[The latter equality in (A5) requires $\gamma > \frac{1}{3}$.]

In parameter space (δ, γ) (A5) are, respectively,

The stability of P_2^* is summarized in Fig. 1.

2. Hopf bifurcation

Hold δ fixed and let γ cross one of the lines (A5) at γ_0, so that the stationary point P_2^* loses stability. As this happens $\mathrm{Re}(\alpha)$ crosses the origin in the positive sense, and $\mathrm{Im}(\alpha)$ approaches ω_0. ($\omega_0 \neq 0$ because $|\alpha|^2 = 0$ only at $\gamma = \delta^2 + \frac{3}{4}$.) Under these conditions, the Hopf bifurcation theorem[17] states that a limit cycle is born at P_2^* with period $2\pi/\omega_0$ and radius growing as $|\gamma - \gamma_0|^{\frac{1}{2}}$. The limit cycle is stable (unstable) and exists for $\mathrm{Re}(\alpha) < 0$ and $[\mathrm{Re}(\alpha) > 0]$ if a certain function of γ, $V(\gamma)$, is less than (greater than) zero at γ_0. The calculation of V from (5) is quite involved, and details are given in Ref. 18. We find that $V(\gamma_0) < 0$ so that the Hopf cycles are attracting for all γ_0 on the critical loci (A5). For $\delta = -6$ we have isolated the three Hopf cycles numerically; they are indicated in Fig. 4.

3. Cantor set

We construct an example of a Cantor set from the unit interval $[0, 1]$ as follows. First remove the open interval $(1/3, 2/3)$, leaving $S_1 = [0, 1/3] \cup [2/3, 1]$. Now remove from S_1 the two open intervals $(1/9, 2/9)$ and $(7/9, 8/9)$, leaving $S_2 = [0, 1/9] \cup [2/9, 1/3] \cup [2/3, 7/9] \cup [8/9, 1]$, and so on. The Cantor set, S, is

$$S \equiv \bigcap_{j=1}^{\infty} S_j.$$

(In general, we could begin by removing any finite, disjoint family of open subintervals from the unit interval. Provided that this first excision does not leave us with only isolated points, iterating the process indefinitely also yields a Cantor set.)

Notice that $S \cap [0, 3^{-j}] = 3^{-j} S$. That is, any one of the closed intervals comprising S_j contains a copy of S reduced by the factor 3^{-j}. This property of S is called "scale invariance." Notice also that the length of S is zero.

[16] M. Wersinger, J. M. Finn, and E. Ott, Phys. Fluids 23, 1142 (1980).
[17] M. I. Rabinovich and A. L. Fabrikant, Zh. Eksp. Teor. Fiz. 77, 617 (1979) [Sov. Phys. JETP 50, 311 (1979)].
[18] B. A. Huberman and J. P. Crutchfield, Phys. Rev. Lett. 43, 1743 (1979).
[19] M. J. Feigenbaum, J. Stat. Phys. 21, 669 (1979).
[20] M. J. Feigenbaum, Phys. Lett. A 74, 375 (1979).
[21] R. M. May, Nature 261, 459 (1976).
[22] J. A. Yorke and D. Yorke, J. Stat. Phys. 21, 263 (1979).
[23] J. L. Kaplan and J. A. Yorke, Commun. Math. Phys. 67, 93 (1979).
[24] T. Shimizu and N. Morioka, Phys. Lett. A69, 147 (1978).
[25] S. Smale, Bull. Am. Math. Soc. 73, 747 (1967).
[26] D. Ruelle and F. Takens, Commun. Math. Phys. 20, 167 (1971).
[27] M. Henon, Commun. Math. Phys. 50, 69 (1976).
[28] G. M. Zaslavskii, Phys. Lett. A 69, 145 (1978).
[29] B. B. Mandelbrot, *Fractals* (Freeman, San Francisco, Calif., 1977).
[30] D. A. Russell, J. D. Hanson, and E. Ott, Phys. Rev. Lett. 45, 1175 (1980).
[31] L. Cesari, *Asymptotic Behavior and Stability Problems in Ordinary Differential Equations* (Springer-Verlag, Berlin, 1959), p. 50.
[32] J. L. Kaplan and J. A. Yorke, in *Functional Differential Equations and Approximation of Fixed Points*, edited by H. O. Peitgen and H. O. Walther (Springer-Verlag, Berlin, 1979), p. 228.
[33] J. E. Marsden and M. McCracken, *The Hopf Bifurcation and Its Applications* (Springer-Verlag, Berlin, 1976), p. 163.

APPENDIX I

I. "Solitons and Ionospheric Heating"

J.C. Weatherall, J. Sheerin, D. Nicholson, G. Payne, and M.V. Goldman

Journal of Geophysical Research A 87, 823-842 (1981)

JOURNAL OF GEOPHYSICAL RESEARCH, VOL. 87, NO. A2, PAGES 823-832, FEBRUARY 1, 1982

Solitons and Ionospheric Heating

J. C. WEATHERALL,[1] J. P. SHEERIN,[2] D. R. NICHOLSON,[2] G. L. PAYNE,[2] M. V. GOLDMAN,[2] AND P. J. HANSEN[2]

For parameters characterizing the Platteville ionospheric heating facility, the Langmuir wave evolution at the exact reflection point of the heater wave involves an oscillating two-stream instability followed by a collisionally damped three-dimensional soliton collapse. The results provides an alternative explanation for certain experimental observations.

1. Introduction

Modification of the ionosphere by intense radio waves launched from the earth's surface continues to be an active area of experimental and theoretical research; reviews can be found in the November 1974 issue of *Radio Science* (volume 9, number 11), in the articles by *Fejer* [1975, 1979], and in the book by *Gurevich* [1978]. The important role of nonlinear wave effects during ionospheric heating is by now well established, and these effects have at least qualitatively explained many of the observational phenomena.

The purpose of this report is to explore the possibility that three-dimensional Langmuir soliton collapse occurs during ionospheric heating. This possibility was first introduced by *Petviashvili* [1975, 1976], who emphasized the importance of the geomagnetic field. Previous analytic theories of nonlinear wave interaction during ionospheric modification, as summarized in the work by *Fejer* [1975, 1979] and by *Nicholson* [1977], have mainly concentrated on three-wave parametric instabilities; see, for example, *Bezzerides and Weinstock* [1972], *Chen and Fejer* [1975], *DuBois and Goldman* [1972], *Kruer and Valeo* [1973], and *Perkins et al.* [1974]. Most of these theories have neglected the four-wave parametric instability, also known as the modulational instability or oscillating two-stream instability, despite the fact that this instability was the one discussed in the original paper of *Perkins and Kaw* [1971] introducing the significance of parametric instabilities to ionospheric modification. The four-wave interactions were usually neglected because they are quite difficult to treat analytically, and because the nonlinear saturation mechanism of these instabilities was unknown. The latter difficulty was remedied by *Zakharov* [1972], who showed that the modulational instability leads to the formation of solitons, regions of intense localized electric field, which in the unmagnetized, three-dimensional situation can collapse catastrophically to a singularity, like a black hole. In this paper we use the term soliton to mean a coherent, nonlinear entity; this contrasts with certain strict mathematical definitions in which a soliton is a one-dimensional object which can pass through another soliton with no change. The difficulty in analytically treating the modulational instability has been circumvented by numerically solving an appropriate nonlinear wave equation. This numerical work has been pursued by Zakharov and co-workers [*Zakharov et al.*, 1974; *Degtyarev and Zakharov*, 1974, 1975; *Degtyarev et al.*, 1975; *Zakharov et al.*, 1975; *Budnev et al.*, 1975; *Degtyarev et al.*, 1976] and by others [*Litvak et al.*, 1974; *Galeev et al.*, 1975; *Pereira et al.*, 1977; *Nicholson et al.*, 1978; *Nicholson and Goldman*, 1978; *Goldman and Nicholson*, 1978; *Weatherall et al.*, 1981].

In this paper, we treat the evolution of Langmuir waves at the exact reflection point of the modifier wave, the point where the modifier frequency is exactly equal to the plasma frequency ($z = 0$ in Figure 1). At this spatial point, it is well known [*Chen*, 1974] that only the four-wave oscillating two-stream instability can occur. Previous theories using three-wave parametric instabilities are appropriate to spatial locations somewhat closer to the earth, including the location where the maximum amplitude of the standing heater wave occurs. The competition among three-wave interactions, four-wave interactions, and soliton formation at these lower spatial locations will be treated by us in future work. Here, we numerically solve a nonlinear wave equation for parameters appropriate to the Platteville modification facility. We find that the Platteville modifier wave is intense enough to excite an oscillating two-stream instability which evolves into a set of three-dimensional collapsing solitons. Because of collisional damping, these solitons do not collapse catastrophically to a singularity, but rather undergo a period of virulent collapse followed by exponential damping due to collisions.

In the next section, we review the wave equation which describes nonlinear Langmuir waves in the absence of a magnetic field, and solve it for parameters appropriate to the Platteville facility. In the succeeding section, the effects of the geomagnetic field are added; this results in a significant change in the shape of the collapsing solitons but does not significantly change the time scale for collapse. In the final section, conclusions are presented and the possible application of the results to explain certain observational facts is discussed.

2. Soliton Collapse Ignoring the Geomagnetic Field

The equations describing the nonlinear evolution of Langmuir waves were introduced by *Zakharov* [1972] and are known as the Zakharov equations. From *Nicholson et al.* [1978], these are

$$\left(i\omega_i + i\nu_i/2 + \frac{3L_i}{2\omega_i m_i}\nabla^2\right)\nabla\cdot\mathbf{E}(\mathbf{x},t) = \frac{2\pi e^2}{m_i\omega_i}\nabla\cdot(n\mathbf{E}) \qquad (1)$$

$$\omega_i^2 + i\nu_i\omega_i - c_i^2\nabla^2)n(\mathbf{x},t) = \frac{1}{4\pi m_i}\nabla^2 E^2 \qquad (2)$$

[1] Astro-Geophysics Department, University of Colorado, Boulder, Colorado 80309
[2] Physics and Astronomy Department, University of Iowa, Iowa City, Iowa 52242

Copyright © 1982 by the American Geophysical Union

Paper number 1A1662
0148-0227/82/001A-1662$01.00

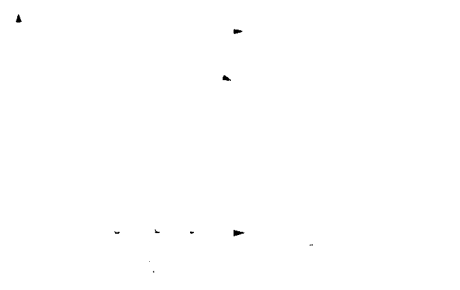

Fig. 1. Standing wave pattern of the heater electric field and direction of the geomagnetic field over Platteville, Colorado.

together with $\tilde{\nabla} \times \tilde{\mathbf{E}} = 0$, where $\tilde{\mathbf{E}}(\tilde{\mathbf{x}}, \tilde{t})$ is the low-frequency envelope of the total high-frequency electric field $\mathbf{E}^{(0)}(\tilde{\mathbf{x}}, \tilde{t}) = \tilde{\mathbf{E}}(\tilde{\mathbf{x}}, \tilde{t}) \times \exp(-i\omega_e \tilde{t})$ plus the complex conjugate; $n(\tilde{\mathbf{x}}, \tilde{t})$ is the deviation of the ion density from its average value n_0; $\omega_e = (4\pi n_0 e^2/m_e)^{1/2}$ is the background electron plasma frequency; m_e (m_i) is the electron (ion) mass; e is the absolute value of the charge of the electron; $\tilde{\nu}_i$ ($\tilde{\nu}_e$) is the high (low) frequency phenomenological energy damping rate (twice the amplitude damping rate); the sound speed $c_s = [(\gamma_e T_e + \gamma_i T_i)/m_i]^{1/2}$, where γ_e (γ_i) is the electron (ion) specific heat ratio characteristic of low-frequency oscillations; T_e (T_i) is the electron (ion) temperature; and $\tilde{\mathbf{x}} = (\tilde{x}, \tilde{y})$ and $\tilde{t}$ represent dimensional space and time, while $\tilde{\nabla}$ is the dimensional gradient operator. Throughout this paper, a tilde represents a dimensional variable. While the Langmuir wave evolution during ionospheric heating is expected to be fully three dimensional, for numerical convenience we work in two spatial dimensions. We discuss below the differences to be expected between our two-dimensional calculations and the true three-dimensional wave evolution. Equations (1) and (2) have been derived heuristically by *Smith and Nicholson* [1979].

It is convenient to introduce the dimensionless variables

$$t = \left(\frac{2\eta}{3}\right)\left(\frac{m_e}{m_i}\right)(\omega_e \tilde{t})$$

$$(x, y) = \frac{2}{3}\left(\frac{\eta m_e}{m_i}\right)^{1/2}\left(\frac{\tilde{x}, \tilde{y}}{\lambda_e}\right)$$

$$n = \left(\frac{3m_i}{4\eta m_e}\right)\left(\frac{\tilde{n}}{n_0}\right) \tag{3}$$

$$E = \frac{1}{\eta}\left(\frac{m_i}{m_e}\right)^{1/2}\left(\frac{3\tilde{E}^2}{16\pi n_0 T_e}\right)^{1/2}$$

$$\nu_{e,i} = \left(\frac{3}{2\eta}\right)\left(\frac{m_i}{m_e}\right)(\tilde{\nu}_{e,i}/\omega_e)$$

where the electron Debye length $\lambda_e = (T_e/m_e\omega_e^2)^{1/2}$ and the dimensionless ratio $\eta = (\gamma_e T_e + \gamma_i T_i)/T_e$. With the definitions (3), (1) and (2) become

$$(i\partial_t + i\nu_e/2 + \nabla^2)\nabla \cdot \mathbf{E}(\mathbf{x}, t) = \nabla \cdot (n\mathbf{E}) \tag{4}$$

$$(\partial_t^2 + \nu_i\partial_t - \nabla^2)n(\mathbf{x}, t) = \nabla^2|\mathbf{E}|^2 \tag{5}$$

The physical effects contained in (4) and (5) have been discussed by *Zakharov* [1972], by *Nicholson et al.* [1978], and by many others. These include the three wave parametric instability often called the decay instability, four-wave parametric instabilities called the stimulated modulational instability and the modulational or oscillating two-stream instability, and soliton formation and collapse.

We consider parameters [*Nicholson*, 1977] characteristic of ordinary-mode nighttime heating by the Platteville, Colorado, facility. The heater frequency is taken to be $\omega_0/2\pi = 4.9$ MHz so that the reflection point occurs at an electron density $n_0 = 3 \times 10^5$ cm^{-3} approximately 300 km above the earth's surface; $T_e = T_i = 0.1$ eV; electron collision frequency due to ions and neutrals (high-frequency amplitude damping rate) $\tilde{\nu}_e/2\omega_e = 2 \times 10^{-5}$; power density incident at the base of the ionosphere 50 μW/m^2; ionospheric density scale length 50 km. We are interested in the electric field of the ordinary-mode heater wave at the exact reflection point where $\omega_e = \omega_0$ ($z = 0$ in Figure 1). Here, the heater electric field is along the geomagnetic field with an effectively infinite wavelength. The formulas of *Ginzburg* [1964], taking into account the Airy enhancement of the heater wave as shown in Figure 1, predict an electric field of 1.0 V/m for the stated incident power density. A natural measure of the intensity of this field is the ratio $W = \tilde{E}^2/4\pi n_0 T_e$ of electric field energy density to background electron kinetic energy density; for these parameters we have $W = W_0 = 4.4 \times 10^{-4}$ at the initial time. This electric field acts as a pump or driver for parametric instabilities. For the parameters being considered here, we shall see below that this instability is an oscillating two-stream instability involving a low frequency perturbation which is purely growing. We find that a typical electron traverses many wavelengths of this low frequency perturbation in one growth time, so that the electrons are isothermal with respect to the low frequency response, and we must use $\gamma_e = 1$ as in an ion-acoustic wave. On the other hand, a typical ion does not move a substantial fraction of a wavelength in one growth time, so the ion motion is adiabatic. The ion collision time is much larger than a growth time, so the adiabatic compression is one dimensional ($d = 1$) and $\gamma_i = (d + 2)/d = 3$. Thus $\eta = 4$. Finally, we need the low frequency damping coefficient. In an equal temperature plasma, this is usually quite large due to ion Landau damping. To avoid the complicated expression for this type of damping, we adopt a simple model damping which after Fourier transformation is $\tilde{\nu}_i(\mathbf{k}) = 2|\mathbf{k}|c_s$ or $\nu_i(\mathbf{k}) = 2|\mathbf{k}|$; this model yields a damping rate of the same order as the undamped linear frequency, and has been shown by *Bardwell and Goldman* [1976] to be sufficiently accurate for the present purposes.

Choosing the heater field $\mathbf{E}_0$ in the $\hat{x}$ direction which is also the direction of the geomagnetic field, we follow *Nicholson et al.* [1978] and study the stability of the heater field by inserting the forms

$$\mathbf{E}(\mathbf{x}, t) = \mathbf{E}_0 + \mathbf{E}_1 \exp(-i\omega t + i\mathbf{k} \cdot \mathbf{x}) + \mathbf{E}_2 \exp(i\omega^* t - i\mathbf{k} \cdot \mathbf{x}) \tag{6}$$

and

$$n(\mathbf{x}, t) = n' \exp(-i\omega t + i\mathbf{k} \cdot \mathbf{x}) + \text{complex conjugate} \tag{7}$$

into (4) and (5). There results the dispersion relation

$$\omega^2 + 2ik\omega - k^2 = k^2 E_0^2 \mu^2 \cdot \left(\frac{1}{\omega + i\nu_e/2 - k^2} - \frac{1}{\omega + i\nu_e/2 + k^2} \right) \quad (8)$$

where

$$\mu^2 = (\hat{\epsilon} \cdot \hat{k})^2 \quad (9)$$

The threshold for a purely growing instability is found by setting $\omega = 0$ in (8); this yields (for $\mathbf{k} = k\hat{x}$)

$$|E_0|^2 = \nu_e/2 \quad (10)$$

or in dimensional units for the present parameters, $E_0 = 0.6$ V/m, which is well below our value of $E_0 = 1.0$ V/m. This conclusion is in agreement with the original prediction of *Perkins and Kaw* [1971].

In order to determine the nonlinear evolution of the oscillating two-stream instability, we solve the Zakharov equations (4) and (5) numerically in two spatial dimensions. The numerical technique is described by *Nicholson et al.* [1978] and by *Nicholson and Goldman* [1978]; it uses 64×64 grids in wave number space and in configuration space. The initial electric field consists of the 'pump' electric field with wave number zero pointing in the $\hat{x}$ direction, representing the heater field, and small random electric fields at all other wave numbers in the two-dimensional wave number grid. The initial density perturbation is zero. All electric field components are subject to the linear damping $\nu_e/2$, except for the pump electric field which has zero linear damping. This is a model which is intended to represent the steady state (in the absence of nonlinear effects) which results from the linear damping of the heater wave balanced by a continuous flux of energy from the heating facility.

At early times, some of the wave number components with initially small amplitudes grow due to the oscillating two-stream instability. The contours of constant growth rate at $\omega_e \tilde{t} = 2.2 \times 10^5$ or $\tilde{t} = 0.007$ s are shown in Figure 2. The maximum growth rate, contour 3 in Figure 2, has a value $\tilde{\gamma}/\omega_e = 1.4 \times 10^{-5}$ or $\tilde{\gamma} = 420\ \text{s}^{-1}$ and occurs at a wave number $\tilde{k}\gamma_e = 0.005$ or $\tilde{\lambda} = 2\pi/\tilde{k} = 5.4$ m. These values are in good agreement with a direct numerical solution of the dispersion relation (8). If we were treating the fully three-dimensional problem, Figure 2 could be rotated about the k_x axis to yield the full three-dimensional growth contours. The maximum vertical extent of the region of substantial growth can be predicted from the dispersion relation (8). If we fix k_x at the value of maximum growth (contour 3 in Figure 2) and study the growth rate as a function of $\theta = \tan^{-1}(k_y/k_x)$, we find from (8) that growth ceases when (very roughly) $\theta \sim 45°$, in agreement with Figure 2. This is due to the fact that $|E_0|^2$ is replaced by $|E_0|^2 \cos^2\theta$ in (8).

Fig. 2. Contours of constant growth rate of electric field amplitude in two-dimensional wave number space at $\omega_e \tilde{t} = 2.2 \times 10^5$ or $\tilde{t} = 0.007$ s. Growth rate $\tilde{\gamma}$ is linearly proportional to the contour label, with contour 3 indicating $\tilde{\gamma}/\omega_e = 1.4 \times 10^{-5}$ or $\tilde{\gamma} = 420\ \text{s}^{-1}$. The point k_x^M is the maximum wave number retained by the computer program, and corresponds to $k_x^M \lambda_e = 0.034$. Likewise, k_y^M corresponds to $k_y^M \lambda_e = 0.017$. The wave number corresponding to the highest value of $\tilde{\gamma}$ is $\tilde{k}_x \lambda_e = \pm 0.005$.

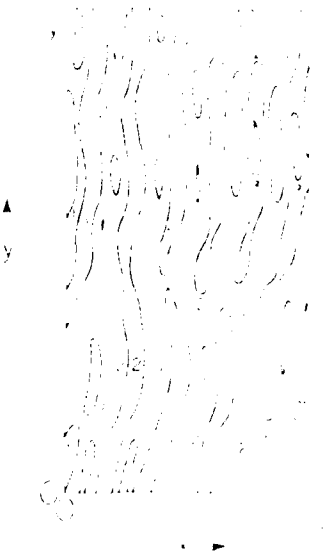

Fig. 3. Contours of absolute value of electric field in configuration space at $\omega_e \tilde{t} = 4.4 \times 10^5$ or $\tilde{t} = 0.014$ s. The spatial region shown is that used by the computer program, with $\tilde{L}_x$ corresponding to $\tilde{L}_x/\lambda_e = 7400$ or $\tilde{L}_x = 32$ m, and $\tilde{L}_y = 64$ m. Contour 2 corresponds to the initial electric field energy density W, contour 1 is 3% below the initial value, and contour 3 is 3% above the initial value.

At a later time in this run, $\omega_e \tilde{t} = 4.4 \times 10^5$ or $\tilde{t} = 0.014$ s, the unstable modes in Figure 2 have exponentiated sufficiently from their initial noise levels that the absolute value of the total electric field, Figure 3, shows regions of substantially enhanced field and regions of substantially depressed field. The lowest contour level 1 corresponds to a value of electric field energy W which is 3% below the initial value W_0, contour level 2 corresponds to the initial value, and contour 3 corresponds to a value 3% above the initial value. Figure 4 shows the contours of constant absolute value of

Fig. 4. Contours of absolute value of electric field in wave number space, the other parameters have the same values as in Figure 3. Most of the energy is still in the $\mathbf{k} = 0$ mode, not shown in this figure.

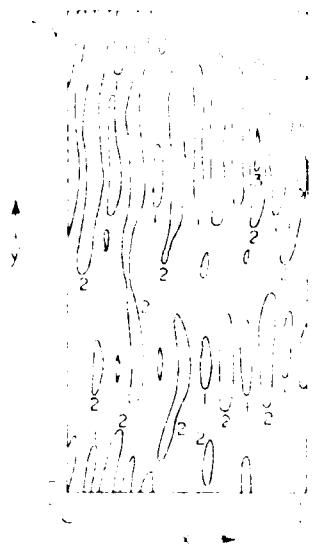

Fig. 5. Contours of absolute value of electric field in configuration space at $\omega_e t = 6.2 \times 10^5$ or $t = 0.020$ s. Contour 1 corresponds to $W = 7.8 \times 10^{-4}$, contour 2 to $W = 9.9 \times 10^{-4}$, and contour 3 to $W = 1.2 \times 10^{-3}$. Other parameters are the same as in Figure 3.

electric field in wave number space at the same time as in Figure 3. Those modes with the highest growth rates in Figure 2 have reached substantial amplitudes in Figure 4. Most of the energy still resides in the $\mathbf{k} = 0$ mode, not shown in Figure 4.

Figure 5 shows the absolute value of electric field in configuration space at $\omega_e t = 6.2 \times 10^5$ or $t = 0.020$ s. Regions of high electric field energy density W at the earlier time of Figure 3 have become even more intense in Figure 5, while regions of low W in Figure 3 have become even lower. The regions of intense field in Figure 5 begin to collapse at this time, so that at $\omega_e t = 7.9 \times 10^5$ or $t = 0.026$ s (Figure 6) they

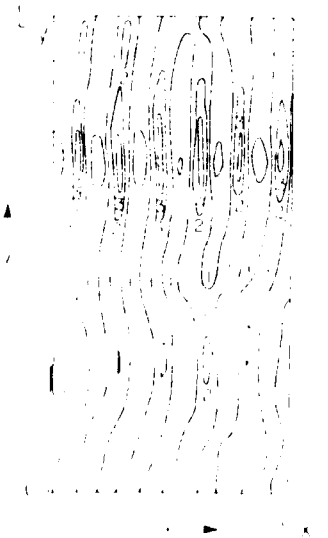

Fig. 6. Contours of absolute value of electric field in configuration space at $\omega_e t = 7.9 \times 10^5$ or $t = 0.026$ s. Contour 1 corresponds to $W = 2.4 \times 10^{-4}$, contour 2 to $W = 9.7 \times 10^{-4}$, and contour 3 to $W = 2.2 \times 10^{-3}$. Other parameters are the same as in Figure 3.

Fig. 7. Low-frequency density variation in configuration space at time $\omega_e t = 7.9 \times 10^5$ or $t = 0.026$ s. Contour 1 corresponds to a zero density variation, contour 2 corresponds to $\tilde{n}/n_0 = -0.002$ or $n = 600$ cm^{-3}, and contour 3 (in four places, unmarked on figure) corresponds to $\tilde{n}/n_0 = -0.004$ or $\tilde{n} = -1200$ cm^{-3}. Other parameters are the same as in Figure 3.

have become even more intense. At this time, the low frequency density variation n (Figure 7) has minima in the same spatial locations as the maxima of the electric field amplitude in Figure 6. This is as expected for the oscillating two-stream instability and the subsequent soliton collapse.

At the final time of this run, $\omega_e t = 8.9 \times 10^5$ or $t = 0.029$ s, the collisionally damped collapsing solitons are quite prominent (Figure 8), and have absorbed most of the wave energy from other spatial regions. The absolute value of the electric field amplitude in wave number space at this time (Figure 9) shows some spreading. However, because of the relatively large collisional damping, the soliton collapse in configuration space and consequent spreading in wave number space is much less pronounced than in situations with no collisional damping [*Nicholson et al.*, 1978; *Nicholson and Goldman*, 1978].

The relative electric field energy density W/W_0 versus time throughout the run is displayed in Figure 10. After time $\omega_e t = 7 \times 10^5$, the unstable modes take a substantial fraction of energy from the original $\mathbf{k} = 0$ pump mode; this energy is subsequently lost due to collisional damping. The net damping is always slower than the collisional damping rate (dashed line in Figure 10) because a substantial fraction of the total wave energy continues to reside in the undamped $\mathbf{k} = 0$ mode at each time. The collisional damping in this case acts fast enough to prevent the collapse of the solitons to such small spatial regions that the accuracy of the computer code is lost. Thus the computer code is accurate over the entire length of the run, in contrast to previous work in the undamped regime [*Nicholson et al.*, 1978].

The numerical work described here is in two spatial dimensions, while the actual soliton collapse during ionospheric heating occurs in three spatial dimensions. Thus the spatial dimensions of the solitons, and the maximum energy density in the center of the solitons, may differ by factors of

two or more in the actual physical situation from those obtained here. However, the time scales involved are probably very close in the two-dimensional and three-dimensional cases.

There has been a fair amount of work on analytic solutions describing collapsing solitons, and this work is reviewed in the appendix. Most of the analytic work does not include the effects of collisional damping (see, however, *Degtyarev et al.* [1976], *Pereira et al.* [1977], and *Goldman et al.* [1980]), so these results cannot be directly compared to our numerical results.

Before discussing the implications of these results for ionospheric heating, we proceed in the next section to add the effect of the geomagnetic field. This results in significant quantitative differences; the overall qualitative scenario, however, remains unchanged.

3. Soliton Collapse Including the Geomagnetic Field

The earth's magnetic field is such that the electron gyrofrequency Ω_e is roughly $\Omega_e/\omega_e = 1/3.5$ for the parameters of interest. For Langmuir waves along the geomagnetic field, there is no effect of the geomagnetic field. However, for linear Langmuir waves with a wave number component k_y perpendicular to the magnetic field, the unmagnetized dispersion relation

$$\tilde{\omega}^2 = \omega_e^2(1 + 3\tilde{k}^2\lambda_e^2) \tag{11}$$

is replaced by

$$\tilde{\omega}^2 = \omega_e^2\left(1 + 3\tilde{k}^2\lambda_e^2 + \frac{\Omega_e^2}{\omega_e^2}\sin^2\theta\right) \tag{12}$$

where $\theta = \tan^{-1}(k_y/k_x)$. Thus we include the effect of the geomagnetic field in our numerical calculation by making the

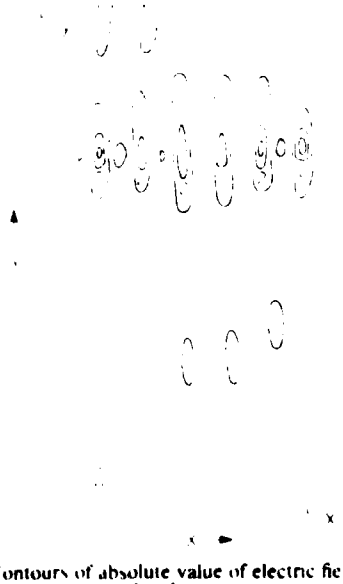

Fig. 8. Contours of absolute value of electric field in configuration space at $\omega_e t = 8.9 \times 10^5$ or $t = 0.029$ s. Contour 1 corresponds to $W = 1.4 \times 10^{-4}$, contour 2 to $W = 5.4 \times 10^{-4}$, and contour 3 (in three places, unmarked) to $W = 1.2 \times 10^{-3}$. Other parameters are the same as in Figure 3.

Fig. 9. Contours of absolute value of electric field in wave number space; the other parameters have the same values as in Figure 8. There is a small amount of energy in the $\mathbf{k} = 0$ mode, not shown in this figure.

following replacement of the dimensionless Fourier representation of the operator $-\nabla^2$ in (4):

$$k^2 \rightarrow k^2 + \frac{3}{4\eta}\frac{\Omega_e^2}{\omega_e^2}\frac{m_i}{m_e}\sin^2\theta \tag{13}$$

There is also a more complicated effect on the low-frequency equation (5) which we include. In previous studies [*Weatherall*, 1980; *Nicholson et al.*, 1978; *Weatherall et al.*, 1981; *Goldman et al.*, 1981], we have found that this low-frequency effect is substantial only in a very limited region of wave number space, with a negligible contribution to the overall wave evolution.

With the replacement (13), the dispersion relation (8) becomes

$$\omega^2 + 2ik\omega - k^2 = k^2|E_0|^2\mu^2\left(\frac{1}{\omega + i\nu_e/2 - k^2 - 450\sin^2\theta}\right.$$

$$\left. - \frac{1}{\omega + i\nu_e/2 + k^2 - 450\sin^2\theta}\right) \tag{14}$$

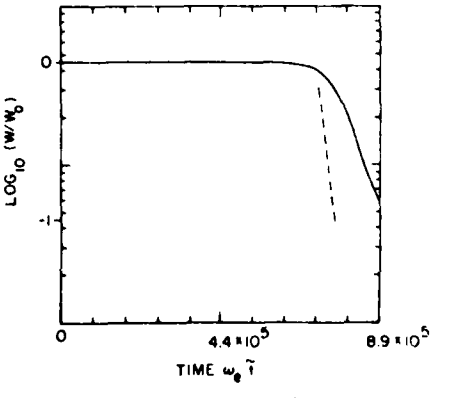

Fig. 10. Log_{10} of the relative electric field energy density W/W_0 versus time for the entire unmagnetized run. The dashed line shows the rate of energy decay which would occur if all modes were collisionally damped. The actual decay is slower than this because at each time a significant fraction of the wave energy is in the undamped $\mathbf{k} = 0$ mode.

Fig. 11. Contours of constant growth rate of electric field amplitude in two-dimensional wave number space at $\omega_c t = 2.2 \times 10^5$ or $t = 0.007$ s, in the magnetized case. Growth rate $\dot{\gamma}$ is linearly proportional to the contour label, with contour 3 indicating $\dot{\gamma}/\omega_c = 1.4 \times 10^{-5}$ or $\dot{\gamma} = 420\ s^{-1}$. The point k_x^M is the maximum wave number retained by the computer program, and corresponds to $k_x^M \lambda_c = 0.034$. The maximum vertical wave number is $k_y^M/k_x^M = 0.02$. Note that this figure has been stretched by a factor of 25 in the vertical direction.

The angular effect in the denominators on the right is now much more important than the μ^2 factor in the numerators. The growth rates for $k_y = 0$ are unaffected by the magnetic field, so the fastest growing mode is the same in the magnetized case as in Figure 2 in the unmagnetized case. Fixing k_x at this value, analysis of (14) shows that growth ceases at an angle $\theta \cong k_y/k_x = 0.05$ radians $\cong 3°$.

With the modification (13) to our computer program, we repeat the calculation of the previous section. Since only wave numbers with small values of k_y are predicted to grow by (14), and since we are limited by computer resources to a grid of 64 × 64 points, we resolve the behavior in wave number space by choosing $L_y/L_x = 50$, with L_x the same as in the unmagnetized case. This implies that the ratio of the sides of the grid in wave number space is $k_y^M/k_x^M = 0.02$, allowing detailed resolution of growth rate contours in wave number space.

With all other parameters the same as in the preceding section, we repeat the previous calculation. Figure 11, analogous to Figure 2 in the unmagnetized case, shows contours of constant growth rate of electric field amplitude in wave number space at $\omega_c t = 2.2 \times 10^5$ or $t = 0.007$ s. Although this figure appears very similar to Figure 2, note that it has been stretched by a factor of 25 in the vertical direction. Thus, growth occurs only for angles k_y/k_x of less than a few degrees, in agreement with the prediction of the dispersion relation (14).

Figure 12, analogous to Figure 5 in the unmagnetized case, shows the electric field in configuration space at $\omega_c t = 6.2 \times 10^5$ or $t = 0.020$ s. The formation of collapsing solitons is observed. Note that this figure is compressed by a factor of 25 in the vertical direction. At the later time $\omega_c t = 7.9 \times 10^5$ or $t = 0.026$ s, the collapsing solitons have intensified (Figure 13, analogous to Figure 6 in the unmagnetized case). The maximum energy densities here are actually twice as large as in the unmagnetized case. We interpret this as follows. In the magnetized case, the spatial configuration is much more one dimensional than in the unmagnetized case. It is well known that dispersion is more effective in inhibiting one-dimensional collapse than in inhibiting two-dimensional collapse. Thus, in the magnetized case, the unstable oscillating two-stream modes can remain in phase with the pump for a longer time. This allows them to absorb more of the pump energy than in the unmagnetized case; at a slightly later time, when the waves do decouple from the pump and begin to collapse, they have a somewhat greater intensity than in the unmagnetized case. This effect is helped by the fact that the magnetized solitons involve the collapsing energy from a spatial volume roughly 50 times larger than in the unmagnetized case; thus it is not surprising that the intensity at the very center of a collapsing soliton is larger in the magnetized case.

Figure 14 shows the electric field amplitude in wave number space at the final time $\omega_c t = 8.9 \times 10^5$ or $t = 0.029$ s. The characteristic spreading in wave number space due to the spatial collapse is again observed.

Figure 15 shows the relative electric field energy density versus time for the entire magnetized run. The energy dissipation at late times is even closer to the collisional damping rate than in the unmagnetized case (Figure 10), consistent with our previous interpretation of a greater efficiency in the conversion of pump energy to unstable mode energy in the magnetized case.

There are two major differences between the present work and the actual physical situation near the reflection point of the heater wave. First, the present calculations are performed in two spatial dimensions, whereas the actual physical situation is fully three dimensional. We do not expect any of the scale lengths in three dimensions to be different than those found here. Since soliton collapse is favored in three dimensions, the time scale for collapse may be somewhat shorter than found here, but probably by less than a factor of 2.

Second, the actual physical situation involves a background ionosphere which is inhomogeneous with scale

Fig. 12. Contours of absolute value of electric field in configuration space at $\omega_c t = 6.2 \times 10^5$ or $t = 0.020$ s, for the magnetized case. L_x corresponds to $L_x/\lambda_c = 7400$ or $L_x = 32$ m, and $L_y/L_x = 50$. Contour 1 corresponds to $W = 7.4 \times 10^{-4}$, contour 2 to $W = 9.5 \times 10^{-4}$, and contour 3 to $W = 1.2 \times 10^{-3}$. Note that this figure has been compressed by a factor of 25 in the vertical direction.

length 50 km rather than homogeneous as assumed here. The effects of inhomogeneity are much more difficult to predict than the effects of three dimensionality, partially because the inhomogeneity enters in three ways: the heater wave profile, assumed to be an Airy function, is inhomogeneous with a scale length of order 100 m; the heater wave frequency is different than the local plasma frequency by an amount depending on the distance from the exact reflection point; the Langmuir waves excited by the modulational instability find themselves in an inhomogeneous plasma. While it is beyond the scope of this paper to attempt even a semiquantitative treatment of inhomogeneity, we can make several observations. The locally homogeneous dispersion relation for the modulational instability at all levels above and below the exact heater reflection point can be easily obtained from (4), (5), and (6) of *Nicholson et al.* [1978] by setting $k_0 = 0$ (since the heater wave is a dipole field if the Airy inhomogeneity is ignored) and by letting ω_0 represent the difference between the heater frequency and the exact local plasma frequency. The solution of this local dispersion relation then predicts that the threshold for modulational instability, and the growth rate above threshold, are both quite insensitive to the distance from the exact reflection point. However, the range of unstable wave numbers is quite sensitive to the height, with a scale length of order 10 m. Thus the fastest growing wave number at the height of the Airy function maximum, roughly 200 m below the exact heater reflection point, is 10 times larger than the fastest growing wave number at the exact reflection point. Furthermore, the fastest growing wave number at the exact reflection point is not growing at all a short distance of order 10 m (or a few wavelengths) below the exact reflection point. Of course, at any location below the exact reflection point, the four-wave modulational instabilities must compete with the three-wave parametric decay instabilities. The rapid change in the magnitude of the fastest growing wave number with height probably means that the collapsing solitons of section 3 will not maintain the coherence over scales of order 100 m in the y direction as shown in Figure 12. However, this would in no way change the time scale for collapse, as section 2 showed similar collapse time scales for solitons with initial dimensions of order 5 m in both directions. Thus we have no reason to think that the proper inclusion of inhomogeneity will affect the importance of collapse or the time scales for collapse; it may strongly affect the variation of spatial scales of the initial collapsing objects. We will treat this subject, and the subject of the competition between three-wave and four-wave processes, in future work.

Fig. 13. Contours of absolute value of electric field in configuration space at $\omega_e t = 7.9 \times 10^5$ or $t = 0.026$ s, for the magnetized case. Contour 1 corresponds to $W = 5.4 \times 10^{-4}$, contour 2 to $W = 2.2 \times 10^{-3}$, and contour 3 to $W = 4.9 \times 10^{-3}$. Other parameters are the same as in Figure 12. Note that this figure has been compressed by a factor of 25 in the vertical direction.

Fig. 14. Contours of absolute value of electric field in wave number space at $\omega_e t = 8.9 \times 10^5$ or $t = 0.029$ s, for the magnetized case. There is some energy in the $\mathbf{k} = 0$ mode, not shown in this figure. Other parameters are the same as in Figure 11. Note that this figure has been stretched by a factor of 25 in the vertical direction.

Previous work on the analytic study of collapsing solitons is summarized in the appendix. Since most of this work does not include collisional dissipation, we cannot directly compare it to our numerical results. In the final section, we summarize our conclusions and discuss the implications of our results.

4. Conclusions and Implications

We have demonstrated numerically that the ordinary mode Platteville modifier is intense enough to cause an

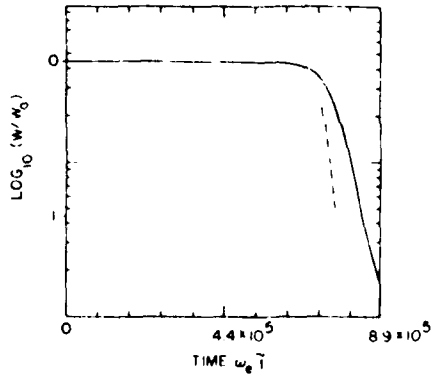

Fig. 15. $\log_{10}$ of the relative electric field energy density W/W_0 versus time for the entire magnetized run. The dashed line shows the rate of energy decay which would occur if all modes were collisionally damped. The actual decay is slower than this because at each time a significant fraction of the wave energy is in the undamped $\mathbf{k} = 0$ mode.

oscillating two-stream instability at its exact reflection point. This instability leads to regions of spatially localized intense electric field which become collisionally damped collapsing solitons. The time scale for collapse is a few milliseconds. The spatial scale of the collapsing solitons is about 1 m along the geomagnetic field, and, because of the geomagnetic field, about 100 m or less perpendicular to the geomagnetic field.

Our results lend an intriguing interpretation to an important observational fact. It has been observed that when the modifier at Arecibo is turned on, the intensity of the plasma line echo is initially quite intense [*Muldrew and Showen*, 1977; *Muldrew*, 1978; *Showen and Behnke*, 1978; *Showen and Kim*, 1978; *Fejer*, 1979]; this phenomenon is called 'plasma line overshoot.' According to linear plasma theory, this result is difficult to understand, since it requires Langmuir waves created by the modifier to travel up or down in an essentially vertical direction. However, the unstable oscillating two-stream instability of the present paper, and the parametric decay instability of the earlier theories of ionospheric modification reviewed in the introduction, both produce Langmuir waves travelling predominantly along the geomagnetic field, not in the vertical direction. However, this difficulty does not occur if one has three-dimensional collapsing solitons. These nonlinear entities contain all wave number components, not merely the ones allowed by the linear Langmuir wave dispersion relation. Thus, at least qualitatively, the three-dimensional collapsing solitons of the present paper could lead to a substantial plasma line intensity. Although the heating powers at Arecibo are lower than at Platteville, they are still quite possibly high enough to excite collapsing solitons. We note that the collapsing solitons have a frequency spectrum characterized by the heater frequency (local plasma frequency), broadened somewhat by the several millisecond collapse time scale. An alternative explanation of the origin of the intense plasma line using linear wave propagation has been presented by *Muldrew* [1978]. It is quite possible that his mechanism and our mechanism occur simultaneously with an additive effect. We do not attempt to explain here the fact that the plasma line decays after its initial overshoot; although the dissipation of pump energy due to soliton formation and collisionally damped collapse could contribute, the complete explanation presumably involves all of the parametric instabilities and nonlinear effects occurring at the reflection point and below it [*Fejer*, 1979].

In future work, we will make a quantitive prediction of the plasma line echo to be expected from the three-dimensional collapsing solitons predicted by the present work, and compare it to that observed.

There are several other implications of our work which can be explored. First, all of our solitons are observed to collapse and collisionally damp. We do not observe the formation of steady state pancake solitons as studied by *Petviashvili* [1975, 1976]. Second, it does not appear that our mechanism will help to explain the production of hot electrons and the resultant airglow observed during ionospheric heating [*Nicholson*, 1977]. The smallest spatial dimension observed in the present work is about 1 m or 200 λ_i. Most theories of electron acceleration due to collapsing solitons require the localization of intense fields to sizes $\sim 10\ \lambda_i$ or less [*Morales and Lee*, 1974; *Bezzerides and DuBois*, 1975]. It is not at all clear at this time whether the change from two dimensions to three dimensions can produce a localization by a factor of 20. We will explore this question in future work, both for Platteville parameters and for parameters of new facilities. Finally, as stated above, we will explore in future work the effects of the ionospheric inhomogeneity on the conclusions of this paper, together with a detailed study of the competition among three-wave interactions, four-wave interactions, and soliton collapse at heights below the exact heater reflection point.

APPENDIX

Analytic descriptions of collapsing solitons were shown by *Zakharov* [1972] to take the form of self-similar solutions (SSS). Discrepancies among the results of various authors [*Zakharov*, 1972; *Litvak et al.*, 1974; *Degtyarev and Zakharov*, 1974, 1975; *Degtyarev et al.*, 1975; *Nishikawa et al.*, 1975] have led to some confusion in their application. *Galeev et al.* [1975] pointed out the important role that scaling laws, inherent in a SSS, play in determining the spectra of strong Langmuir turbulence. Thus it is imperative to use a SSS in its appropriate context. In what follows, a generalized SSS is developed for the Zakharov model (equations (4)–(5)) without damping ($\nu_e = \nu_i = 0$) for both the magnetized and unmagnetized cases. All previously obtained results are regained and a unified perspective is possible. In addition, directions for further development and applications to results of computer simulations are suggested.

The general SSS for (4)–(5) with $\nu_e = \nu_i = 0$ is of the form

$$\begin{aligned} E &= (t_0 - t)^{\alpha}\psi(\xi, \eta) \exp\{i \int \mu(t)\, dt\} \\ \xi &= (t_0 - t)^{\beta}x \\ \eta &= (t_0 - t)^{\gamma}y \\ n &= (t_0 - t)^{\delta}\mathcal{N}(\xi, \eta) \\ \mu &= (t_0 - t)^{\varepsilon} \end{aligned} \tag{A1}$$

where E, t, x, y, n are the dimensionless variables defined in (3). In the unmagnetized case, previous work, mentioned in the preceding paragraph, assumed the soliton collapses symmetrically. This is equivalent to setting $\xi = \eta$. With this assumption, substitution of (A1) into (4) yields the following relationships between exponents:

$$2\beta = 2\gamma + \delta = \varepsilon \tag{A2}$$

This leaves two exponents to be determined: α is fixed by the dynamical equation used for the ions, depends upon how the electric field envelope changes in time.

Ion dynamics. The form assumed for the ion-acoustic equation (5) divides solutions into the following regimes.

1. The first is the 'supersonic' regime. For very intense fields ($W \gg m_e/m_i$), (5) is approximated as

$$\partial_t^2 n = \nabla^2 E^2 \tag{A3}$$

Substitution of (A1) with (A2) into (A3) yields

$$\alpha = -1 \tag{A4}$$

2. The second is the 'trans-sonic' regime. For less intense fields, the full ion-acoustic equation is used. Again, the result is $\alpha = -1$. The last exponent is also determined, however,

$$\delta = -2$$

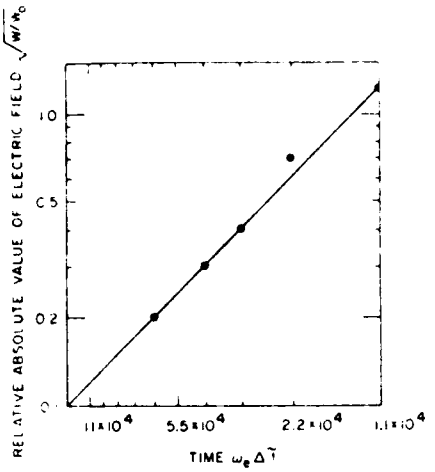

Fig. 16. Relative absolute value of electric field as a function of $\omega_e \Delta t = \omega_e (t_{0a} - t)$ for the magnetized run. The collapse time, t_{0a}, is defined as the time at which the collapsing soliton would have reached singularity if there was no damping. Δt decreases toward the right so that real time is increasing toward the right. The value $\omega_e t_{0a}$ corresponds to $\omega_e t = 6.05 \times 10^5$ in Figure 15.

3. The third is the 'static' regime. For weaker fields ($W \ll m_i/m_e$), the density is given by

$$n = -E^2 \tag{A5}$$

In this case, $\alpha = -1/2$.

Electric field envelope. The remaining exponent is determined by how the electric field envelope changes in time: (1) the slowly varying envelope—if the time dependent equation (4) is used, then

$$\delta = -1 \tag{A6}$$

This solution, however, does not conserve the first integral of motion, plasmon number; (2) the adiabatic envelope approximation—this approximation ignores the time dependence of the envelope; the first integral of motion must be invoked to determine δ; the plasmon number is given by

$$I_1 = \int E^2 \, d^D r \tag{A7}$$

where D is the dimensionality of the system. Substitution of the SSS in (A7) yields

$$\delta = -4/D \tag{A8}$$

Thus, assuming the time rate of change of the envelope is a constant and plasmons are conserved, the scaling laws for the collapse become dependent on the dimensionality of the system.

The introduction of an ambient magnetic field into the model breaks the symmetry previously assumed. *Petviashvili* [1975] and *Galeev* [1975] derived a modified version of (4) to include the weak dispersion transverse to the ambient magnetic field.

$$\frac{\partial^2}{\partial x^2}\left[i\omega_t E + \frac{\partial^2 E}{\partial \tilde{x}^2} - nE\right] = \frac{\partial^2 E}{\partial y^2} \tag{A9}$$

For the asymmetric collapse, (A2) is replaced by

$$2\beta = \gamma = \delta - 1 \tag{A10}$$

The shape of the solution is that of a 'pancake.' The rate of collapse of this pancake is twice as fast in the larger dimension transverse to the magnetic field line than along the field line. Thus, during the asymmetric stage of collapse, the pancake becomes more symmetric. The discussions of ion dynamics to determine the exponent α, and the envelope approximation to determine δ, carry over from before. Note, however, the form for the integral in (A7) changes to include the asymmetric geometry. In this case, the assumption of conservation of plasmon number leads to

$$\delta = -4/(2D - 1) \tag{A11}$$

The general SSS, (A1), includes all previously obtained results as special cases. These results [e.g., *Zakharov*, 1972] typically assumed spherical symmetry and conservation of plasmon number. Computer simulations [*Lipatov*, 1977] suggest, however, that these approximations may not hold in the case of highly distorted structures such as pancakes. The asymmetric collapse parameters, (A10), apply to solitons in a magnetic field. Interestingly, the asymmetric collapse may be applicable to highly distorted wave packets in unmagnetized plasma as well. Computer simulations by *Pereira et al.* [1977] show collapsing pancakes for $B_0 = 0$ with the transverse dimension decreasing at twice the rate of the longitudinal dimension. Indeed, this presents some of the best evidence to date for differential scaling of a collapsing pancake.

Comparison of the SSS with simulation results presented in this paper is hampered by the inclusion of damping. Qualitatively, we can see the production of highly elongated pancakes which collapse faster lengthwise than along the width. This is observed in both the magnetized and unmagnetized runs.

The relative absolute value of the electric field is plotted on a double logrithmic scale, as a function of $\Delta t (= t_{0a} - t)$, for the magnetized run (Figure 16). Note that Δt is decreasing toward the right so as to preserve the sense of real time which is increasing toward the right. The collapse time, t_{0a}, is defined as the time at which the collapsing soliton would have reached singularity if there was no damping. The slope of the line in the log-log plot gives

$$\alpha = -1$$

This result is exactly that predicted for dynamic ions (equation (A4)). A breakdown of the static approximation (equation (A5)) is indicated, as expected for the large values of electric field obtained. It is interesting to note that results in the unmagnetized case [*Pereira et al.*, 1977] compare more closely with predictions for static ions. To make more detailed comparisons, the theory must be modified to include the effect of damping.

Acknowledgments. We thank D. F. DuBois, L. M. Duncan, J. A. Fejer, K. Papadopoulos, H. L. Pécseli, F. W. Perkins, and H. A. Rose for useful conversations. This work was supported by the National Science Foundation, Atmospheric Research Section, grant ATM78-22487 and ATM79-18778, and by USDOE grant DE-AC02-76ET53034. The work of two of us (M. G. and J. W.) was also supported by the National Science Foundation, Atmospheric Research Section, under ATM79-16837 and ATM80-20826, by the Air Force Office of Scientific Research under contract F49620-76-C-0005, and by NASA NAGW-91. We thank the National Center for Atmospheric Research, supported by the National Science Foundation, for computer time used in this research. Part of this work was

performed while two of us (M.G. and D.N.) were the guests of the Aspen Institute for Physics and Astrophysics, whose hospitality is appreciated.

REFERENCES

Bardwell, S., and M. V. Goldman, Three-dimensional Langmuir wave instabilities in type III solar radio bursts, *Astrophys. J.*, *209*, 912, 1976.

Bezzerides, B., and D. F. DuBois, Electron heating and Landau damping in intense localized electric fields, *Phys. Rev. Lett.*, *34*, 1381, 1975.

Bezzerides, B., and J. Weinstock, Nonlinear saturation of parametric instabilities, *Phys. Rev. Lett.*, *28*, 481, 1972.

Budneva, O. B., V. E. Zakharov, and V. S. Synakh, Certain models for wave collapse (in Russian), *Fiz. Plazmy*, *1*, 606, 1975. (*Sov. J. Plasma Phys. Engl. Transl.*, *1*, 335, 1975.)

Chen, F. F., *Introduction to Plasma Physics*, Plenum, New York, 1974.

Chen, H. C., and J. A. Fejer, Saturation spectrum of the parametric decay instability in the presence of an external magnetic field, *Phys. Fluids*, *18*, 1809, 1975.

Degtyarev, L. M., and V. E. Zakharov, Dipole character of the collapse of Langmuir waves (in Russian), *Zh. Eksp. Teor. Fiz. Pis'ma Red.*, *20*, 365, 1974. (*JETP Lett. Engl. Transl.*, *20*, 164, 1974.)

Degtyarev, L. M., and V. E. Zakharov, Supersonic collapse of Langmuir waves (in Russian), *Zh. Eksp. Teor. Fiz. Pis'ma Red.*, *21*, 9, 1975. (*JETP Lett. Engl. Transl.*, *21*, 4, 1975.)

Degtyarev, L. M., V. E. Zakharov, and L. I. Rudakov, Two examples of Langmuir wave collapse (in Russian), *Zh. Eksp. Teor. Fiz.*, *68*, 155, 1975. (*Sov. Phys. JETP Engl. Transl.*, *41*, 57, 1975.)

Degtyarev, L. M., V. E. Zakharov, and L. I. Rudakov, Dynamics of Langmuir collapse (in Russian), *Fiz. Plazmy*, *2*, 438, 1976. (*Sov. J. Plasma Phys. Engl. Transl.*, *2*, 240, 1976.)

DuBois, D. F., and M. V. Goldman, Nonlinear saturation of parametric instability: Basic theory and application to the ionosphere, *Phys. Fluids*, *15*, 919, 1972.

Fejer, J. A., Alteration of the ionosphere by man-made waves, *Philos. Trans. R. Soc. London Ser. A*, *280*, 151, 1975.

Fejer, J. A., Ionospheric modification and parametric instabilities, *Rev. Geophys. Space Phys.*, *17*, 135, 1979.

Galeev, A. A., Plasma turbulence in the magnetosphere with special regard to plasma heating, in *The Physics of Hot Plasma in the Magnetosphere*, edited by B. Hulqvist and L. Stenflo, Plenum, New York, 1975.

Galeev, A. A., R. Z. Sagdeev, Yu. S. Sigov, V. D. Shapiro, and V. I. Shevchenko, Nonlinear theory of the Langmuir-wave modulational instability (in Russian), *Fiz. Plazmy*, *1*, 10, 1975. (*Sov. J. Plasma Phys. Engl. Transl.*, *1*, 5, 1975.)

Ginzburg, V. L., *The Propagation of Electromagnetic Waves in Plasmas*, Pergamon, New York, 1964.

Goldman, M. V., and D. R. Nicholson, Virial theory of direct Langmuir collapse, *Phys. Rev. Lett.*, *41*, 406, 1978.

Goldman, M. V., K. Rypdal, and B. Hafizi, Dimensionality and dissipation in Langmuir collapse, *Phys. Fluids*, *23*, 945, 1980.

Goldman, M. V., J. C. Weatherall, and D. R. Nicholson, Langmuir collapse in a weak magnetic field, *Phys. Fluids*, *24*, 668, 1981.

Gurevich, A., *Nonlinear Phenomena in the Ionosphere*, *Phys. and Chem. in Space*, vol. 10, Springer, New York, 1978.

Kruer, W. L., and E. J. Valeo, Nonlinear evolution of the decay instability in a plasma with comparable electron and ion temperatures, *Phys. Fluids*, *16*, 675, 1973.

Lipatov, A. S., Numerical investigation of the collapse of Langmuir waves in a magnetic field (in Russian), *Pis'ma Zh. Eksp. Teor. Fiz.*, *26*, 516, 1977. (*JETP Lett. Engl. Transl.*, *26*, 377, 1977.)

Litvak, A. G., G. M. Fraiman, and A. D. Yunakovskii, Self-focusing of Langmuir oscillations (in Russian), *Zh. Eksp. Teor. Fiz. Pis'ma Red.*, *19*, 23, 1974. (*JETP Lett. Engl. Transl.*, *19*, 13, 1974.)

Morales, G. J., and Y. C. Lee, Effect of localized electric fields on the evolution of the velocity distribution function, *Phys. Rev. Lett.*, *33*, 1534, 1974.

Muldrew, D. B., The role of field-aligned ionization irregularities in the generation of the HF-induced plasma line at Arecibo, *J. Geophys. Res.*, *83*, 2552, 1978.

Muldrew, D. B., and R. L. Showen, Height of the HF-enhanced plasma line at Arecibo, *J. Geophys. Res.*, *82*, 4793, 1977.

Nicholson, D. R., Magnetic field effects on electrons during ionospheric modification, *J. Geophys. Res.*, *82*, 1839, 1977.

Nicholson, D. R., and M. V. Goldman, Cascade and collapse of Langmuir waves, *Phys. Fluids*, *21*, 1766, 1978.

Nicholson, D. R., M. V. Goldman, P. Hoyng, and J. C. Weatherall, Nonlinear Langmuir waves during type III solar radio bursts, *Astrophys. J.*, *223*, 605, 1978.

Nishikawa, K., Y. C. Lee, and C. S. Liu, Langmuir wave turbulence—Condensation and collapse, *Commun. Plasma Phys.*, *2*, 63, 1975.

Pereira, N. R., R. N. Sudan, and J. Denavit, Numerical study of two-dimensional generation and collapse of Langmuir solitons, *Phys. Fluids*, *20*, 936, 1977.

Perkins, F. W., and P. K. Kaw, On the role of plasma instabilities in ionospheric heating by radio waves, *J. Geophys. Res.*, *76*, 282, 1971.

Perkins, F. W., C. Oberman, and E. J. Valeo, Parametric instabilities and ionospheric modification, *J. Geophys. Res.*, *79*, 1478, 1974.

Petviashvili, V. I., Three-dimensional solitons of extraordinary and plasma waves (in Russian), *Fiz. Plazmy*, *1*, 28, 1975. (*Sov. J. Plasma Phys. Engl. Transl.*, *1*, 15, 1975.)

Petviashvili, V. I., Formation of three-dimensional Langmuir solitons by an intense radio wave in the ionosphere (in Russian), *Fiz. Plazmy*, *2*, 450, 1976. (*Sov. J. Plasma Phys. Engl. Transl.*, *2*, 247, 1976).

Showen, R. L., and R. A. Behnke, The effect of HF-induced plasma instabilities on ionospheric electron temperatures, *J. Geophys. Res.*, *83*, 207, 1978.

Showen, R. L., and D. M. Kim, Time variations of HF-induced plasma waves, *J. Geophys. Res.*, *83*, 623, 1978.

Smith, D. F., and D. R. Nicholson, Nonlinear effects involved in the generation of type III solar radio bursts, in *Wave Instabilities in Space Plasmas*, edited by P. J. Palmadesso and K. Papadoupoulos, D. Reidel, Hingham, Mass., 1979.

Weatherall, J. C., Nonlinear Langmuir waves in a weak magnetic field, Ph.D. thesis, Univ. of Colo., Boulder, 1980.

Weatherall, J. C., M. V. Goldman, and D. R. Nicholson, Parametric instabilities in weakly magnetized plasma, *Astrophys. J.*, *246*, 306, 1981.

Zakharov, V. E., Collapse of Langmuir waves (in Russian), *Zh. Eksp. Teor. Fiz.*, *62*, 1745, 1972. (*Sov. Phys. JETP Engl. Transl.*, *35*, 908, 1972.)

Zakharov, V. E., A. F. Mastryukov, and V. S. Synakh, Two-dimensional collapse of Langmuir waves (in Russian), *Zh. Eksp. Teor. Fiz. Pis'ma Red.*, *20*, 7, 1974. (*JETP Lett. Engl. Transl.*, *20*, 3, 1974.)

Zakharov, V. E., A. F. Mastryukov, and V. S. Synakh, Dynamics of plasma-wave collapse in a hot plasma (in Russian), *Fiz. Plazmy*, *1*, 614, 1975. (*Sov. J. Plasma Phys. Engl. Transl.*, *1*, 339, 1975.)

(Received April 21, 1981;
revised October 22, 1981;
accepted October 26, 1981.)

APPENDIX J

J. "Azimuthal Coherent Ion Ring--Beam Generation in Unstable Magnetized Plasmas"

R.A. Stern, D.N. Hill, and N. Rynn
Physical Review Letters 47, 792 (1981)

Azimuthal Coherent Ion-Ring–Beam Generation in Unstable Magnetized Plasmas

R. A. Stern
Department of Astro-Geophysics, University of Colorado, Boulder, Colorado 80309

and

D. N. Hill and N. Rynn
Department of Physics, University of California, Irvine, California 92664

(Received 1 June 1981)

A laser diagnostic yielding detailed space and time resolution of the ion-velocity distribution function reveals that ions ejected by electrostatic instabilities can form a frequency-coherent beam circulating diamagnetically at large radii around the unstable region. This results in anomalous transport with fluxes and over distance scales much larger than conventional processes.

PACS numbers: 52.40.Mj, 52.25.Fi

In collisionless (hot or rarefied) plasmas, transport and dissipation are caused by wave-particle interactions. Such processes are generally stochastic (noncoherent), as in current studies[1] of electrostatic ion-cyclotron waves (EICW), eigenmodes of magnetized plasmas with wide occurrence.[2-4] Using novel diagnostics, we have observed and maximized a new type of wave-particle interaction in which coherence is dominant. It causes ion transport in EICW with much larger intensities and distance scales, totally unrelated to the usual parameters (gradients and wave fields), and also leads to secondary wave excitation. Besides their basic interest, our results bear directly on magnetospheric transport,[2] fusion physics,[3] and isotope separation.[4]

Elementary physical concepts underlie this process. In electrostatic oscillations, half-cycles of potential rise and fall, which cause particle acceleration and deceleration, alternate and nearly cancel. Transport and dissipation are therefore caused by stochastic, high-order noncoherent processes. Under inhomogeneous conditions, however, particles can be irreversibly expulsed during a fraction of each cycle from an intense localized potential wave channel. If the orbits of expelled particles close on themselves in a time equal to the wave period, feedback and reinforcement can occur. Such synchronization is possible in EICW, where the collective mode frequency ω is very close to the free-particle (orbital) cyclotron frequency ω_{ci}.

This process is demonstrated by exciting EICW within a narrow channel in a plasma, and measuring the details of the ion distribution function $f(v, r, t)$ in velocity v, in space r, and time t. A single-ended Q machine[5] generates a 5-cm-diam Ba II plasma column in a uniform magnetic field $1 < B < 6$ kG [Fig. 1(a)]. Charge densities are below 10^9 cm^{-3}, and neutral pressure $< 10^{-6}$ Torr, to minimize collisions. Ion background temperatures are typically 3000 °K. A metal electrode is inserted across the plasma column. When an electron current to the hot plate exceeds 100 μA cm^{-2}, potential oscillations at $\omega \gtrsim \omega_{ci}$ become excited. The very small electron-cyclotron radii

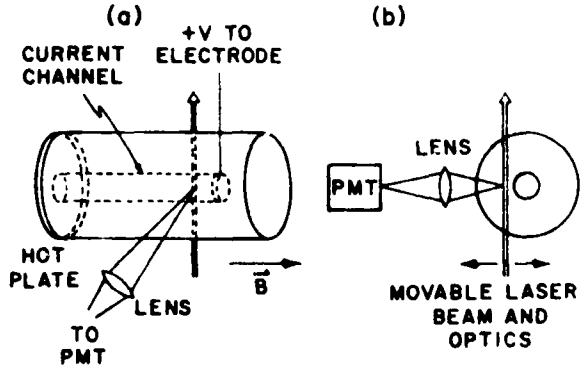

FIG. 1. Schematic of experiment and geometry.

© 1981 The American Physical Society

($\ll$0.1 mm) ensure that the current channel, and consequently the source potential oscillations, are entirely localized within the electrode radius $r \approx 3$ mm.

To measure $f(v, r, t)$, we develop an extension of selective excitation spectroscopy.[7] A single-mode dye laser is beamed across the plasma column and its wave number k is electronically scanned across the D_1 resonance line of Ba II at 4934 Å. The emitted fluorescence intensity F is proportional to f at $v = \vec{k} \cdot \vec{v}/k$, where k is the laser propagation vector. Velocity resolution is maximized by the narrow laser linewidth (<1 MHz): ions which fluoresce have velocities in a range less than 10^{-2} of the mean (thermal) ion speed. The fluorescence is detected by a long-focal-length lens mechanically coupled to the laser, so that both can be indexed simultaneously across the plasma [Fig. 1(a) and Fig. 1(b)]. Their intersection determines a diagnosed volume with resolution of order 1 mm^3. The time behavior of f is obtained from a frequency analysis of $F(v, r, t)$ with use of a radio receiver and phase-sensitive detector. Bandwidth and phase resolution are less than 10^{-3} and 5°, respectively. In summary, we obtain the Fourier transform, $F(v, r, \omega)$, of $f(v, r, t)$ with unprecedented detail.

Below are presented examples of the most significant new observations: (I) Generation and localization of an ion beam, (II) identification of coherent and incoherent beam density components, (III) excitation of secondary density oscillations, and (IV) unfolding of the ion-circulation process.

(I) Figure 2 shows the behavior of the time-averaged value of $F = \bar{F}(v, r)$. In the absence of EICW, $\bar{F}$ is the same at all positions r, as in trace (*a*). Note that $\bar{F}$ is symmetric in v, except for a flattening at high velocities, which is due to hyperfine structure. At finite EICW excitations, traces (*b*)–(*f*), $\bar{F}$ becomes strongly altered, depending on position. First, at the center of the current channel ($r = 0$), trace (*b*), $\bar{F}$ remains symmetrical but is appreciably broadened. This represents heating of the unstable plasma by the localized oscillating fields.[1] Traces (*c*)–(*e*) follow $\bar{F}$ at successively increasing radii *outside* the current channel, all measured along the same azimuthal angle, at 90° to the laser axis. $\bar{F}$ remains narrow as at (*a*), but becomes strongly asymmetrical; a velocity space resonance is seen to emerge (arrow). The resonance is centered, for these conditions, at the speed $V_R = 4 \times 10^4$ cm sec^{-1} in velocity space, and the position $R_R = 12$ mm in configuration space. Finally,

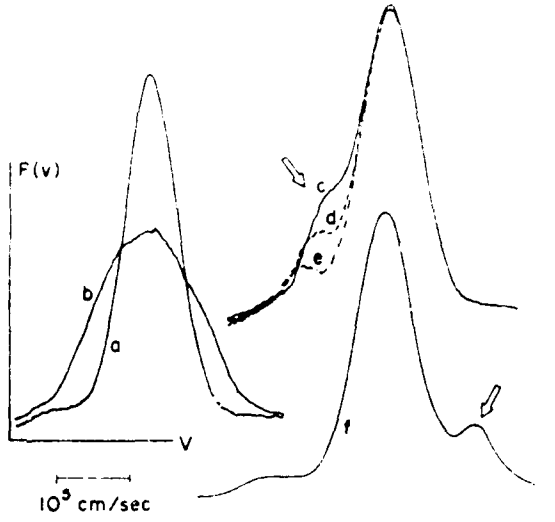

FIG. 2. Evolution of the ion beam in velocity and coordinate space. Vertical: $F(v, r)$, time average of ion distribution function, linear scale, and arbitrary units. Horizontal: ion velocity v, linear scale indicated. Trace (*a*), no excitation; (*b*)–(*f*), excitation at positions (*b*) $r = 0$; (*c*) $r = 9$ mm; (*d*) $r = 10$ mm; (*e*) $r = 12$ mm, on same azimuth; (*f*) $r = 12$ mm, opposite azimuth.

trace (*f*) shows $\bar{F}$ at the same radius as trace (*e*), but on the diametrically opposite side of the channel center (i.e., opposite azimuth). Here the resonance is seen (arrow) to occur with the opposite speed in velocity space, $v = -V_R$. Systematic measurements of this type reveal that EICW excitation creates a localized ion beam, with azimuthal circulation in the *direction of the diamagnetic ion current*, surrounding and concentric with the current channel.

(II) We now study the time dependence of F in the region where the ion beam is localized, e.g., $r = 12$ mm. First, using a phase-sensitive detector, we resolve $F(v, r, t)$ at discrete phase points 1 (90°), 2 (0° and 180°), and 3 (270°) within an individual EICW oscillation period. As seen, the bulk (low-velocity core) of F undergoes little change in comparison with the velocity-space regime centered on V_R. Within the latter—the ion beam—the distribution function is almost entirely *modulated in coherence* with the wave-potential oscillations of the source region at $r \approx 3$ mm. The modulated beam density amounts to about 25% of the background plasma density. Evidently particle transport is occurring on a massive scale, and over a distance scale one order of magnitude larger than the thermal-ion

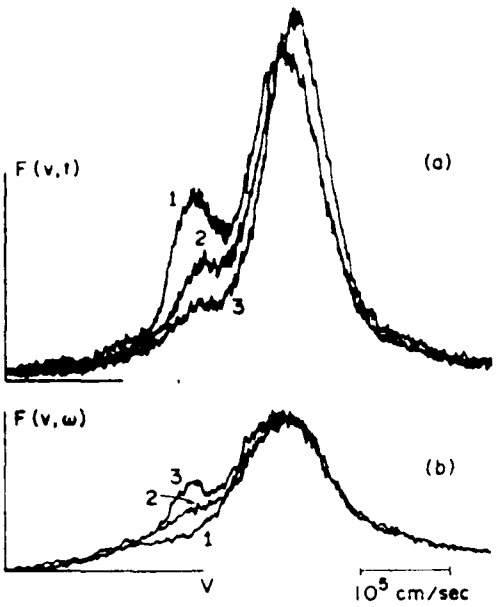

FIG. 3. Evolution of the ion beam in time. Vertical: $F(v,r,t)$, ion distribution function, linear scale, and arbitrary units. Horizontal: ion velocity v, linear scale indicated. Position is $r = 12$ mm. (a) Phase locked with reference from EICW oscillation and (b) radio signal. (1) and (3), radio tuned to ω, excitation on and off, respectively; (2), radio detuned (ω'), excitation on.

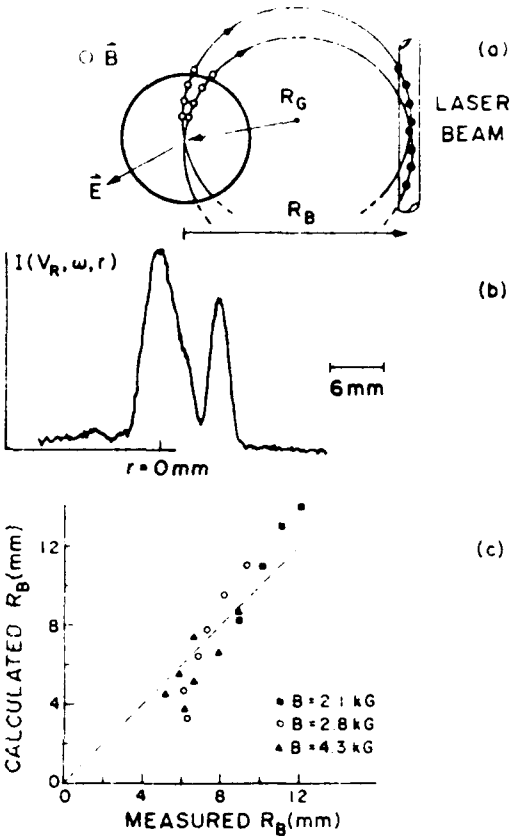

FIG. 4. Ion-circulation analysis and test. (a) Model of ion circulation. (b) Radial scan of $F(V_R, \omega, r)$; horizontal, radius (on same azimuth); vertical, intensity, and linear scale. (c) Measured vs calculated ion beam radius, R_B.

Larmor orbit (~1 mm for these conditions).

At larger excitations the plasma also acquires an appreciable incoherent component, i.e., non-oscillatory distribution function changes, induced by the EICW. To identify these, the detector (PMT) signal is fed to a radio receiver. This can be tuned to the EICW center frequency ω, or to another frequency ω' outside the bandwidth of the EICW oscillations. In Fig. 3(b), traces (1) and (3) show F with (1) and without (3) EICW oscillations, at the ion beam position $r = 12$ mm with the receiver tuned to ω. As seen, these exhibit a net difference in the beam region V_R, and correspond to traces (1) and (3) in Fig. 3(a). Trace (2) represents $F(\omega', r = 12$ mm, $t)$, in the presence of intense EICW. The sharp resonance at V_R has been replaced by a filling in of the distribution function tail. These incoherently accelerated ions comprise about 10% of the background, and we presume they represent diffusion of ions heated within the source.

(III) At intense excitation levels the modulation extends over both positive and negative velocities, with a minimum at $v = 0$. It acquires the appearance of an instability driven nonlocally by the coherent ion beam. We note that conventional (Langmuir) probes in the beam region yield signals which could be misinterpreted as denoting the presence of a local destabilizing current.

(IV) From the preceding, we obtain a physical model for the creation of the ion beam [Fig. 4(a)]: (i) The potential oscillation within the current channel has radial gradients which accelerate ion bunches during a half-cycle of each oscillation period. (ii) Ions "falling" down this potential "hill" leave the channel and enter into ballistic (free) orbits with a gyromagnetic radius R_c determined by their exit speed V_R and the magnetic field B according to the Lorentz formula: $R_c = (V_R/B)(Mc/e)$, where e/M is the ion charge mass ratio. Two adjacent orbits are sketched in Fig. 4(a), with open circles representing ions being expelled. (iii) One-half an EICW period

later, these ions reach the apogee of their orbit (closed circles). As seen, they are now bunched and nearly collimated in both configuration and velocity spaces. (iv) The envelope of the expelled ion orbits therefore constitutes an ion-beam circulation in the azimuthal-diamagnetic direction, with radius R_b *twice* the size of the gyromagnetic radius R_G.

To verify this concept, we measure R_b as a function of the parameters (V_R, B) which determine $R_G = \frac{1}{2} R_b$. (i) For a given B, the laser wavelength is tuned to excite ions with a selected V_k, (ii) their fluorescence is fed to a radio receiver tuned to ω, (iii) the diagnosed volume is scanned across the radius r of the plasma. Records of $F(V_R, \omega, r)$, Fig. 4(b), exhibit *two* resonances. The outermost, sharply peaked at R_b, represents the spatial localization of ion orbits determined by the choice of (V_k, B). The inner, confined to the wave channel region $r \lesssim 3$ mm, represents the *return circulation* of ion orbits with the same R_G but centered on the opposite azimuth. Radii R_b obtained by this method are plotted in Fig. 4(c). The straight line is the theoretical value $R_b = 2R_G$; no fitted parameters are involved. A possible intercept at 2 mm may be due to the finite radius of the source (~3 mm), not considered in our simple model.

Our observations and model describe a stationary saturated state where source-potential oscillations are strongly coupled to beam ions, which comprise roughly 50% of the source density, "load" the potential, and maintain a balance between mean beam energy and potential excursions. Probe-measured potential peaks of 1 V max are consistent with peak beam speeds of 10^6 cm/sec and magnetic field-determined radii, Fig. 4. Hence beam ions retain mean energy on successive orbits, while ions scattered out of phase constitute the "incoherent" broad background (above).

Extrapolating to magnetospheres[4] with potentials $e\varphi \sim kT = 1$ eV at 10^{-1} T, cross-field radii are 0.1 – 1 km. In fusion plasmas[3] with 10 kV, radii range from 1 cm at 10 kG to ∞ (machine size) at critical field-reversed layers ($B = 0$).

In conclusion, we present a new mode of wave-particle interactions which generates anomalous particle fluxes and nonlocal field excitations. In multiply filamented plasmas,[2,3] the flux driven by one filament may pass through another filament, be expelled in turn, and cause multistage transport over scales independent of conventional parameters.

It is a pleasure to acknowledge useful discussions and suggestions from I. B. Bernstein, S. P. Gary, S. W. Fornaca, J. L. Hirshfield, D. E. Murnick, and P. G. Pappas. This work was supported in part by the National Science Foundation under Grant No. Phy 80-09809 and in part by the Air Force Office of Scientific Research under Grant No. 80-0022.

[1]H. Okuda, C. Z. Cheng, and W. W. Lee, Phys. Rev. Lett. 46, 427 (1981); A. Fukuyama *et al.*, Phys. Rev. Lett. 38, 701 (1977); R. A. Stern, D. L. Correll, H. Bohmer, and N. Rynn, Phys. Rev. Lett. 37, 833 (1976).

[2]M. Temerin, M. Woldorff, and F. S. Mozer, Phys. Rev. Lett. 43, 1941 (1979); F. S. Mozer *et al.*, Phys. Rev. Lett. 38, 292 (1977).

[3]In tokomaks, for example: TFR Group, Phys. Rev. Lett. 41, 113 (1978); J. P. M. Schmitt and T. Lehner, Phys. Rev. Lett. 45, 1185 (1980). In mirrors, for example: W. C. Turner *et al.*, Phys. Rev. Lett. 39, 1087 (1977); F. H. Coensgen *et al.*, Phys. Rev. Lett. 35, 1051 (1975).

[4]J. M. Dawson *et al.*, Phys. Rev. Lett. 37, 1547 (1976); E. S. Weibel, Phys. Rev. Lett. 41, 377 (1980).

[5]N. Rynn, Rev. Sci. Instrum. 35, 40 (1964).

[6]R. A. Stern, Phys. Fluids 21, 1287 (1978); R. A. Stern and J. A. Johnson, III, Phys. Rev. Lett. 36, 1047 (1976).

APPENDIX K

K. "Modulational Interaction of Non-linear Waves and Recurrence"

B. Hafizi
Submitted to Physics of Fluids, June, 1981

Modulational interaction of nonlinear waves and recurrence

B. Hafizi

Department of Astro-Geophysics, University of Colorado
Boulder, Colorado 80309

Abstract

Modulational interaction of nonlinear waves is modeled using three-, five-, seven-, nine-, and sixty-four-wave truncations of the nonlinear Schrödinger equation. A detailed description of the phase-space for the three-wave systems is given, showing the various modes of evolution. It is shown that under certain circumstances the saturation level of the side-bands is computable from the linear dispersion relation for the instability. The quantitative accuracy of the three-wave system as regards the recurrence-time and the distribution of energy over the modes is verified by comparison with the other truncations.

I. INTRODUCTION

The collective interaction of many diverse phenomena in fluids is described by the nonlinear Schrödinger equation; for example, the modulational instability and propagation of Langmuir waves in a warm, collisionless plasma,[1] or the modulational interaction of progressive waves of finite amplitude on deep-water (Stokes waves).[2,3] To be specific, we take the Schrödinger equation to have the form

$$i\,\omega_t E + \omega_x^2 E + \left(|E|^2 - \langle |E|^2 \rangle \right) E = 0 \ , \tag{1}$$

where E is proportional to the complex envelope of the electric field for Langmuir waves and $\langle \ldots \rangle$ denotes a spatial average. Since $\langle |E|^2 \rangle$ is a constant [see Eq. (3)], by a suitable change of variables, Eq. (1) can be transformed into the form given in Ref. 2, with E representing the free-surface elevation of Stokes waves on deep water. [All the variables in Eq. (1) are in dimensionless form.]

Noting that a spatially and temporally uniform field E_o satisfies this equation, the stability of this solution is determined by examining perturbations of the form $E \exp(\omega t + ikx)$, leading to the well-known dispersion relation for modulational instability

$$\omega = k\left(2|E_o|^2 - k^2\right)^{1/2} \ , \tag{2}$$

as plotted in Fig. 1.

In an interesting set of water-tank experiments on Stokes waves,[3,4] it was discovered that following the modulationally unstable stage, the waves showed a remarkable behavior in that after the saturation of the instability, the original form of the wave-packet was reconstituted over and over again. The small deterioration in the process of reconstituting the original form of the packet along the length of the water tank was attributed to effects such as the viscous dissipation of surface waves.

To understand the essential physical mechanism underlying this process of recurrent temporal behavior, we show in this paper that it is imperative to note that the boson number B, given by

$$B \int |E|^2 \, dx \quad ,$$

is a constant motion of Eq. (1). In k space one has

$$B = \sum_k |E_k|^2 = |E_o|^2 + \sum_{|k|>0} |E_k|^2 \tag{3}$$

We thus find that as the perturbation grows, $|\hat{E}_o|$ must decrease. Provided $|k|$ is not too small (compared to $\sqrt{2}|\hat{E}_o|$), we show that the instability is quenched when the pump mode has been depleted to such an extent that the radicand in Eq. (2) becomes negative. The subsequent development of the system involves a periodic interchange of energy amongst the modes. (See also Fig. 3, Ref. 2.) For small values of $|k|$, this picture fails since such perturbations

cause considerable depletion of the pump and the linear analysis upon which Eq. (2) rests breaks down. Notwithstanding, for these perturbations, too, the system evolves periodically.

A detailed picture of the phase flow is constructed for the three-mode system, classifying the fixed points and determining the periods of oscillation (when applicable) about them. This analysis is not limited to small amplitude perturbations unlike the case in a recent study[5] where, in addition, the pump amplitude was not allowed to vary.

The results of the three-mode system are then compared with those of five-, seven-, nine-, and sixty-four-mode systems. We find that the recurrence-time is almost exactly the same in all cases. Further, the distribution of energy over the modes for the three-mode and the sixty-four-mode systems are in fair accord and as more and more modes are added to the three-wave systems there is a rapid approach to the results of the sixty-four-wave truncation.

II. THREE-WAVE TRUNCATION OF SCHRÖEDINGER EQUATION

Our aim is to examine only the case of "simple" recurrence.[2] Thus, we neglect the harmonics of the perturbation. In particular, we choose

$$\hat{E} = E_o \exp(i\Phi_o) + E \exp(ikx+i\Phi) + E \exp(-ikx+i\Phi) \quad ,$$

$$(k \neq 0;\ E_o,\ E,\ \Phi,\ \Phi_o \text{ are real})$$

subsitute into Eq. (1), and separate real and imaginary terms to obtain (using a super dot to denote the time derivative)

$$\dot{E} = EE_o^2 \sin\theta \quad , \tag{4}$$

$$\dot{E}_o = -2E^2E_o \sin\theta \quad , \tag{5}$$

$$\dot{\theta} = -2E_o^2 (1+\cos\theta) - 4E^2 \cos\theta - 2E^2 - 2k^2 \quad , \tag{6}$$

where

$$\theta = 2\phi - 2\phi_o \quad . \tag{7}$$

Note that in the expression for $\dot{E}$, we have chosen the amplitude for the perturbation at k to be equal to that for -k. This is done because if these amplitudes are the same initially, as in the computations,[2] one can show their equality for all time. Eq. (3) then becomes

$$B = E_o^2 + 2E^2 = \text{constant} \quad . \tag{8}$$

Using B, we need only consider, in lieu of Eqs. (4)-(6),

$$\dot{E}_o = -(B-E_o^2)E_o \sin\theta \quad , \tag{9}$$

$$\dot{\theta} = 2E_o^2(1+\cos\theta) - 2(B-E_o^2)\cos\theta - (B-E_o^2) - 2k^2 \quad . \tag{10}$$

There exists another constant of motion

$$H = k^2(B-E_o^2) - \frac{1}{2}(B-E_o^2)\left[\frac{1}{2}(B-E_o^2) + 2E_o^2(1+\cos\theta)\right] \quad , \tag{11}$$

which is the Hamiltonian of the system.

III. PHASE-FLOW OF THE TRUNCATED EQUATIONS

As usual,[6] we regard Eqs. (9) and (10) as determining a vector field in the two-dimensional phase-space (E_o, ϕ); i.e., defining a unique direction along which the system evolves. However, there are exceptions to this: at the fixed points of the flow, where the right-hand-sides vanish, there is no defined direction. The fixed points are

$$E_o = \sqrt{B} \quad , \quad \phi = \arccos\left(\frac{k^2}{B} - 1\right) \quad ; \quad (2B > k^2) \qquad (12i)$$

$$E_o = \sqrt{\frac{3B+2k^2}{7}} \quad , \quad \phi = 0, \pm 2\pi \quad ; \qquad (12ii)$$

$$E_o = \sqrt{B-2k^2} \quad , \quad \phi = \pm\pi \quad ; \qquad (B > 2k^2) \qquad (12iii)$$

$$E_o = 0 \quad , \quad \phi = \arccos\left(\frac{-k^2}{B} - \frac{1}{2}\right) \qquad (B > 2k^2) \qquad (12iv)$$

Since physically the phase difference of E_o and E_k is restricted to $-\pi < \phi - \phi_o < \pi$, the condition on ϕ is $-2\pi < \phi < 2\pi$, where ϕ_o is defined by Eq. (7). Using the fact that $E_o < \sqrt{B}$ [see Eq. (8)], we see that the phase-space of Eqs. (9) and (10) is a cylinder of length $\sqrt{B}$ and radius 2, obtained by identifying the lines $\phi = 2\pi$ and $\phi = -2\pi$.

We now determine the nature of the phase flows close to the fixed points by studying their stability; i.e., linearize Eqs. (9) and (10) about each of the fixed points in turn and substitute in perturbations of the form δE_o, $\delta\phi \exp(\lambda t)$. The following characteristic exponents λ are then obtained:

$$\left.\begin{aligned} \lambda &= 2B\sin\theta \quad , \quad \frac{\delta E_o}{\delta\theta} = -\frac{2B\sin\theta}{\tilde{E}_o[(4k^2/B)-1]} \quad , \\ \lambda &= -2B\sin\theta \quad , \quad \delta E_o = 0 \quad ; \end{aligned}\right\} \tag{13i}$$

$$\lambda = \pm i\left[\frac{4(3B+2k^2)(2B-k^2)}{7}\right]^{1/2} \quad , \quad \frac{\delta E_o}{\delta\theta} = \frac{\lambda}{14E_o} \quad ; \tag{13ii}$$

$$\lambda = \pm i2k(B-2k^2)^{1/2} \quad , \quad \frac{\delta E_o}{\delta\theta} = -\frac{\lambda}{2E_o} \quad ; \tag{13iii}$$

$$\left.\begin{aligned} \lambda &= -B\sin\theta \quad , \quad \delta\theta = 0 \quad , \\ \lambda &= 2B\sin\theta \quad , \quad \delta E_o = 0 \quad ; \end{aligned}\right\} \tag{13iv}$$

corresponding to the fixed points given in Eqs. (12i)-(12iv), respectively. In these equations, we have also given the eigenvectors. The exponents given by Eqs. (13i) and (13iv) show that the fixed points given by Eqs. (12i) and (12iv) are <u>saddle</u> points, with a one-dimensional <u>stable</u> <u>manifold</u> $R^{1-}_{i,iv}$ (corresponding to $\lambda < 0$), a one-dimensional <u>unstable</u> <u>manifold</u> $R^{1+}_{i,iv}$ (corresponding to $\lambda > 0$), and with the phase curves having a hyperbolic structure, as shown in Figure 2. The exponents given by Eqs. (13ii) and (13iii) show that the fixed points given by Eqs. (12ii) and (12iii) are <u>centers</u> with elliptical phase curves, as shown in Figure 2. Note that the sense of rotation of the phase curves around these fixed points are opposite to each other, as is easily checked from the linearized forms of Eqs. (9) and (10).

IV. EXAMPLES OF RECURRENT FLOW

Let us first consider the results of Ref. 2. In these computations, the initial fields are real-valued and the perturbation is of an amplitude much smaller than that of the (uniform) pump. Thus we begin at $\theta = 0$ and near the top of the phase-space, below the line $E_o = \sqrt{B}$ in Fig. 2. The trajectory then moves clockwise parallel to the stable manifold R_i^{1-} for awhile, sharply bends downwards, moves towards $\theta = 0$, turns upwards, and then returns to the vicinity of where it started from, parallel to the unstable manifold R_i^{1+}. Fig. 3, obtained by solving Eqs. (9) and (10) numerically for $k = 1.2$ and the initial conditions $E_o = 1$ and $E = 0.05$, shows clearly the structure just described. Thus, initially, as seen from Eq. (2) the system is unstable and the modulation of the uniform field grows. From Fig. 3, we see that the pump decays to an amplitude of ≈ 0.828, at which point the instability is quenched, since the radicand in Eq. (2) now equals $2\times(0.828)^2 - 1.2^2 = -0.069$. The subsequent periodic flow is obvious from the phase curve.

In Fig. 4 we show a phase curve that comes under the influence of most of the fixed points as it transverses the phase-space. In this figure, we have indicated the relative positions of the fixed points, which induce the particular form of this phase curve.

V. EFFECT OF HIGHER HARMONICS ON 3-MODE SYSTEM

In order to evaluate the extent to which our results, based on the solution of Eqs. (9) and (10), faithfully capture the

essence of the actual problem, we have solved Eq. (1) using five , seven , nine , and sixty-four modes. For reference we give the equations for the five-mode system only:

$$\dot{E}_1 = E_1 E_o^2 \sin\theta + 2E_1 E_2 [E_o \sin(\theta-\psi) - E_2 \sin(2\psi-\theta)], \qquad (14)$$

$$\dot{E}_o = -2E_o (E_1^2 \sin\theta + E_2^2 \sin 2\psi) - 2E_1^2 E_2 [2\sin\psi + \sin(\theta-\phi)], \qquad (15)$$

$$\dot{\theta} = 2[-k^2 + E_o^2 - E_1^2 + 4E_2 (E_o - \frac{E_1^2}{E_o}) \cos\psi + (E_o^2 - 2E_1^2)\cos\theta - 2E_2^2 \cos 2\phi$$
$$+ 2E_2 (E_o - \frac{E_1^2}{E_o}) \cos(\phi-\psi) + 2E_2^2 \cos(2\psi-\theta)] \quad , \qquad (16)$$

$$\dot{\psi} = -4k^2 + E_o^2 - E_2^2 + 2E_1^2 (\frac{E_o}{E_2} - 2\frac{E_2}{E_o}) \cos\psi - 2E_1^2 \cos\theta + (E_o^2 - 2E_2^2)\cos 2\phi$$
$$+ E_1^2 (\frac{E_o}{E_2} - 2\frac{E_2}{E_o}) \cos(\theta-\psi) + 2E_1^2 \cos(2\psi-\theta) \quad , \qquad (17)$$

where

$$B_5 = E_o^2 + 2E_1^2 + 2E_2^2$$

is the conserved boson number for the five-mode system, and the Fourier expansion of the electric field in Eq. (1) has the form

$$E = E_o \exp(i\phi_o) + E_1 [\exp(ikx+i\phi_1) + \exp(-ikx-i\phi_1)]$$
$$+ E_2 [\exp(i2kx+i\phi_2) + \exp(-i2kx-i\phi_2)] \quad ,$$

and we have re-defined the following linear combinations of phase-angles for the five-mode system (cf. Eq. (7)

$$\theta = 2\phi_1 - 2\phi_o \quad ,$$
$$\psi = \phi_2 - \phi_o$$

As in the case of the three-mode system one can try to determine the fixed points of Eqs. (14)-(17). As an example, the fixed point corresponding to that given in Eq. (12i) is

$$\tilde{E}_o = \sqrt{B},\ \phi = \arccos\left(\frac{k^2}{B} - 1\right),\ \psi = \frac{1}{2}\arccos\left(\frac{4k^2}{B} - 1\right),$$

$$E_1 = E_2 = 0,$$

provided one uses $\frac{E_1^2}{E_2} = 0$ in Eqs. (16) and (17).

Unfortunately considerable difficulties are encountered in determining some of the other fixed points. To illustrate, we note that $\phi = \psi = 0$ are fixed points for Eqs. (14) and (15). Substituting these into Eqs. (16) and (17) one ends up with the following bi-quartic algebraic equation

$$12(E_o^2-E_1^2)^2(2E_o^2-4k^2)(k^2-2E_o^2+3E_1^2)+216E_1^2(E_o^2-E_1^2)^3$$
$$-E_o^2(k^2-2E_o^2+3E_1^2)^3-12E_1^2(k^2-2E_o^2+3E_1^2)^2(E_o^2-E_1^2) = 0\ .$$

Although there is a formula[7] that expresses the roots of this equation in terms of combinations of radicals of rational functions of the coefficients, the result is so messy that not much can be gained from it.

In order to make further progress as regards the effects of higher harmonics on the three-mode system, we have numerically solved the five-, seven-, nine-, and sixty-four-mode truncations of Eq. (1). In all cases we find that the system behaves according to what Yuon and Ferguson[2] termed "simple"-recurrence, with almost identical recurrence times. Table 1 gives the distribution of energy over the modes at half the recurrence time, when

the energy content of the satellites with respect to the pump mode is maximal. The table clearly shows the rapid approach to an "asymptotic" energy distribution as the number of modes used in the computations increases. This behavior is shown more graphically in Fig. 5, where we have plotted $R(\tau_r/2) \equiv \sum_{k \neq 0} E_k(\tau_r/2)^2 / E_0(t=0)^2$ as a function of number of modes retained in the computations; here τ_r denotes the recurrence time in the system. Fig. 6(a) shows R(t) as a function of time for the system with 64 modes and Fig. 6(b) shows the k spectrum of Langmuir waves obtained from Eq. (1) at the time when the maximum value of R is attained. At this time there are a number of very intense solitary waves in x space [see Fig. 3 in Ref. 1 and Fig. 1(a) *in* Ref. 2]. Fig. 6(b) is shown here in order to give an indication of the extent to which our three-mode truncation of the Schrödinger equation is a valid description of the process. The solitary waves formed in x space, although very intense, are smooth structures. To form these, one needs the high mode-number parts of the spectrum, with appropriate phases, in addition to the low wave number components. In Fig. 6(b), we see that at their peak the amplitudes of the former group are at least a factor of four smaller than those of the latter group.

It is important to note the following. The finite separation of the modes that inevitably arises in any numerical experiment and shown graphically in Fig. 6(b) might lead some to suspect

that by including more and more modes, as in a real experiment, the phenomenon of recurrence would give place to irregular motion. We have two comments against this presumption. First, the very nonlinear coupling that transfers energy in between the modes strongly couples nearby modes to each other, thus causing some degree of ever-present coherence among them. Second, the phenomenon of recurrence has already been observed in actual water-tank experiments of Stokes waves on deep water.[3]

VI. CONCLUSION

We have presented here a detailed description of the phase space of the nonlinear Schrödinger equation, describing the modulational interaction of three waves. It is shown that one can determine the nonlinear saturation level of the modes from the linear dispersion relation of the system provided the wavenumber of the pump is not too small. We have also shown that the three-mode model is fairly accurate, by comparing its predictions for the recurrence time and the distribution of energy over the modes with those of five-, seven-, nine-, and sixty-four-mode truncations.

After the completion of this work we were made aware of similar work on the three-wave systems by Rabinovich and Fabrikant[8], and the integration of the three-mode equations by Infeld[9].

ACKNOWLEDGMENTS

The author thanks M.V. Goldman for bringing Ref. 2 to his attention. Critical comments by H.A. Rose and the referees are gratefully acknowledged.

This work was supported by the National Science Foundation under Grant ATM 7916837, the Air Force Office of Scientific Research under Contract F49620-76-C-0005, the National Aeronautics and Space Administration under Contract NAGW-91, and the National Center for Atmospheric Research Computing Facility in Boulder, Colorado.

REFERENCES

1. G.J. Morales, Y.C. Lee, and R.B. White, Phys. Rev. Lett. 32 457 (1974).

2. H.C. Yuen and W.E. Ferguson, Jr., Phys. Fluids 21, 1275 (1978).

3. B.M. Lake, H.C. Yuen, H. Rungaldier, and W.E. Ferguson, J. Fluid Mech. 83, 49 (1977).

4. B.M. Lake and H.C. Yuen, J. Fluid Mech. 83, 75 (1977).

5. P.A.E.M. Janssen, Phys. Fluids 24, 23 (1981).

6. V.I. Arnol'd, Oridindary Differential Equations (MIT Press, Cambridge, Mass., 1973).

7. M. Abramowitz and I.A. Stegun (Ed.), Handbook of Mathematical Functions, p. 17 (Dover, New York).

8. M.I. Rabinovich and A.L. Fabrikant, Zh. Eksp. Teor. Fiz. 77, 617 (1979). [Sov. Phys. - JETP 50, 311 (1979)].

9. E. Infeld, Phys. Rev. Lett., 47, 717 (1981).

FIGURE CAPTIONS

Fig. 1. Growth rate γ of modulation $E \exp(\gamma t+ikx)$ on uniform pump field E_o, as a function of wavenumber k. Dashed line shows effect of pump depletion: an initially unstable mode k causes instability to be quenched by extracting energy from the pump.

Fig. 2. Phase-space for $k^2 < B/2$. Note that this is a cylinder, obtained by identifying lines $\theta = -2\pi$ and $\theta = 2\pi$; $\tan\theta = 2B\sin\theta/[E_o(4k^2/B^{-1})]$. Dot-dash curve shows relative position of phase-curve of Fig. 3.

Fig. 3. Phase-curve for initial conditions $E_o = 1$, $E = 0.5$, and $k = 1.2$. Location of hyperbolic fixed points is shown.

Fig. 4. Example of phase-curve traversing phase-space. Initially, $E_o = .531$, $E = .86$, $k = .6$, and $\theta = .987$. Location of fixed points is indicated.

Fig. 5. $R(\tau_r/2) \sum_{k\neq o} |\hat{E}_k(\tau_r/2)|^2/|E_o(t=o)|^2$ as a function of number of modes used in computations; τ_r denotes the recurrence time.

Fig. 6. (a) $R \sum_{k\neq 0} |\hat{E}_k(t)|^2/|\hat{E}_o(t=0)|^2$ as function of time, using 64 modes. (b) Spectrum of Langmuir waves in k space at instant when R is maximum.

TABLE CAPTION 1

Table 1. Distribution of energy amongst the modes for various levels of truncation of the nonlinear Schrödinger equation at half the recurrence time. Mode number n corresponds to the term $\hat{E}_n \exp(inkx)$ in a Fourier representation of the electric field; n = o being the pump mode.

TABLE I

MODE NUMBER / NUMBER OF MODES IN COMPUTATION	0	4	8	12	16
	AMPLITUDE AT HALF THE RECURRENCE TIME				
3	16.96	10.57	-	-	-
5	14.20	11.82	3.244	-	-
7	13.39	12.06	3.821	1.109	-
9	13.19	12.08	4.030	1.326	0.4324
64	13.14	12.07	4.095	1.391	0.4727

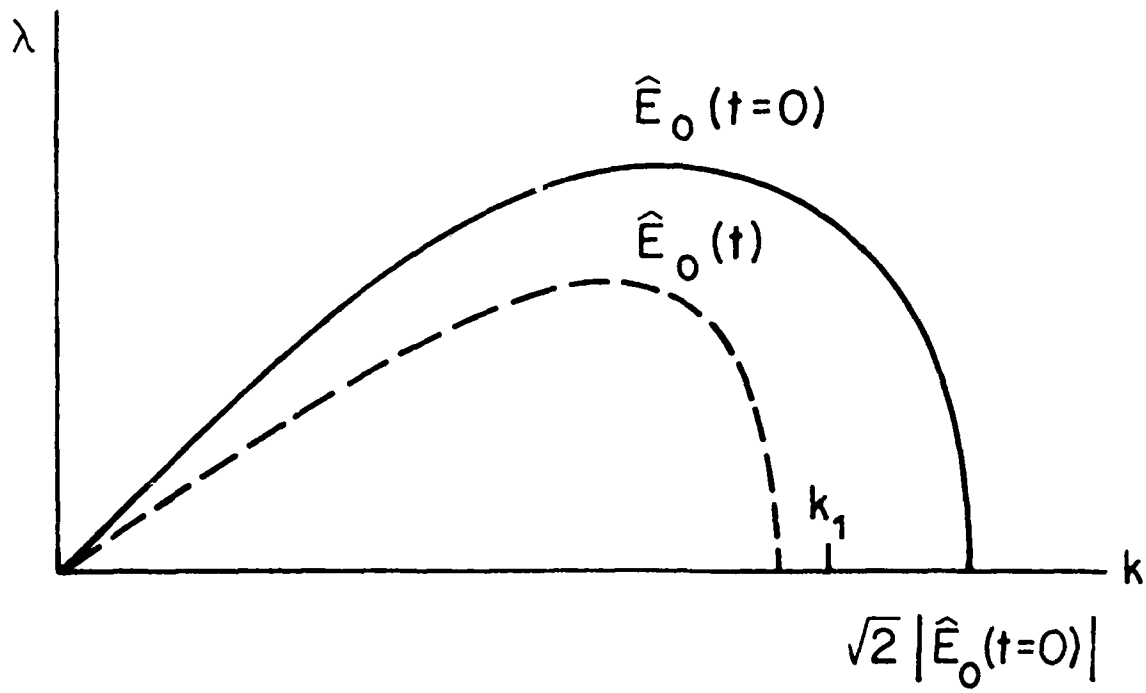

FIGURE 1

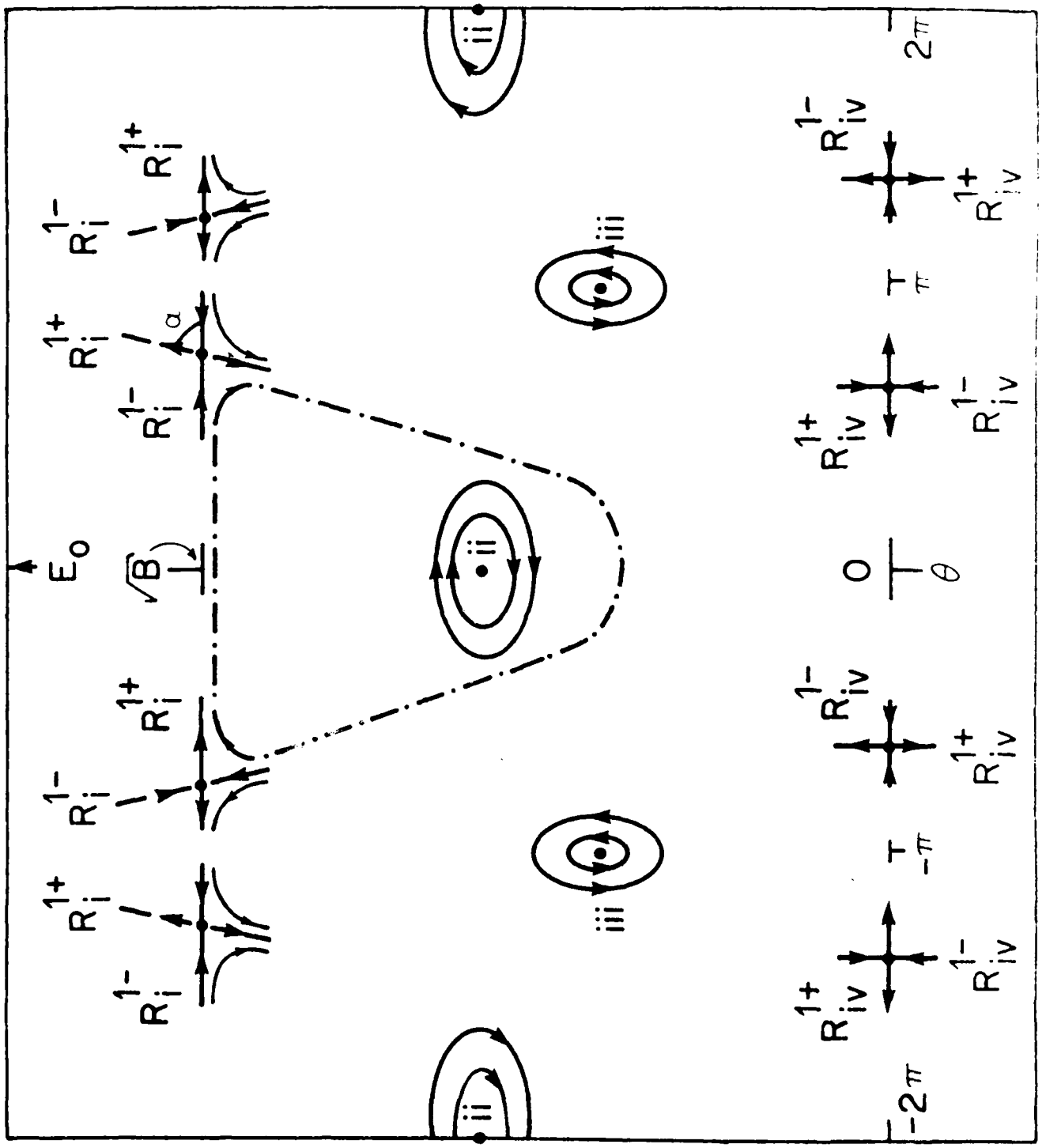
E_o
$\vec{B}$
α
R_i^{1+}
R_i^{1-}
R_{iv}^{1+}
R_{iv}^{1-}
i
ii
iii
iv
2π
π
0
$-\pi$
-2π
θ

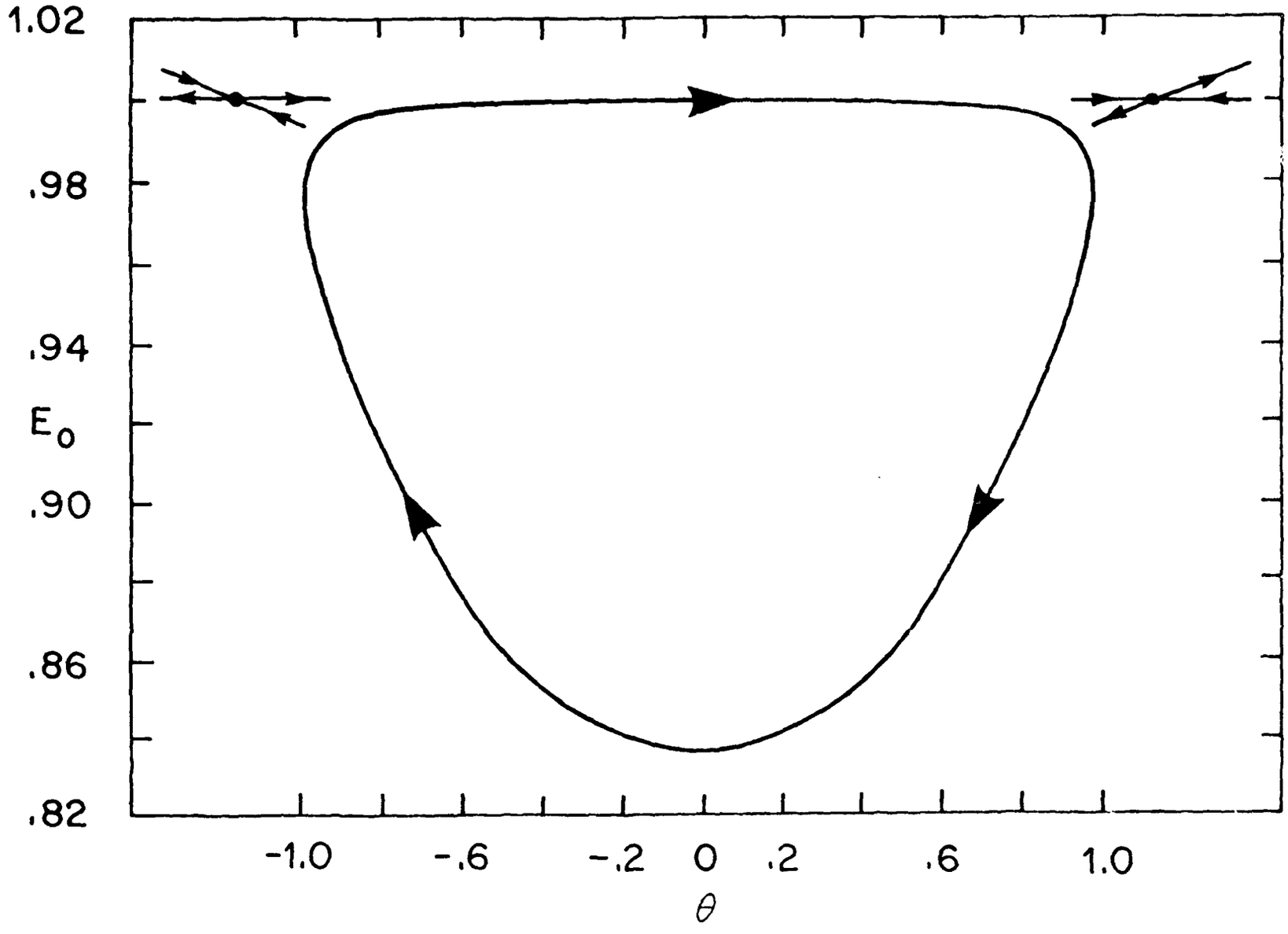

FIGURE 3

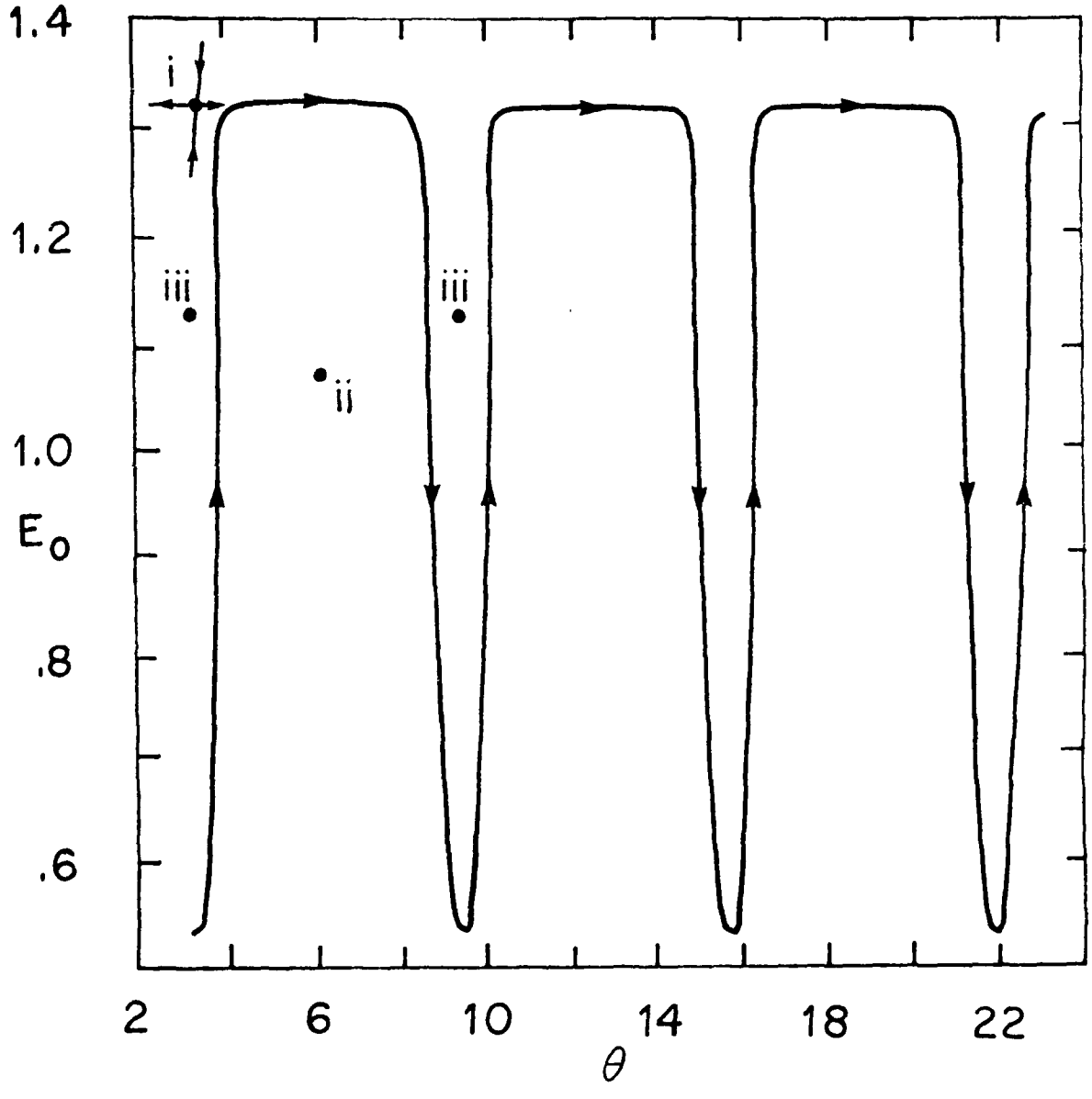

FIGURE 4

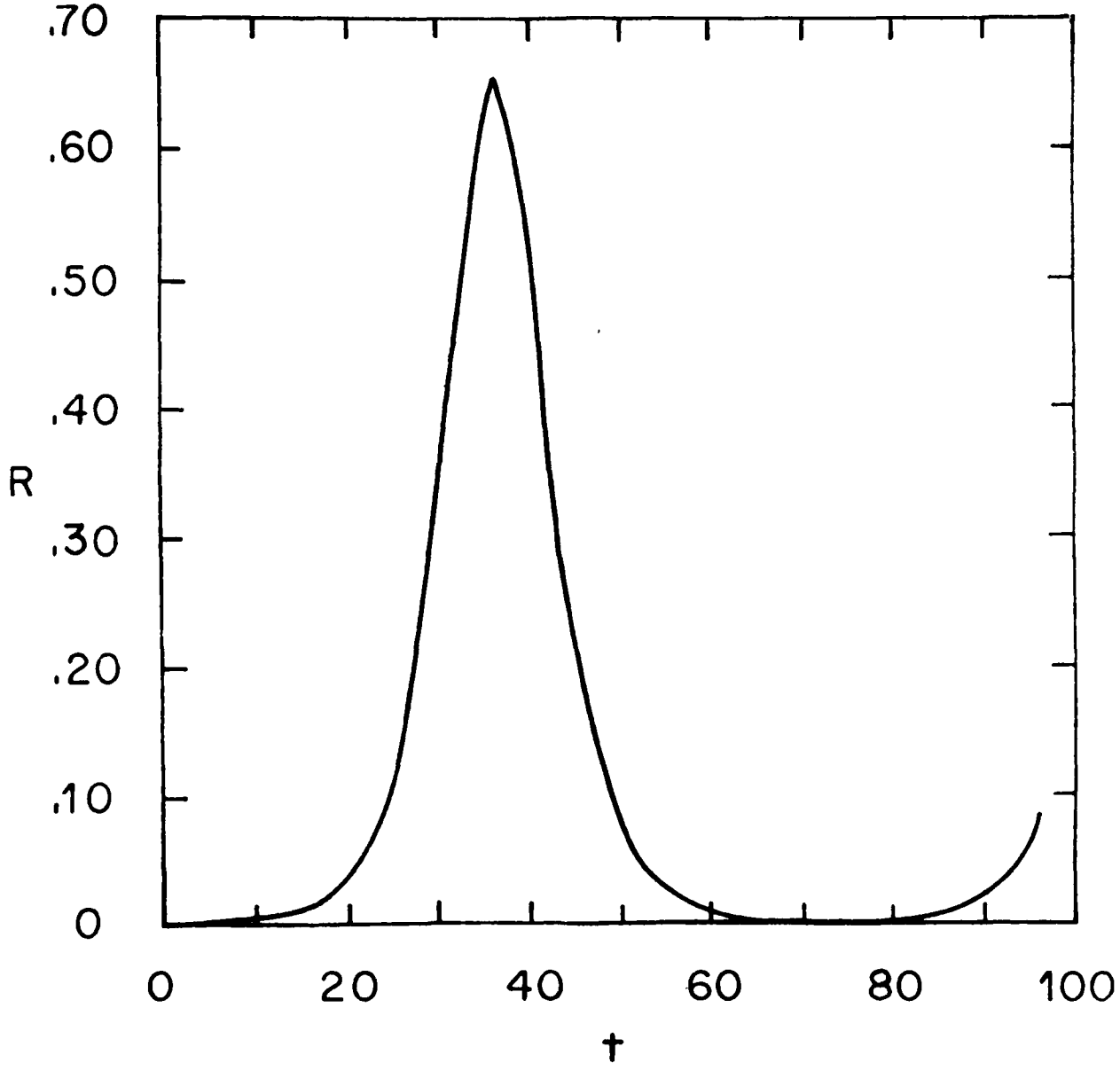

FIGURE 5(a)

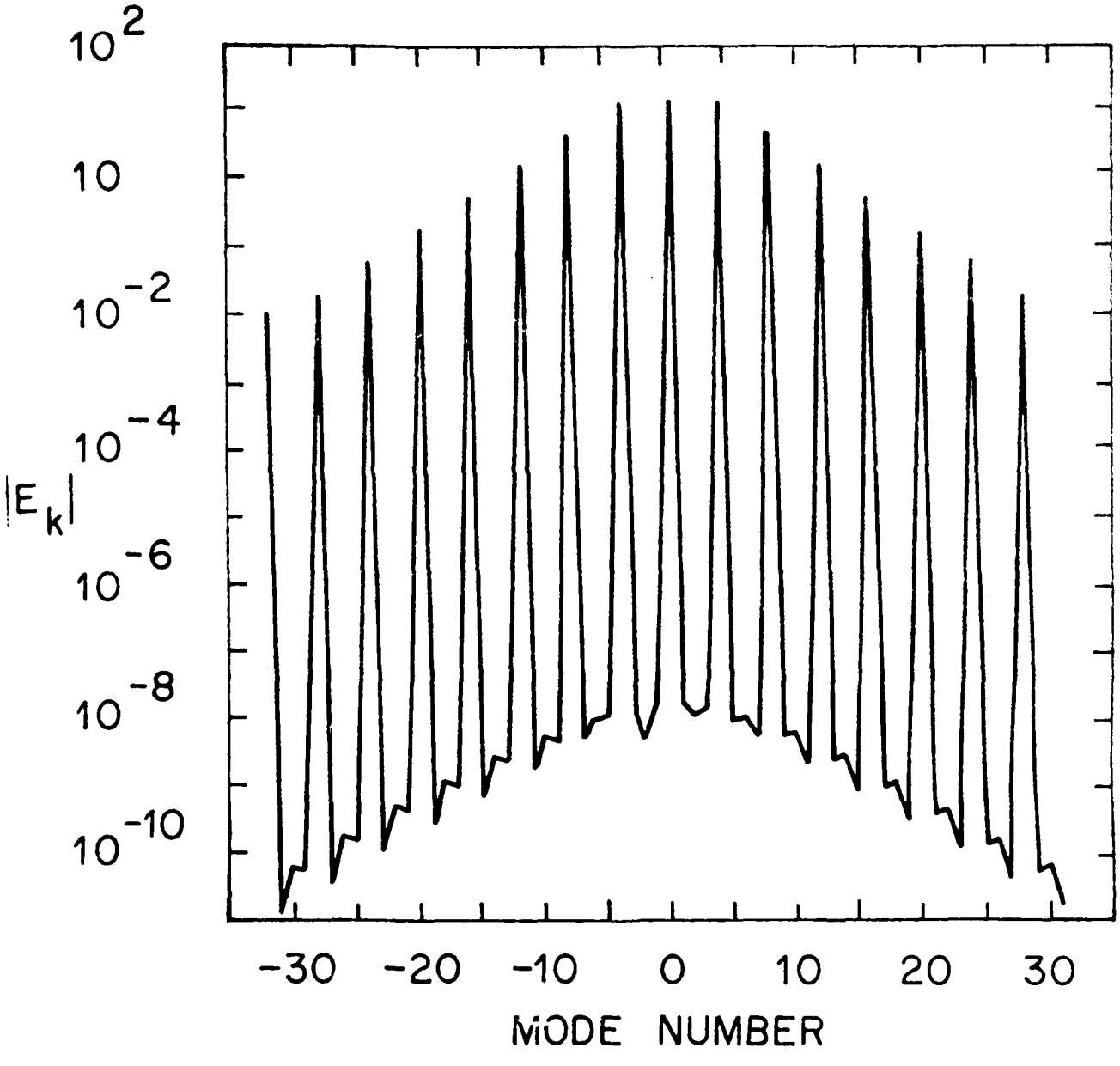

FIGURE 5(b)

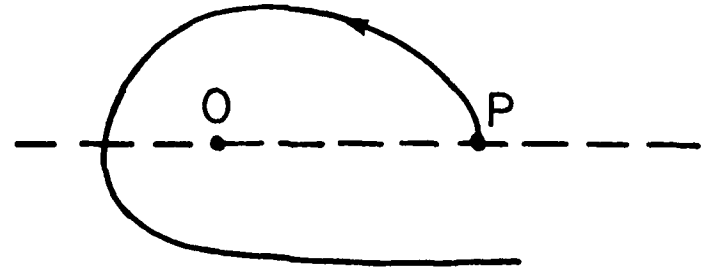

(a)

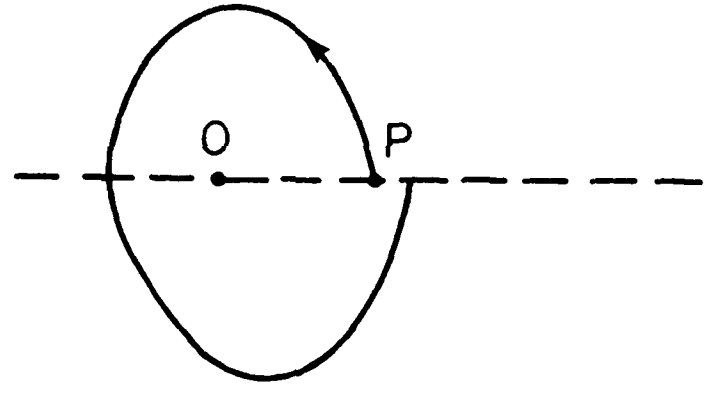

(b)

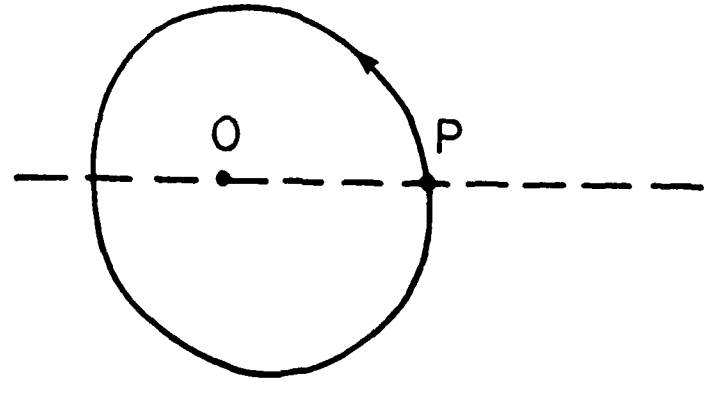

(c)

FIGURE 6

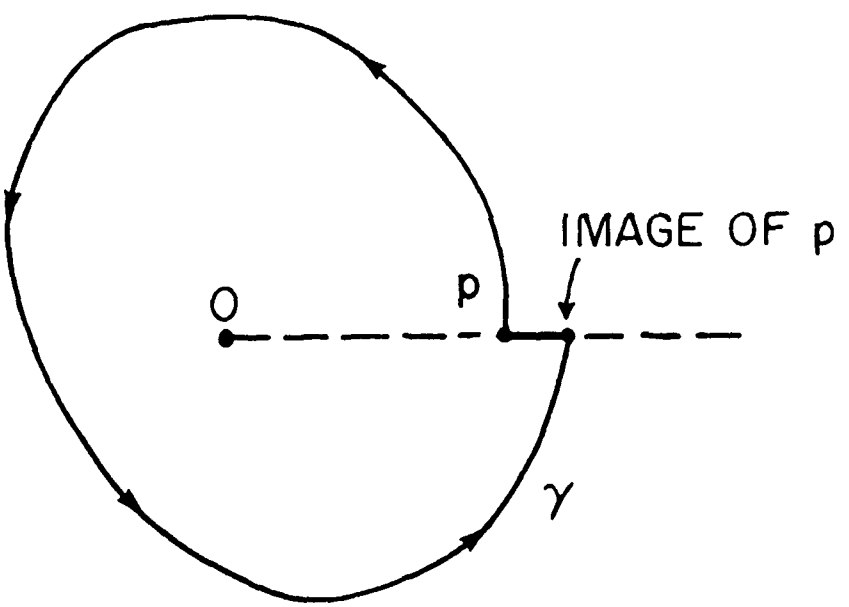

FIGURE 7

APPENDIX L

L. "Modulational Interaction of Langmuir Waves in One Dimension"

B. Hafizi
Submitted to Physics of Fluids, March, 1981

Modulational Interaction of Langmuir Waves in One Dimension

B. Hafizi*
Department of Astro-Geophysics
University of Colorado
Boulder, Colorado 80309

Abstract

The modulational interaction of Langmuir waves in the absence of forcing and of dissipation is studied by perturbation theory and by numerically solving 4-mode and 128-mode truncations of the Zakharov equations. In the 128-mode system, following the usual weak-turbulence process of inverse cascade a Langmuir condensate forms whose self-modulations lead to the formation of intense Langmuir wave packets which propagate with fluctuating amplitudes and velocities. The behavior of the 4-mode system follows that of the 128-mode system for a brief time interval before the formation of the condensate in the latter. In both cases several diagnostics, such as the two-time autocorrelation function, indicate a partially stochastic late-time behavior. It is shown that this behavior is consistent with the rigorous perturbation theorem of Kolmogoroff, Arnol'd and Moser, and that the non-integrability of Zakharov's equations is due to the presence of everywhere overlapping resonances.

*Permanent address: Science Applications, Inc., Boulder, Colorado 80302.

I. Introduction

The efficacy with which a powerful laser or relativistic electron beam may be used to heat a plasma is intimately connected with the problem of Langmuir turbulence. The understanding of the latter was greatly advanced by Zakharov[1] who derived a self-consistent pair of equations describing the interaction of Langmuir and sound waves. These fluid-like equations provide a succinct description of many phenomena, including the modulational interaction and incipient collapse of plasma waves.[1,2,3,4]

Recent progress[5] in the study of plasma turbulence based on the direct interaction approximation uses externally-generated sources of noise, and damping in the Zahkarov equations. The application of the dynamical renormalization group is also based on an open system.[6]

In view of the tremendous excitement that has been generated by the studies of intrinsic stochasticity exhibited by a number of nonlinear evolution equations[7,8,9] it would appear worthwhile to examine the Zakharov equations in a similar vein. In particular, there is already some evidence that the Zakharov equations are not solvable by the method of the inverse scattering problem and that they do not possess any symmetries (and therefore constants of motion) apart from those associated with the invariance group of their Lagrangian density [namely the Hamiltonian, the momentum, and the boson (or plasmon) number]. The evidence alluded

to in the foregoing - and this is only circumstantial evidence - comes about in computational studies[10] in which, rather than the more well-known elastic collisions of the solitons described by, say, the Korteweg-deVries equation[11] , the solitons of the Zakharov equations under certain circumstances fuse on collision.

It is well-known that the nonlinear Schrödinger equation (which is a limiting form of the Zakharov equations) is solvable by the method of the inverse-scattering problem and that it possesses an infinite set of constants of motion.[12] Thus a trajectory of this equation, lying at the intersection of the level-surfaces of all these motion-invariants, is severly constrained in its topology and its disposition relative to nearby trajectories. One thus finds that waves of finite amplitude on deep water (i.e., Stokes waves) described by this equation show such remarkable properties as recurrence and phase-coherence over long distances.[13] Then, if it is true that the Zakharov equations have only a few integrals of motion one might expect non-recurrent behavior.

In the present work we describe some initial-value solutions of the Zakharov equations in one spatial dimension. Starting from a single monochromatic wave and small-amplitude noise in the other modes we find that a Langmuir condensate forms through the process of inverse-cascade[14] (or parametric instability). The self-modulational[14,15] interaction of the condensate then develops intense Langmuir waves[1] that propagate in x space with fluctuating velocity and amplitude. Based on these and other information, such as the behavior of the autocorrelation functions for the various modes,

it is concluded that the Zakharov equations can show intrinsic stochasticity. The theoretical foundation for this behavior is provided by the rigorous perturbation theory of Kolmogoroff, Arnol'd and Moser.[7,8] It turns out that the Hamiltonian of the Zakharov equations is degenerate and the the tori of the zero-order Hamiltonian are destroyed under the influence of arbitrarily small perturbations. Further, the presence of everywhere overlapping resonances accounts for the nonintegrability of these equations.

II. Parametric instability and 4-wave interaction

There are basically two processes involved in reaching the late-time behavior of the solutions of the Zakharov equations: First, there is the parametric instability of a (large-amplitude) wave leading to the formation of a Langmuir condensate in k space[14] and second, the self-modulational interaction[14,15] of the condensate, which results in the appearance of flutuating, intense Langmuir waves in x space.

As noted in the Introduction both of these processes find a self-consistent description in the form of Zakharov's equations:

$$[i\partial_{\tilde{t}}+(3T_e/2m\omega_p)\partial_{\tilde{x}}^2]\tilde{E}(\tilde{x},\tilde{t}) = (2\pi e^2/m\omega_p)\tilde{N}\tilde{E},$$

$$(\partial_{\tilde{t}}^2-C_s^2\partial_{\tilde{x}}^2)\tilde{N}(\tilde{x},\tilde{t}) = (1/4\pi M)\partial_{\tilde{x}}^2|\tilde{E}|^2,$$

where $\tilde{E}(\tilde{x},\tilde{t})$ is the low-frequency envelope of the Langmuir field: $\tilde{E}_{Lang}(\tilde{x},\tilde{t}) = (1/2)\tilde{E}(\tilde{x},\tilde{t})\exp(-i\omega_p\tilde{t})+c.c.$; $\tilde{N}(\tilde{x},\tilde{t})$ is the perturbation in the background ion density, N_o; $\omega_p = (4\pi N_o e^2/m)^{1/2}$ is the plasma frequency, m(M) being the electron (ion) mass and e the electronic charge; $C_s = [(\gamma_e T_e+\gamma_i T_i)/M]^{1/2}$ is the sound speed, $T_e(T_i)$ being the temperature and $\gamma_e(\gamma_i)$ the adiabaticity index of electrons (ions).

Defining dimensionless variables through

$$t = \frac{2\eta}{3}\frac{m}{M}\omega_p\tilde{t} \quad ,$$

$$x = \frac{2}{3}\left(\frac{\eta m}{M}\right)^{1/2}\frac{\tilde{x}}{r_D} \quad ,$$

$$N = \frac{3M}{4m\eta}\frac{\tilde{N}}{N_o} \quad ,$$

$$E = \frac{1}{\eta}\left(\frac{M}{m}\right)^{1/2}\left(\frac{3\tilde{E}^2}{16\pi N_o T_e}\right)^{1/2} \quad ,$$

the equations become

$$(i\partial_t+\partial_x^2)E = NE \quad , \tag{1}$$

$$(\partial_t^2-\partial_x^2)N = \partial_x^2|E|^2 \quad ; \tag{2}$$

here $r_D \equiv (T_e/4\pi N_o e^2)^{1/2}$ is the Debye radius and

$$\eta \equiv (\gamma_e T_e+\gamma_i T_i)/T_e \quad .$$

In Eq. (2) the term $\partial_x^2|E|^2$ is (proportional to) the pressure force of the Langmuir oscillations on the sound waves. The completely integrable nonlinear Schrödinger equation is obtained when $\frac{\tilde{E}^2}{8\pi N_o T_e}$, $\left(r_D\frac{\partial \ln\tilde{E}}{\partial\tilde{x}}\right)^2 << \frac{m}{M}$. On the other hand, the validity of the Zakharov equations is guaranteed provided

$$\frac{\tilde{E}^2}{8\pi N_o T_e} << 1 \quad , \tag{3}$$

and

$$kr_D << 1 \quad , \tag{4}$$

in the last inequality k represents the dominant wavenumber in the spectrum. In general, the wavenumber is given by $2\pi\ell/L$, where ℓ is an integer representing the mode number and L is the periodicity length.

We now derive a set of evolution equations for 4 wave processes, one of whose diagrams is shown in Fig. 1, where two pump waves of amplitude E_o and wavenumber k_o interact via an intermediate sound wave of amplitude N_k and wavenumber k, producing a Stokes (down-shifted) and an anti-Stokes (up-shifted) Langmuir wave of amplitude E_1 and E_2 and wavenumber k_o+k and k_o-k, respectively ($k<0$); i.e.,

$$E(x,t) = \frac{1}{L}\{E_o\exp(-ik_ox)+E_1\exp[-i(k_o+k)x]+E_2\exp[-i(k_o-k)x]\} \quad ,$$

$$N = \frac{1}{L}[N_k\exp(-ikx)+N_k^*\exp(ikx)] \quad ,$$

$$V = \frac{1}{L}[V_k\exp(-ikx)+V_k^*\exp(ikx)] \quad ,$$

where V, the "hydrodynamic" velocity, satisfies

$$\partial_t N + \partial_x V = 0 \quad .$$

Substitution of these expressions into Eqs. (1) and (2) yields

$$\dot{e}_o + \frac{n}{L}(e_2\sin\psi+e_1\sin\theta) = 0 \quad , \tag{5}$$

$$\dot{e}_1 - \frac{ne_o}{L}\sin\theta = 0 \quad , \tag{6}$$

$$\dot{e}_2 - \frac{ne_o}{L}\sin\psi = 0 \quad , \tag{7}$$

$$\dot{n}-kv\sin\phi = 0 \quad , \tag{8}$$

$$\dot{v} + k\{n\sin\phi + \frac{e_o}{L}[e_2\sin(\psi+\phi) - e_1\sin(\theta-\phi)]\} = 0 \quad , \tag{9}$$

$$\dot{\theta} - k(k+2k_o+\frac{v}{n}\cos\phi) + \frac{n}{L}[\frac{e_2}{e_o}\cos\psi + (\frac{e_1}{e_o} - \frac{e_o}{e_1})\cos\theta] = 0 \quad , \tag{10}$$

$$\dot{\phi} - \frac{k}{v}\{\frac{v^2-n^2}{n}\cos\phi - \frac{e_o}{L}[e_2\cos(\psi+\phi) + e_1\cos(\theta-\phi)]\} = 0 \quad , \tag{11}$$

$$\dot{\psi} + k(k-2k_o-\frac{v}{n}\cos\phi) + \frac{n}{L}[\frac{e_1}{e_o}\cos\theta + (\frac{e_2}{e_o} - \frac{e_o}{e_2})\cos\psi] = 0 \quad , \tag{12}$$

wherein a super dot denotes a time derivative, and

$$E_o \equiv e_o\exp(i\phi_o) \quad ,$$

$$E_1 \equiv e_1\exp(i\phi_1) \quad ,$$

$$E_2 \equiv e_2\exp(i\phi_2) \quad ,$$

$$N_k \equiv n\exp(i\phi_n) \quad ,$$

$$V_k \equiv v\exp(i\phi_v) \quad ,$$

$$\theta \equiv \phi_o - \phi_1 + \phi_n \quad ,$$

$$\psi \equiv \phi_o - \phi_2 - \phi_n \quad ,$$

$$\phi \equiv \phi_n - \phi_v \quad ,$$

with e_o, e_1, e_2, n, v, ϕ_o, ϕ_1, ϕ_2, ϕ_n, and ϕ_v being real-valued functions of time.

Examining Eqs. (5)-(12) one can extract the following constants of the motion

$$b = e_o^2 + e_1^2 + e_2^2 \quad ,$$

$$p = k_o e_o^2 + (k_o+k) e_1^2 + (k_o-k) e_2^2 - 2nv \cos\phi \quad ,$$

$$h = k_o^2 e_o^2 + (k_o+k)^2 e_1^2 + (k_o-k)^2 e_2^2 + n^2 + v^2 + \frac{2ne_o}{L}(e_1 \cos\theta + e_2 \cos\psi) \quad , \tag{13}$$

representing the boson number, the momentum and the Hamiltonian, respectively.

The corresponding invariants of the untruncated Zakharov equations are proportional to[10,16]

$$B = \int dx |E(x,t)|^2 \quad ,$$

$$P = \frac{i}{2} \int dx (E \partial_x E^* - E^* \partial_x E) + \int dx NV \quad ,$$

$$H = \int dx [|\partial_x E|^2 + N|E|^2 + (1/2)(N^2+V^2)] \quad ,$$

in the integral representation.

As is well-known,[14] a monochromatic pump-mode of wavenumber $\tilde{k}_o r_D > \frac{1}{3}\sqrt{m/M}$ is unstable to the inverse-cascade process whereby it decays successively into daughter waves until a Langmuir condensate is formed in the region $o \leq |\tilde{k} r_D| \leq \frac{1}{3}\sqrt{m/M}$. With the formation of the condensate there arises the question of the means by which to dissipate this energy in a region of phase-space where the usual process of Landau damping, radiation, etc. are ineffective. [By dissipation we mean the transformation of the electrostatic energy residing in the condensate to other forms, via processes lying outside the scope of Eqs. (1) and (2).]

The way out of this difficulty was first pointed out by Vedenovand Rudakov[15] who showed that the Langmuir condensate is unstable to spatial modulations when $\frac{\tilde{E}^2}{8\pi N_o T_e} \gtrsim (\Delta\tilde{k} r_D)^2$, where $\Delta\tilde{k}$ is the average spread in the wavenumbers of the condensate. It was later shown that the self-modulation can lead to the formation of intense solitary waves, thus transferring energy into the dissipative region.[1]

III. Computations

The computations were performed by the Galerkin[17] method of using a finite number (128) of Fourier modes spanning the solution space. The integration of Eqs. (1) and (2) was carried out by splitting the evolution operator into its linear and nonlinear parts. The linear part of the integration was carried out exactly in k space and the nonlinear part by implicit methods in x space. Aliasing errors were avoided by the usual method.[18] The errors sustained in B, P, and H were less than 1%.

Landau damping is neglected since $\tilde{k} r_D << 1$ and $T_e >> T_i$; further, following the definition given after Eq. (2), $n = \gamma_e = 1$ since the electrons are isothermal on the ion-sound time-scale. The periodicity length used in these computations is $\tilde{L} = 64x\frac{3}{2}(\frac{M}{m})^{\frac{1}{2}} r_D$.

The initial-value problem was set-up with $\tilde{k}_o r_D = 2.4 \times \frac{1}{3}\sqrt{m/M}$ ($E_{k_o} \equiv E_o = 45.2$), $(\tilde{k}_o+\tilde{k}) r_D = -0.6 \times \frac{1}{3}\sqrt{m/M}$ ($E_{k_o+k} \equiv E_1 = 0.021$) and all the other modes at round-off amplitudes ($\tilde{=}10^{-15}$). The Stokes mode chosen $(\tilde{k}_o+\tilde{k})$ is the one with the fastest parametric growth rate, obtained by solving the usual dispersion relation[19] for parametric instabilities for constant $E_{k_o} \equiv E_o$:

$$\omega^4 - 4kk_o\omega^3 + (4k_o^2 - k^2 - 1)k^2\omega^2 + 4k^3k_o\omega - (4k_o^2 - k^2 + 2|E_o|^2/L^2)k^4 = 0 \; ; \qquad (14)$$

with the imaginary part of ω determining the growth-rate.

Fig. 2 shows the spectrum of Langmuir waves at $\omega_p t = 192(M/m)$. In this figure we see the pump-mode and a strongly driven Stokes mode. Since the magnitude of the wave number of the latter, $0.6 \times \frac{1}{3}\sqrt{m/M}$, is less than $\frac{1}{3}\sqrt{m/M}$ it cannot decay. As usual, one can also see a prominant anti-Stokes (up-shifted) mode. The standard normal-mode analysis[19] determines the ratio of the Stokes mode E_1 to the anti-Stokes E_2 to be

$$\left|\frac{E_1}{E_2}\right| = \left|\frac{\omega_o - \omega^* - (k_o - k)^2}{\omega_o + \omega - (k_o + k)^2}\right|$$

where ω_o is the frequency of the pump-mode. Note that this ratio is independent of the pump-amplitude, E_o. The ratio of the amplitudes determined from Fig. 2 is within a factor of three of that given by this expression. Of course, this agreement is very rough because the above formula is obtained from a normal-mode analysis with a fixed pump amplitude, whereas the computations refer to a system (and in particular a pump-mode) that changes considerably.

Although the Stokes component cannot decay into another Langmuir wave with the emission of a sound wave, it is still unstable with respect to the 4-wave instability shown in Fig. 1. We have checked that, making a rough estimate for the amplitude of the Stokes mode (as the pump-mode), the unstable modes predicted by Eq.(14) correspond to the sub-satellites of the Stokes mode, designated ss in Fig. 2. The sub-satellites on the right-side of the pump-mode and the right-side of the anti-Stokes mode could possibly be generated by parametric interaction with the sub-satellite on the right-side of the Stokes mode. Thus, the

wavenumber and frequency selection rules for the 3-wave process[20] (neglecting the anti-Stokes mode) Langmuir→Langmuir+Sound are respectively

$$k_o = (k_o+k) - k \quad , \tag{15}$$

$$k_o^2 = (k_o+k)^2 - |k| \quad , \tag{16}$$

in dimensionless units.

One can now excite a sub-satellite of the pump-mode, with only a small mis-match for the frequency selection rule using the existing sound wave:

$$[(k_o+k)+\delta k]-k \rightarrow k_o+\delta k \quad , \tag{17}$$

$$[(k_o+k)+\delta k]^2-|k| \rightarrow (k_o+\delta k)^2 \quad . \tag{18}$$

If Eq. (15) is satisfied then so is Eq. (17); if Eq. (16) is also satisfied, then Eq. (18) has a frequency mis-match $o(\delta k)$. In Eqs. (17) and (18) $(k_o+k)+\delta k$ is the wavenumber of the sub-satellite on the Stokes mode and $k_o+\delta k$ that for the sub-satellite on the pump-mode.

One can also generate sub-satellites to the sound waves (as observed in the computations) by beating a sub-satellite of the Stokes mode with the pump-mode:

$$k_o \rightarrow [(k_o+k)+\delta k] - (k+\delta k) \quad ,$$

$$k_o^2 \rightarrow [(k_o+k)+\delta k]^2 - |k+\delta k| \quad ,$$

in obvious notation.

As regards to the sub-sub-satellites and the sub-sub-sub-satellites we believe that they are excited through the modulational (4-wave) instability of the Stokes mode, and harmonic generation.

This is suggested by the disposition of the sub-sub-satellites and the sub-sub-sub-satellites with respect to the Stokes mode and its sub-satellites in k space.

Fig. 3(a) shows the k spectrum of the Langmuir waves at $\omega_p t = 624(M/m)$. The Langmuir condensate has already been formed and its self-modulational interaction[1] has led to the development of an intense solitary wave as shown in Fig. 3(b).

Fig. 4 shows a plot of $R(t) \equiv \sum_{k \neq k_o} |E_k(t)|^2 / |E_{k_o}(t=0)|^2$ as a function of time. After a period of recurrent energy exchange - principally between the pump and the Stokes mode - an apparently time - asymptotic state is reached, with fluctuations of about 5% on the mean value of R. In this late-time stage the pump mode is almost completely depleted and most of the plasmon energy resides around the origin of k space.

At this juncture it must be pointed out that a picture similar to that in Fig. 3 is obtained if one starts with a broad-band pump, since in both cases the Stokes wave and its sub-satellites form a broad spectrum around $k = 0$.[21]

IV. Theory and Discussion

We now proceed to examine Fig. 4 in more detail in order to gain an understanding of its two main features, namely the initial periodic behavior and the final random oscillations superimposed on a mean level.

Examination of the k spectra of the Langmuir oscillations reveals that in the initial stages most of the energy resides in the pump and the decay mode, which exchanges energy in a periodic manner. Eqs. (5)-(12) for the four-wave system have been solved for the same set of initial conditions as that for the many-mode computations. Fig. 5 shows the amplitude of the pump mode as a function of time, which can easily be compared with Fig. 4. From Fig. 5, the pump is depleted to a value $\simeq 12.6$, at which time $R = \frac{45.2^2-12.6^2}{45.2^2} = 0.92$, compared to 0.725, 0.9, and 0.73 for the first three maxima of R in Fig. 4, for the 128-mode system. The oscillation period for the pump in Fig. 5 is $37\ \frac{M}{m}\omega_p^{-1}$ and that for the initial oscillations in Fig. 4 is $44\ \frac{M}{m}\omega_p^{-1}$. We note that the oscillatory part can also be accurately described by a 3-wave system[20] in which the anti-Stokes mode e_2 is neglected in Eqs. (5)-(12); this being due to the fact that this mode has relatively small amplitude.

We now proceed to examine the late-time behavior of our solutions. After the formation of the Langmuir condensate and its self-modulation, there appear intense Langmuir waves in x space which propagate with fluctuating amplitude and velocity. It is well-known that the decay instability is subsonic provided[14]

$$\frac{E_o^2}{8\pi N_o T_e} \lesssim \frac{m}{M} ,$$

wherein E_o is the peak value of the electric field in x space. For the parameters of our problem we find $\frac{E_o^2}{8\pi N_o T_e} = \frac{1}{3}\frac{m}{M}$ at $t = 0$. Further, due to the decay process and the associated emission of sound, weak turbulence is accompanied by sound turbulence. Under these circumstances one observes break-up and fusion of Langmuir wave packets.[10] Fig. 6 shows the space-time path of the fluctuating wave packets. One can see that as it progresses its speed on occasions approaches that of sound and then abruptly slows down. Its terminal speed is close to $0.4C_s$ with small fluctuations about this value and little emitted sound energy. However, the amplitude of the wave-packet varies within a factor of 3 in this time interval, $630\ \frac{M}{m} \leq \omega_p t \leq 720\ \frac{M}{m}$. It must be noted that at about $\omega_p t = 636\ \frac{M}{m}$, for example, one observes the wave packet to slow-down considerably and to break-up into two wave-packets one of which then intensifies and moves away from the other. (An example of break-up is given later, Fig. 10). The displacement plotted in Fig. 6 is that of the dominant wave packet observed. (In the snap-shots obtained in our computations there has always been one dominant wavepacket even when two wavepackets have collided or one has broken up.) The largest value of $\frac{|E_o|^2}{8\pi N_o T_e}$ in this problem is $4\ \frac{m}{M}$ in the course of computation. Fig. 7 shows the sound momentum [$= \int NV dx$, as given in the expression for P, following Eq. (13)], indicating a fluctuating interaction with the Langmuir oscillations in the late stages.

Let f(t) be one of the variables characterizing the system. The two-time autocorrelation function for this variable is given by

$$C(\tilde{\tau}) = \frac{1}{\tilde{T}-\tilde{\tau}} \int_0^{\tilde{T}-\tilde{\tau}} dt[f^*(t+\tilde{\tau}) - \langle f^* \rangle][f(\tilde{t}) - \langle f \rangle] \quad , \qquad (19)$$

where $\langle \ldots \rangle$ denotes the time average. We have computed the (real-part of the) two-time autocorrelation function for the Langmuir modes zero through fifteen, two of which are shown in Fig. 8. The integral in Eq. (19) was performed for the time interval $630\ \frac{M}{m} \leq \omega_p \tilde{t} \leq 720\ \frac{M}{m}$. The decay of the autocorrelation function to zero as $\tilde{\tau} \to \infty$ is regarded as a signature of stochastic flow.[22] Bearing in mind the limited time-length of our computations, Fig. 8 indicates that our particular problem is partially stochastic. The definition of autocorrelation function given in Eq. (19) is that usually used in real experiments as opposed to idealized mathematical systems where the time-averaging is performed over an infinite time interval. The finite number of sample points implies that relatively large errors are incurred in evaluating the autocorrelation function, which error increases as $\tilde{\tau}$ increases due to the reduced number of sampling points. For the eigth mode, Fig. 8(a), the error at $\omega_p\tilde{\tau} = 5$ is 3%, that at $\omega_p\tilde{\tau} = 25$ is 20% and that at $\omega_p\tilde{\tau} = 40$ is 60%. We have referred to the state of the 128-mode system as partially stochastic since, given the errors involved and the limited time over which the system has evolved, once cannot conclude that the two-time autocorrelation function decays to zero. In fact, the very presence of one or more intense Langmuir waves implies that there is a certain coherence amongst the Fourier components that make up the wave packet(s). Particularly

in the late-time stages of the computations we have observed that the wave packets propagate for distances corresponding to at least a few decorrelation-times (i.e., the time duration in which the correlation function falls by a factor e) while maintaining their integrety, albeit with fluctuating amplitudes and velocities. Thus, although the autocorrelation functions decay to about 1/3 of their peak value, there is certainly the remanent of organized behavior in the 128-mode system, for the particular parameters used here. We refer to such behavior as partially stochastic. The autocorrelation functions for the other modes have a similar behavior except that the numer of oscillations per unit time interval increases as the mode number increases. We have also analyzed the temporal spectrum of the Langmuir oscillations (at a fixed point in x space), obtaining a continuous, broad-band spectrum over a decade and half of frequency.

The next obvious question is how these results are altered as one increases the initial pump amplitude? For this purpose we need to rewrite the four-wave Hamiltonian in action-angle variables so as to be able to use the Kolmogoroff-Arnol'd-Moser stability theorem[23] and some of the numerous numerical studies performed to investigate the stochastic behavior of Hamiltonian systems.[7,8,9] The details of the calculations are given in the Appendix; the four-wave Hamiltonian has the form

$$\begin{aligned} h = {} & [k_o^2 J_o + (k_o+k)^2 J_1 + (k_o-k)^2 J_2] + |k|(J_3+J_4) \\ & + 2\left(\frac{|k|J_o}{L}\right)^{\frac{1}{2}} (J_3\cos^2\phi_3 + J_4\sin^2\phi_4)^{\frac{1}{2}} [J_1^{\frac{1}{2}} \cos(\phi_0-\phi_1-\phi_n) \\ & + J_2^{\frac{1}{2}} \cos(\phi_0-\phi_2+\phi_n)] \end{aligned} \tag{20}$$

wherein the J's denote the action variables and the ϕ's the angles, with

$$
\begin{aligned}
E_j &= (LJ_i)^{\frac{1}{2}} \exp(-i\phi_j), \qquad (j = 0, 1, 2) \\
N_k &= (L|k|)^{\frac{1}{2}}(J_3^{\frac{1}{2}} \cos\phi_3 + iJ_4^{\frac{1}{2}} \sin\phi_4) \quad , \\
\phi_n &= \arctan[(\frac{J_4}{J_3})^{\frac{1}{2}} \frac{\sin\phi_4}{\cos\phi_3}] \quad , \\
V_k &= i(L|k|)^{\frac{1}{2}}(J_3^{\frac{1}{2}} \sin\phi_3 + iJ_4^{\frac{1}{2}} \cos\phi_4) \quad ;
\end{aligned}
\tag{21}
$$

note the change in the sign of the exponential for the electric field as compared to that given following Eq. (12) (For the transformation to action-angle variables it is natural to use the variable U defined in the Appendix, Eq. (A2). However, for our computational work for reasons of symmetry we have found it natural to use the "hydrodynamic" velocity V, defined just before Eq. (5); they are related via $V+\partial_x U=0$.)

The basic question is if the Kolmogoroff-Arnol'd-Moser theorem can guarantee the preservation of the tori of the unperturbed system. The basic requirements of this theorem for stability are[7,8,23]

i) The nondegeneracy condition

$$\det|\omega_{\ell m}| \neq 0 \quad , \qquad \ell,m = 0,1,\ldots,4$$

ii) The condition for isoenergetic nondegeneracy

$$\det \begin{vmatrix} \omega_{\ell m} & \omega_\ell \\ \omega_m & 0 \end{vmatrix} \neq 0 \qquad \ell,m = 0,1,\ldots,4$$

iii) Absence of low-order resonances, i.e., no relations $\sum_{i=0}^{4} \ell_i \omega_i = 0$ with integers ℓ_i such that $0 < \sum_{i=0}^{4} |\ell_i| \leq 4$.

In these formulas ω_ℓ is the frequency corresponding to the action variable J_ℓ; i.e. $\omega_2 = \dot{\phi}_2 = \frac{\partial h_o}{\partial J_2} = (k_o - k)^2$, h_o being the zeroth order Hamiltonian

$$h_o = k_o^2 J_o + (k_o+k)^2 J_1 + (k_o-k)^2 J_2 + |k|(J_3+J_4);$$

in addition, $\omega_{\ell m}$ denotes the derivative of ω_ℓ with respect to J_m.

Straightforward calculations show that conditions i) and ii) fail for this Hamiltonian.

Now consider the decay mode corresponding to the perturbation term $\cos(\phi_o - \phi_1 - \phi_n)$. By definition, and using Eq. (21).

$$\dot{\phi}_o = \frac{\partial h_o}{\partial J_o} = k_o^2 \quad ,$$

$$\dot{\phi}_1 = \frac{\partial h_o}{\partial J_1} = (k_o+k)^2 \quad ,$$

$$\dot{\phi}_n = \frac{\cos(\phi_4 - \phi_3)}{\cos^2\phi_3 + (J_4/J_3)\sin^2\phi_3} \; |k| \to |k| \quad ,$$

where in the last step we have specialized to a diagram of the kind shown in Fig. 1 in which $J_3 = J_4$ and $\phi_3 = \phi_4$.

The decay is resonantly driven when

$$k_o^2 + (-1)(k_o+k)^2 + (-1)|k| = 0 \quad , \qquad (22)$$

and the coefficients of this relation give

$$1 + |-1| + |-1| = 3 < 4$$

whence condition iii) fails.

The other angle dependent term, $\cos(\phi_o - \phi_2 + \phi_n)$, leads to another resonance

$$k_o^2 + (-1)(k_o - k)^2 + (+1)|k| = 0 \qquad (23)$$

which again fails to satisfy condition iii).

As is well-known,[7,8,9] the presence of two or more resonances is the basic ingredient required for chaotic behavior. A graphic confirmation of this is shown in Fig. 9, which is discussed in the sequel. But first we wish to point out some of the pecularities of the Zakharov system.

In general, the resonance conditions for a Hamiltonian system depend on the action variables, with the result that the resonance is satisfied on a certain subspace of the phase space. Given two or more resonance conditions the proximity of the resonant subspaces is a crucial factor in determining the threshold for stochasticity, which will be limited to the region formed by the union of the resonant subspaces. But, the resonance conditions given by Eqs. (22) and (23) are independent of J_o, J_1, and J_2. Thus, in the action space spanned by $(J_o, J_1, J_2, J_3, J_4)$, these two resonances overlap on the hypersurface $J_3 = J_4$ for all J_o, J_1, J_2 (provided these are small enough for the validity of perturbation theory). We therefore reach the important conclusion that the Zakharov equations may be stochastic for <u>arbitrarily small</u> values of J_o, J_1, and J_2 (but not zero). It should perhaps be pointed out that the extent to which, for example, the temporal behavior of the electric field would appear to be irregular or random, is determined by the absolute value of the nonlinearity, and the randomness would grow as the nonlinearity increased.

It must be remarked that the presence of a single resonance and the failure of the Kolmogorov-Arnol'd-Moser theorem means that the tori of the zero-order Hamiltonian are severly distorted, but the system is still integrable. As soon as two or more resonances overlap, the global invariants (or constants of motion) of the system are destroyed, leading to a nonintegrable motion.[7,8] In otherwords, the speculation that the Zakharov equations are nonintegrable, which arose from numerical studies[10] in which Zakharov solitons were observed to fuse on collision, or breakup, has its fundamental basis in the presence of (everywhere) overlapping resonances. It should also be pointed out that the Kolmosoroff-Arnol'd-Moser theorem is basically a theorem of stability; i.e., it guarantees the preservation, under perturbation, of the tori on which the unperturbed flow takes place when certain conditions are satisfied. When these conditions are not satisfied, the destruction of the tori is possible. The numerical results presented are therefore necessary in order to confirm this possibility, as is the usual practise.[7,8]

Now consider the subspace $J_3 = J_4 \equiv J$ on which the Hamiltonian is

$$h_o' = k_o^2 J_o + (k_o+k)^2 J_1 + (k_o-k)^2 J_2 + 2|k|J$$

$$+ 2\varepsilon\left(\frac{|k|J_o J}{L}\right)^{\frac{1}{2}}\left[J_1^{\frac{1}{2}}\cos(\phi_0-\phi_1-\phi_n) + J_2^{\frac{1}{2}}\cos(\phi_0-\phi_2+\phi_n)\right] ,$$

where an ε has been appended to the nonlinear term to indicate smallness, and the following (time-dependent) canonical transformation

$$F(\phi_0, j_0; \phi_1, j_1; \phi_2, j_2; \phi_n, j) = \sum_{\ell=0}^{2} j_\ell(\phi_\ell - \omega_\ell t) + j(\phi_n - \omega_n t) \quad .$$

The new angle variables are, by definition,[23]

$$\alpha_\ell \equiv \frac{\partial F}{\partial j_\ell} = \phi_\ell - \omega_\ell t \qquad \ell = 0, 1, 2$$

$$\alpha_n = \frac{\partial F}{\partial j} = \phi_n - \omega_n t$$

and the new Hamiltonian is

$$h_o^{new} = h_o' + \frac{\partial F}{\partial t} = 2\varepsilon\left(\frac{|k| j_o j}{L}\right)^{\frac{1}{2}} [j_1^{\frac{1}{2}} \cos(\alpha_0 - \alpha_1 - \alpha_n) + j_2^{\frac{1}{2}} \cos(\alpha_0 - \alpha_2 + \alpha_n)] .$$

In consequence of this expedient we find that if h_o' governs a stochastic motion, this stochasticity will persist for $\varepsilon \to o+$, since ε is just a multiplicative factor which only affects the time scale.

Eqs. (5)-(12) for the 4-wave system have been derived with no assumption as regards the value of k_o; thus, the resonance overlap in Eqs. (13) and (20) exists also for interactions involving four waves in the condensate, and therefore the condensate itself can be stochastic.

Without going into details, we report that as the pump amplitude is increased, the 4-wave system becomes (more and more) chaotic; that is, the two-time autocorrelation functions for the variables decay to zero (approximately) in a very short time τ [See Eq. (19)]. Fig. 9 shows the chaotic temporal behavior of the pump mode for the four-wave system, starting from a pump amplitude $e_o = 88.6$, all other parameters being the same as for Fig. 5. A similar behavior is true of the many-mode system. Starting from a state in which $\frac{|E_o|^2}{8\pi N_o T_e} \sim \frac{2}{3}\frac{m}{M}$, after the formation of the Langmuir condensate and its self-modulation, there appears a

very intense Langmuir wave and one much less so, both of which propagate with fluctuating amplitude and velocity. Fig. 10 shows an example in which a wave at x ~ 13 breaks-up into two and two at x ~ 35 and 38 merge into one another; Fig. 10(a) is at $\omega_p t = 140 \frac{M}{m}$, Fig. 10(b) is at $\omega_p t = 144 \frac{M}{m}$. The peak value of $\frac{|E_o|^2}{8\pi N_o T_e}$ equals $70 \frac{m}{M}$ in the course of computation. The two-time autocorrelation functions for the Langmuir modes, Fig. 11, have a form similar to that shown in Fig. 8, with the difference that, for each mode, the decorrelation time is decreased as compared to the previous one in Fig. 8. The decorrelation time is defined to be the time separation $\omega_p \tau$ at which the correlation function falls to a value 1/e. Comparing Figs. 8 and 11 one can descern a somewhat more rapid fall-off in the autocorrelation functions in the latter. If one imagines fitting an envelope of the form $\exp(-\tau/\tau_c)$ to these curves, with τ_c being the decorrelation time, the envelopes would hug the vertical axis in Fig. 11 more tightly than in Fig. 8, because of the more rapid fall-off in the former. Futher, the first "recovery" of the autocorrelation function after its first dip towards zero is smaller in Fig. 11. (The errors involved in Fig. 8 and 11 are about the same.) This indicates (but not prove) that the degree of stochasticity increases with the intensity of the initial Langmuir field. This result and the suggestions that the many-mode system is chaotic should not be surprising in view of our foregoing arguments as regards to the presence of overlapping resonance in the 4-wave system. Thus for the many mode system one might expect a large number of overlapping resonances whose simultaneous "pulling" on a phase-space trajectory leads to complicated and stochastic flow,[7,8,9] specially in view of the indications that the Zakharov equations possess very few constants of motion.

For simplicity, let us now consider the following form of Zakharov's equations

$$(i\partial_t+\Delta)E = NE \quad , \tag{24}$$

$$(\partial_t^2-\Delta)N = \Delta|E|^2 \quad , \tag{25}$$

wherein $\Delta \equiv \partial_x^2 + \partial_y^2 + \partial_z^2$; similar equations have been used to study the stability of solitons [which are special solutions of the one dimensional Zakharov equations, Eqs. (1) and (2)], to perturbations.[24,25,26] Using the Lagrangain density

$$\mathscr{L} = \frac{i}{2}[E^*\partial_t E - E(\partial_t E^*)] - \nabla E^*\cdot\nabla E + \frac{1}{2}(\partial_t U - |E|^2)^2 - \frac{1}{2}(\nabla U)^2 \quad ,$$

the Fourier expansions

$$E = \frac{1}{L^3}\sum_{\underset{\sim}{k}} E_{\underset{\sim}{k}}\exp(-i\underset{\sim}{k}\cdot\underset{\sim}{r}) \quad ,$$

$$N = \frac{1}{L^3}\sum_{\underset{\sim}{k}} N_{\underset{\sim}{k}}\exp(-i\underset{\sim}{k}\cdot\underset{\sim}{r}) \quad ,$$

($N=\partial_t U-|E|^2$ being the momentum conjugate to U) and following the procedure outlined in the Appendix, the Hamiltonian for Eqs. (24) and (25) in action-angle variables is

$$H = \sum_{\underset{\sim}{k}}[k^2 J_{\underset{\sim}{k}} + |\underset{\sim}{k}|(I_{\underset{\sim}{k}}+K_{\underset{\sim}{k}})] + \frac{1}{(2L^3)^{\frac{1}{2}}}\sum_{\underset{\sim}{k},\underset{\sim}{k}'}(|\underset{\sim}{k}|J_{\underset{\sim}{k}'}J_{\underset{\sim}{k}+\underset{\sim}{k}'})^{\frac{1}{2}}$$

$$\times\ (I_{\underset{\sim}{k}}\cos^2\xi_{\underset{\sim}{k}} + K_{\underset{\sim}{k}}\sin^2\zeta_{\underset{\sim}{k}})^{\frac{1}{2}}\exp[-i(\phi_{\underset{\sim}{k}'}-\phi_{\underset{\sim}{k}+\underset{\sim}{k}'}-\alpha_{\underset{\sim}{k}})] \tag{26}$$

wherein

$$E_{\underset{\sim}{k}} = (L^3 J_{\underset{\sim}{k}})^{\frac{1}{2}} \exp(-i\phi_{\underset{\sim}{k}}) \quad ,$$

$$U_{\underset{\sim}{k}} = \left(\frac{2L^3 I_{\underset{\sim}{k}}}{|\underset{\sim}{k}|}\right)^{\frac{1}{2}} \sin\zeta_{\underset{\sim}{k}} + i\left(\frac{2L^3 K_{\underset{\sim}{k}}}{|\underset{\sim}{k}|}\right)^{\frac{1}{2}} \cos\zeta_{\underset{\sim}{k}} \quad ,$$

$$N_{\underset{\sim}{k}} = (2L^3 |\underset{\sim}{k}| I_{\underset{\sim}{k}})^{\frac{1}{2}} \cos\xi_{\underset{\sim}{k}} + i(2L^3 |\underset{\sim}{k}| K_{\underset{\sim}{k}})^{\frac{1}{2}} \sin\zeta_{\underset{\sim}{k}} \quad ,$$

$$\alpha_{\underset{\sim}{k}} = \arctan\left[\left(\frac{K_{\underset{\sim}{k}}}{I_{\underset{\sim}{k}}}\right)^{\frac{1}{2}} \frac{\sin\zeta_{\underset{\sim}{k}}}{\cos\xi_{\underset{\sim}{k}}}\right] \quad ,$$

and L^3 is the volume.

The linear dependence of the zero-order part of Eq. (26) implies the violation of the nondegeneracy conditions. Consideration of decay processes of the type $\dot{\phi}_{\underset{\sim}{k}} - \dot{\phi}_{\underset{\sim}{k}+\underset{\sim}{k}'} - \dot{\alpha}_{\underset{\sim}{k}} = 0$, (cf. Fig. 1) for example, will bring in overlapping resonances and the consequent stochastic flows.

It must be mentioned that in all the computations presented here the maximum wave number (or the number of modes used) have been chosen in such a way that a negligible fraction of the energy lies in the large wave number region. Indeed, this is a necessary condition for the accuracy of the code [as measured by the (semi-) conservation of the Hamiltonian and of the momentum.]

In closing we note that several computations have been performed with different periodicity lengths L, using the same (initial) boson number per unit length and the same modes with no change in the results obtained. Further, we have also performed computations in which modes -32 through +32 (c.f. Fig. 2) were initially at the same level (=0.021), the pump mode at E_{k_o} = 45.2 and modes 33 through 64 and -33 through -64 at $\sim 10^{-15}$ (c.f. Section III). In this case the late-time behavior was stochastic and similar to the previous cases, except that the transition to the time-asymptotic (in the context of our computations) state was faster. This is because there were fewer

large-amplitude oscillations initially (c.f. Fig. 4, for $\omega_p t \lesssim 150$). The reason is, of course, that with so many modes in the condensate region at relatively large amplitudes and the fact that for a given pump mode there is band of modes that are parametrically unstable, the condensate forms much faster.

V. Conclusions

The results of computations on wave-wave interactions in a plasma described by the Zakharov equations have been reported. A number of diagnostics, such as the two-time autocorrelation function, used in those experiments indicate that the interaction of plasma waves in the absence of forcing and of dissipation leads to partially stochastic flow, wherein there remains, in the parameter range reported here, remanents of organized behavior, such as intense, large amplitude Langmuir waves.

It is argued that the fundamental theoretical basis for such behavior lies in the fact that the Hamiltonian Zakharov equations are degenerate (in the sense of the rigorous perturbation theory of Kolmogorov, Arnol'd and Moser) with everywhere overlapping resonances. Herein lies the reason for the non-integrability of the Zakharov equations, a conclusion which is independent of the dimensionality of the system. For the parameter range of interest to this work the effects of Landau damping are negligibly small. If the width of the wave-number spectrum is sufficiently large so that the influence of dissipation need be included it is possible that with appropriate amounts of forcing the wandering phase point corresponding to a solution of Zakharov's equations falls into the basin of an attractor introduced by the dissipation. In this case it is possible that the chaotic motion would take place on a strange attractor.

Acknowledgements

I wish to thank A.O. Barut, D.F. DuBois, M.V. Goldman, H.A. Rose, and D.A. Russell for helpful discussions.

This work was supported by the National Science Foundation under Grant ATM 7916837, and the Air Force Office of Scientific Research under Contract F49620-76-C-0005, the National Aeronautics and Space Administration under Contract NAGW-91, and the National Center for Atmospheric Research Computing Facility in Boulder, Colorado.

AD-A117 862 COLORADO UNIV AT BOULDER F/G 20/9
PLASMA WAVE TURBULENCE AND PARTICLE HEATING CAUSED BY ELECTRON --ETC(U)
MAY 82 M V GOLDMAN AFOSR-80-0022
UNCLASSIFIED CU-1533143 AFOSR-TR-82-0592 NL

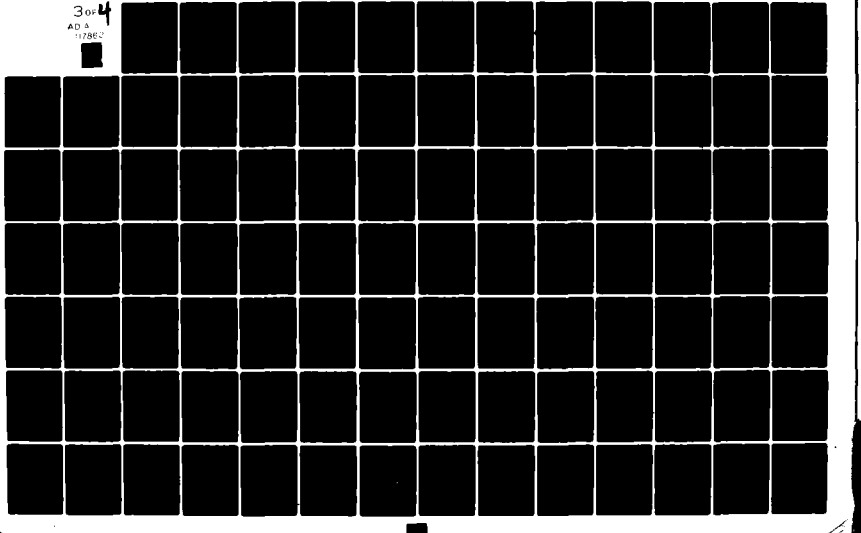

Appendix

The purpose of this Appendix is to cast the four-wave Hamiltonian, Eq. (13), in the form required for stability analysis via the Kolmogoroff-Arnol'd-Moser theorem. To do this we must determine the action-angle variables for the Langmuir and for the sound waves.

It can easily be verified that[10,16]

$$\mathscr{L} = \frac{i}{2}[E^*\partial_t E - (\partial_t E^*)E] - (\partial_x E^*)(\partial_x E) + \frac{1}{2}(\partial_t U - |E|^2)^2 - \frac{1}{2}(\partial_x U)^2 \quad \text{(A1)}$$

is a Lagrangian density for Zakharov's equations, Eqs. (1) and (2), where U is related to the density perturbation N (which is the momentum conjugate to U)

$$N = \partial_t U - |E|^2 . \quad \text{(A2)}$$

We need to consider a single mode only,

$$E = \frac{1}{L} E_k \exp(-ikx) \quad ,$$

$$U = \frac{1}{L}[U_k \exp(-ikx) + U_k^* \exp(ikx)] \quad ,$$

and the bare Lagrangian densities for the Langmuir wave, L_L, and for the sound waves, L_S,

$$L_L = \int dx \mathscr{L}_L = \frac{i}{2L}(E_k^* \dot{E}_k - \dot{E}_k^* E_k) - \frac{k^2}{L}|E_k|^2 \quad , \quad \text{(A3)}$$

$$L_S = \int dx \mathscr{L}_S = \frac{1}{L}(|N_k|^2 - k^2|U_k|^2) \quad , \quad \text{(A4)}$$

in obvious notation. The respective Hamiltonians are, following the usual procedure,

$$H_L = \frac{k^2}{L}|E_k|^2 \quad \text{(A5)}$$

$$H_S = \frac{1}{L}(|N_k|^2 + k^2|U_k|^2) \quad \text{(A6)}$$

We first determine the action-angle variables for the Langmuir waves. This is particularly simple since

$$E_k = (LJ)^{\frac{1}{2}} \exp(-i\phi) \tag{A7}$$

with J being the action variable and ϕ the angle variable is the required transformation. To see this note that the Langmuir Hamiltonian (A5) in terms of J and ϕ is

$$H_L = k^2 J$$

which is independent of ϕ, justifying the designation of (J,ϕ) as the action-angle variable. We now need to show that the transformation (A7) is canonical[27], i.e.,

$$dJ \wedge d\phi = dp_k \wedge dE_k + c.c. \tag{A8}$$

where $\wedge$ is the symbol of wedge product and $p_k = \frac{iE_k^*}{2L}$ is the momentum conjugate to the coordinate E_k, as follows from Eq. (A3). The right-hand-side of this expression is

$$\begin{aligned} dp_k \wedge dE_k + dp_k^* \wedge dE_k^* &= \frac{i}{2L} dE_k^* \wedge dE_k - \frac{i}{2L} dE_k \wedge dE_k^* \\ &= id[J^{\frac{1}{2}} \exp(i\phi)] \wedge d[J^{\frac{1}{2}} \exp(-i\phi)] \\ &= i\left[\frac{\exp(i\phi)}{2J^{\frac{1}{2}}} dJ + iJ^{\frac{1}{2}} \exp(i\phi)\, d\phi\right] \\ &\quad \wedge \left[\frac{\exp(-i\phi)}{2J^{\frac{1}{2}}} dJ - iJ^{\frac{1}{2}} \exp(-i\phi)\, d\phi\right] \\ &= \frac{i}{2}[-idJ \wedge d\phi - idJ \wedge d\phi] \end{aligned}$$

$$= dJ \wedge d\phi ,$$

which equals the left-hand-side of Eq. (A8), showing that Eq. (A7) represents a canonical transformation. (In manupulating the above wedge product we have used the usual rules[27], such as $dx \wedge dx = 0$, $dx \wedge dy = -dy \wedge dx$, for any x and y.)

Next we examine the sound waves and write the Hamiltonian (A6) as

$$H_S = \frac{1}{L}[Q_3^2+k^2P_3^2) + (Q_4^2+k^2P_4^2)] \qquad (A9)$$

where $U_k = P_3+iP_4$; and $N_k=Q_3+iQ_4$. The Hamiltonian is now similar to that of two simple harmonic oscillators, whose action-angle variables are well-known[28]

$$P_3 = (\frac{LJ_3}{|k|})^{\frac{1}{2}}\sin\phi_3, \quad Q_3 = (LJ_3|k|)^{\frac{1}{2}}\cos\phi_3 \qquad (A10)$$

$$P_4 = (\frac{LJ_4}{|k|})^{\frac{1}{2}}\cos\phi_4, \quad Q_4 = (LJ_4|k|)^{\frac{1}{2}}\sin\phi_4 \qquad (A11)$$

Now,

$$N_k = Q_3 + iQ_4 = (L|k|)^{\frac{1}{2}}(J_3^{\frac{1}{2}}\cos\phi_3+iJ_4^{\frac{1}{2}}\sin\phi_4)$$

$$= n(\cos\phi_n+i\sin\phi_n) ,$$

wherein the expression for N_k given following Eq. (12) has been used in the last step. It follows that

$$\phi_n = \arctan\left[\left(\frac{J_4}{J_3}\right)^{\frac{1}{2}} \frac{\sin\phi_4}{\cos\phi_3}\right] \tag{A12}$$

$$n = (L|k|)^{\frac{1}{2}}(J_3\cos^2\phi_3 + J_4\sin^2\phi_4)^{\frac{1}{2}} \tag{A13}$$

Using Eqs. (A7), (A9), (A10), (A11), and (A13) we have the four-wave Hamiltonian, Eq. (13), in action-angle variables:

$$\begin{aligned} h = {} & [k_o^2 J_o + (k_o+k)^2 J_1 + (k_o-k)^2 J_2] + |k|(J_3+J_4) \\ & + 2\left(\frac{|k|J_o}{L}\right)^{\frac{1}{2}}(J_3\cos^2\phi_3 + J_4\sin^2\phi_4)^{\frac{1}{2}}[J_1^{\frac{1}{2}}\cos(\phi_o-\phi_1-\phi_n) \\ & + J_2^{\frac{1}{2}}\cos(\phi_o-\phi_2+\phi_n)] \end{aligned} \tag{A14}$$

in obvious notation.

References

1. V.E. Zakharov, Zh. Eksp. Teor. Fiz. 62, 1745 (1972) [Sov. Phys. - JETP 35, 908 (1972)].
2. N.R. Pereira, R.N. Sudan, and J. Denavit, Phys. Fluids 20, 271 (1977).
3. M.V. Goldman and D.R. Nicholson, Phys. Rev. Lett. 41, 406 (1978).
4. L.M. Degtyarev, R.Z. Sagdeev, G.I. Solol'ev, V.D. Shapiro, and V.I. Shevchenko, Fiz. Plasmy. 6, 485 (1980) [Sov. J. Plasma Phys. 6, 263 (1980)].
5. D.F. DuBois and H.A. Rose, Phys. Rev. A24, 1476 (1981).
6. G. Pelletier, J. Plasma Phys. 24, 421 (1980).
7. G.H. Walker and J. Ford, Phys. Rev. 188, 416 (1969).
8. J. Ford, in Lectures in Statistical Physics, edited by W.C. Schieve and J.S. Turner, in Lecture Notes in Physics 28 (Springer-Verlag, New York, 1974), p. 204.
9. Nonlinear Dynamics, edited by R.H.G. Helleman Ann. N.Y. Acad. Sci. 357 (New York Academy of Sciences, 1980).
10. L.M. Degtyarev, V.G. Nakhan'kov, and L.I. Rudakov, Zh. Eksp. Teor. Fiz. 67, 533 (1974) [Sov. Phys. - JETP 40, 264 (1975)].
11. N.J. Zabusky and M.D. Kruskal, Phys. Rev. Lett. 15, 240 (1965).

12. V.E. Zakharov and A.B. Šabat, Zh. Eksp. Teor. Fiz. 61, 118 (1971) [Sov. Phys. - JETP 34, 62 (1972)].

13. B.M. Lake, H.C. Yuen, H. Rungaldier, and W.E. Ferguson, J. Fluid Mech. 83, 49 (1977).

14. LI. Rudakov and V.N. Tsytovich, Phys. Reports C40, 1 (1978).

15. A.A. Vedenov and L.I. Rudakov, Dok. Akad. Nauk. SSSR 159, 767 (1965) [Sov. Phys. Doklady 9, 1073 (1965)].

16. A.G. Litvak and G.M. Fraiman, Zh. Eksp. Theor. Fiz. 68, 1288 (1975) [Sov. Phys. - JETP 41, 640 (1976)].

17. L.V. Kantorovich and V.I. Krylov, Approximate Methods of Higher Analysis (Interscience Publishers, New York, 1958) p. 261.

18. S.A. Orszag, Phys. Fluids Suppl. 12, II-250 (1969).

19. S. Bardwell and M.V. Goldman, Astrophys. J. 209, 912 (1976).

20. V.N. Oraevskii and R.Z. Sagdeev, Zh. Tekh. Fiz. 32, 1291 (1962) [Sov. Phys. - Tech. Phys. 7, 955 (1963)].

21. B. Hafizi, J.C. Weatherall, M.V. Goldman, and D.R. Nicholson, Phys. Fluids 25, 902 (1982).

22. D. Reulle and F. Takens, Commun. Math. Phys. 20, 167 (1971).

23. V.I. Arnol'd, Usp. Mat. Nauk 18, 91 (1963) [Russian Math. Surveys 18, 85 (1963)].

24. V.E. Zakharov and A.M. Rubenchik, Zh. Eksp. Teor. Fiz. 65, 997 (1973) [Sov. Phys. - JETP 38, 494 (1974)].

25. L.M. Degtyarev, V.E. Zakharov, and L.I. Rudakov, Zh. Eksp. Teor. Fiz. 68, 115 (1975) [Sov. Phys. - JETP 41, 57 (1975)].

26. N.R. Pereira, R.N. Sudan, and J. Denavit, Phys. Fluids 20, 936 (1977).

27. V.I. Arnol'd and A. Avez, Ergodic Problems of Classical Mechanics, (Benjamin, New York, 1968), p. 235.

28. L.D. Landau and E.M. Lifshitz, Mechanics (Addison-Wesley, 1960), p. 156.

Figure Captions

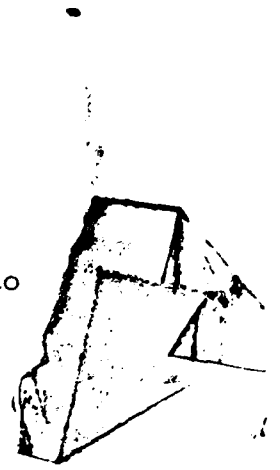

Fig. 1. Scattering of two Langmuir waves (k_o) into a Stokes (k_o+k) and an anti-Stokes (k_o-k) mode, mediated by a (virtual) sound wave (k).

Fig. 2. Spectrum of Langmuir waves versus mode number at $\omega_p\tilde{t} = 192\,\frac{M}{m}$. (If $k = \frac{2\pi}{L}\,n$ is a wavenumber, the integer n is the mode number.) p: pump mode; s: Stokes mode; as: anti-Stokes mode; ss: sub-satellite to Stokes mode; pss: sub-satellite to pump mode; sss: sub-sub-satellite to Stokes mode; ssss: sub-sub-sub-satellite to Stokes mode.

Fig. 3. (a) Spectrum of Langmuir waves at $\omega_p\tilde{t} = 624\,\frac{M}{m}$.
(b) Corresponding electric field distribution in x space, showing an intense packet of Langmuir oscillations (dashed line) trapped in a local rarefaction in ion density (full line).

Fig. 4. Plot of $R(\tilde{t}) \equiv \sum_{k\neq k_o} |E_k(\tilde{t})|^2/|E_{k_o}(t=0)|^2$ as a function of time. (Values on the abscissa must be multiplied by the mass ratio $\frac{M}{m}$ to obtain actual $\omega_p\tilde{t}$.) k_o labels the wavenumber of the pump-mode.

Fig. 5. Amplitude of pump-mode versus time for the four-wave system. (Values on the abscissa must be muliplied by the mass ratio $\frac{M}{m}$ to obtain actual $\omega_p t$.)

Fig. 6. Displacement versus time for the solitary wave shown in Fig. 3(b) (Values on the abscissa must be multiplied by the mass ratio $\frac{M}{m}$ to obtain actual $\omega_p t$.) $\frac{V_s}{C_s}$ denotes speed of the solitary wave in units of sound speed C_s.

Fig. 7. Momentum in the sound waves as a function of "time". (The values on the abscissa must be multiplied by the mass ratio $\frac{M}{m}$ to obtain actual $\omega_p t$.)

Fig. 8. Real part of two-time auto-correlation function $C(\tilde{\tau})$ versus time separation $\omega_p \tilde{\tau}$ (values on the abscissa must be multiplied by the mass ratio $\frac{M}{m}$ to obtain actual $\omega_p t$.) (a) Eigth mode; (b) eleventh mode. At $\tilde{t} = 0$, $\frac{\tilde{E}_o^2}{3\pi N_o m_o} \simeq \frac{1}{3}\frac{m}{M}$.

Fig. 9. Amplitude of pump-mode versus time for the four-wave system, in the chaotic regime. (Values on the abscissa must be multiplied by the mass ratio $\frac{M}{m}$ to obtain actual $\omega_p t$.)

Fig. 10. Electric field (dashed line) and density perturbation (full line) in x space, showing solitary wave break-up.
(a) $\omega_p t = 140 \frac{M}{m}$; (b) $\omega_p t = 144 \frac{M}{m}$.

Fig. 11. Real part of two-time auto-correlation function $C(\tilde{\tau})$ versus time separation $\omega_p \tilde{\tau}$ (values on the abscissa must be multiplied by the mass ratio $\frac{M}{m}$ to obtain actual $\omega_p \tilde{\tau}$.)
(a) Eighth mode; (b) eleventh mode.
At $\tilde{t} = 0$, $\frac{\tilde{E}_o^2}{8\pi N_o T_e} \simeq \frac{2}{3} \frac{m}{M}$.

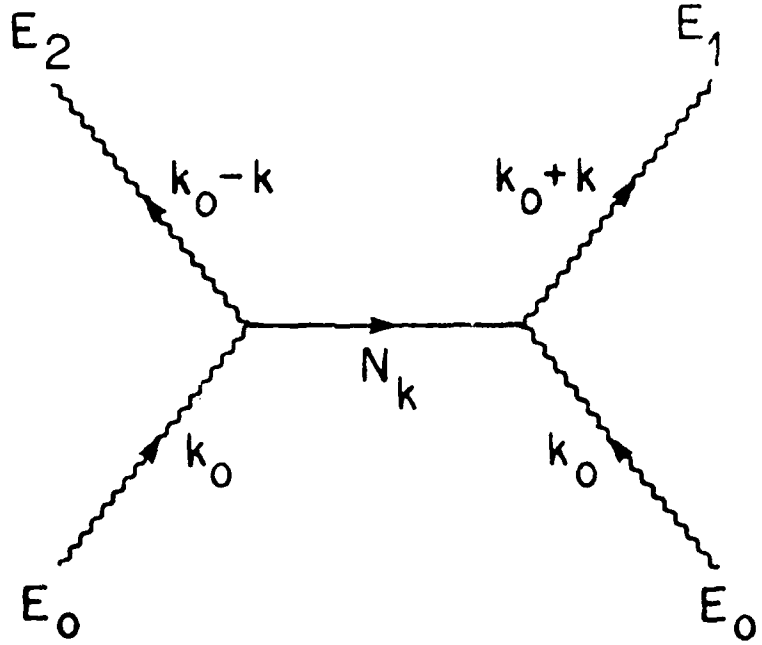

FIG. 1

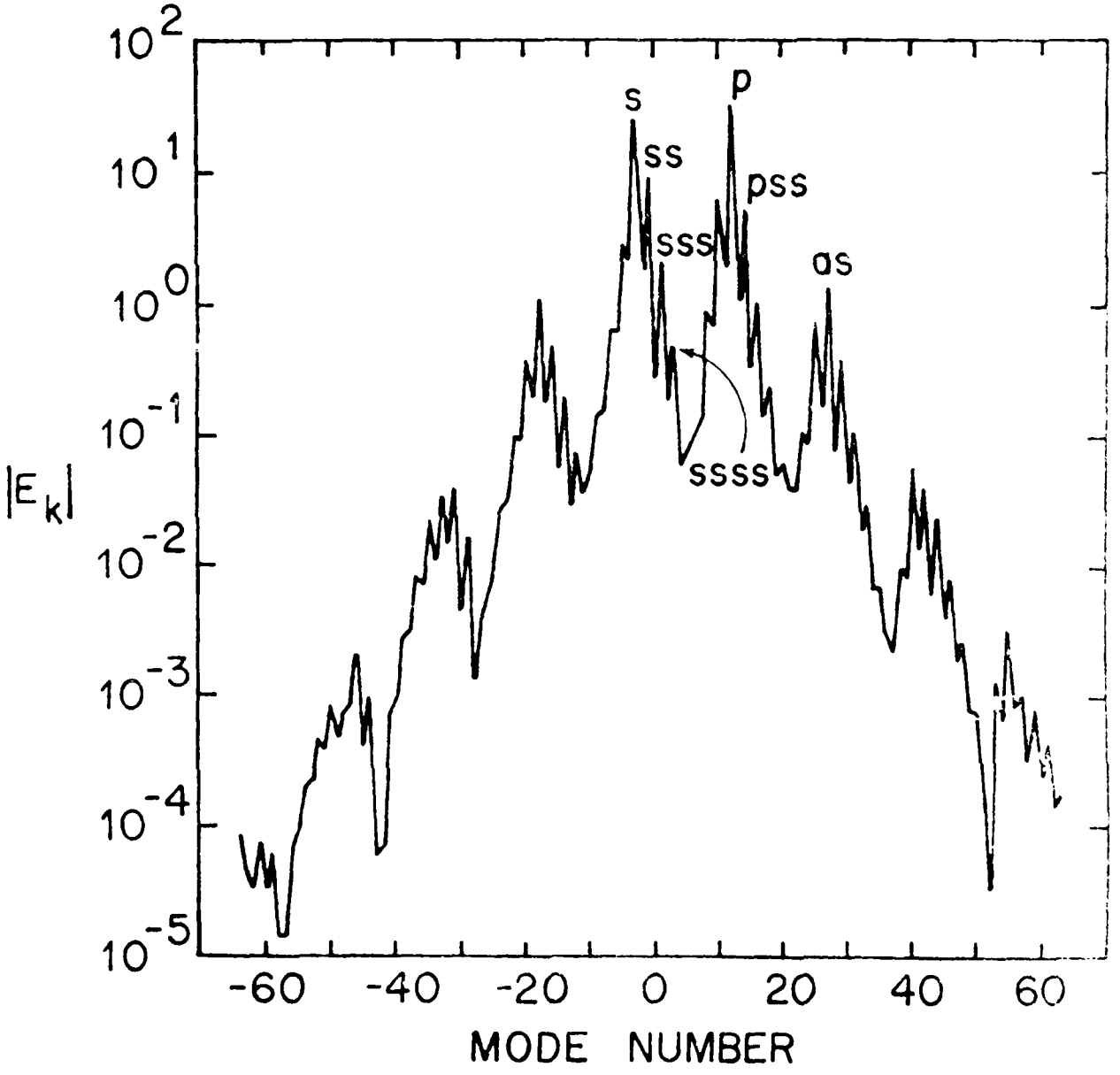
10^2
10^1
10^0
10^{-1}
10^{-2}
10^{-3}
10^{-4}
10^{-5}
$|E_k|$
s
ss
sss
ssss
p
pss
as
-60
-40
-20
0
20
40
60
MODE NUMBER

FIG. 2

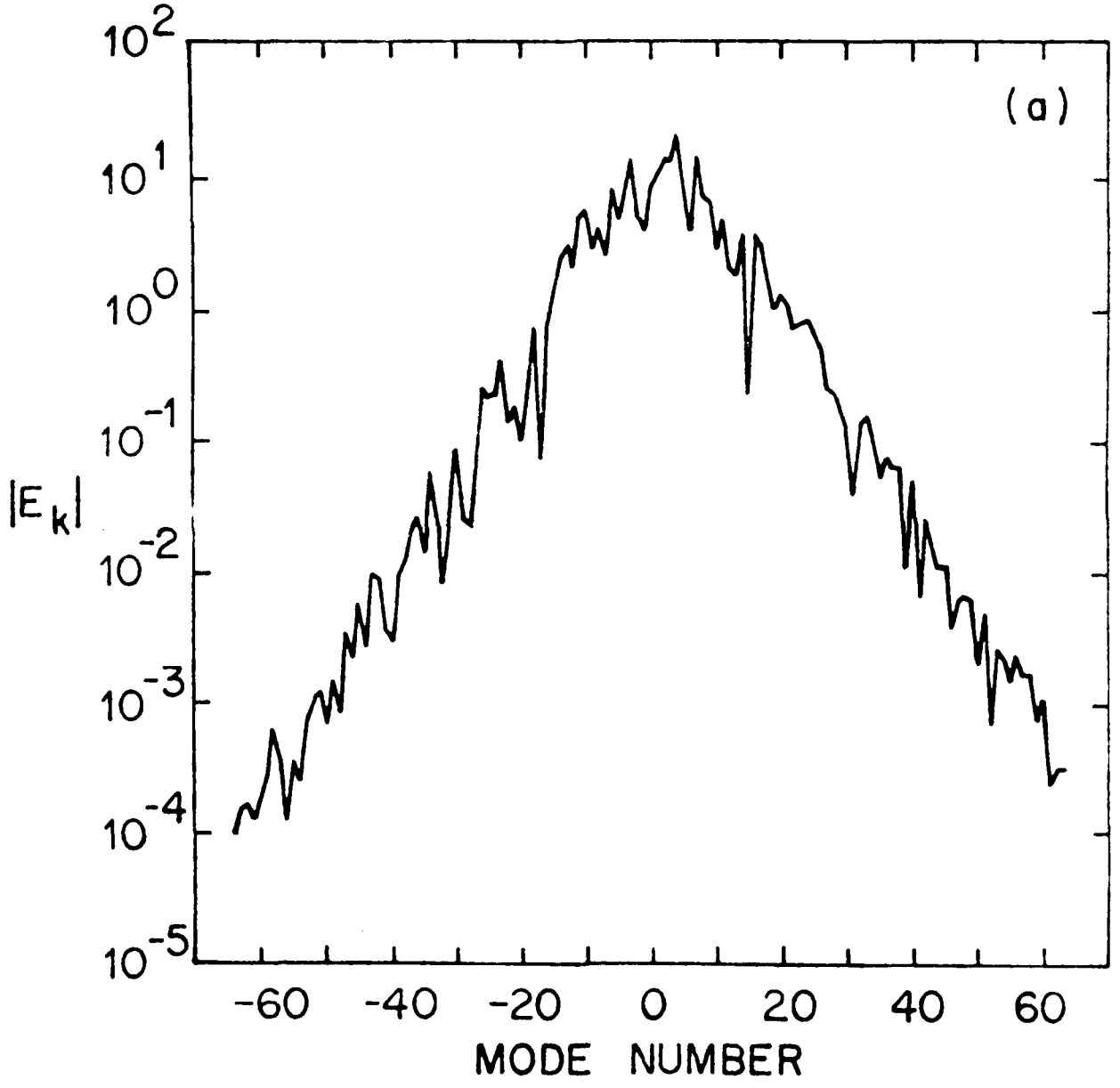
(a)
10^2
10^1
10^0
10^{-1}
10^{-2}
10^{-3}
10^{-4}
10^{-5}
$|E_k|$
-60
-40
-20
0
20
40
60
MODE NUMBER

FIG. 3(a)

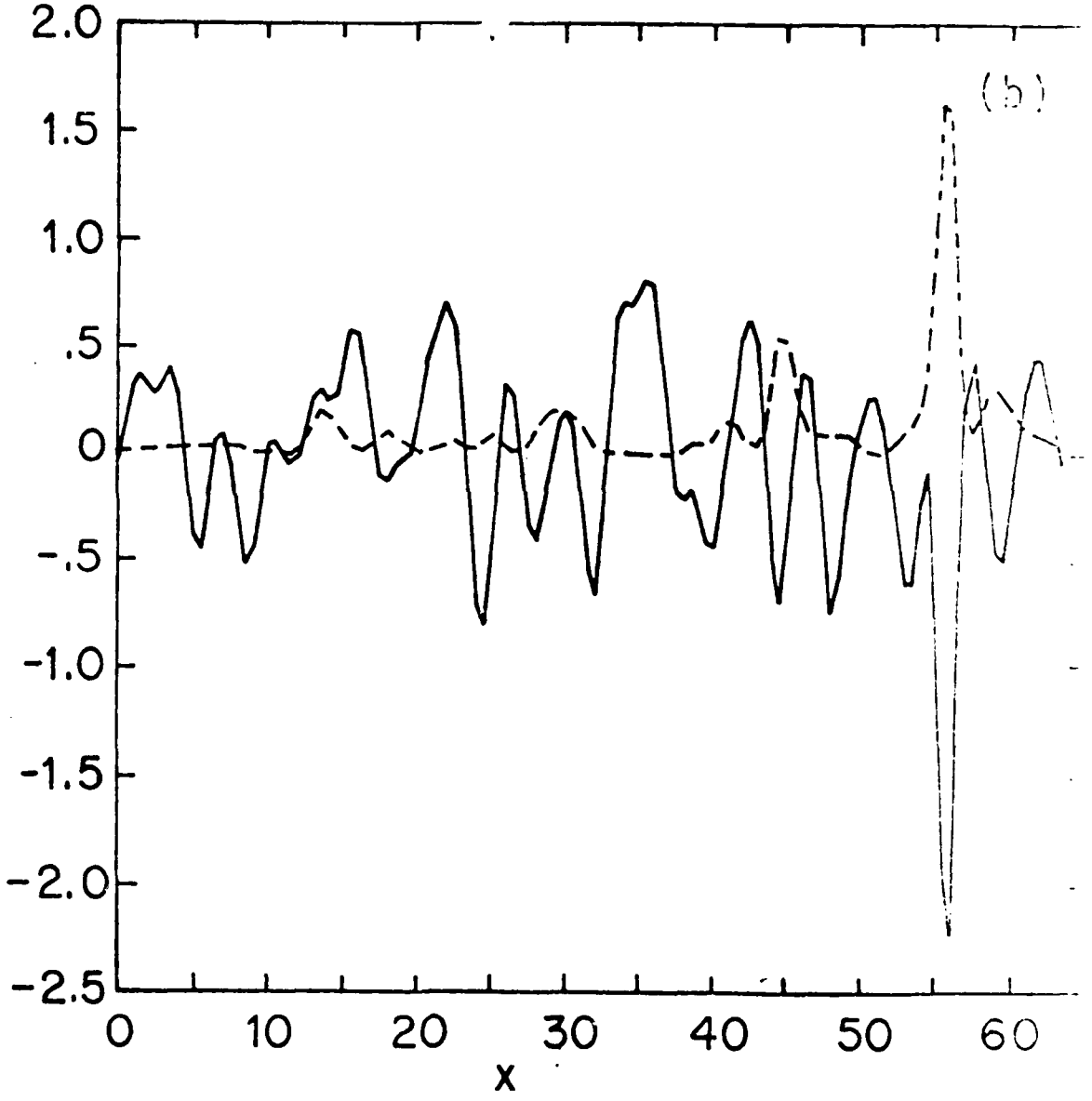

Fig. 3(b)

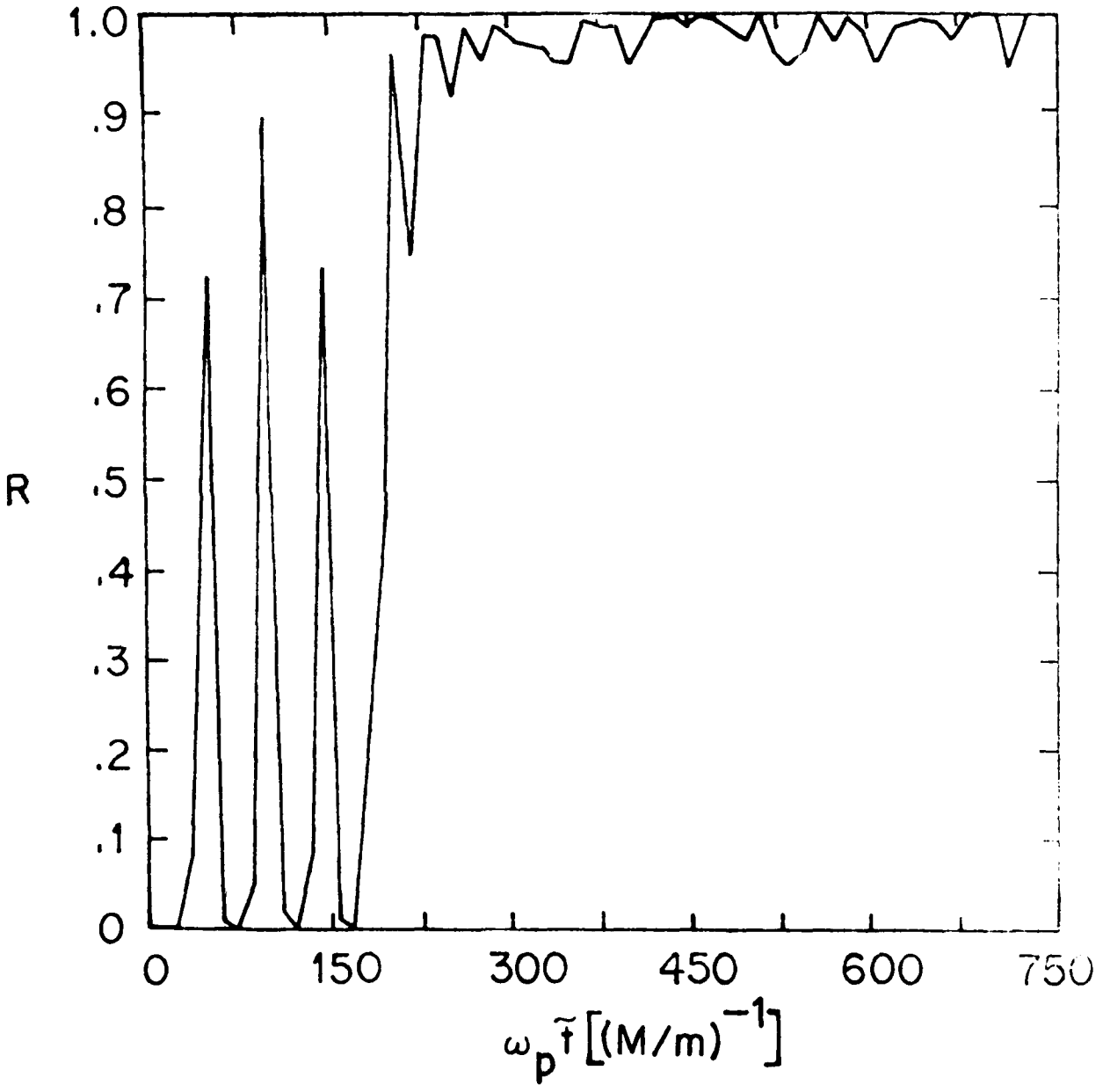

FIG. 4

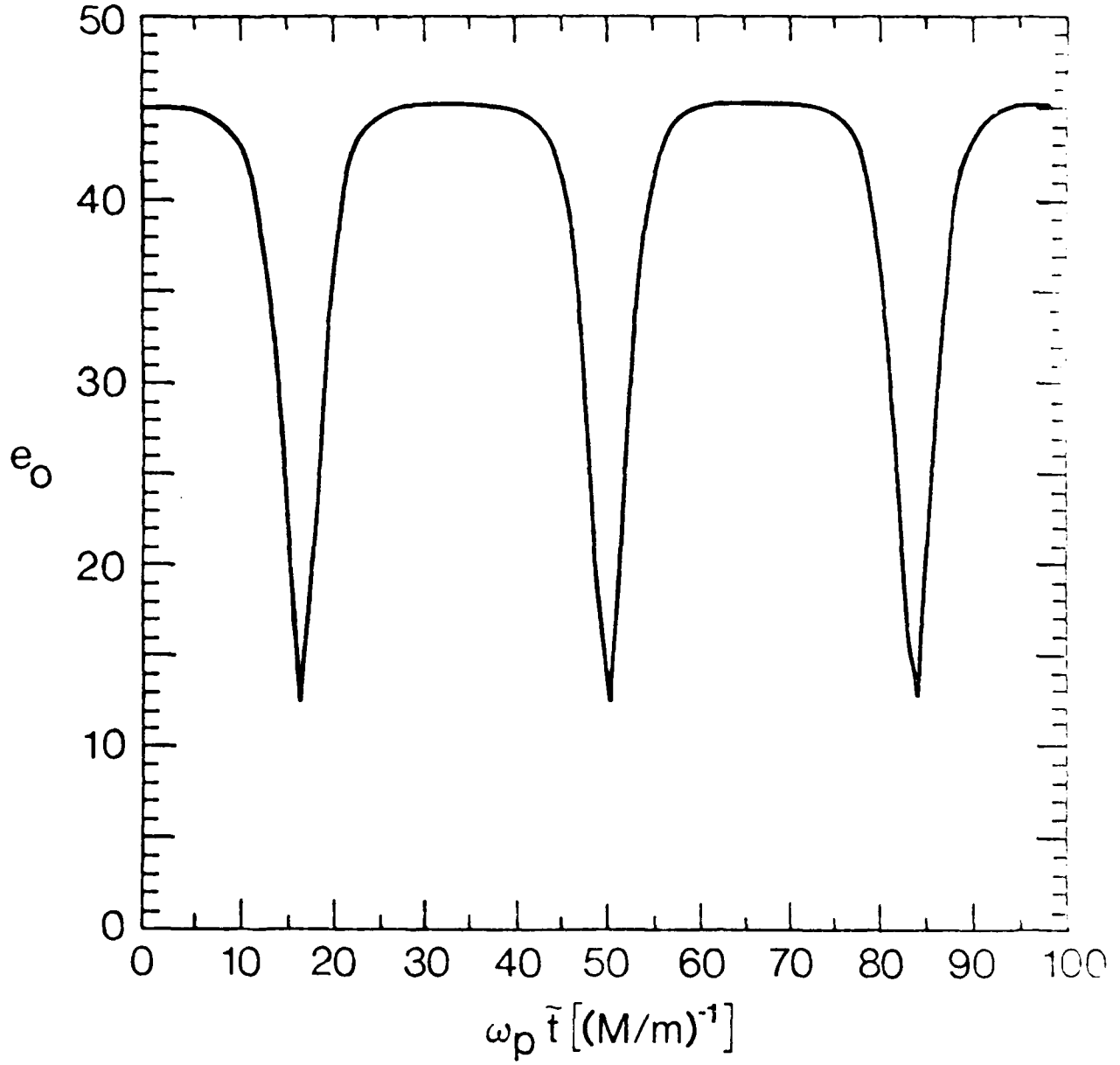
50
40
30
20
10
0
e_o
0
10
20
30
40
50
60
70
80
90
100
$\omega_p \tilde{t}\,[(M/m)^{-1}]$

Fig. 5

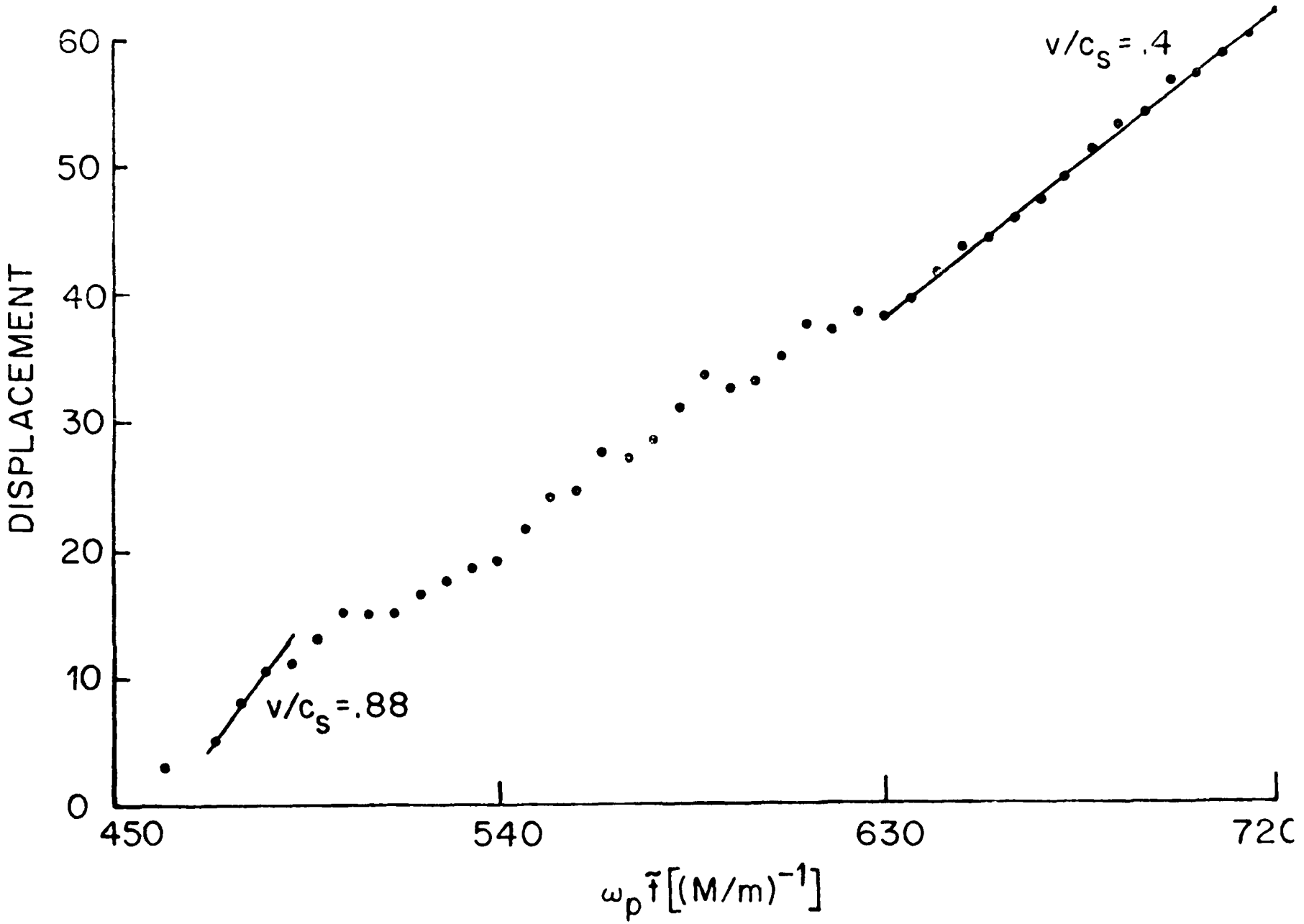
60
50
40
30
20
10
0
DISPLACEMENT
v/c_s = .4
v/c_s = .88
450
540
630
720
ω_p t̃ [(M/m)^-1]

FIG. 6

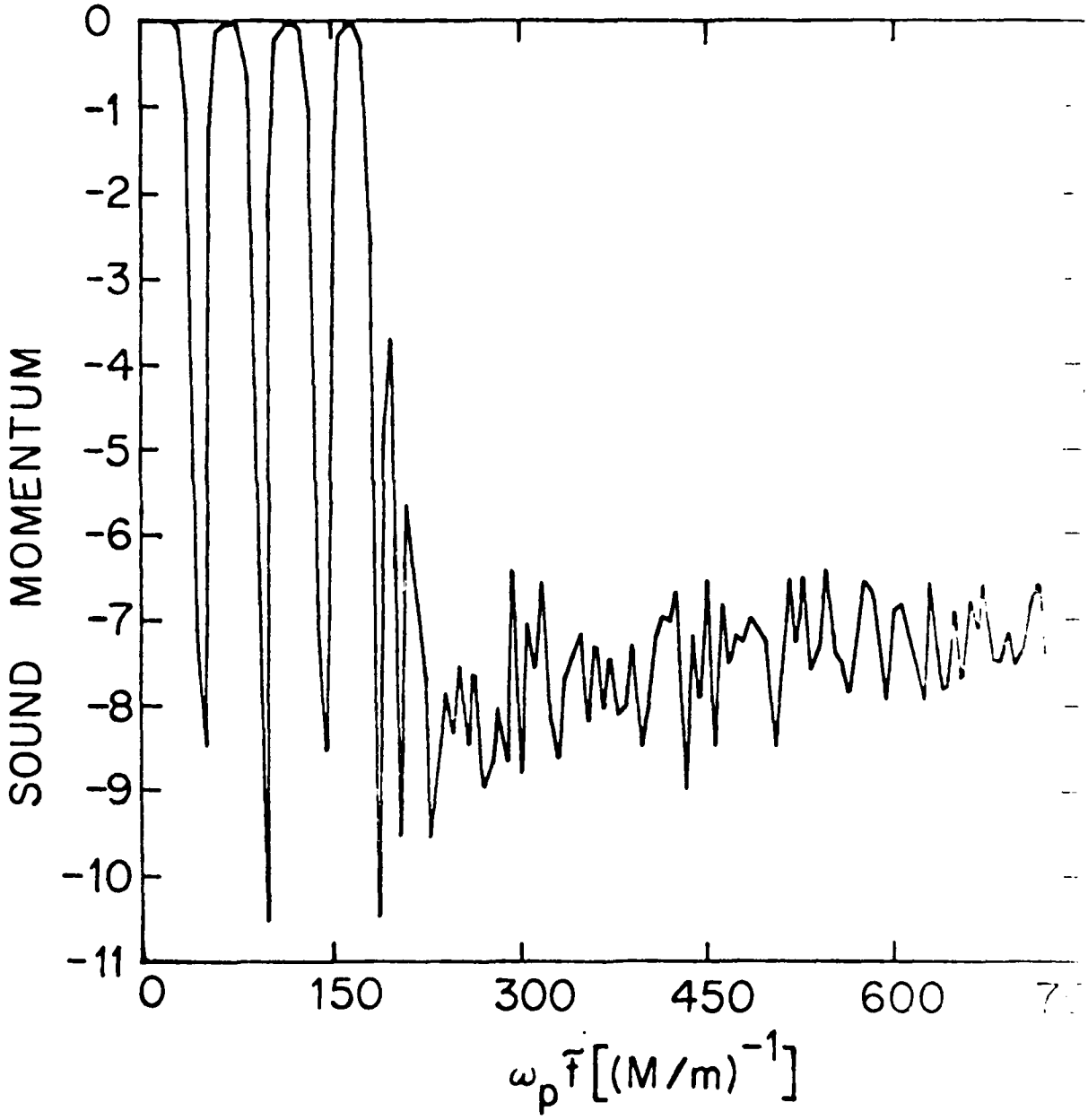
SOUND MOMENTUM
0
-1
-2
-3
-4
-5
-6
-7
-8
-9
-10
-11
0
150
300
450
600
$\omega_p \tilde{t}\,[(M/m)^{-1}]$

Fig. 7

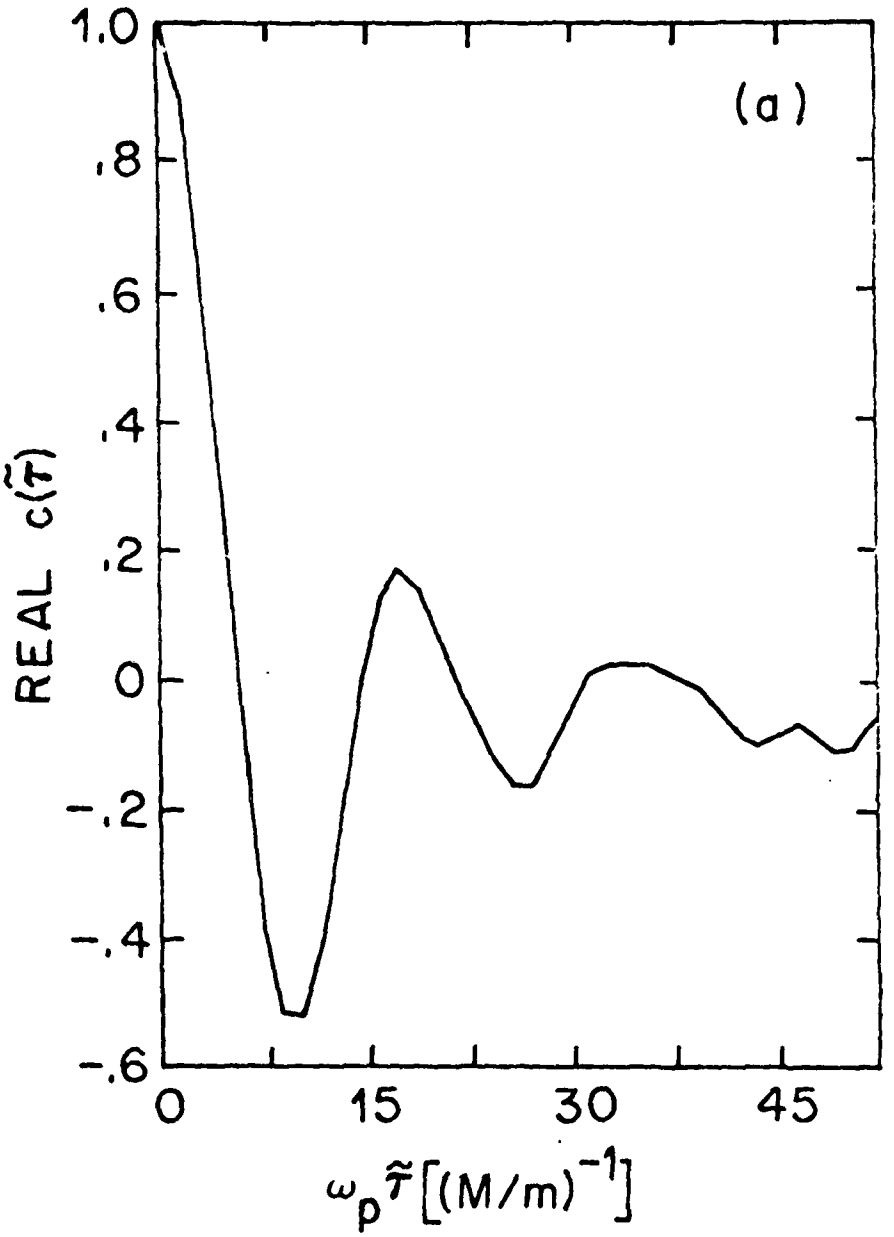

Fig. 8(a)

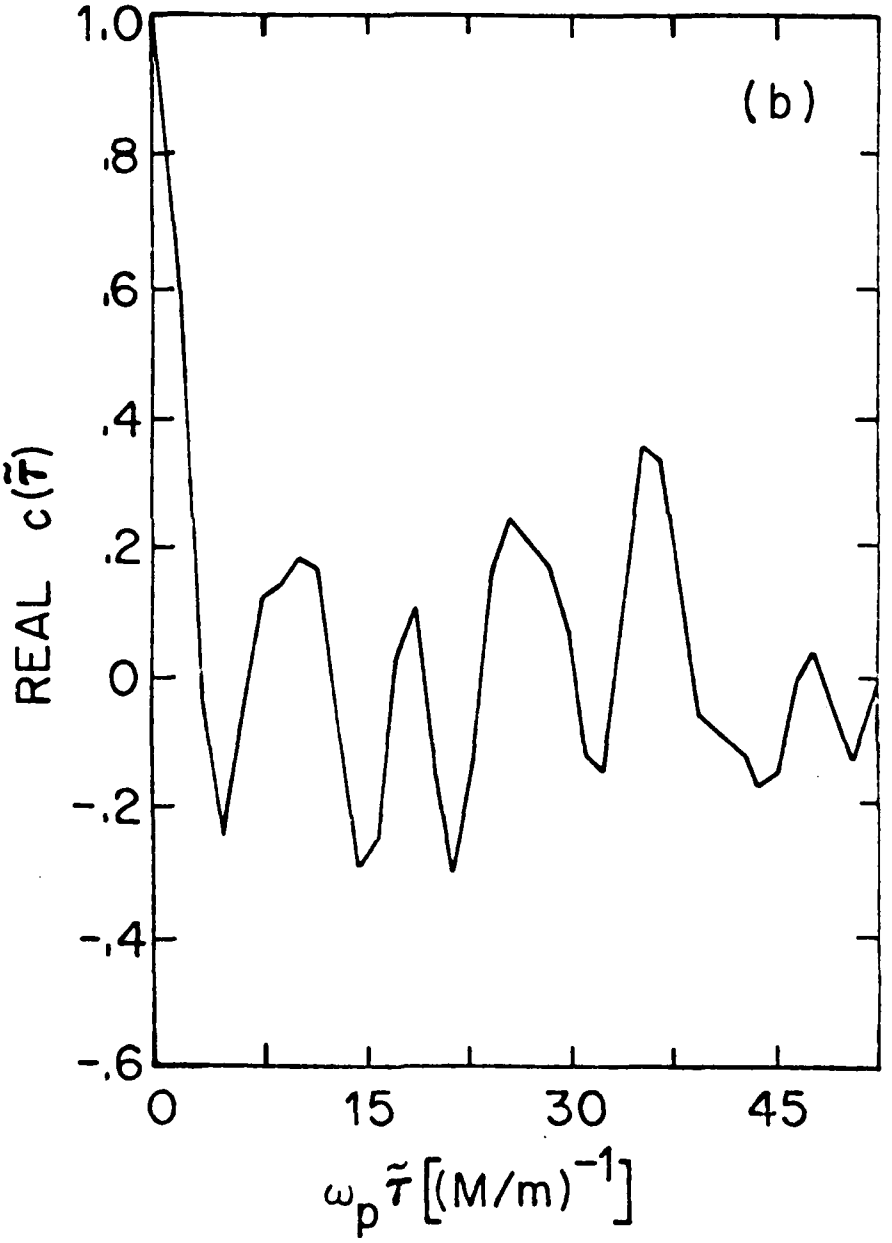

Fig. 8(b)

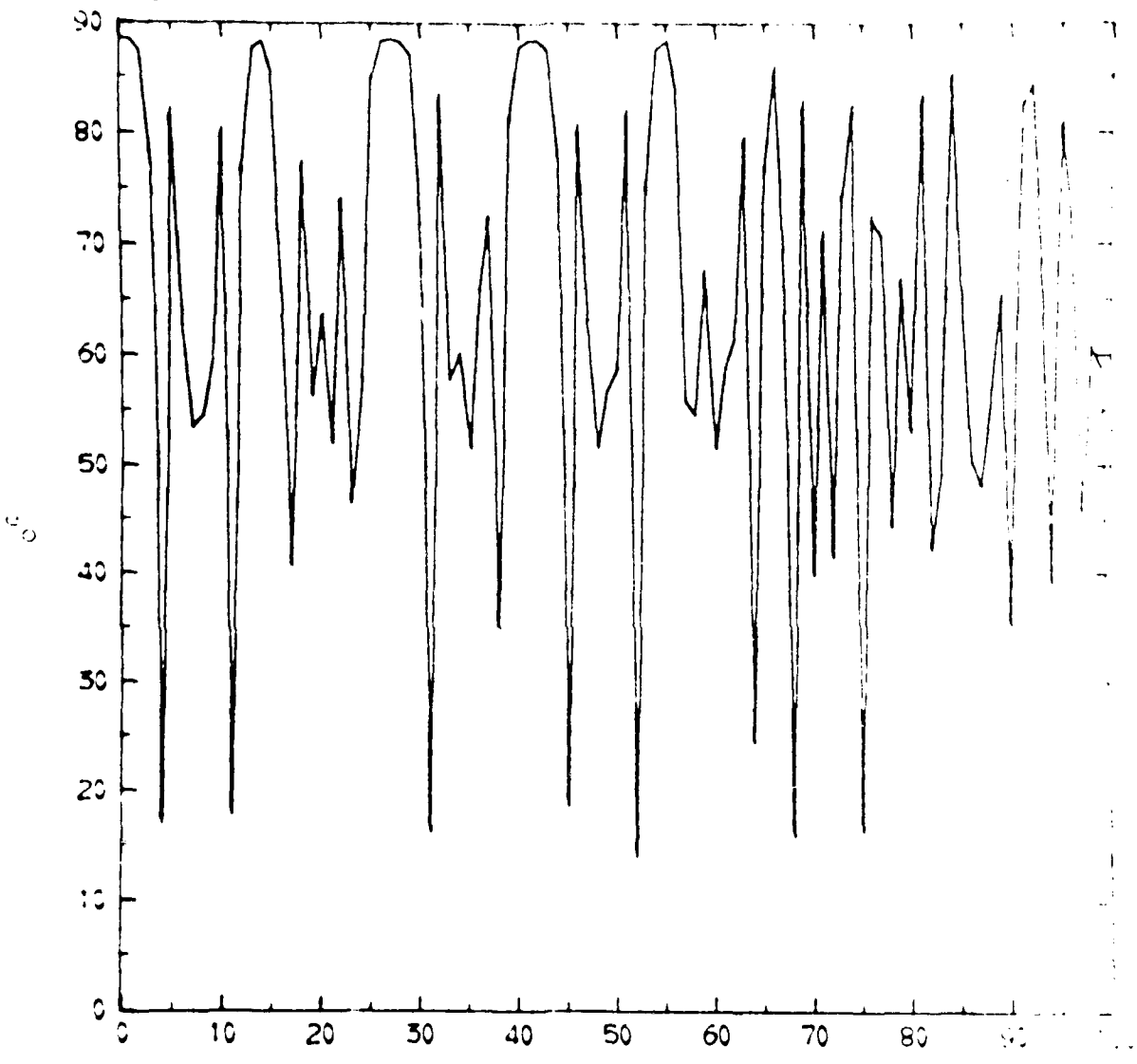

Fig. 9

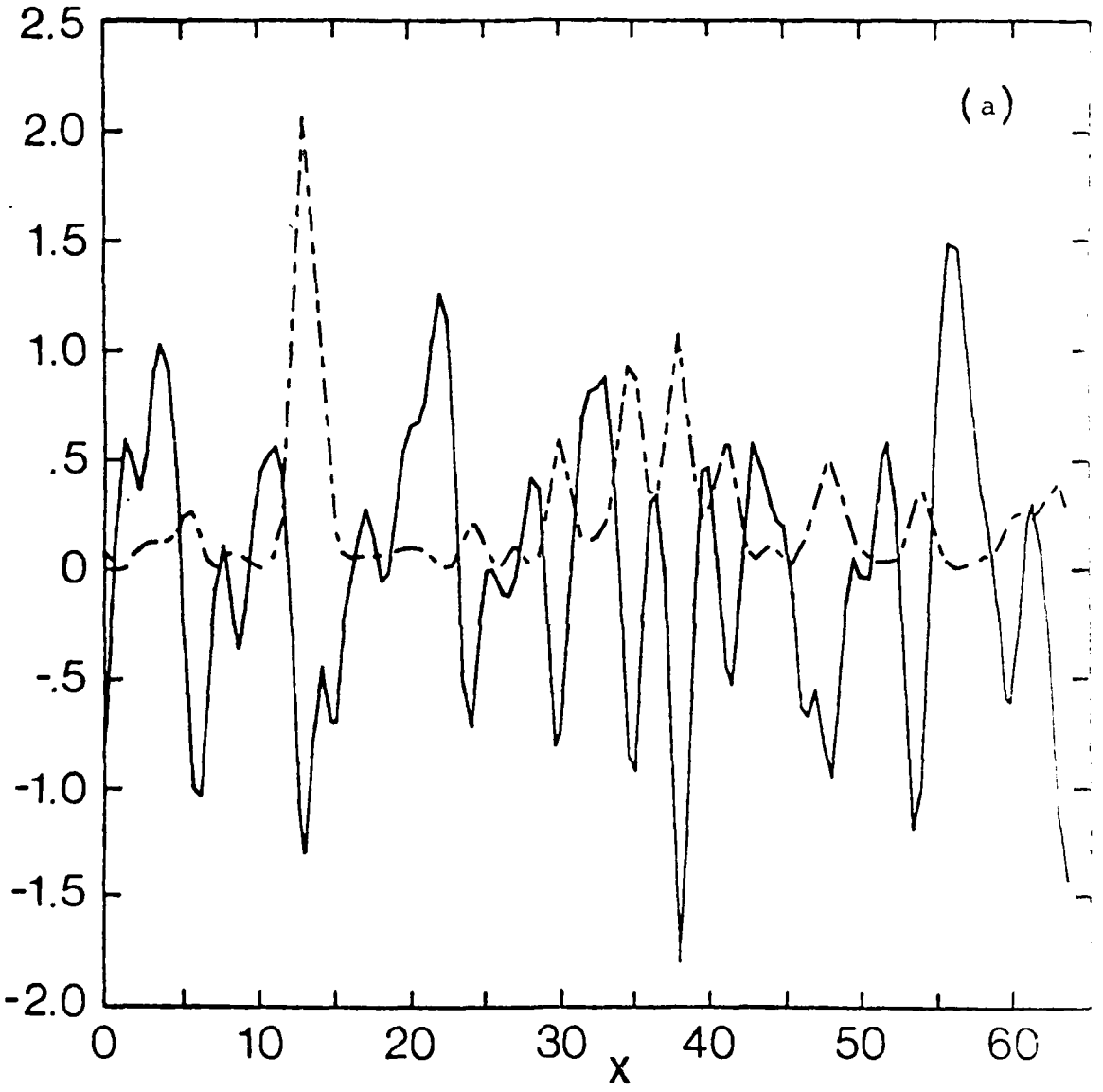

Fig. 10(a)

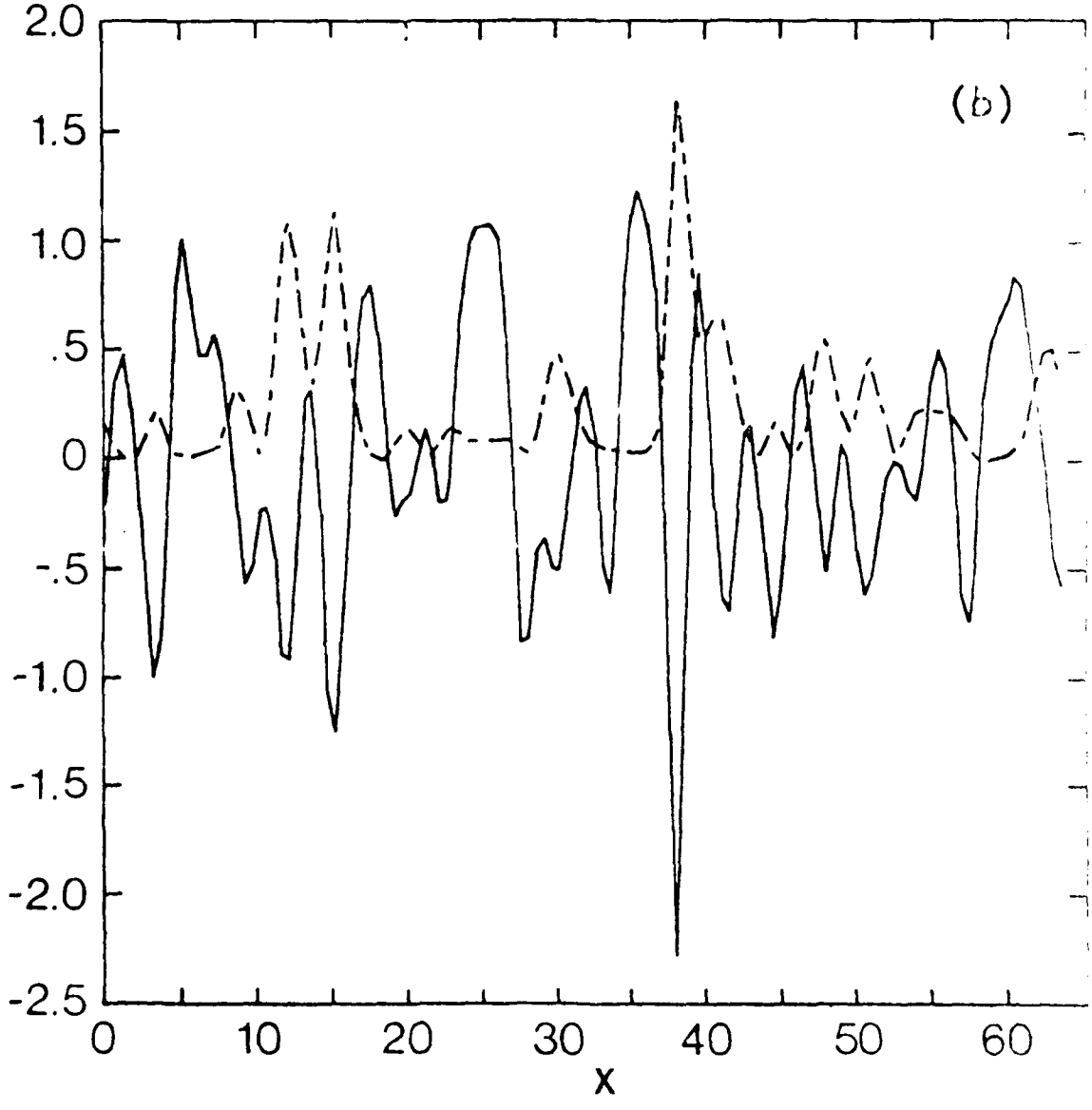

Fig. 10(b)

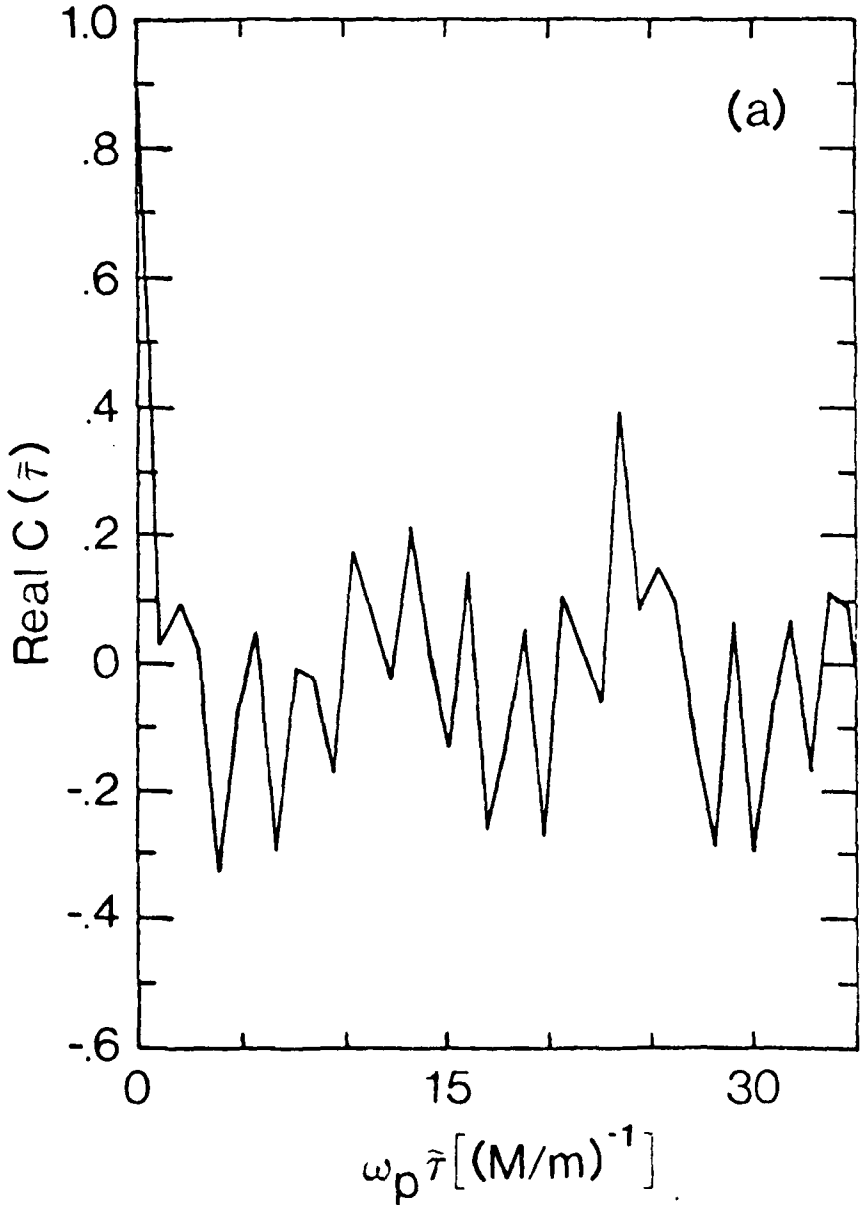

Fig. 3 (a)

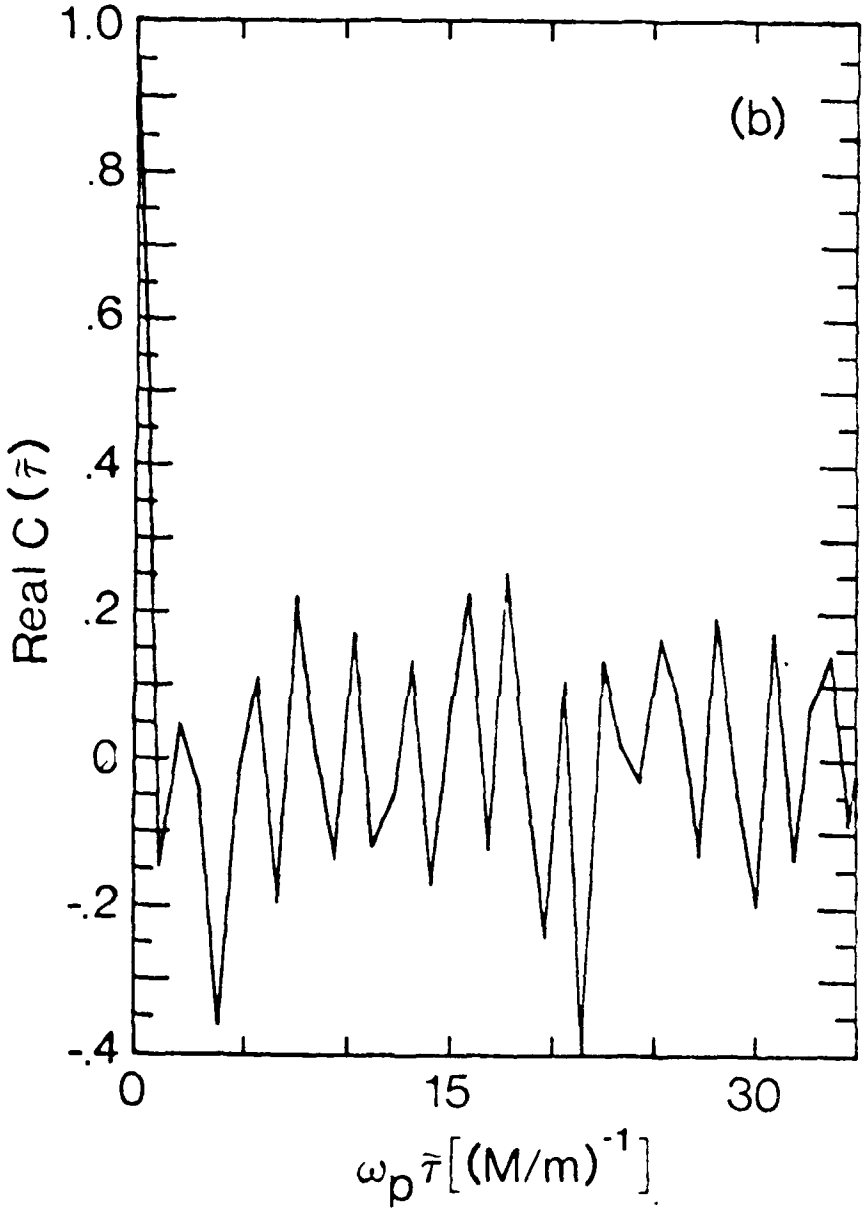

Fig. 11(b)

APPENDIX M

M. "Ion Trajectories in a Space Charge Wave on a Relativistic Electron Beam"

D.A. Russell and E. Ott
Submitted to Physics of Fluids, 1981

Ion trajectories in a space charge wave on a relativistic electron beam

D. A. Russell
Department of Astro-Geophysics, University of Colorado,
Boulder, Colorado 80309
and
E. Ott
Department of Physics and Astronomy,
University of Maryland, College Park, Maryland 20742

Motivated by the possibility of collective acceleration of ions trapped in an accelerating space charge wave on a strongly magnetized electron beam, the ion trajectories in such a configuration are studied. The motions perpendicular and parallel to the beam direction are coupled by a nonlinear term in the ion Hamiltonian that is proportional to the wave amplitude. Because of this coupling, the motion deviates markedly from that of a linear harmonic oscillator in certain resonant regions of phase space. A sequence of canonical transformations is used to study the motion in these regions. It is shown that wave amplitudes that are too small to trap beam electrons are too small to cause these resonances to overlap. In the absence of such overlap, the motion is not discernably ergodic in any three-dimensional subspace of the energy hypersurface because there exists a third

constant of the motion in addition to the total energy and angular momentum. These conclusions are verified using surface-of-section techniques to study numerically integrated ion trajectories. It is observed that the third constant of the motion constrains an ion initially trapped in a potential well of the wave to remain trapped in that well. Therefore, within the bounds of the physical model presented here, ergodic behavior poses no threat to attempts at collective ion acceleration in space charge waves on an electron beam.

I. INTRODUCTION

We consider the motion of an ion in a space-charge wave on a strongly magnetized electron beam. In cylindrical geometry, the wave has both radial and axial potential variations which couple the ion motion parallel to the beam to that perpendicular to the beam. Due to this coupling, there is not, in general, a constant of the ion motion in addition to the total energy and angular momentum. The absence of a third constant of the motion could permit the ion's radial oscillational energy to be converted into axial translational energy and thus defeat attempts to trap the ion in the potential wells of the wave. For example, if ions are loaded with zero velocity from the edge of an electron beam, then, when they reach the center of the beam, they have kinetic energy in radial motion approximately equal to the radial electrostatic well depth. This kinetic energy will typically exceed the axial well depth since the amplitude of space charge waves cannot be larger than a critical value at which wave breaking (overturning) occurs. Thus, if at some time during the particle's orbit a large enough fraction of the kinetic energy of the particle is converted to axial kinetic energy, then the particle will no longer be trapped in the potential well of the space charge wave.

In § II we derive the ion Hamiltonian. A canonical transformation to action-angle variables is introduced in

§ III.A which allows us to study the ion motion in a convenient toroidal representation. In § III.B we prove the existence of an approximate third constant of the motion using perturbation methods. These analytical findings are supported by studying the numerically integrated ion trajectories using surface-of-section techniques. Summarizing remarks and conclusions appear in § IV.

II. THE ION HAMILTONIAN

Consider a cylindrically symmetric electrostatic wave perturbation of a cold electron beam of uniform density, n_0, which fills a conducting cylinder of radius a (cf. Fig. 1). A strong magnetic field in the z-direction is assumed to constrain the electrons to move only parallel to the z-axis. In the beam frame (i.e., a reference frame at rest with respect to the beam electrons) we take

$$\phi_e(r,z,t) = \phi_0(r) + \phi_1(r)\exp[i(k_{||}z + \omega t)] ,$$

$$v_e(r,z,t) = v_1(r)\exp[i(k_{||}z + \omega t)] ,$$

and

$$n_e(r,z,t) = n_0 + n_1(r)\exp[i(k_{||}z + \omega t)] ,$$

where ϕ_e is the electric potential due to the electrons, v_e is the electron velocity in the z-direction, and n_e is the electron number density. ϕ_1, v_1 and n_1 are small quantities.

To zeroth order, Poisson's equation,

$$\nabla^2\phi_e = 4\pi e n_e ,$$

implies that

$$\phi_0(r) = \pi n_0 e r^2$$

where e is the magnitude of the charge of an electron. Linearizing the electron continuity equation,

$$\frac{\partial n_e}{\partial t} + \frac{\partial}{\partial z}(n_e v_e) = 0$$

in the small quantities n_1 and v_1, we find that

$$i\omega n_1 + ik_{||} n_0 v_1 = 0 . \qquad (1)$$

The linearized electron equation of motion

$$m_e \frac{\partial v_e}{\partial t} = e \frac{\partial \phi_e}{\partial z}$$

implies that

$$i\omega v_1 = ik_{||} e\phi_1 / m_e . \qquad (2)$$

m_e is the mass of the electron. Eliminating v_1 between (1) and (2) we find that

$$n_1 = \frac{-ek_{||}^2 n_o}{m_e \omega^2} \phi_1 ,$$

which, when substituted into Poisson's equation for $\phi_1(r)$,

yields

$$\frac{d^2}{dr^2}\phi_1(r) + \frac{1}{r}\frac{d}{dr}\phi_1(r) + k_{||}^2\left(\frac{\omega_p^2}{\omega^2} - 1\right)\phi_1(r) = 0 \qquad (3)$$

where $\omega_p \equiv (4\pi n_o e^2/m_e)^{1/2}$ is the background electron plasma frequency measured in the beam frame.

Equation (3) is to be solved subject to the condition that $\phi_1(r)$ vanish at $r = a$, so that the electric field, $-\nabla\phi_c$, has no component tangent to the wall of the conducting cylinder. Furthermore, $\phi_1(r)$ must be non-singular at $r = 0$. We find that

$$\phi_1(r) = \sum_{n=1}^{\infty}\phi_n J_0(p_n r/a) ,$$

where J_0 is the Bessel function of the first kind of order zero. p_n is the n-th zero of J_0, and we demand that

$$k_{||}^2 = \left(\frac{\omega_p^2}{\omega^2} - 1\right)^{-1}\frac{p_n^2}{a^2} \equiv \frac{\kappa_n^2}{a^2} . \qquad (4)$$

(4) is the dispersion relation of the wave with amplitude ϕ_n. Obviously $\omega_p^2 > \omega^2$ if the wave is to propagate (i.e., $k_{||}$ must be real). For simplicity, we retain only one wave, that having the lowest radial wavenumber, so that

$$\phi_1(r) = \phi_1 J_0(p_1 r/a) . \qquad (5)$$

Here and henceforth we suppress the subscript 1 on ϕ_1, p_1, and κ_1, and assume that $\kappa > 0$.

In the wave frame [$z \to z - (\omega/k_{\|})t$], the electric potential is independent of time:

$$\phi_e(r,z) = \pi n_0 e r^2 - \phi J_0(pr/a)\cos(\kappa z/a) \ . \qquad (6)$$

An ion (charge = Ze, mass = m_i) in the wave has potential energy $Ze\phi_e(r,z)$. Since ϕ_e is independent of the angle α, the angular momentum about the z-axis, $L_\alpha \equiv m_i r^2(d\alpha/dt)$, is a constant of the ion motion,[1] and the ion Hamiltonian is

$$H(r,z;P_r,P_z) = \frac{1}{2m_i}(P_r^2 + P_z^2) + \frac{L_\alpha^2}{2m_i r^2} + Z\pi n_0 e^2 r^2$$

$$- Ze\phi J_0(pr/a)\cos(\kappa z/a) \ . \qquad (7)$$

(P_r,P_z) are the canonical momenta conjugate to (r,z). Since H does not depend explicitly on the time, the total energy, E, is also a constant of the motion:

$$H(r,z;P_r,P_z) = E \ .$$

Let

$$\omega_0^2 \equiv Z4\pi n_0 e^2/2m_i = Z\omega_p^2 m_e/2m_i \ .$$

We divide the Hamiltonian (7) by $m_i a^2 \omega_0^2$ and make the following substitutions:

$$r \to r/a \ , \quad z \to z/a \ ,$$

$$P_r \to P_r/(m_i\omega_0 a) \ , \quad P_z \to P_z/(m_i\omega_0 a) \ ,$$

and

$$t \to \omega_0 t \ .$$

Now the ion motion is described by the dimensionless Hamiltonian,

$$H(r,z;P_r,P_z) = \frac{1}{2} P_r^2 + \frac{1}{2} P_z^2 + \frac{\ell^2}{2r^2} + \frac{1}{2} r^2$$

$$- \varepsilon J_0(pr)\cos(\kappa z) \ , \qquad (8)$$

where

$$\ell^2 \equiv L_\alpha^2/(m_i^2 a^4 \omega_0^2) \ ,$$

$$\varepsilon \equiv e\phi/(\tfrac{1}{2} m_e a^2 \omega_p^2) \ , \qquad (9)$$

and $(r,z;P_r,P_z;t)$ are dimensionless dynamical variables. We take (8) to be the fundamental ion Hamiltonian. However, we have neglected the magnetic field $\underset{\sim}{B} = B_o e_z$, which, we have assumed, constrains the electrons to move only parallel to the z-axis. In Appendix A we show that including the magnetic field in the ion dynamics only adds a constant term to the ion Hamiltonian (8) (and requires us to redefine the parameters ε and ℓ^2). Therefore, the motion described by the Hamiltonian (8) is qualitatively identical to the ion motion including the effects of the magnetic field so that our conclusions, based on an analysis of (8), are easily generalized.

The ion moves along a trajectory in the four-dimensional $(r,z;P_r,P_z)$-phase space described by Hamilton's equations:

$$\dot{r} = \frac{\partial H}{\partial P_r} = P_r \ , \quad \dot{z} = \frac{\partial H}{\partial P_z} = P_z \ ,$$

$$-\dot{P}_r = \frac{\partial H}{\partial r} = -\frac{\ell^2}{r^3} + r + \epsilon p J_1(pr)\cos(\kappa z) \ ,$$

and

$$-\dot{P}_z = \frac{\partial H}{\partial z} = \epsilon\kappa J_0(pr)\sin(\kappa z) \ .$$

(The dot denotes differentiation with respect to t.) Each trajectory is constrained by the conservation of energy to lie on a three-dimensional subspace of the four-dimensional phase space. This subspace is described by Eq. (8) and is called the energy hypersurface. If there were a third constant of the motion, the trajectories would lie on a two-dimensional surface in phase space.

For definiteness, we take ϵ and ℓ to be greater than zero. These two parameters are then bounded above. ℓ is bounded by requiring that there be at least one point of stable equilibrium with $r < 1$. This must be so if an ion is to be trapped in a potential well without striking the walls of the cylinder. For our purposes it is sufficient to monitor this constraint on ℓ numerically.

ϵ is bounded by requiring that the wave not trap beam electrons. Trapped electrons would violate the assumptions made in deriving the expression for the Hamiltonian (8). Using the dispersion relation (4) we find that

$$\epsilon = \frac{e\phi}{\frac{m_e}{2} v_p^2 (p^2+\kappa^2)} ,$$

where v_p is the phase velocity of the wave in the beam frame. But, to zeroth order, v_p is the velocity of a beam electron in the wave frame. Thus, the requirement that the wave not trap beam electrons is

$$\epsilon < (p^2 + \kappa^2)^{-1} \equiv \epsilon_{max} . \qquad (10)$$

The primary conclusion of this paper is that, with the wave amplitude ϵ so bounded, the kind of ergodic behavior that would discourage attempts to trap and accelerate the ion does not occur. This conclusion is also valid when the effects of the magnetic field on the ion motion are considered (cf. Appendix A).

III. ION TRAJECTORIES

A. $\epsilon = 0$: Conserved Action Variables

It is convenient to study the ion motion in a coordinate system different from the cylindrical system of §II. To introduce this new coordinate system we first consider the case $\epsilon = 0$. In this case, there is no wave on the beam, and the ion motion is described by the Hamiltonian

$$H_0(r,z;P_r,P_z) \equiv \frac{1}{2} (P_r^2+P_z^2) + \frac{\ell^2}{2r^2} + \frac{1}{2} r^2 = E . \qquad (11)$$

We specify a canonical transformation to action-angle variables

$$(r,z;P_r,P_z) \rightarrow (\theta_r,\theta_z;J_r,J_z)$$

using Hamilton's characteristic function $W(r,z;J_r,J_z)$.[2] W is defined, to within an additive constant, by the relations

$$P_r = \frac{\partial W}{\partial r} \quad \text{and} \quad P_z = \frac{\partial W}{\partial z} \ . \tag{12a}$$

From (11) it follows that W must solve the Hamilton-Jacobi equation,

$$\frac{1}{2}\left(\frac{\partial W}{\partial r}\right)^2 + \frac{1}{2}\left(\frac{\partial W}{\partial z}\right)^2 + \frac{\ell^2}{2r^2} + \frac{1}{2}\,r^2 = E \ . \tag{12b}$$

The dependence of W on the action variables (J_r,J_z) is given by the defining relations

$$J_r \equiv \frac{1}{2\pi}\oint P_r dr = \frac{1}{2\pi}\oint \frac{\partial W}{\partial r}\,dr \ , \tag{12c}$$

and

$$J_z \equiv \frac{1}{2\pi}\oint P_z dz = \frac{1}{2\pi}\oint \frac{\partial W}{\partial z}\,dz \ , \tag{12d}$$

where the integrals are over a complete period of r and z. (We adopt the convention that H_0 is periodic in z with period 2π.) Notice that $J_r \geq 0$ because the motion is bounded in r. Once Eqs. (12b)-(12d) have been solved for W, the angle variables (θ_r,θ_z) are defined by

$$\theta_r = \frac{\partial W}{\partial J_r} \quad \text{and} \quad \theta_z = \frac{\partial W}{\partial J_z} \ . \tag{12e}$$

W is called the generating function of the canonical transformation given by Eqs. (12a) and (12e).

We easily find (cf. Appendix B) that

$$W(r,z;J_r,J_z) = \int^r \left(2E - J_z^2 - s^2 - \frac{\ell^2}{s^2}\right)^{1/2} ds + zJ_z \quad , \tag{13}$$

where

$$E = \frac{1}{2} J_z^2 + 2J_r + \ell \quad . \tag{14}$$

It follows from (14) that in the action-angle variables the Hamiltonian is

$$K_0(J_r,J_z) = \frac{1}{2} J_z^2 + 2J_r + \ell \quad . \tag{15}$$

Since K_0 is independent of θ_r and θ_z, both actions are conserved:

$$J_r(t) = J_r(t=0) \equiv J_r^0 \tag{16a}$$

and

$$J_z(t) = J_z(t=0) \equiv J_z^0 \quad . \tag{16b}$$

Therefore, Hamilton's equations for $\dot{\theta}_r$ and $\dot{\theta}_z$,

$$\dot{\theta}_r = \frac{\partial K_0}{\partial J_r} = 2 \quad \text{and} \quad \dot{\theta}_z = \frac{\partial K_0}{\partial J_z} = J_z \quad ,$$

are trivial to integrate:

$$\theta_r(t) = 2t + \theta_r^0 \tag{16c}$$

and

$$\theta_z(t) = tJ_z + \theta_z{}^0 \ . \tag{16d}$$

Using (13), Eqs. (12a), (12c), and (12d) are easily solved for $(r,z;P_r,P_z)$ in terms of $(\theta_r,\theta_z;J_r,J_z)$ (cf. Appendix B):

$$z = \theta_z \ , \quad P_z = J_z \ , \tag{17a}$$

$$r = [\beta + \sqrt{\beta^2 - \ell^2}\cos\theta_r]^{1/2} \ , \tag{17b}$$

and

$$P_r = \frac{-(\beta^2-\ell^2)^{1/2}\sin\theta_r}{r} \ , \tag{17c}$$

where $\beta \equiv 2J_r + \ell$.

It is convenient to think of the motion, Eqs. (16), as taking place on a torus (cf. Fig. 2). For given initial conditions, $(\theta_r{}^0,\theta_z{}^0;J_r{}^0,J_z{}^0)$, the ion's trajectory subsequently will be confined to the torus with radii $(J_r{}^0,|J_z{}^0|)$. The two characteristic frequencies of this motion,

$$\omega_r \equiv \frac{\partial K_0}{\partial J_r} = 2 \ , \tag{18a}$$

and

$$\omega_z \equiv \frac{\partial K_0}{\partial J_z} = J_z \ , \tag{18b}$$

are constant on each trajectory. Clearly this motion consists of simple harmonic oscillation in (r,P_r)-space and uniform translation in (z,P_z)-space.

At this point we introduce a technique that will be used in § III.B to study the trajectories of the full Hamiltonian (8) numerically. We record the points of intersection of a given trajectory with the plane $\kappa z = 0 \pmod{2\pi}$. This plane is our surface of section. For definiteness, only those points with $P_z > 0$ will be recorded. (Obviously, taking z equal to any constant would do for a surface of section if $\epsilon = 0$, and the same pattern of intersections would result no matter what constant we chose. $z = 0$ is a good choice if $\epsilon \neq 0$ because this plane contains all points of stable equilibrium; all of the trajectories that we observed punctured this plane repeatedly as the equations of motion were advanced in time numerically.)

In the case $\epsilon = 0$, we know from Eqs. (17b) and (17c) that the points in the surface of section lie on the curve

$$P_r^2 r^2 + (r^2-\beta)^2 = \beta^2 - \ell^2 , \qquad (19)$$

corresponding to the (J_r^0, J_z^0) torus determined by our choice of initial conditions. Of course, in the toroidal $(\theta_r, \theta_z; J_r, J_z)$-representation any trajectory will puncture the surface of section $(\kappa\theta_z = 0, \text{ mod } 2\pi)$ along a circle in the (θ_r, J_r)-plane.

If there exist non-zero integers (m,n) such that $m\omega_r + n\omega_z = 0$, where ω_r and ω_z are defined by Eqs. (18), then the motion is periodic, and the trajectory will intersect

the surface of section in finitely many points. (The period of the motion is the least common multiple of $2\pi/\omega_r$ and $2\pi/\omega_z$.) If, on the other hand, $m\omega_r + n\omega_z = 0$ implies that $n = m = 0$, then the trajectory never intersects the surface of section in the same point twice. The intersections fill in the circle in the (θ_r, J_r)-plane, and the curve (19) in the (r, P_r)-plane, densely as time increases without bound. Such motion is called "conditionally periodic." On the (J_r, J_z) torus it is known[3] that conditionally periodic motion is ergodic: as time increases without bound, the fraction of the total elapsed time spent by the phase point in a small neighborhood of any point on the torus approaches the fraction of the total area of the torus contained in that small neighborhood.

We have seen that if $\epsilon = 0$ the ergodic motion is confined to the surfaces of two-dimensional tori whose characteristic frequencies (ω_r, ω_z) are not rationally related. If $\epsilon > 0$ there may exist three-dimensional regions of phase space in which the motion is ergodic and a third constant of the motion does not exist. In this case, a single trajectory would intersect the surface of section densely in a region of finite area. For our purposes it is necessary to determine whether or not such three-dimensional chaos exists and the effect such behavior would have on our ability to trap an ion in the potential wells of the wave.

B. $\epsilon > 0$: Resonant Island Overlap

If $\epsilon > 0$, there exist trajectories for which $|\kappa z(r)| < \pi$, and such motion is observed to be oscillatory in both r and z. If the energy, E, is sufficiently large ($E \geq \ell+\epsilon$) there also exist trajectories for which the motion is unbounded in z. Both types of trajectories are illustrated in Figure 3. Notice that these trajectories puncture the surface of section along simple closed curves that are in fact very close to the curves given by Eq. (19). Thus, these trajectories must lie on two-dimensional surfaces embedded in phase space. We conclude that for these trajectories there exists a third constant of the motion.

If E and ϵ are held fixed and κ is increased, some of the simple closed curves of Figure 3a are distorted into chains of islands, as shown in Figure 4. A single trajectory generated the chain of two islands, while a different trajectory generated the chain of three islands. Yet all observed trajectories intersect the surface of section in simple closed curves, so there still exists a third constant of the motion for these trajectories. Both island chains correspond to unbounded motion in z. Only those simple curves nearest the energy curve (i.e., the outermost curve in Figure 4, where all of the energy is in radial oscillations) correspond to bounded motion.

If now E and κ are held fixed at the values they have in Figure 4 and ϵ is increased, the two-island chain is

completely destroyed, as are the simple curves near the energy curve. That is, there is an annular region between the energy curve and the three-island chain (i.e., what remains of the three-island chain) that trajectories puncture randomly. The annular region shown in Figure 5a was generated by a single trajectory. Apparently, a third constant of the motion does not exist in this region. The corresponding motion in z (cf. Fig. 5b) vascillates randomly between bounded oscillations in the potential wells and unchecked flight over the crests of the wave. Obviously, such behavior must be avoided if we are to trap the ion in a potential well. Our main conclusion is that motion such as that depicted in Figure 5 does not occur for $\epsilon < \epsilon_{max}$. Indeed, the parameters used to generate Figure 5 are not physical since they correspond to $\epsilon > \epsilon_{max}$.

We may attempt to understand the behavior depicted in Figures 3 through 5 using perturbation techniques as follows.

Employing the canonical transformation given by Eqs. (17), the ion Hamiltonian (8) becomes

$$K(\theta_r,\theta_z;J_r,J_z) = K_0(J_r,J_z)$$

$$- \epsilon \sum_{i=0}^{\infty} C_i(J_r)\left[\cos(i\theta_r-\kappa\theta_z) + \cos(i\theta_r+\kappa\theta_z)\right] , \qquad (20)$$

where K_0 is given by Eq. (15),

$$C_i(J_r) \equiv \frac{1}{2\pi}\int_0^{2\pi} J_0[p(\beta + \sqrt{\beta^2-\ell^2}\cos\theta_r)^{1/2}]\cos(i\theta_r)d\theta_r \tag{21}$$

and $\beta \equiv 2J_r + \ell$. Clearly $|C_i(J_r)| \leq 1$ so that from Hamilton's equations,

$$-\dot{J}_r = \frac{\partial K}{\partial \theta_r} \quad \text{and} \quad -\dot{J}_z = \frac{\partial K}{\partial \theta_z} ,$$

we see that $\dot{J}_r$ and $\dot{J}_z$ are of order ε; that is, J_r and J_z are conserved to zeroth order in the small parameter ε. [J_r and J_z are the actions of (8) only if $\varepsilon = 0$.]

We specify a canonical transformation to new dynamical variables,

$$(\theta_r, \theta_z; J_r, J_z) \rightarrow (\psi_r, \psi_z; j_r, j_z) ,$$

using a generating function, T:

$$T(\theta_r, \theta_z; j_r, j_z) \equiv j_r\theta_r + j_z\theta_z + \varepsilon S(\theta_r, \theta_z; j_r, j_z) . \tag{22}$$

The transformation equations are given by[4]

$$\psi_r = \frac{\partial T}{\partial j_r} = \theta_r + \varepsilon\frac{\partial S}{\partial j_r} , \tag{23a}$$

$$\psi_z = \frac{\partial T}{\partial j_z} = \theta_z + \varepsilon\frac{\partial S}{\partial j_z} , \tag{23b}$$

$$J_r = \frac{\partial T}{\partial \theta_r} = j_r + \varepsilon\frac{\partial S}{\partial \theta_r} , \tag{23c}$$

and

$$J_z = \frac{\partial T}{\partial \theta_z} = j_z + \epsilon \frac{\partial S}{\partial \theta_z} \quad . \tag{23d}$$

Replacing the old variables with the new ones in (20) gives us the transformed Hamiltonian, K':

$$K'(\psi_r,\psi_z;j_r,j_z) = K_0(j_r,j_z) + \epsilon \left\{ \frac{\partial K_0}{\partial j_r} \frac{\partial S}{\partial \psi_r} + \frac{\partial K_0}{\partial j_z} \frac{\partial S}{\partial \psi_z} \right.$$

$$\left. - \sum_{i=0}^{\infty} C_i(j_r)[\cos(i\psi_r - \kappa\psi_z) + \cos(i\psi_r + \kappa\psi_z)] \right\}$$

$$+ O(\epsilon^2) \quad . \tag{24}$$

[Here we have used the Taylor expansion of K_0 and are treating S as a function of (ψ_r,ψ_z), correct to lowest order in ϵ.]

If the term proportional to ϵ in (24) vanishes, then j_r and j_z are conserved to order ϵ^2. Furthermore, if $\partial S/\partial \theta_{r,z}$ does not become large, then Eqs. (23c) and (23d) imply that j_r and j_z differ from J_r and J_z by terms of order ϵ. In other words, if we can find a sufficiently smooth function S for which the term in brackets in (24) vanishes, then the ion trajectories will lie on surfaces that differ very little ($\sim\epsilon$) from the tori of § III.A. Such trajectories would puncture the surface of section along simple curves as in Figure 3a.

Equation (24) suggests that we take S to be of the form

$$S(\theta_r,\theta_z;j_r,j_z) \equiv \sum_{\substack{\ell=0 \\ m=\pm 1}}^{\infty} A_{\ell,m}(j_r,j_z)\sin(\ell\theta_r+m\kappa\theta_z) \ . \tag{25}$$

Substituting (25) in (24) we easily discover a suitable definition for $A_{\ell,m}$:

$$A_{\ell,\pm 1} \equiv \left\{ \begin{array}{ll} \dfrac{C_\ell(j_r)}{\ell\omega_r \pm \kappa\omega_z} & \text{if } |C_\ell(j_r)| \le |\ell\omega_r \pm \kappa\omega_z| \\ \\ 0 & \text{otherwise} \end{array} \right\}. \tag{26}$$

Here, $(\omega_r,\omega_z) = (\partial K_0/\partial j_r, \partial K_0/\partial j_z) = (2, j_z)$.

In those regions of phase space where no denominator $(2\ell \pm \kappa j_z)$ is small, we may expect the trajectories to lie on surfaces similar to the tori of § III.A. In this case, the motion is described by the Hamiltonian

$$K_0(j_r,j_z) = \tfrac{1}{2} j_z^2 + 2j_r + \ell \ .$$

Therefore, j_r and j_z are constants of the motion (up to terms of order ϵ^2 which we are neglecting). But, according to Eqs. (23), J_r and J_z differ from j_r and j_z by sinusoidal functions of θ_r and θ_z that are of order ϵ. The trajectories are therefore constrained to lie on surfaces in $(\theta_r,\theta_z;J_r,J_z)$

space resembling slightly rippled tori. Because these rippled tori are topologically equivalent to the tori in the case $\epsilon = 0$, they are said to be preserved by the transformation T. (Two surfaces are topologically equivalent if one can be continuously deformed into the other.) A preserved torus intersects the surface of section in a simple closed curve. The curve is approximately described by Eq. (19), up to sinusoidal wiggles which are imperceivable in the numerically generated surface of section plots shown in Figure 3a.

Let

$$j_z^N \equiv \pm 2N/\kappa \ , \tag{27a}$$

and

$$j_r^N \equiv \frac{1}{2}\left(E - \ell - \frac{2N^2}{\kappa^2}\right) \ . \tag{27b}$$

We cannot expect the ion trajectories in regions of phase space near (j_r^N, j_z^N) to lie on surfaces closely resembling tori. Those tori corresponding to (j_r^N, j_z^N) (i.e., $J_r^N \cong \frac{1}{2}[E-\ell-(2N^2/\kappa^2)]$ and $J_z^N \cong \pm 2N/\kappa$) are said to be resonant under the transformation T. [Tori close enough to (J_r^N, J_z^N) to be strongly distorted by T are considered to be resonant as well.]

Recall that J_r is by definition positive. J_r and j_r differ by terms of order ϵ. Therefore j_r^N must be positive, up to terms of order ϵ. Clearly, if

$$\kappa^2 < \frac{2}{E-\ell}$$

then there are no resonant tori ($N \geq 1$) present. This result depends only on the form of H_0 in Eq. (11) and on the fact that there is a single $k_{||}$ on the beam.

Near the N-th resonance, $A_{N,-1} = 0$, according to Eq. (26), and the motion is described approximately by the Hamiltonian

$$K^N(\psi_r,\psi_z;j_r,j_z) \equiv K_0(j_r,j_z) - \varepsilon C_N(j_r)\cos(N\psi_r-\kappa\psi_z) \quad . \quad (28)$$

(Our conclusions do not depend on which sign is chosen for j_z^N in (27a). We have taken the + sign for definiteness.) From Hamilton's equations,

$$-\dot{j}_r = \frac{\partial K^N}{\partial \psi_r} = N\varepsilon C_N \sin(N\psi_r-\kappa\psi_z)$$

and

$$-\dot{j}_z = \frac{\partial K^N}{\partial \psi_z} = -\kappa\varepsilon C_N \sin(N\psi_r-\kappa\psi_z) \quad ,$$

it is clear that

$$I^N \equiv \kappa j_r + N j_z \quad (29)$$

is a constant of the motion for Hamiltonian K^N. Let

$$j_r = j_r^N + \delta j_r \quad ,$$

eliminate j_z from Eq. (28) using (29) and set $\psi_z = 0$

to see how resonant tori intersect the surface of section. Solving Eq. (28) for δj_r we find that

$$\delta j_r \cong -\frac{1}{2}\left(E - \ell - \frac{2I^N}{\kappa}\right) - \frac{N^2}{\kappa^2}$$

$$\pm \frac{N}{\kappa}\left[2\left(E - \ell - \frac{2I^N}{\kappa}\right) + \frac{4N^2}{\kappa^2} + 2\varepsilon C_N(j_r{}^N)\cos(N\psi_r)\right]^{1/2} . \tag{30a}$$

(We have neglected the dependence of C_N on δj_r and have set $K^N = E$ to get this approximate result.)

For given I^N the radicand in Eq. (30a) may be positive only for values of ψ_r in one of N intervals between 0 and 2π. The corresponding resonant torus would intersect the surface of section in a chain of N islands as in Figure 4. Since we have kept only terms of order ε in K^N, the islands are called "first order resonant islands." (Higher order perturbation techniques would reveal chains of much smaller second order resonant islands surrounding the first order chains, etc.) If the radicand is positive for all ψ_r, the corresponding torus is not resonant but is only rippled by the transformation T, in accord with the description of preserved tori given above. Between the preserved and resonant tori there is a separatrix given by Eq. (30a) when I^N is chosen so that

$$E - \ell - \frac{2I^N}{\kappa} + \frac{2N^2}{\kappa^2} = \varepsilon\left|C_N(j_r{}^N)\right| . \tag{30b}$$

Since in this case

$$\delta j_r = -\frac{\epsilon}{2} |C_N(j_r^N)| \pm \frac{N}{\kappa} \left[2\epsilon |C_N(j_r^N)| (1 \pm \cos N\psi_r) \right]^{1/2} ,$$

we see that the maximum island width is

$$W_N \equiv \frac{4N}{\kappa} \left[\epsilon |C_N(j_r^N)| \right]^{1/2} . \tag{31}$$

If the motion can be described to order ϵ by either K_0 or by K^N, for some N, then in all of phase space there exists an approximate third constant of the motion which, we observe, keeps the ion from escaping from a potential well once it is trapped. If, however, there are regions of phase space in which two or more denominators $(2N \pm \kappa j_z)$ are simultaneously small this may not be the case.

It is well known[5] that for conservative dynamical systems of two degrees of freedom the motion is ergodic in those three-dimensional regions of phase space where resonant island overlap occurs. For our purposes it is sufficient to determine whether or not the motion is observably ergodic due to the overlapping of first order resonant islands. Resonant island overlap occurs approximately when the distance between two resonant tori is less than the sum of the half-widths of the corresponding island chains. That is, when

$$j_r^N - j_r^{N+1} < \frac{1}{2} (W^N + W^{N+1}) , \tag{32}$$

we should expect trajectories to puncture the surface of

section chaotically in a roughly annular neighborhood of J_r^N and J_r^{N+1}. Using Eqs. (27b) and (31) we obtain from (32) the resonant islant overlap criterion:

$$2N+1 < 2N\kappa\left[\varepsilon|C_N(j_r^N)|\right]^{1/2} + 2(N+1)\kappa\left[\varepsilon|C_{N+1}(j_r^{N+1})|\right]^{1/2} . \tag{33}$$

This is, of course, an approximate condition.

It is interesting to notice that if $\ell = 0$, C_N is zero if N is odd, and

$$C_{2m}(j_r^m) = (-1)^m J_m^2\left[p\left(\tfrac{1}{2}\, j_r^m\right)^{1/2}\right] , \qquad m = 0,1,2,...$$

where now

$$j_r^m = E - \frac{2m^2}{\kappa^2} ,$$

and J_m is the Bessel function of the first kind of order m. (See Appendix C for a discussion of the case $\ell = 0$.) Thus, the m-th resonant torus intersects the surface of section in a chain of 2m islands. The overlap criterion corresponding to (33) is

$$2m+1 < 2m\kappa\varepsilon^{1/2}\left|J_m\left[p\left(\tfrac{1}{2}\, j_r^m\right)^{1/2}\right]\right| + 2(m+1)\kappa\varepsilon^{1/2}\left| J_{m+1}\left[p\left(\tfrac{1}{2}\, j_r^{m+1}\right)^{1/2}\right]\right| , \tag{34}$$

and it is easy to see that this inequality cannot be satisfied if $\varepsilon < \varepsilon_{max}$ unless m = 0. This corresponds to

overlap of the 2-island chain and the energy curve in the surface of section. This overlap and the chaotic motion it engenders are shown in Figure 6 for $\epsilon > \epsilon_{max}$. (We took a large, forbidden value of ϵ to produce apparent chaotic behavior.)

If $\ell > 0$, our numerical calculations reveal no resonant island overlap for $N \geq 1$ and $\epsilon < \epsilon_{max}$. Presumably this is because the overlap criterion (33) cannot be satisfied. The only observed chaotic behavior for $\epsilon < \epsilon_{max}$ results from overlap of the energy curve and the 1-island chain. This overlap and the chaotic motion it produces are shown in Figure 7 for $\epsilon > \epsilon_{max}$. (Of course it is possible that this chaos is a product of the overlap of higher-order, smaller resonant islands whose theoretical origins we have ignored in our first order perturbation analysis and whose existence we were not able to document numerically. Nevertheless, the observed chaos <u>appears</u> to result from overlap of the 1-island chain and the energy curve.)

All N-island chains ($N \geq 1$) are observed to be produced by motion that is unbounded in z if $\epsilon < \epsilon_{max}$. We may understand this observation as follows. Using the constant of the motion, Eq. (29) to eliminate j_r from the resonant Hamiltonian, Eq. (28) we find that on the separatrix, Eq. (30b),

$$j_z \cong \frac{2N}{\kappa} \pm \left\{ 2\epsilon \left| C_N(j_r^N) \right| \left[1 \pm \cos(N\psi_r - \kappa\psi_z) \right] \right\}^{1/2} .$$

Thus, the most negative value of j_z in the N-island chain is approximately

$$\frac{2N}{\kappa} - 2\left[\epsilon|C_N(j_r^N)|\right]^{1/2} ,$$

which cannot be less than zero if $\epsilon < \epsilon_{max}$ and $N \geq 1$ because $|C_N| \leq 1$. Because the energy curve is a resonance of no width, the 1-island chain must get very close to it to produce chaotic behavior. But then there are few, if any, bounded trajectories left to protect. (Obviously, the energy curve itself cannot be destroyed by overlap.) Thus, the Hamiltonian (8) manifests no chaotic behavior that would discourage attempts to trap the ion and keep it trapped.

IV. CONCLUSIONS

We have considered the motion of an ion in an electrostatic wave on a cold, uniform electron beam. We find that if the amplitude of the wave, ϵ, is insufficient to trap beam electrons then there exists a third constant of the ion motion, in addition to the angular momentum and total energy. This third constant of the motion constrains the ion trajectories to lie on two-dimensional tori embedded in the four-dimensional ion phase space. The motion on these tori may be either periodic or doubly

periodic. If ϵ exceeds the critical value for wave breaking, the ion motion is observed to be chaotic in certain three-dimensional regions of phase space where resonant tori overlap and a third constant of the motion does not exist. Were this chaotic behavior physical (i.e., if the wave were not broken) it would undermine attempts to trap and accelerate the ion in the potential wells of the space charge wave. However, if ϵ is less than the critical value for wave breaking, the existence of the third constant of the motion throughout all of phase space ensures that radial oscillational energy cannot be converted to axial translational energy so as to liberate an ion initially trapped in the potential wells of the wave.

ACKNOWLEDGMENTS

We are grateful to Professor Richard Lovelace for suggesting the easy generalization of our results to include the effects of the magnetic field on the ion dynamics.

This work was supported by the Air Force Office of Scientific Research under grant no. AFOSR-80-0087, and in part (D.A.R. only) by AFOSR grant no. 80-0022, the National Aeronautics and Space Administration under grant no. NAGW-90, and by the National Science Foundation, Atmospheric Research Section, under grant no. 7916837.

APPENDIX A

Magnetic Field Effects on the Ion Motion

Since we have assumed that a uniform axial magnetic field, $\underset{\sim}{B} = B_o \underset{\sim}{e}_z$, constrains the electrons to move only parallel to the z-axis, we must include the effects of this field on the ion motion. We do so using the vector potential,

$$\underset{\sim}{A}(r) = B_o r \, \underset{\sim}{e}_\alpha \ ,$$

such that $\underset{\sim}{B} = \underset{\sim}{\nabla} \times \underset{\sim}{A}$. Including this vector potential, the ion Hamiltonian analogous to (8) is:[6]

$$H(r,z;P_r,P_z) = \frac{1}{2m_i}\,(P_r^2+P_z^2) + \frac{1}{2m_i}\left(\frac{P_\alpha}{r} - \frac{Ze}{c}\,B_o r\right)^2$$

$$+ Ze\phi_e(r,z) \ .$$

Here c is the speed of light in vacuo and (P_r,P_z,P_α) are the canonical momenta conjugate to (r,z,α), respectively:

$$P_r = m_i\dot{r} \ , \quad P_z = m_i\dot{z} \ , \text{ and}$$

$$P_\alpha = m_i r^2\dot{\alpha} + \frac{Ze}{c}\,r^2 B_o \ .$$

Because the Hamiltonian is independent of α, P_α is a constant of the motion.

Introducing the ion cyclotron frequency,

$$\Omega_c = ZeB_o/m_i c \ ,$$

and a frequency ω_o,

$$\omega_o^2 = \Omega_c^2 + Z\omega_p^2 m_e/2m_i \ ,$$

we divide H by $m_i a^2 \omega_o^2$ and make the following substitutions:

$$r \to r/a \ , \quad z \to z/a \ ,$$

$$P_r \to P_r/(m_i \omega_o a) \ , \quad P_z \to P_z/(m_i \omega_o a) \ ,$$

and

$$t \to \omega_o t \ .$$

Under this change of variables, the dimensionless Hamiltonian is

$$H(r,z;P_r,P_z) = \frac{1}{2} P_r^2 + \frac{1}{2} P_z^2 + \frac{\ell^2}{2r^2} + \frac{1}{2} r^2 - \varepsilon J_o(pr)\cos(\kappa z) - \delta \ ,$$

where

$$\ell^2 \equiv P_\alpha^2/(m_i^2 a^4 \omega_o^2) \ ,$$

$$\varepsilon \equiv Ze\phi/(m_i a^2 \omega_o^2) \ ,$$

and

$$\delta \equiv \Omega_c P_\alpha/(m_i a^2 \omega_o^2) \ .$$

Since this Hamiltonian and (8) differ only by the added constant δ, the motions they generate are qualitatively identical.

Using the dispersion relation (4) we may rewrite ϵ as

$$\epsilon = \frac{e\phi/(\frac{1}{2}m_e v_p^2)}{p^2+\phi^2+m_i a^2 \omega_c^2/(Z\frac{1}{2}m_e v_p^2)} ,$$

where v_p is the phase velocity of the wave in the beam frame. In order that the wave not break, the numerator must be less than 1, or:

$$\epsilon < [p^2+\phi^2+m_i a^2 \omega_c^2/(Z\frac{1}{2}m_e v_p^2)]^{-1} .$$

This upper bound on ϵ is even smaller than $\epsilon_{max} \quad [p^2+\phi^2]^{-1}$ used to bound when the magnetic field is neglected. Therefore: if wave amplitudes that are too small to trap beam electrons are too small to foil attempts to trap and accelerate an ion when the effects of the magnetic field on the ion motion are neglected, then (because the respective Hamiltonians are of the same form) the same is true when the effects of the magnetic field are included in the ion dynamics.

APPENDIX B

Action-Angle Variables

We assume a solution of the Hamilton-Jacobi equation,

$$\frac{1}{2}\left(\frac{\partial W}{\partial z}\right)^2 + \frac{1}{2}\left(\frac{\partial W}{\partial z}\right)^2 + \frac{1}{2}\,r^2 + \frac{\ell^2}{2r^2} = E \ ,$$

of the form

$$W(r,z) = W_1(r) + W_2(z) \ .$$

It follows that dW_2/dz = a constant $\equiv J_z$, say. Notice that

$$J_z = \frac{1}{2\pi}\int_0^{2\pi} \frac{\partial W}{\partial z}\, dz \ ,$$

in agreement with the definition of action, Eq. (12d). The action in the (r,P_r)-plane is

$$J_r \equiv \frac{1}{2\pi}\oint \frac{dW_1}{dr} = \frac{1}{2\pi}\oint \pm\left(2E - J_z^2 - r^2 - \frac{\ell^2}{r^2}\right)^{1/2} dr \ , \tag{B1}$$

where we must take the plus sign for increasing r and the minus sign for decreasing r. It is convenient to rewrite the action integral (B1) as

$$J_r = \frac{1}{2\pi}\oint_{C_{12}}\left[\frac{(r_2^2-z^2)(z^2-r_1^2)}{z^2}\right]^{1/2} dz \tag{B2}$$

and to evaluate this integral in the complex plane. The integrand [±I(z)] in (B2) is singular at the origin and at the point at infinity. There are four branch points: $\pm r_{1,2}$. We choose one branch cut between r_1 and r_2 and another between $-r_1$ and $-r_2$, both along the real axis. The action is given by the integral along the contour C_{12}, as shown in Figure 8, where the integrand is taken to be positive above the cut and (therefore) negative below. Deforming the contour C_{12} around the origin, the point at infinity, and the cut between $-r_1$ and $-r_1$, we find that

$$2J_r = \frac{1}{2\pi} \oint_{C_0} I(z)dz + \frac{1}{2\pi} \oint_{C_0} \frac{I(1/z)}{z^2}\, dz \quad . \qquad \text{(B3)}$$

Here we have used the fact that the integral around C'_{12} is equal to $-J_r$ and have transformed the integral around the point at infinity to one around the origin using the substitution, $z \to 1/z$. In evaluating both integrals in (B3) we take care to choose the signs of $I(z)$ and $I(1/z)$ consistent with the choice in (B2). We find that the residue at $z = 0$ of $I(z)$ is $i\ell$ ($\ell > 0$). The residue of $I(1/z)/z^2$ at $z = 0$ is $-i(E - \frac{1}{2} J_z^2)$. Applying the residue theorem, we find that

$$2J_r = -\ell + E - \frac{1}{2} J_z^2 \ ,$$

that is,

$$E = \frac{1}{2} J_z^2 + 2J_r + \ell \quad . \tag{B4}$$

To determine the old variables $(r,z; P_r,P_z)$ in terms of the new variables $(\theta_r,\theta_r;J_r,J_z)$ we first note that $W_2(z) = zJ_z$ + a constant, which we take to be zero. Therefore

$$W(r,z) = zJ_z + \int^r \left(4J_r+2\ell -r'^2 - \frac{\ell^2}{r'^2}\right)^{1/2} dr' \ ,$$

where we have used (B4). Two of the transformation equations,

$$\theta_z = \frac{\partial W}{\partial J_z} \quad \text{and} \quad P_z = \frac{\partial W}{\partial z} \ ,$$

are trivial to solve:

$$\theta_z = z \quad \text{and} \quad P_z = J_z \ .$$

We also have

$$\theta_r = \frac{\partial W}{\partial J_r} = \int^r \frac{2dr'}{[4J_r+2\ell-r'^2-(\ell^2/r'^2)]^{1/2}} \quad . \tag{B5}$$

Changing the variable of integration in (B5) from r' to ϕ, where

$$\cos\phi \equiv \frac{r'^2-\beta}{(\beta^2-\ell^2)^{1/2}}$$

and $\beta \equiv 2J_r+\ell$, we find that

$$r = [\beta+(\beta^2-\ell^2)^{1/2}\cos\theta_r]^{1/2} \quad . \tag{B6}$$

Finally, substituting this expression into the Hamiltonian, Eq. (11), we find that

$$P_r^2 = \frac{(\beta^2 - \ell^2)\sin^2\theta_r}{r} \quad . \tag{B7}$$

Because P_r is positive for increasing r and negative for decreasing r, we must take

$$[\sin^2\theta_r]^{1/2} = -\sin\theta_r \quad ,$$

as in Eq. (17c), if r is given by (B6).

APPENDIX C

The Case $\ell = 0$

In the case $\ell = 0$, we do not obtain correct expressions by setting $\ell = 0$ in (B4) through (B7). This is because the action integral, Eq. (B1), is discontinuous in ℓ at $\ell = 0$. The integral is, however, elementary in this case, and we easily find that

$$J_r = E - \frac{1}{2} J_z^2 \ .$$

Proceeding as before, it is now straightforward to show that the canonical transformation to action-angle variables is given by the following equations:

$$z = \theta_z \ , \quad P_z = J_z \ ,$$

$$r = \sqrt{2J_r} \cos\theta_r \ , \quad P_r = -\sqrt{2J_r} \sin\theta_r \ .$$

In this case, the N-th Fourier-cosine coefficient in the expansion of $J_0(pr)$ is

$$\frac{1}{2\pi} \int_0^{2\pi} J_0(p\sqrt{2J_r} \cos\theta_r) \cos N\theta_r \, d\theta_r \ .$$

Therefore, in the notation of Eq. (20),

$$C_N(J_r) = \frac{1}{2\pi} \int_0^{2\pi} J_0(p\sqrt{2J_r} \cos\theta_r) \cos N\theta_r \, d\theta_r \ ,$$

if $\ell = 0$. It is easy to see that $C_N = 0$ if N is odd. If N is even,[7]

$$C_{2m}(J_r) = (-1)^m J_m^2(p\sqrt{J_r/2}) , \qquad m = 0,1,2,...$$

Therefore, in action-angle variables, the Hamiltonian (8) is

$$H(\theta_r, \theta_z; J_r, J_z) = \frac{1}{2} J_z^2 + J_r$$

$$- \varepsilon \sum_{m=0}^{\infty} C_{2m}(J_r) \left[\cos(2m\theta_r - \kappa\theta_z) + \cos(2m\theta_r + \kappa\theta_z) \right] .$$

The resonant tori, analagous to Eqs. (27a) and (27b) are found at

$$j_z^m = \pm 2m/\kappa$$

and

$$j_r^m = E - \frac{2m^2}{\kappa^2} ;$$

but now these tori intersect the surface of section in chains of 2m islands. We find that the m-th chain will overlap the m+1-st chain if

$$2m+1 \leq 2m\kappa[\varepsilon|C_{2m}(j_r{}^m)|]^{1/2}$$

$$+ 2(m+1)\kappa[\varepsilon|C_{2(m+1)}(j_r{}^{m+1})|]^{1/2} ,$$

which is expression (34) in the text.

REFERENCES

1. H. Goldstein, Classical Mechanics (Addison Wesley, Reading, Mass., 1950), Sec. 7-3.
2. H. Goldstein, Classical Mechanics (Addison Wesley, Reading, Mass., 1950), Sec. 9-3.
3. V. I. Arnol'd, Russian Math. Surveys 18, 85 (1963).
4. H. Goldstein, Classical Mechanics (Addison Wesley Reading, Mass., 1950), p. 241.
5. M. Henon and C. Heiles, Astron. J. 69, 73 (1964); G. H. Walker and J. Ford, Phys. Rev. 188, 416 (1969).
6. D. L. Landau and E. M. Lifshitz, The Classical Theory of Fields (Pergamon, New York, 1971), 3rd ed., p. 46.
7. I. S. Gradshteyn and I. M. Ryshik, Table of Integrals, Series and Products (Academic Press, New York, 1965), p. 738, no. 5.

FIGURE CAPTIONS

FIG. 1. The cylindrical coordinate system used to analyze the ion trajectories.

FIG. 2. The toroidal representation of the ion phase space. ($J_r < |J_z|$ is assumed.)

FIG. 3. Ion trajectories unaffected by nonlinear resonances. (a): Intersections of the surface of section by ion trajectories that are (A) bounded in z and (B) unbounded in z. No nonlinear resonances are present. E = 0.6, ℓ = 0.1, κ = 1.0, ε = 0.02. (b): κz as a function of the time t for trajectories (A) and (B) of Fig. 3(a). (c): r as a function of the time t for trajectories (A) and (B) of Fig. 3(a).

FIG. 4. Intersections of the surface of section by ion trajectories on strongly distorted, resonant tori. (A) is the energy curve, (B) is a chain of two islands, and (C) is a chain of three islands. E = 0.6, ℓ = 0.1, κ = 7.0, ε = 0.02, $\varepsilon_{max} \cong 0.018$.

FIG. 5. Ion trajectories strongly affected by resonant island overlap. (a): Intersections of the surface of section by two ion trajectories. One trajectory produced the chain of three islands; another trajectory produced the stippled region. $E = 0.6$, $\ell = 0.1$, $\kappa = 7.0$, $\varepsilon = 0.1$, $\varepsilon_{max} \cong 0.018$. (b): κz as a function of the time t for the ion trajectory that produced the stippled region in Fig. 5(a).

FIG. 6. Intersections of the surface of section by several ion trajectories, in the case $\ell = 0$, when the two-island chain (B) overlaps the energy curve (A). The stippled region was produced by a single trajectory. $E = 0.6$, $\ell = 0$, $\kappa = 5.0$, $\varepsilon = 0.1$, $\varepsilon_{max} \simeq 0.0324$.

FIG. 7. Intersections of the surface of section by several trajectories when the one-island chain (B) overlaps the energy curve (A). The stippled region was produced by a single trajectory. $E = 0.65$, $\ell = 0.1$, $\kappa = 5.0$, $\varepsilon = 0.1$, $\varepsilon_{max} \simeq 0.0324$.

FIG. 8. Contours in the complex plane used to find the action, J_r.

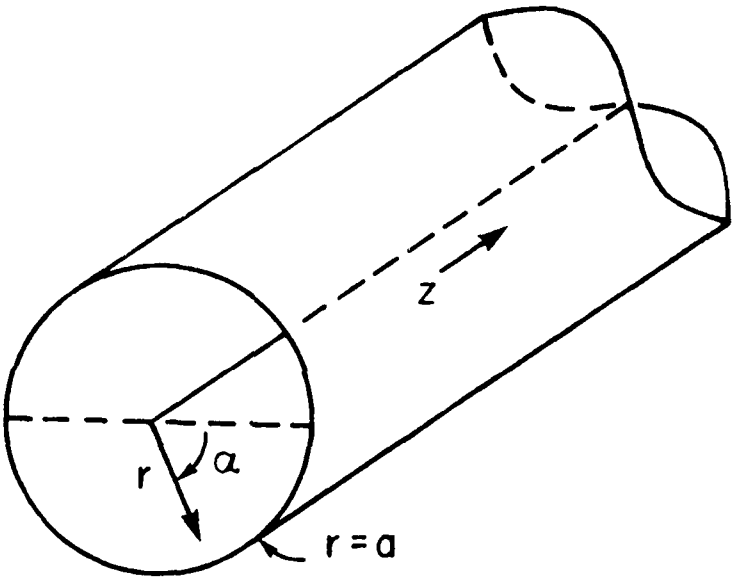

FIGURE 1

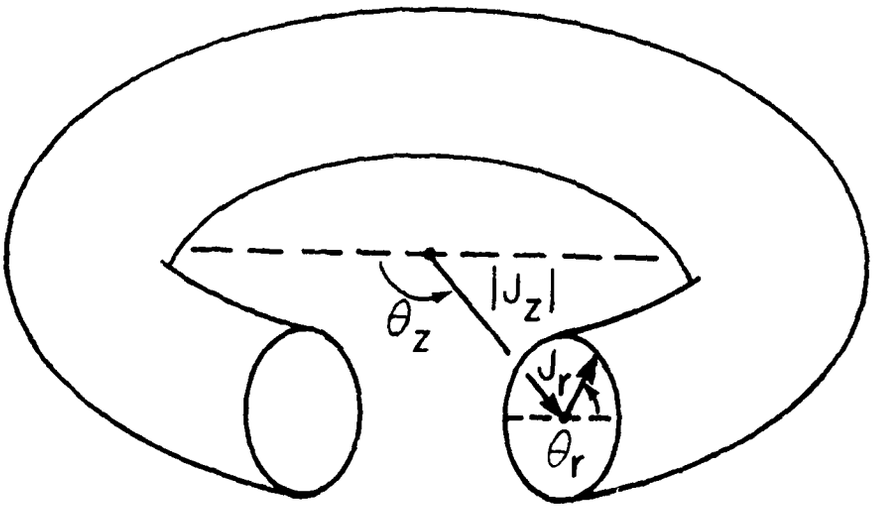

FIGURE 2

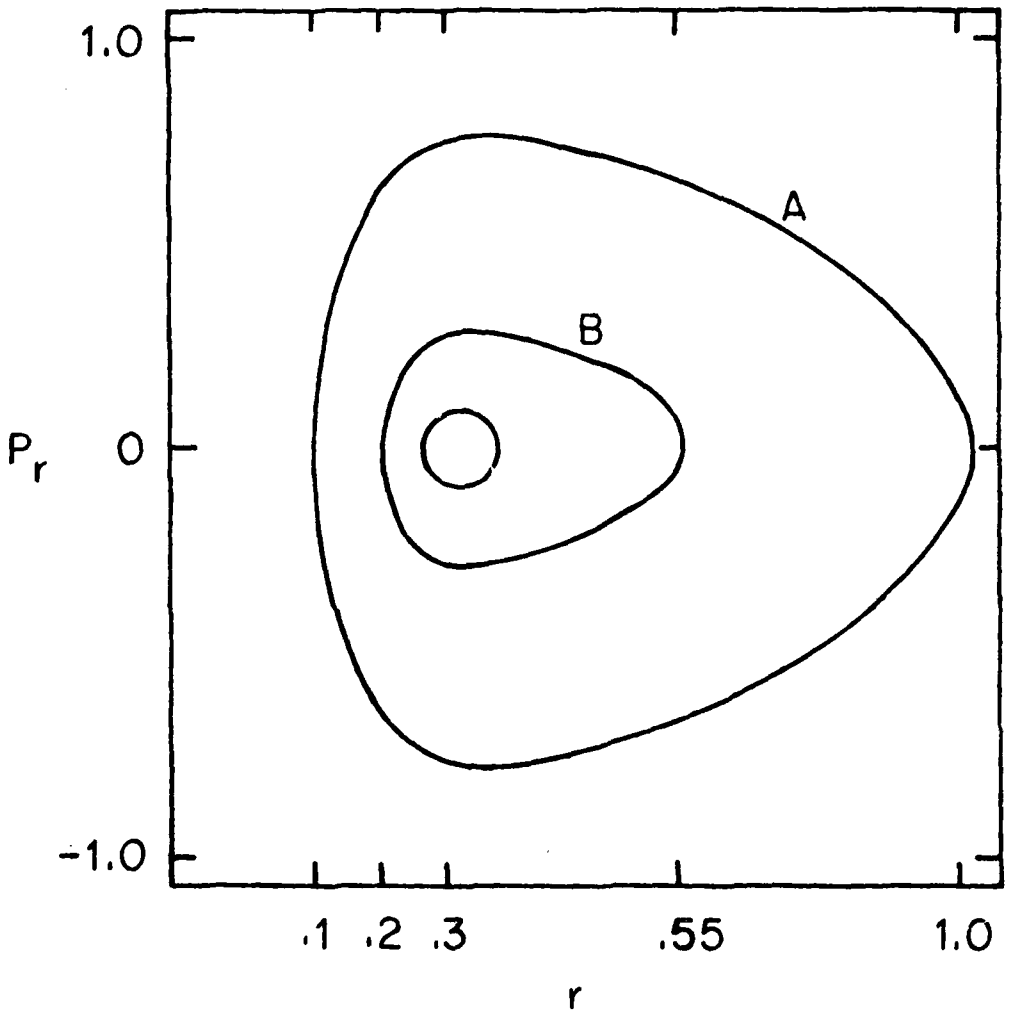

FIGURE 3(a)

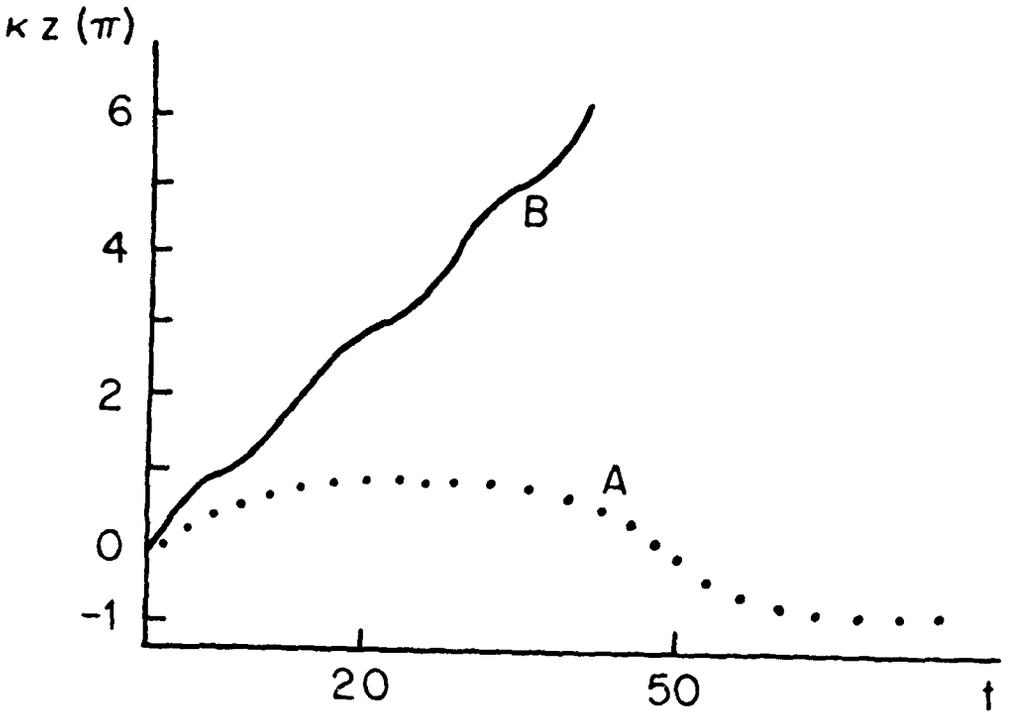

FIGURE 3(b)

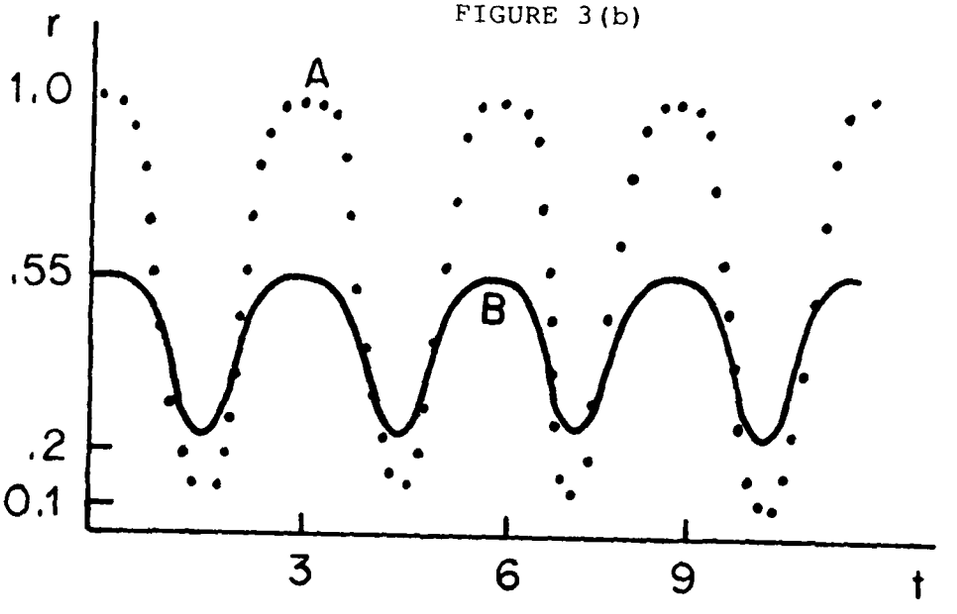

FIGURE 3(c)

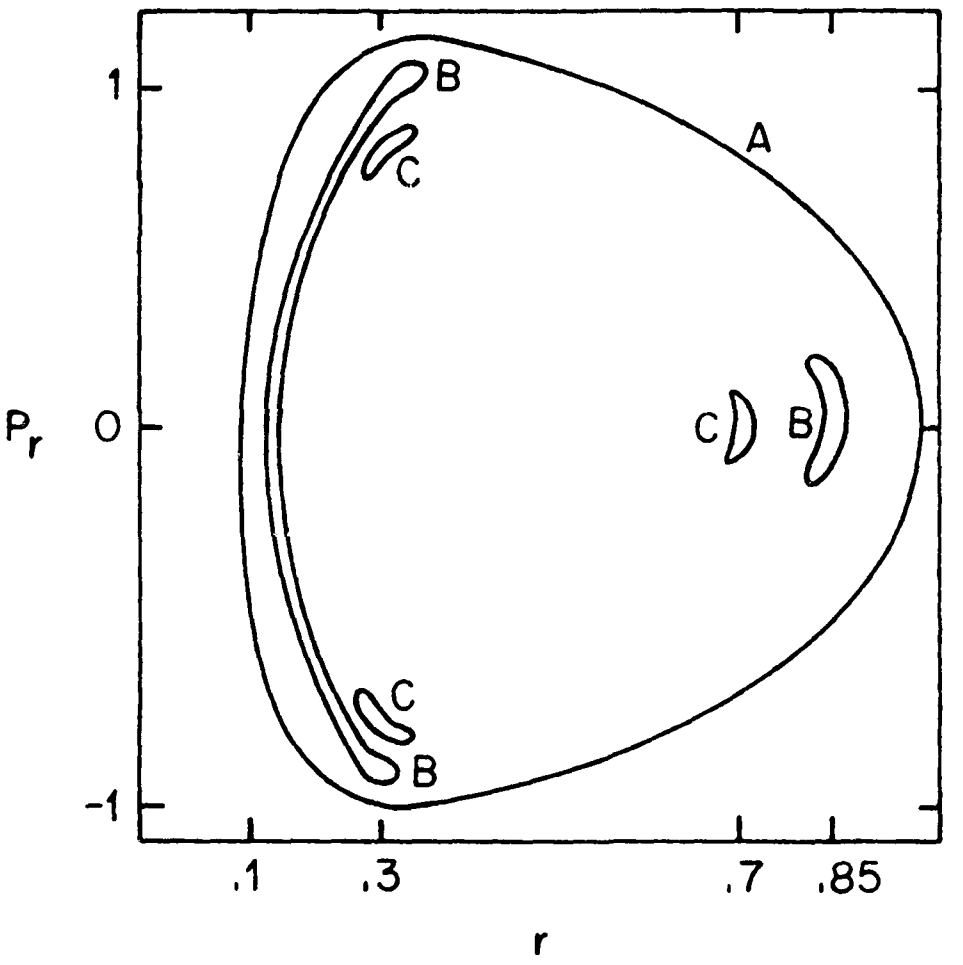

FIGURE 4

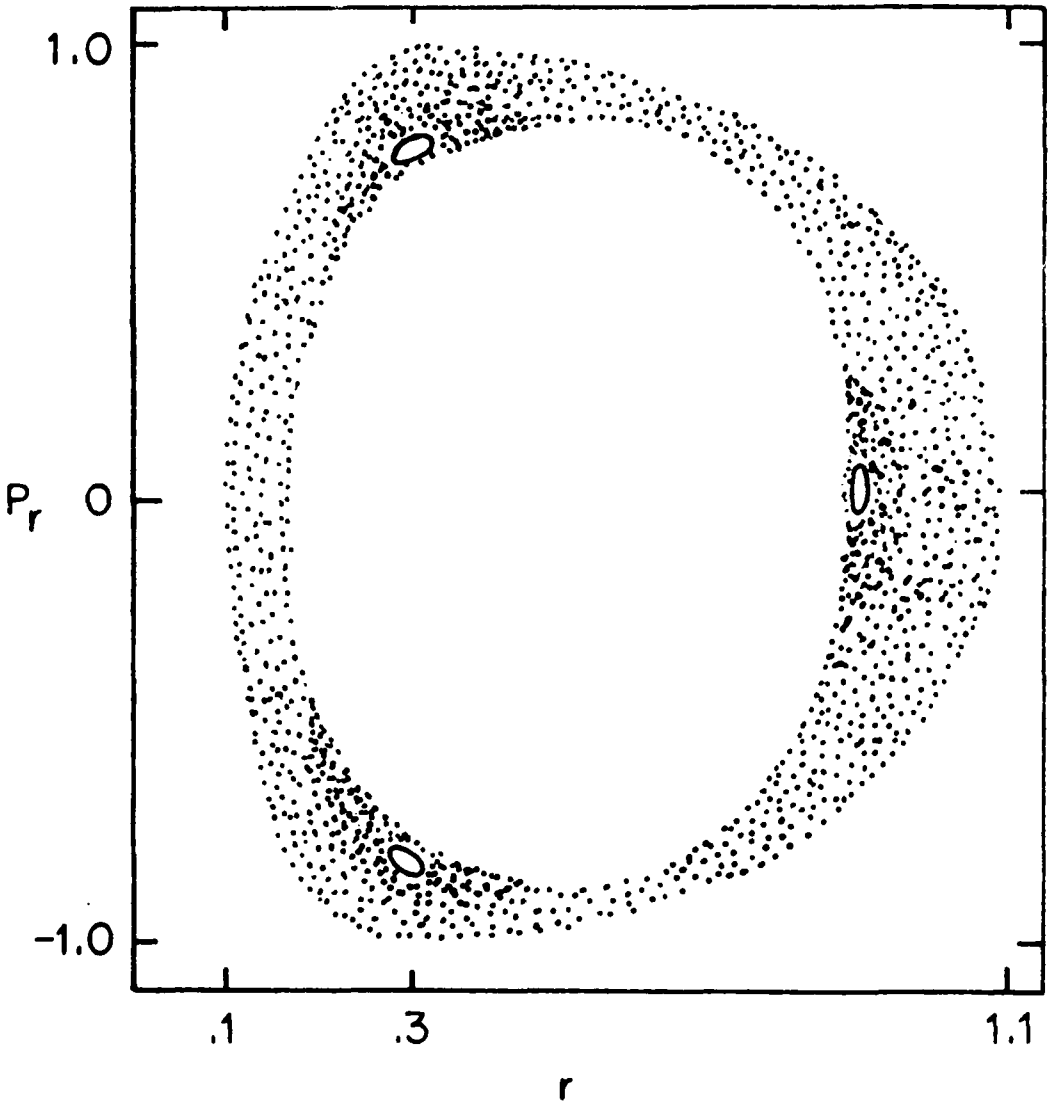

FIGURE 5(a)

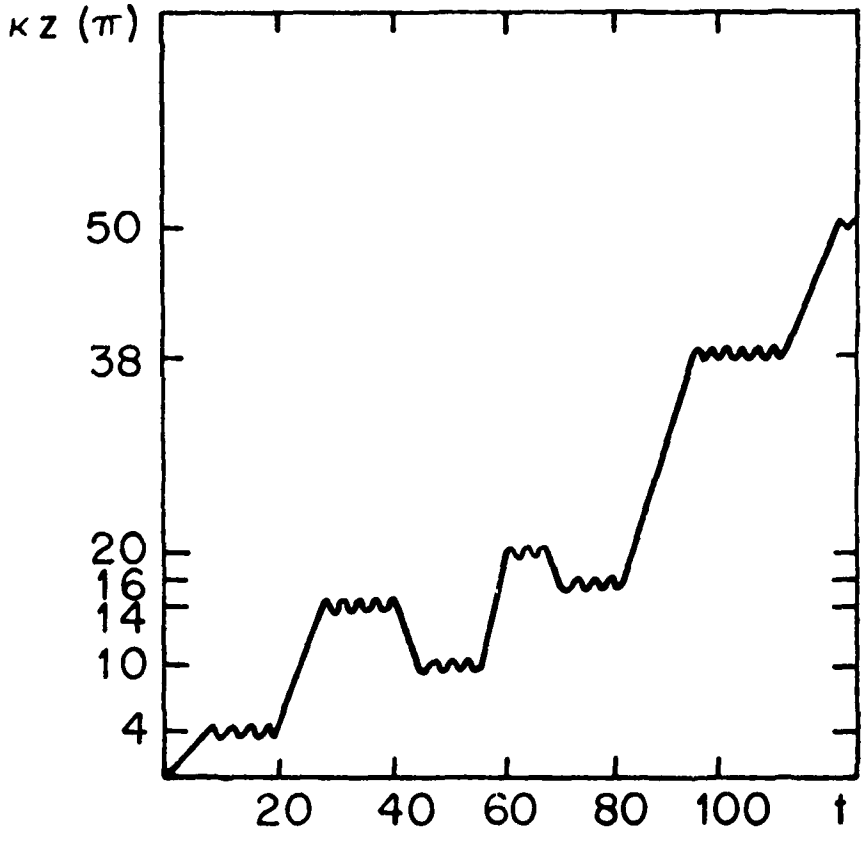

FIGURE 5(b)

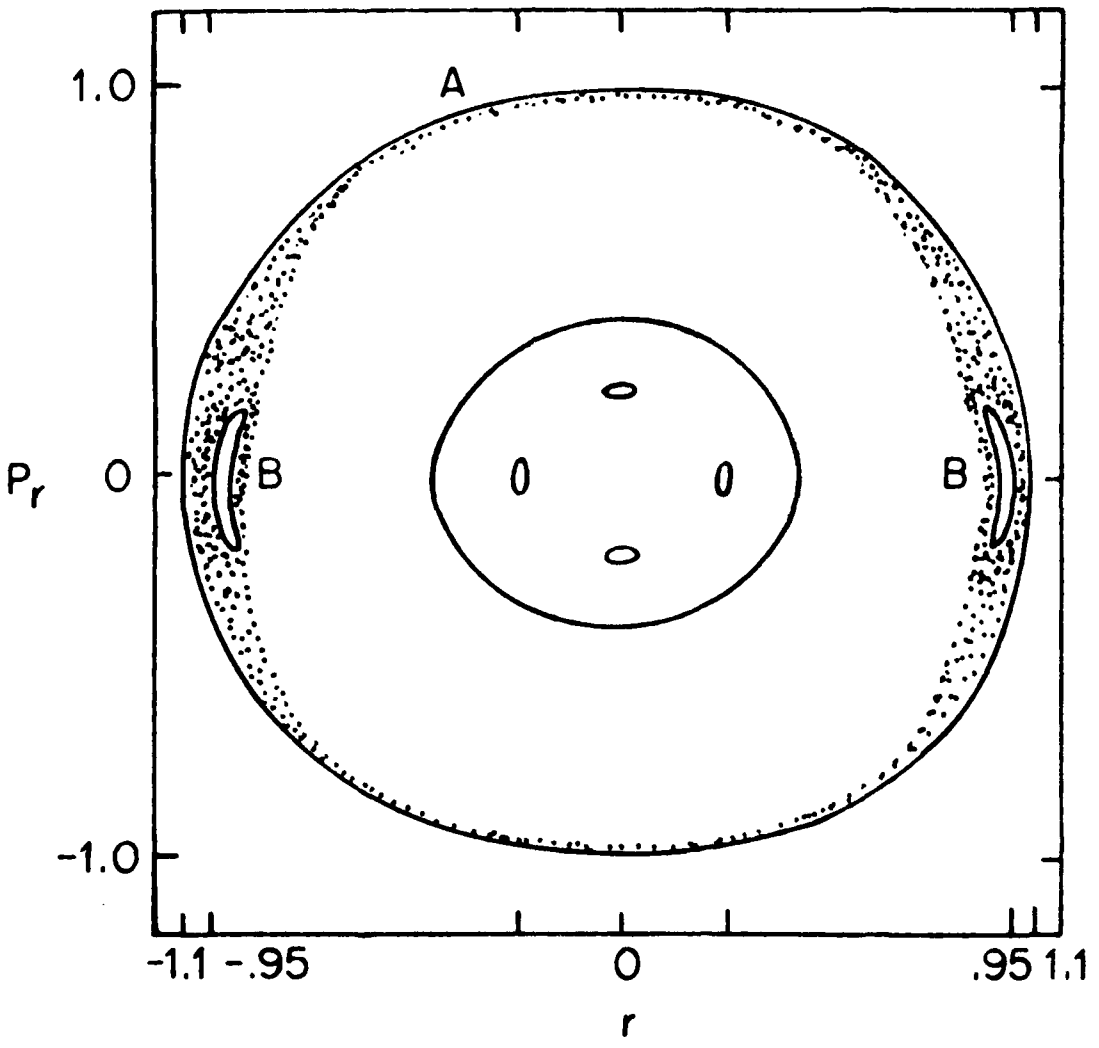

FIGURE 6

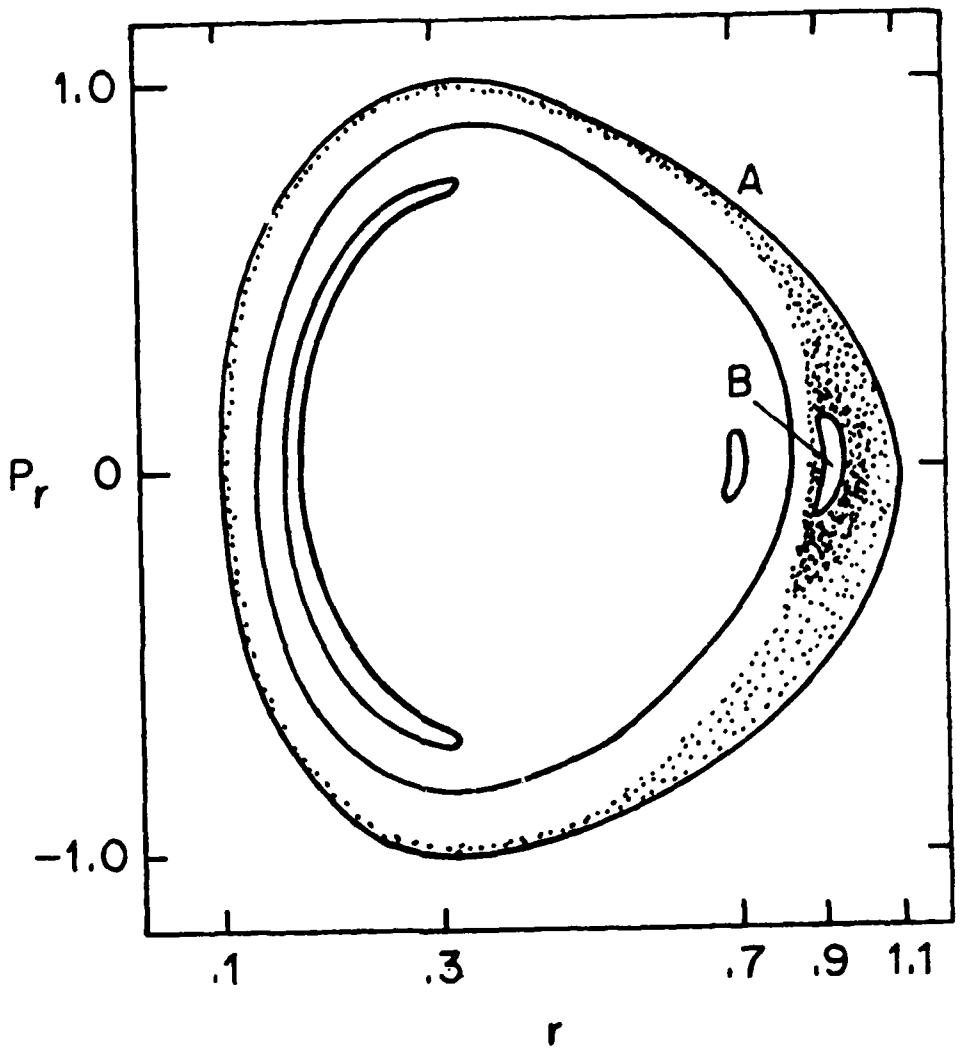

FIGURE 7

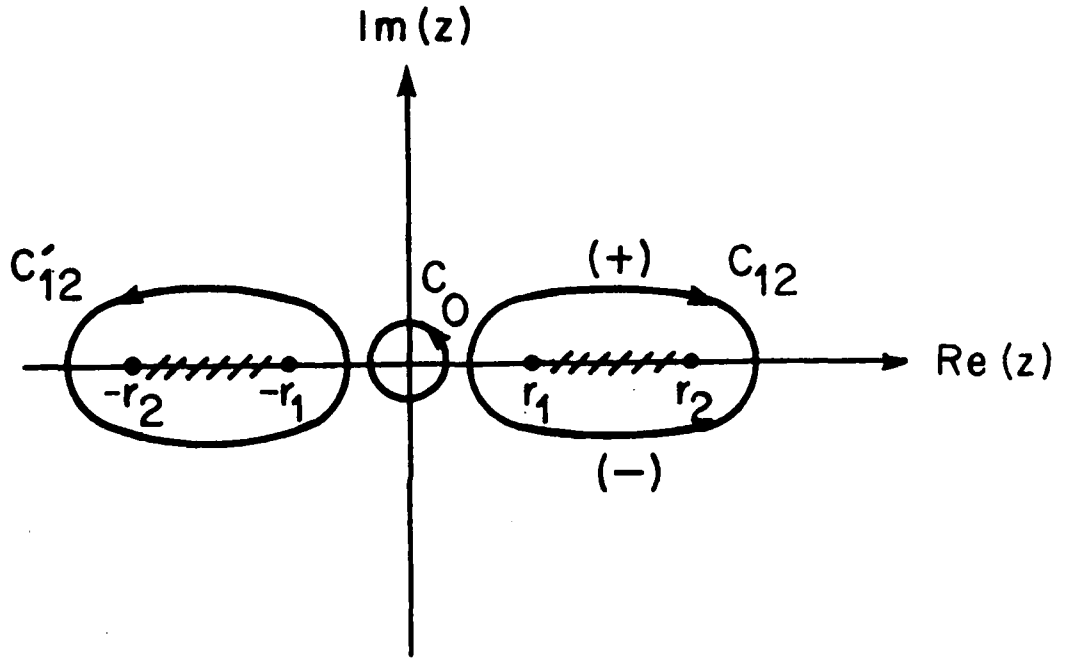

FIGURE 8

APPENDIX N

N. "Summary of Simulations Relevant to the Benford Beam Emission Experiment"

J.C. Weatherall and M.V. Goldman
Private Research Note, May, 1981

Summary of Simulations Relevant to the Benford Beam Emission Experiment

J. C. Weatherall and M. V. Goldman

Department of Astro-Geophysics, University of Colorado,
Boulder 19809

Research Note

May 1981

This computer simulation differs from the Type III driven problem in using a larger amplitude pump, and smaller wave-number pump:

$$W = 5\times10^{-4}$$

$$k_0\lambda_e = 0.005 \ .$$

This is a new parameter regime ($W \gtrsim 10\ k_0^2\lambda_e^2$) for which wave-packets are expected to be unstable to short wavelength perturbations, and break-up may precede collapse.

We are motivated by Benford's experiment, for which

$$\omega_{pe} = 1.8\times10^{11} \quad (n_0 = 10^{13})$$

$$\theta_e = \theta_i = 10 \text{ eV}$$

$$\frac{\gamma_b}{\omega_{pe}} = 0.03 \quad (W \to 1)$$

$$\frac{\Delta k_{\parallel}}{k_0} = \frac{1}{10} \ , \quad \frac{\Delta k_{\perp}}{k_0} = \frac{1}{4}$$

$$\frac{\omega_{ce}}{\omega_{pe}} = 0.01$$

$$k_0\lambda_e = 0.005 \ .$$

Our work uses a broadband, initial value pump (no beam growth rate), $E_0 = 0.283$ ($W = 5\times10^{-4}$); 64x64 grid of length

and maximum growth at $k = E_0$, or $k\lambda_e = 0.006$. In this problem, wavepacket dimension is $2\pi/\Delta k = 2\pi/\frac{1}{4}k_0 = 5000\ \lambda_e$. The instability wavelength is $2\pi/0.006 = 1000\ \lambda_e$.

II. Computer simulation, $\omega_{ce} = 0$ (Figures 2 through 8).

Shows modulational instability and collapse.

III. Computer simulation, $\omega_{ce} = 0.033\ \omega_{pe}$
(Figures 9 through 15).

From J. C. Weatherall's thesis, a sufficient condition for a magnetic field to alter collapse is

$$\frac{\Delta k_\perp^2}{3k_o^2}\frac{\omega_{ce}^2}{\omega_{pe}^2} > \frac{W}{24} ,$$

$$2.6\times10^{-5} \sim 2.1\times10^{-5} .$$

The condition for the magnetic field to affect parametric instability is

$$\frac{k_\perp}{k}\frac{\omega_{ce}}{\omega_{pe}} \gtrsim \sqrt{3}\,\frac{k}{k_{De}} ,$$

$$\frac{1}{2}\,(0.033) \gtrsim \sqrt{3}\,(0.006)$$

$$0.018 \gtrsim 0.010$$

$L = 10{,}000\ \lambda_e$. Pump modes consist of a box in k-space of six modes, $\Delta k_\perp = 2\Delta k_\parallel = \frac{1}{4} k_0$. (Dimensionless units are as in Nicholson, et al., 1978.) We observe modulational breakup and collapse. With a magnetic field of $\omega_{ce} = .035\ \omega_{pe}$, collapse is enhanced, not inhibited.

I. The behavior of parametric instability for $k_0 = 0.005\ k_D$ is shown in Figure 1.

As W becomes large with respect to k_0 ($W > 10\ k_0^2 \lambda_e^2$), the wave is unstable to a modulational (OTS) instability. The counter-streaming waves produced by these instabilities will break up wavepackets into smaller packets.

We can estimate size of perturbation from dispersion relation (Dwight Nicholson, Private Communication, January 1981)

$$-\omega^2 - i\omega\nu_i + k^2 = -k^2 E_0^2 \cdot \left(\frac{1}{\omega + \frac{i\nu_e}{2} - k^2} + \frac{1}{-\omega - \frac{i\nu_e}{2} - k^2} \right) ,$$

assuming $|\omega^2| << k^2$, $|\omega\nu_i| << k^2$, $\omega = i\gamma$ (purely growing). The growth rate is found to be

$$\gamma = -\frac{\nu_e}{2} + \sqrt{2E_0^2 k^2 - k^4} ,$$

FIGURE 1

Behavior of linear parametric instability of a monochromatic wave with $k_0 = 0.005\ k_D$ (growth rate contours in k-space).

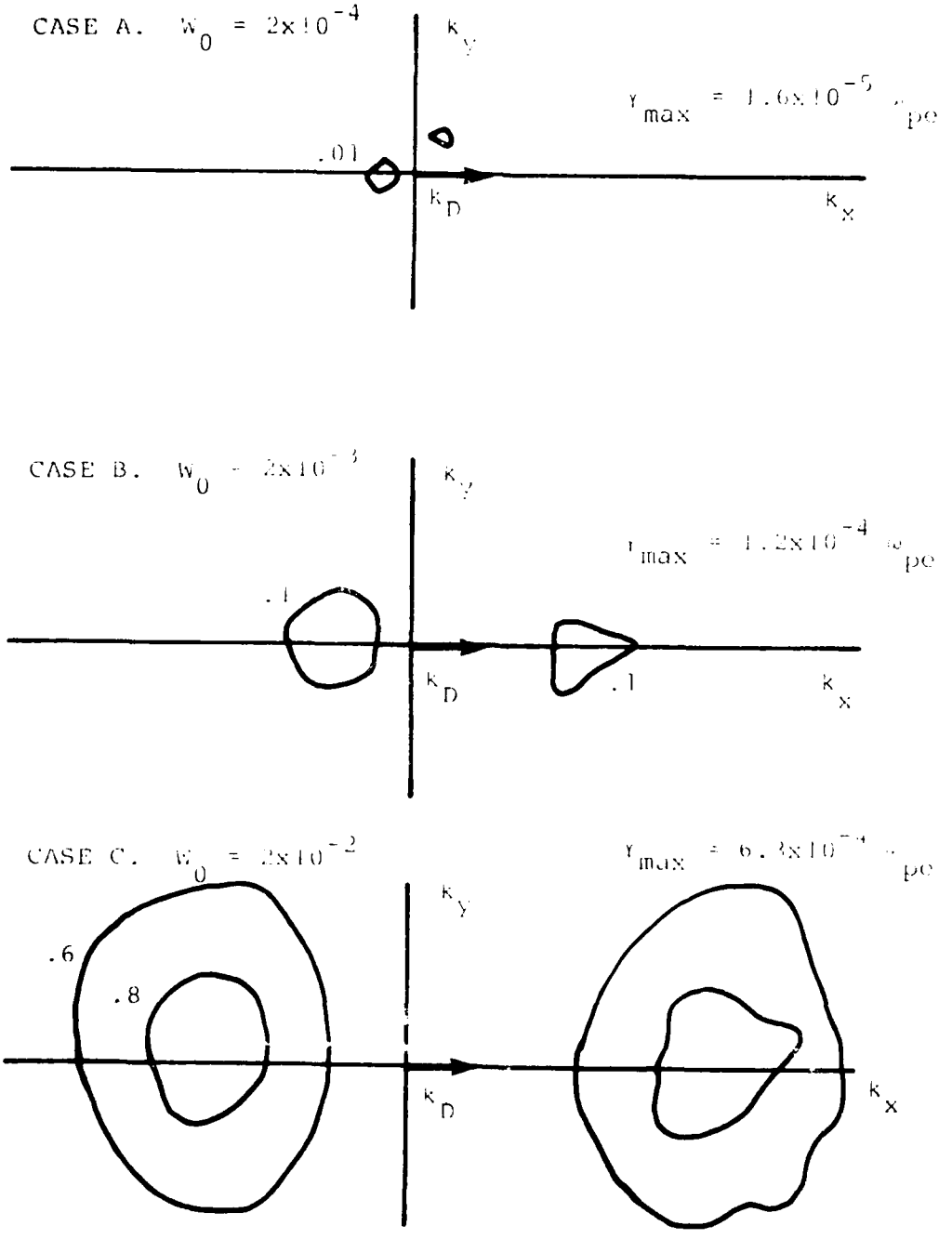

We conclude that this magnetic field will not strongly affect collapse. It may have a stronger affect on instability.

The modulational breakup is faster with a magnetic field (because instability has smaller bandwidth transverse to the field?), and collapse is enhanced, for example, at $T = 72$ ($T = 1$ corresponds to $1377\ \omega_{pe}^{-1}$).

FIGURE 2

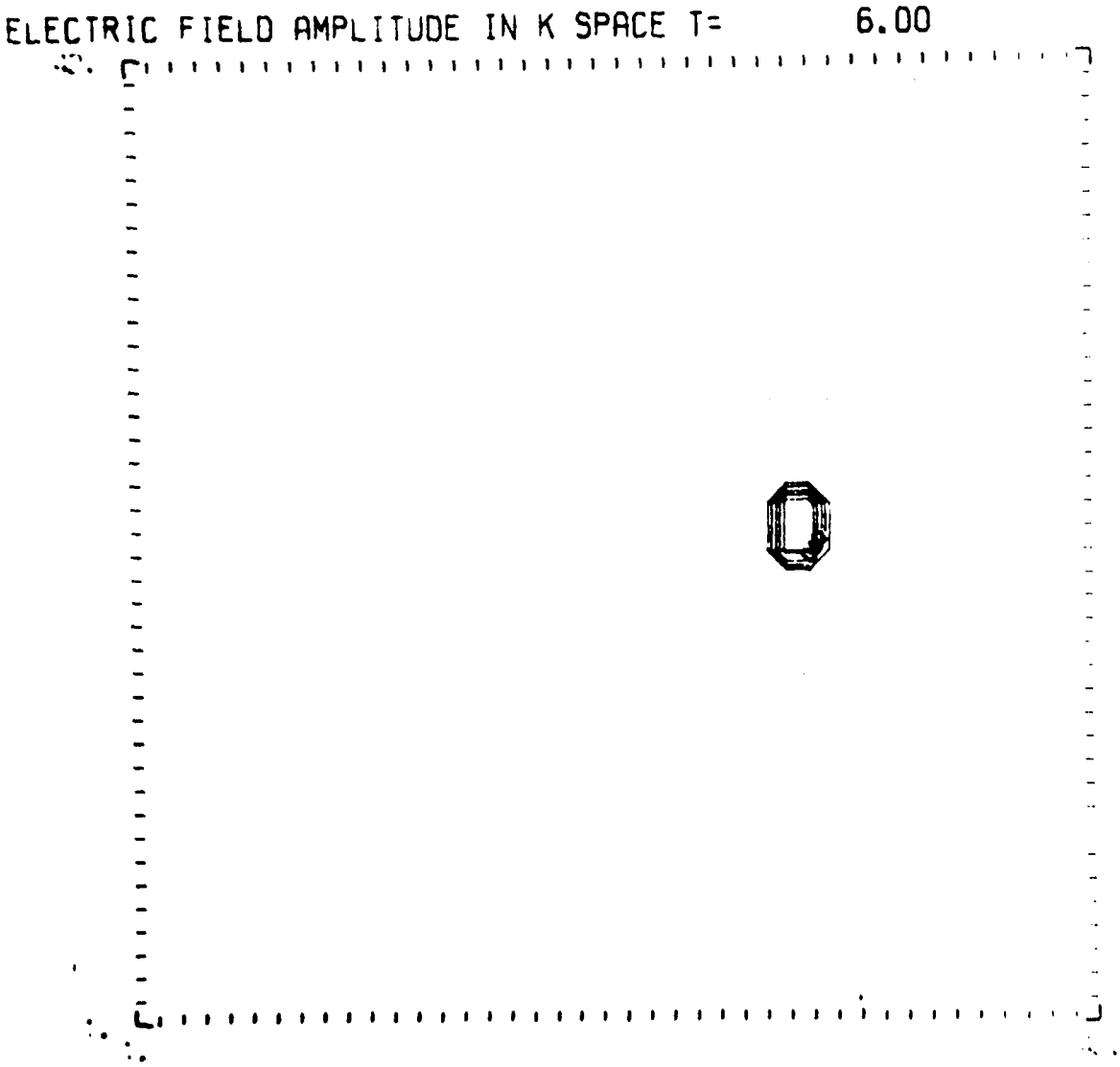

FIGURE 3

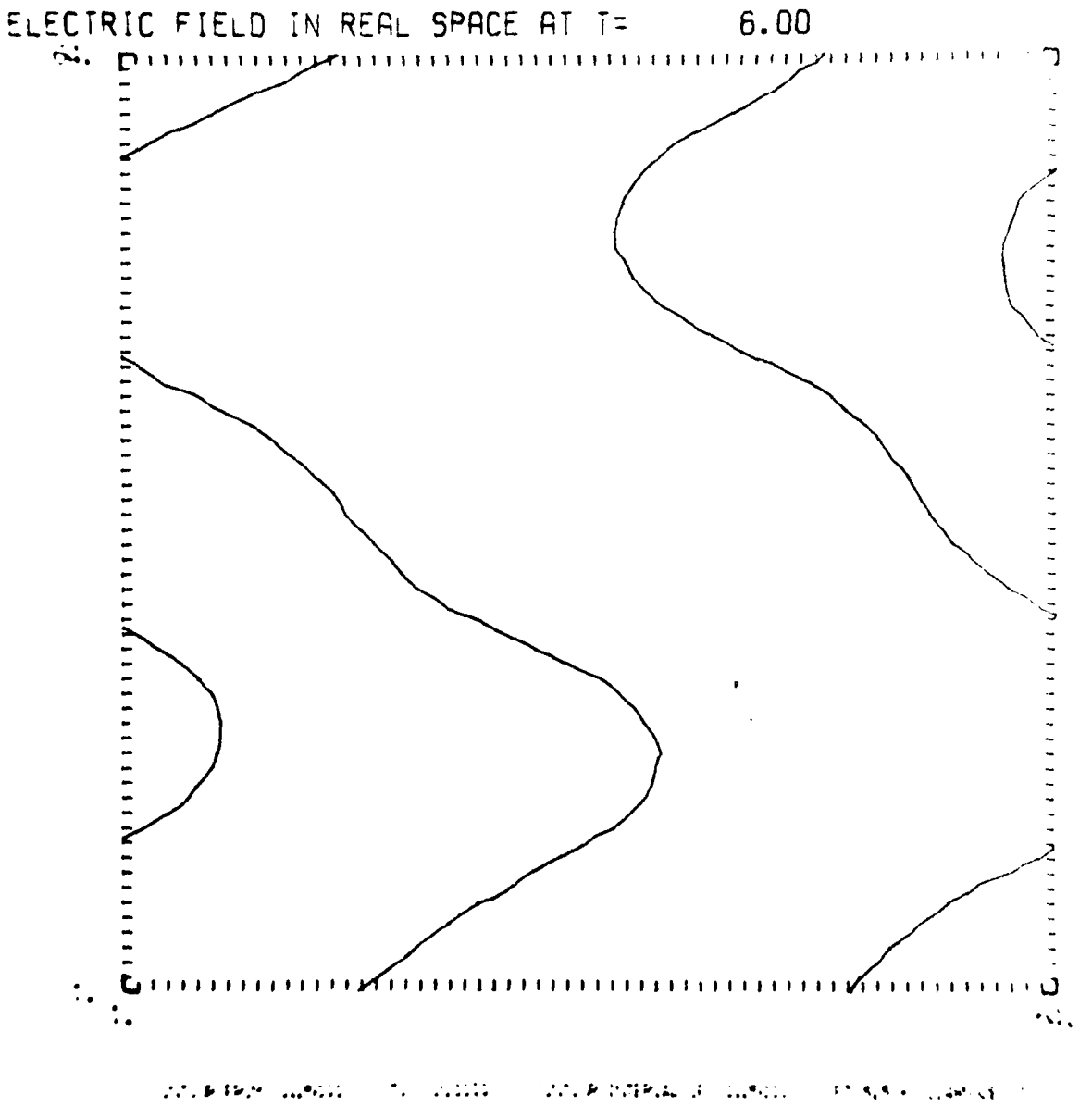

FIGURE 4

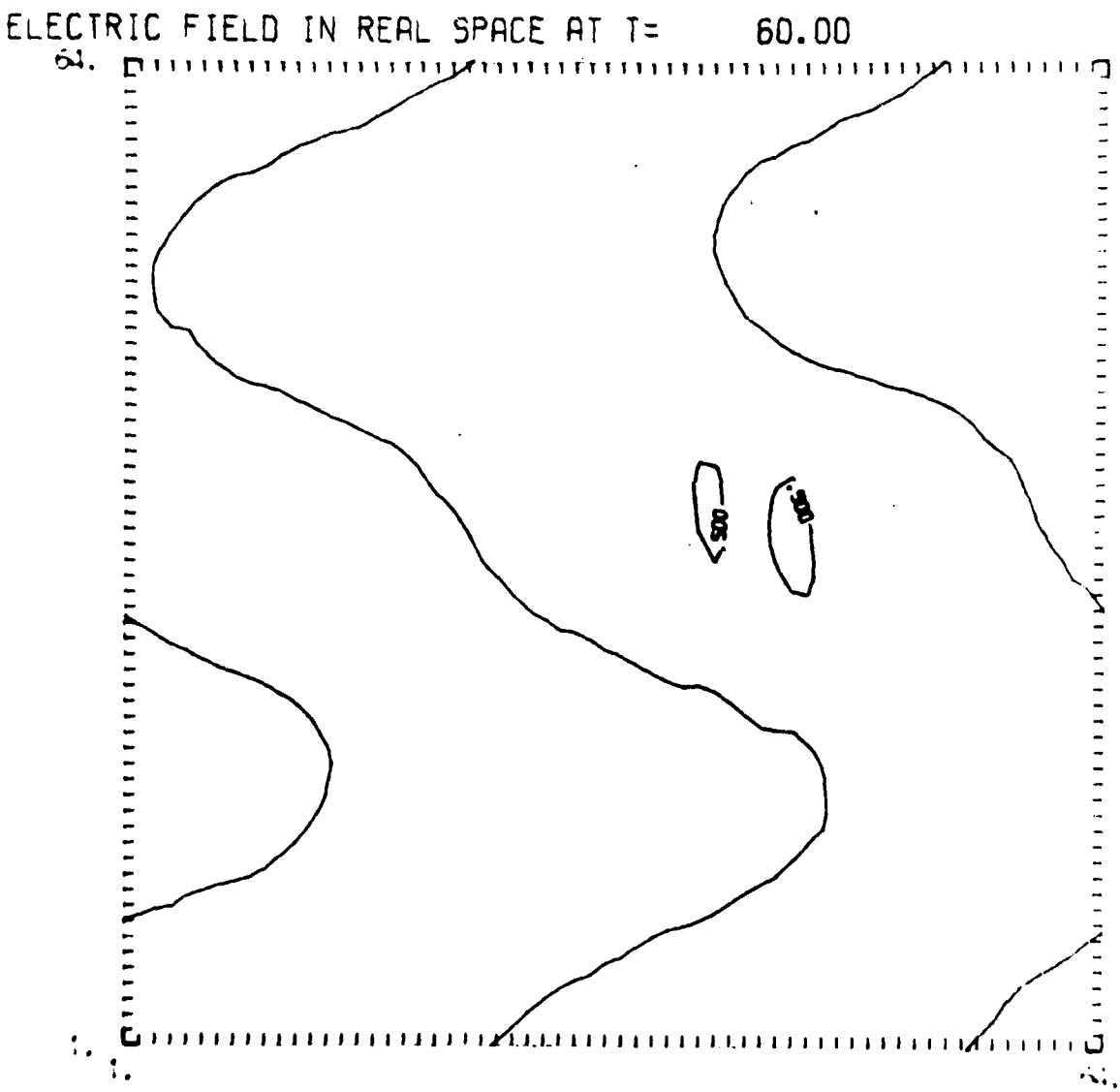

FIGURE 5

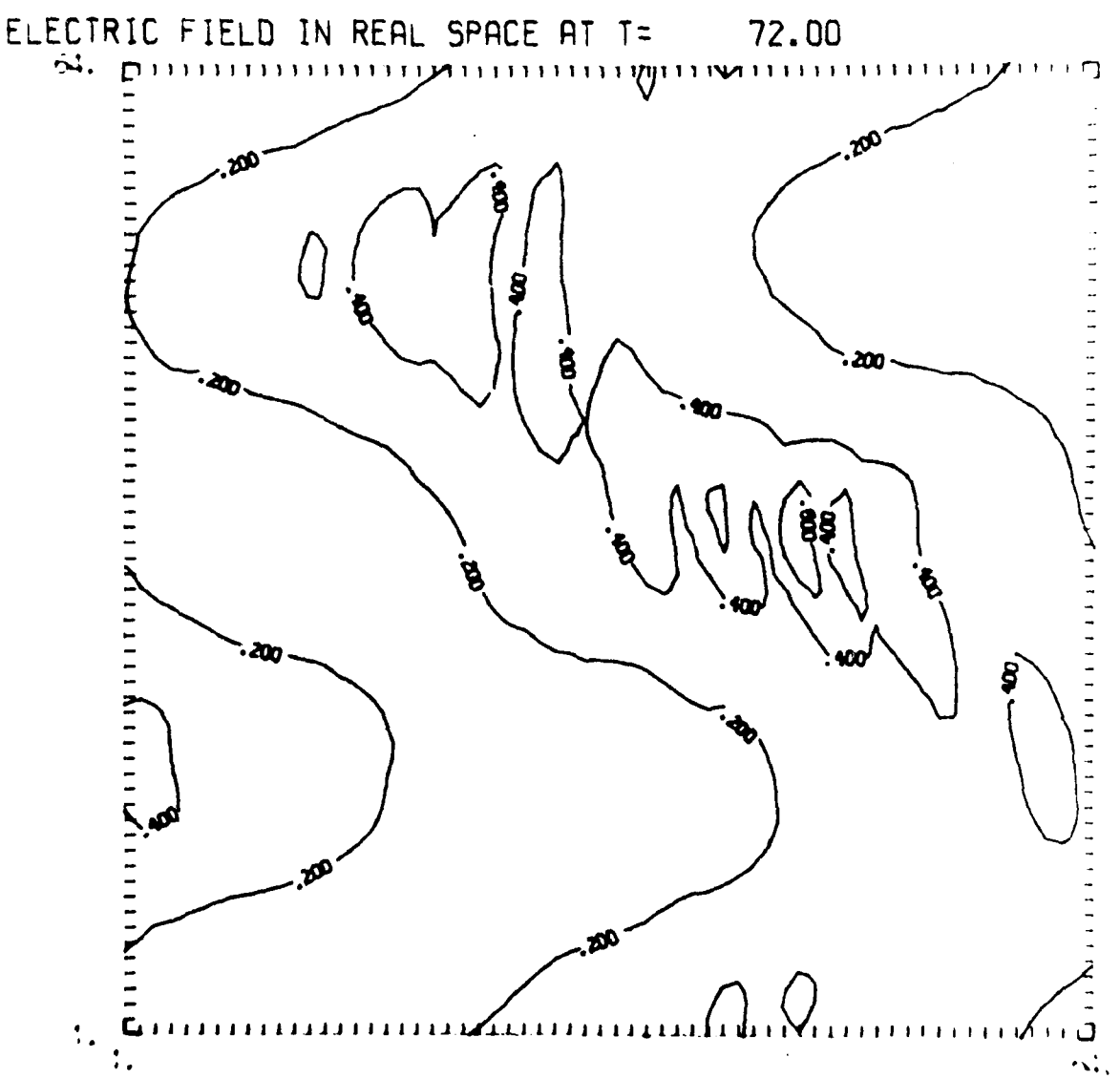

FIGURE 6

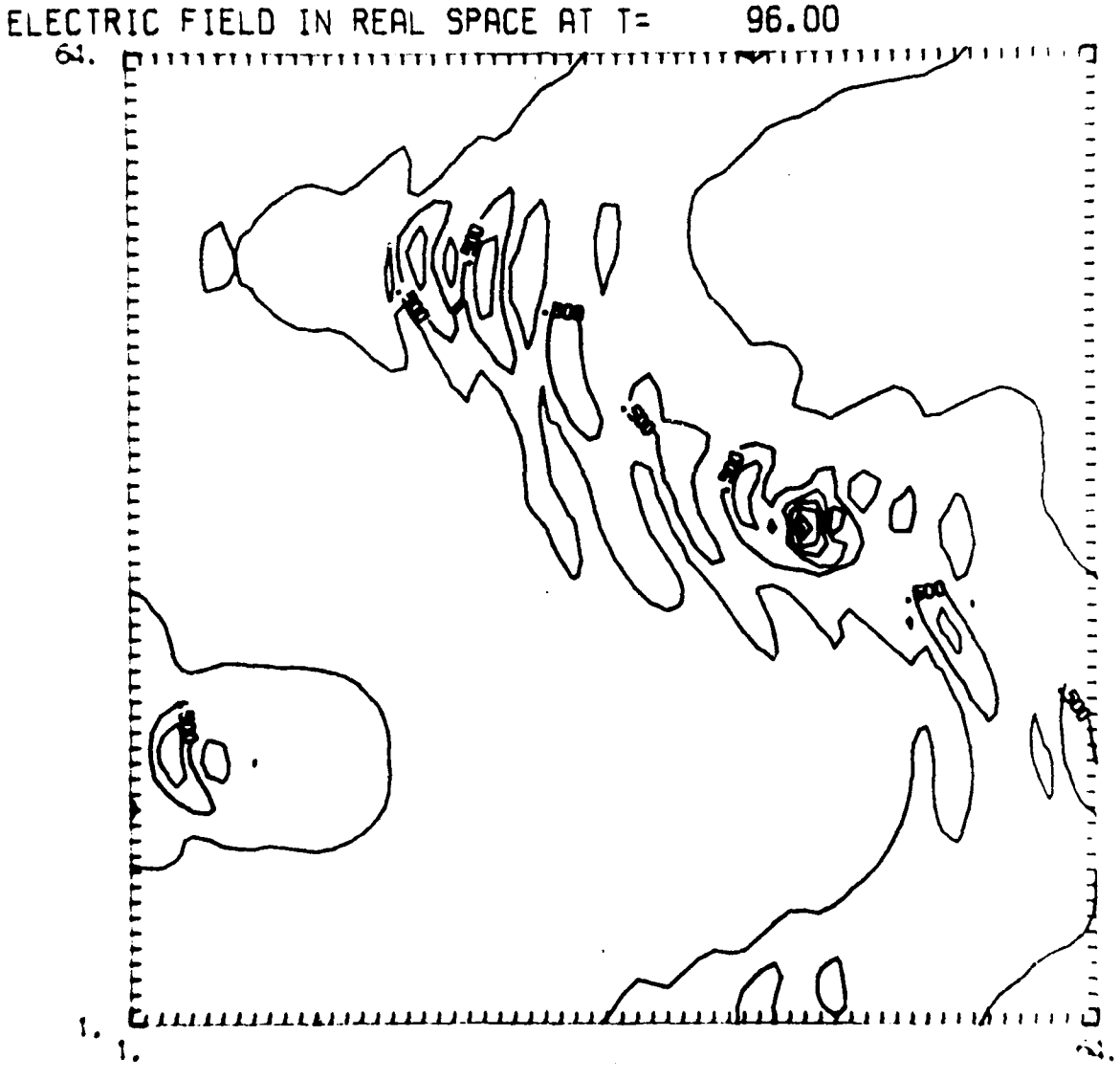
ELECTRIC FIELD IN REAL SPACE AT T= 96.00
64.
1.
1.
64.
CONTOUR FROM 0.25000 TO 2.0000 CONTOUR INTERVAL OF 0.25000

FIGURE 7

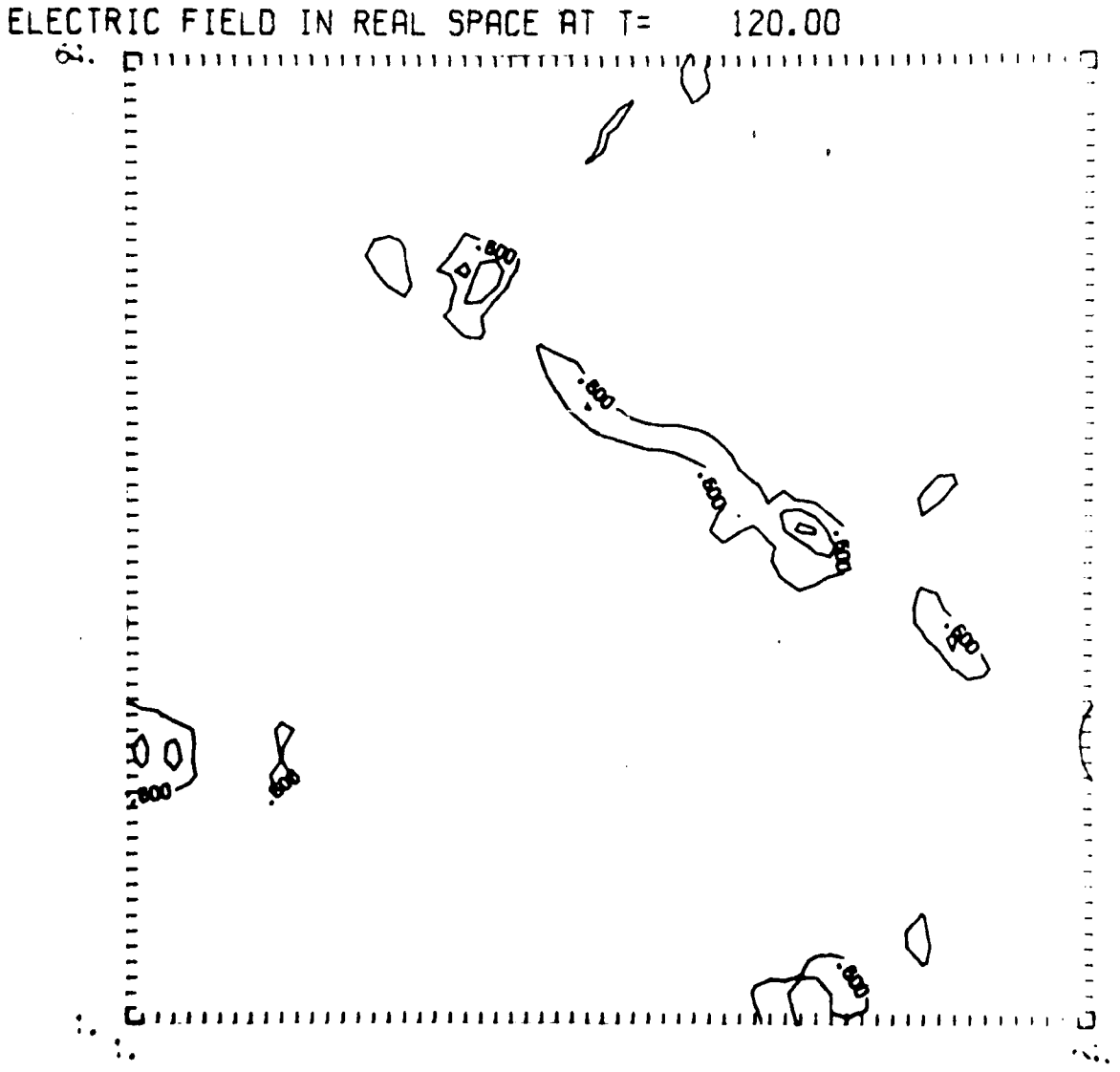

FIGURE 8

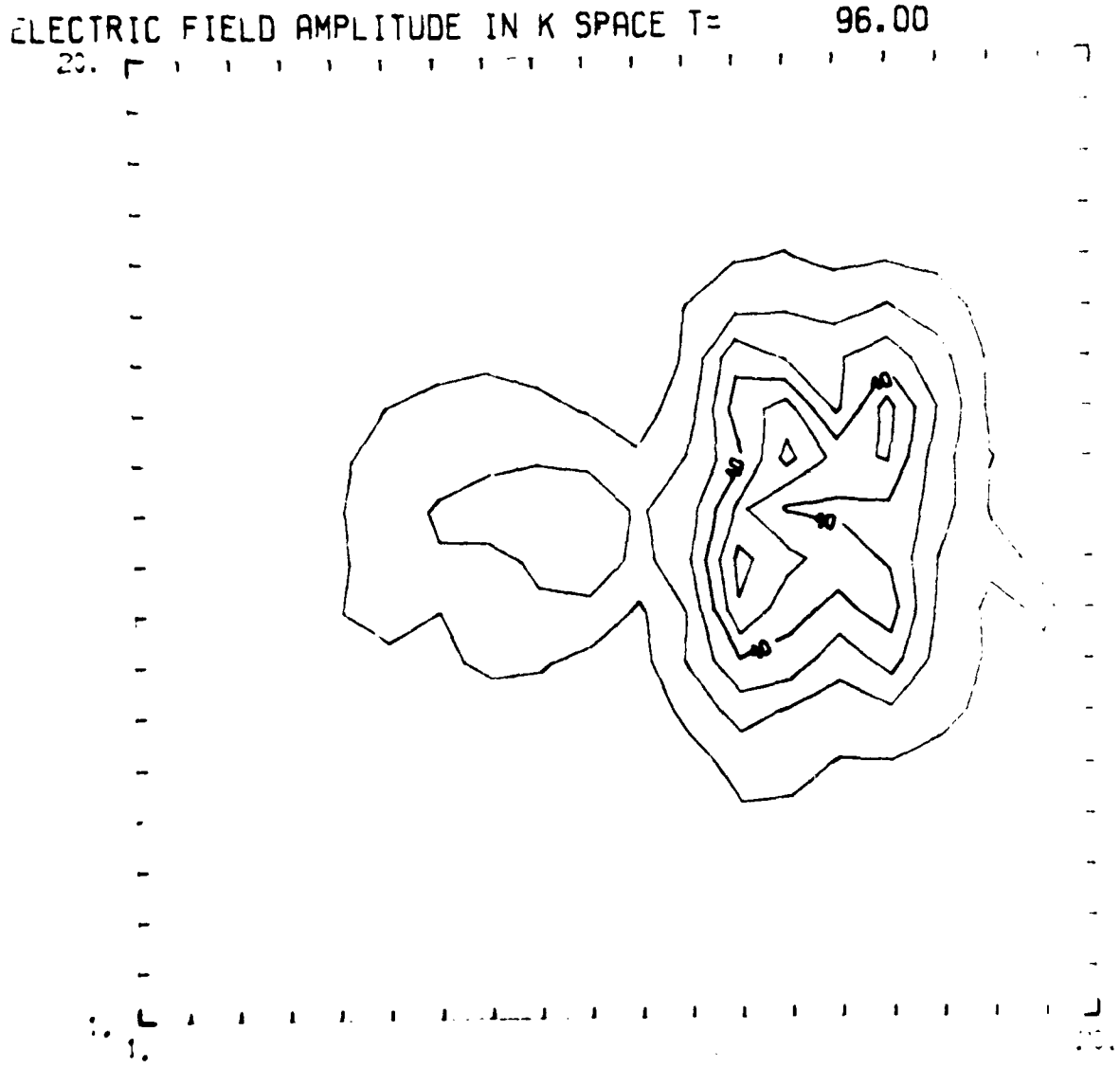

FIGURE 9

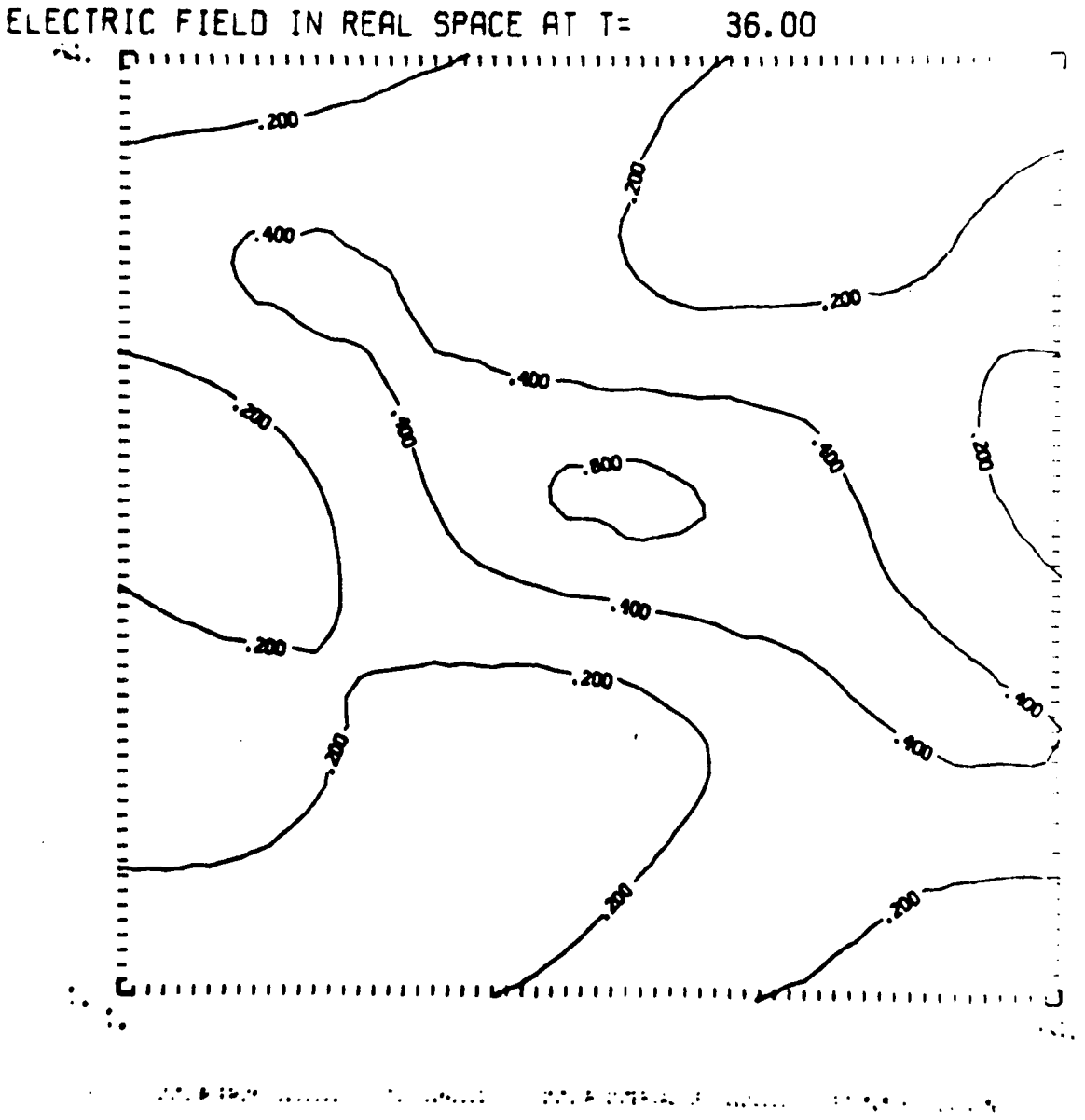

FIGURE 10

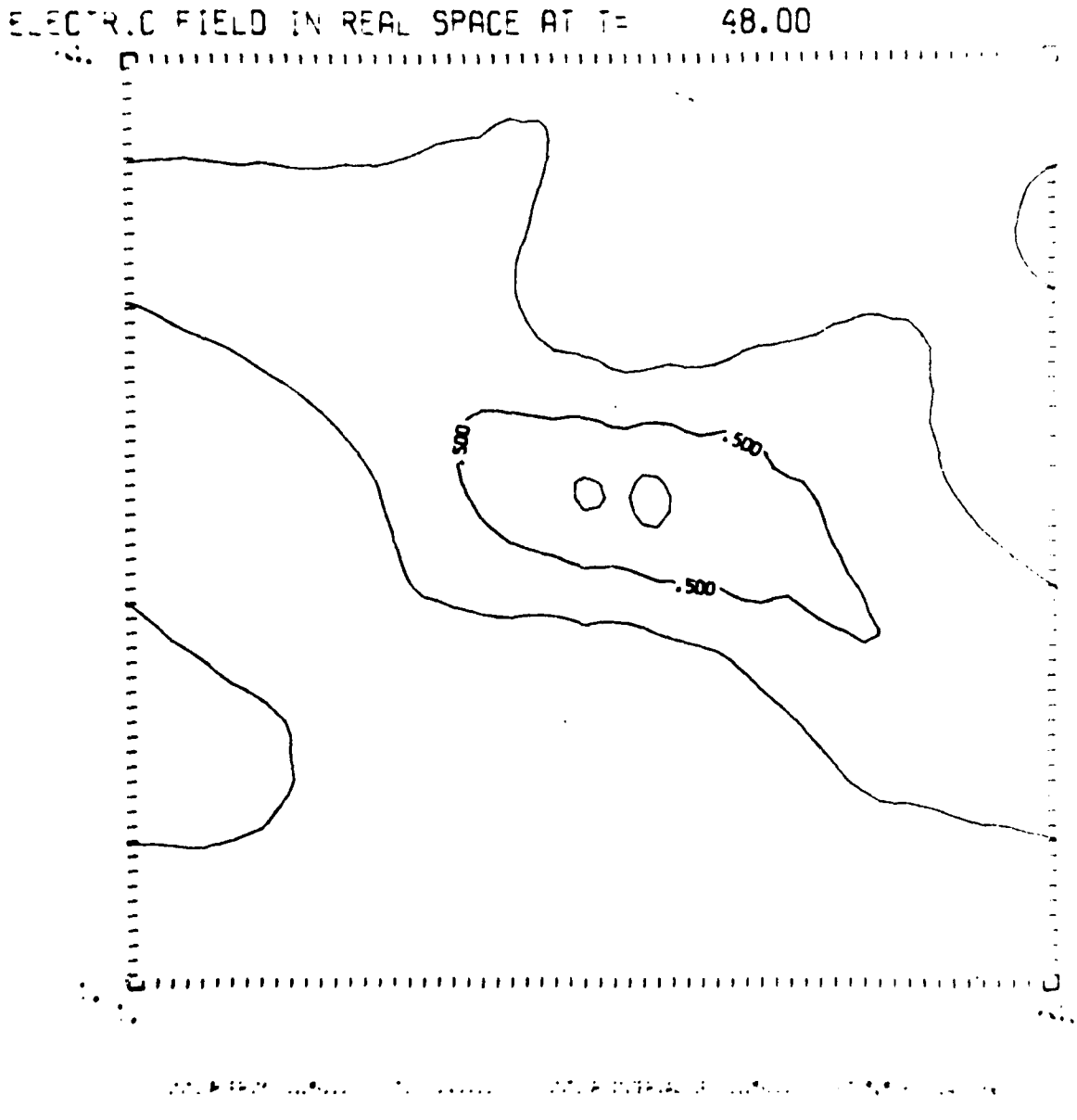

FIGURE 11

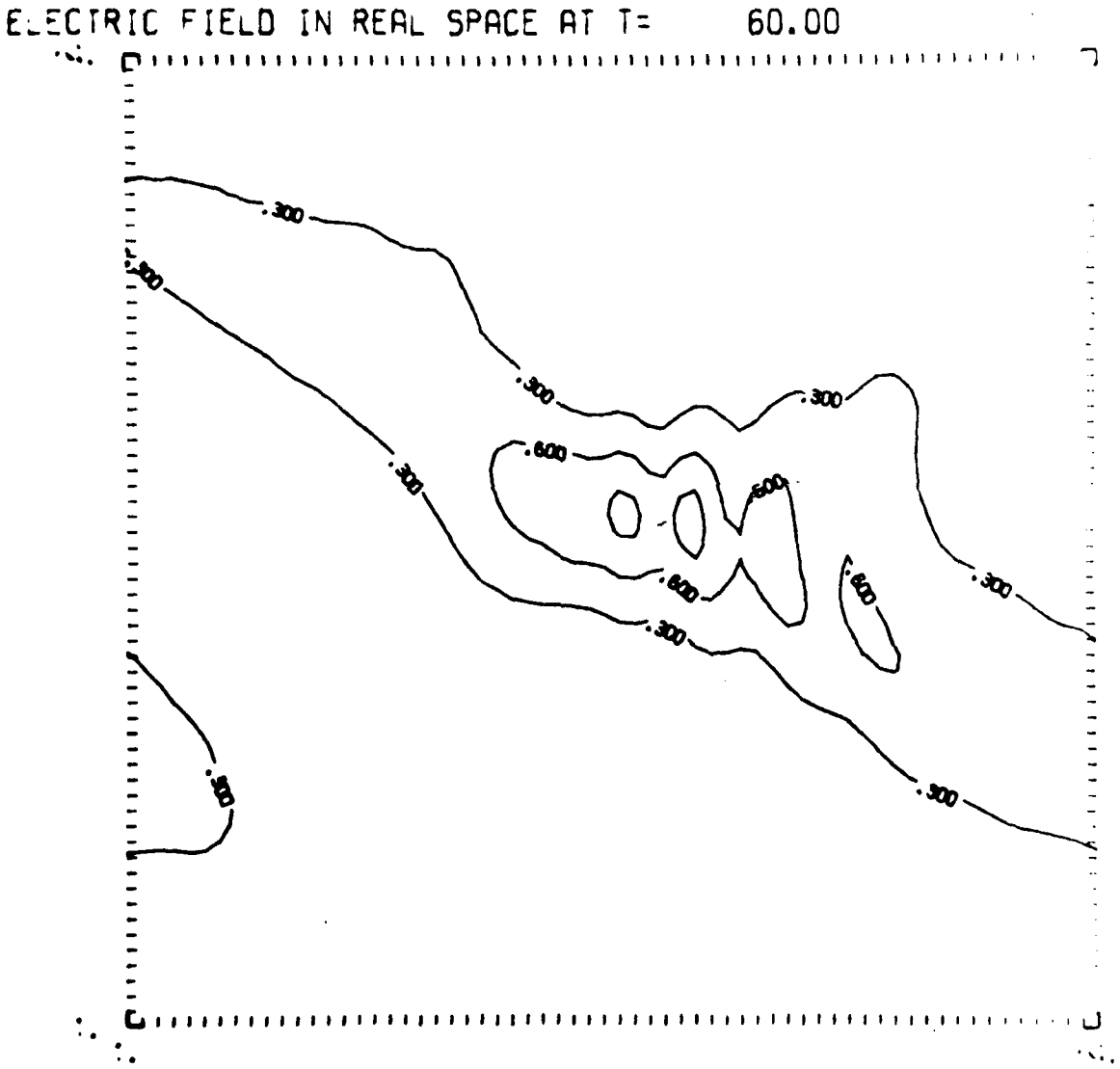

FIGURE 12

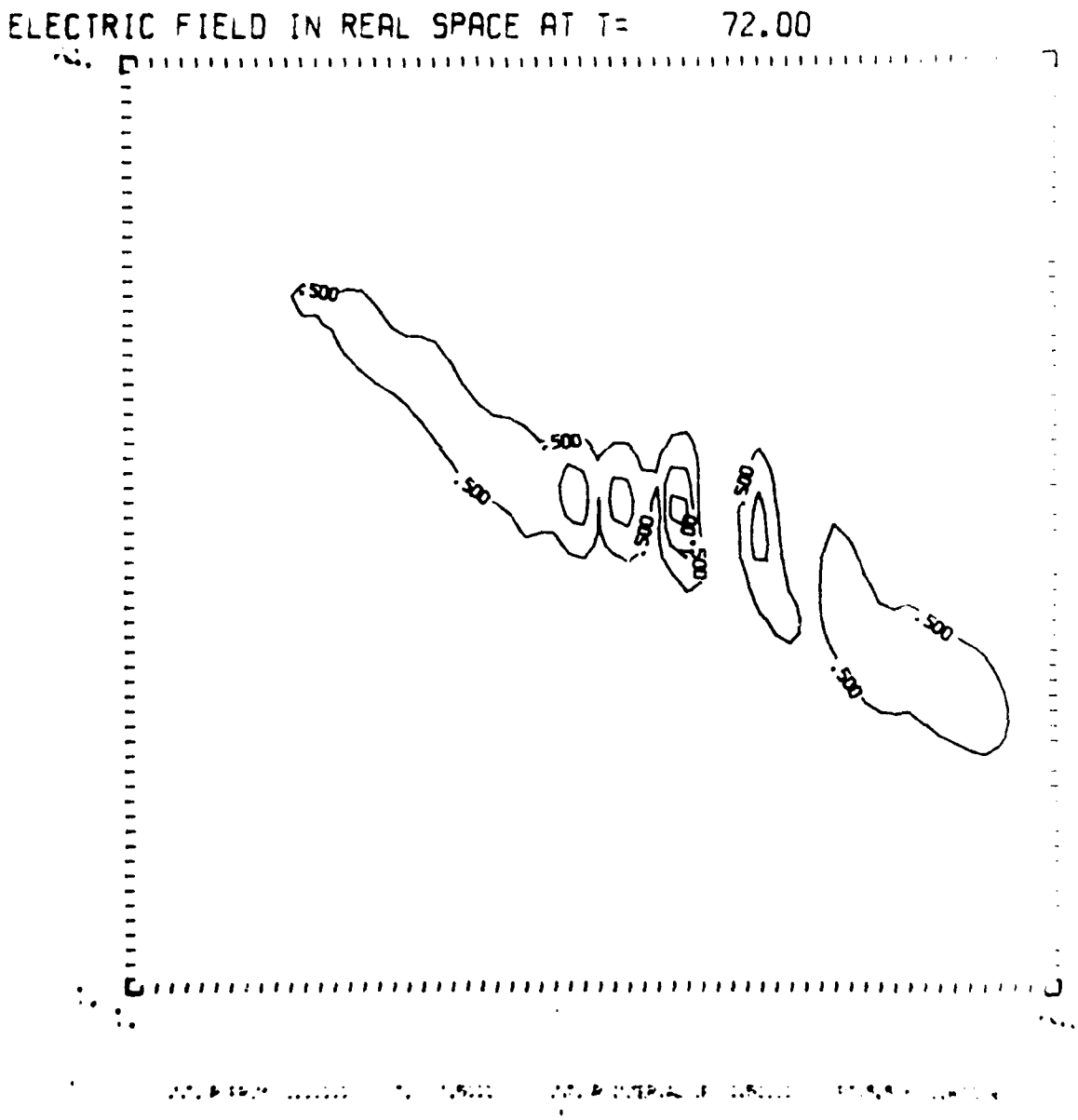
ELECTRIC FIELD IN REAL SPACE AT T= 72.00
.500
.500
.500
.500
.500
.500
.500
.500

FIGURE 13

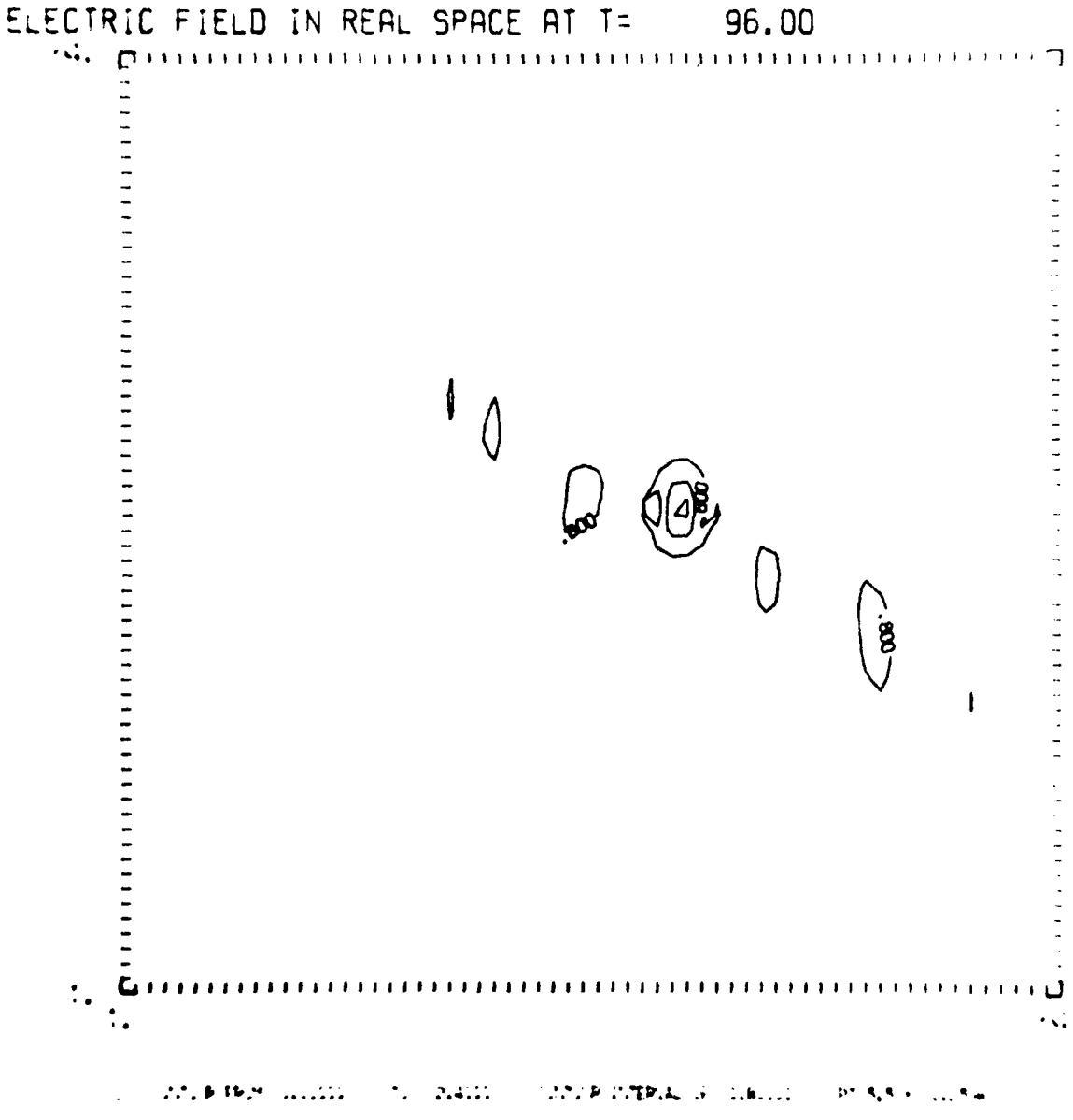

AD-A117 862 COLORADO UNIV AT BOULDER F/G 20/9
PLASMA WAVE TURBULENCE AND PARTICLE HEATING CAUSED BY ELECTRON --ETC(U)
MAY 82 M V GOLDMAN AFOSR-80-0022
UNCLASSIFIED CU-1533143 AFOSR-TR-82-0592 NL

FIGURE 14

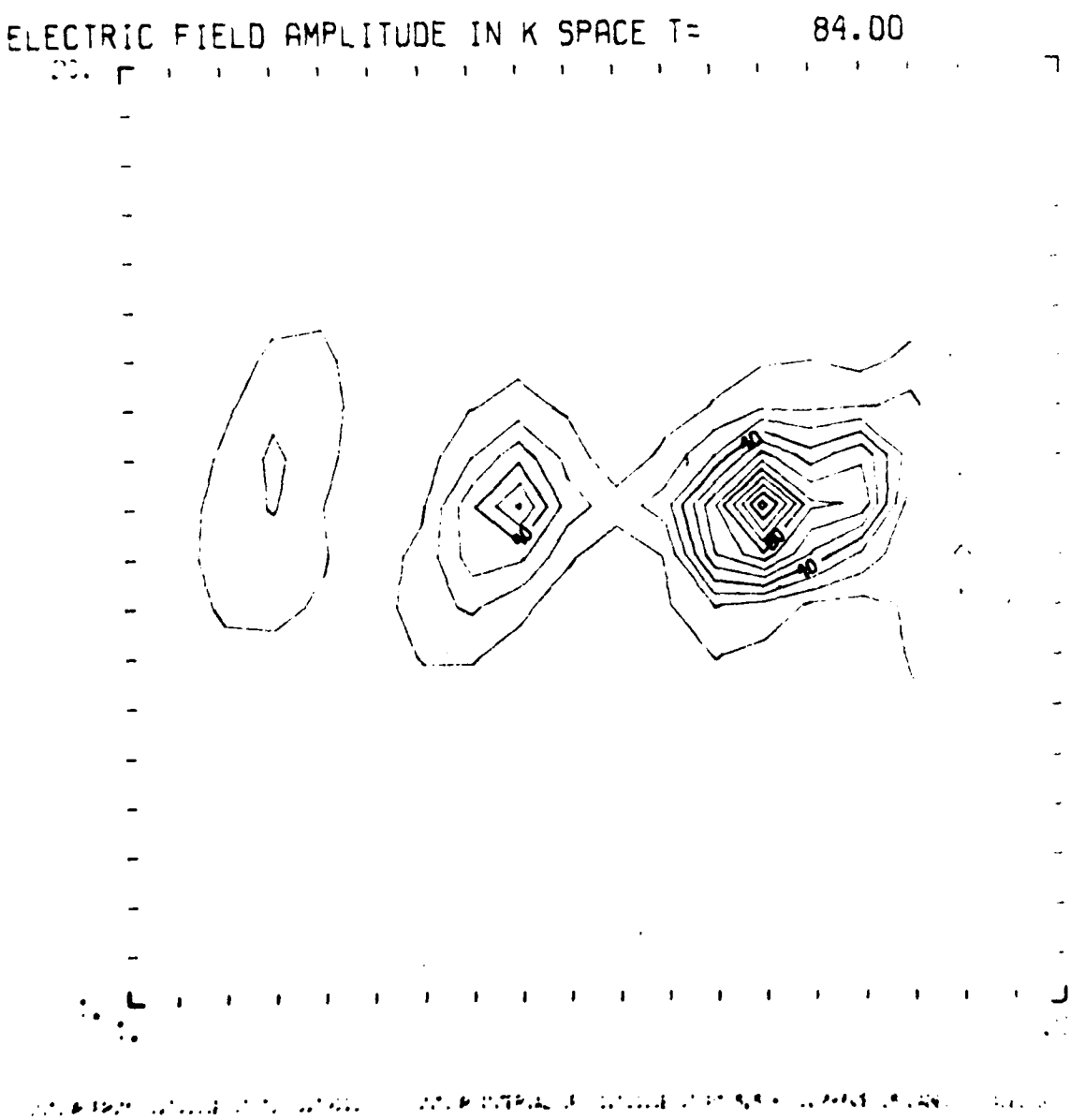

FIGURE 15

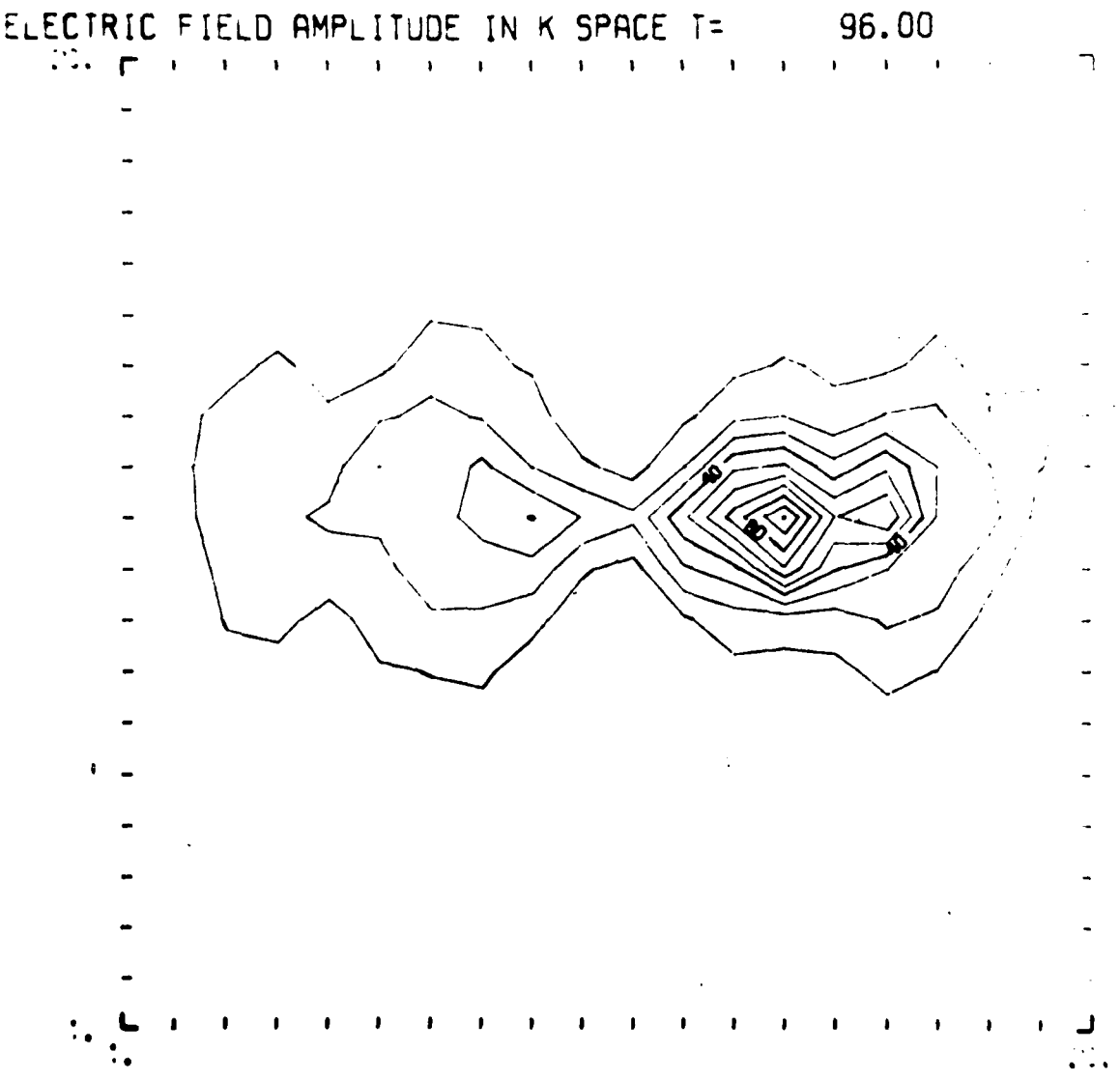


DATE
ILME